UMONS
Université de Mons
Faculté Polytechnique

Optimizing Control of Fed-batch Cultures of Microorganisms with Overflow Metabolism

Laurent Dewasme
Graduate Electrical Engineer
(Faculté Polytechnique de Mons)

Ph.D. Thesis

submitted at the

Université de Mons

and presented on June 11th, 2010,

in fulfilment of the requirements for the degree of

Docteur en Sciences de l'Ingénieur

Jury members

Prof. Dr. Ir. **A.-L. Hantson** (Université de Mons) – *President*
Prof. Dr. Ir. **M. Remy** (Université de Mons) – *Secretary*

Dr. **Ph. Dehottay** (GlaxoSmithKline Biologicals, Rixensart)
Prof. Dr. Ir. **E. C. Ferreira** (Universidade do Minho, Braga)
Prof. Dr. **D. Dumur** (Ecole Supérieure d'Electricité, Gif-sur-Yvette)

Prof. Dr. Ir. **Ph. Bogaerts** (Université Libre de Bruxelles) – *Thesis Co-advisor*
Prof. Dr. Ir. **A. Vande Wouwer** (Université de Mons) – *Thesis Advisor*

POLYTECH MONS

2009-2010

ACADÉMIE UNIVERSITAIRE WALLONIE-BRUXELLES

Optimizing Control of Fed-batch Cultures of Microorganisms with Overflow Metabolism

Laurent Dewasme

THESIS
submitted at the
FACULTE POLYTECHNIQUE DE MONS

Remerciements

Une étape se termine, mais la vie commence seulement. C'est ainsi que je résumerai mon sentiment sur l'aboutissement de cette thèse de doctorat de plus de 4 années et demi au sein du service d'Automatique de la Faculté Polytechnique de Mons. Cette thèse est née du projet PEPSI, fruit des accords et efforts financiers de la Faculté Polytechnique de Mons (FPMs), de l'Université Libre de Bruxelles (ULB) et de la société GlaxoSmithKline Biologicals (GSK), Rixensart.

Je commencerai donc évidemment par exprimer toute ma gratitude à mes promoteur et co-promoteur, Messieurs les Professeurs Alain Vande Wouwer et Philippe Bogaerts, sans qui ce projet n'aurait pas existé. Plus particulièrement, je tiens à remercier Monsieur le Professeur Alain Vande Wouwer pour la confiance qu'il m'a accordée, pour tous ses bons conseils et surtout pour m'avoir régulièrement encouragé tout au long de ma thèse. Je remercie également Monsieur le Professeur Philippe Bogaerts pour les nombreuses discussions fructueuses que nous avons pu avoir durant ces 4 dernières années et pour le chaleureux accueil qu'il m'a toujours réservé à chacune de mes visites dans son service.

Je tiens à remercier Monsieur le Professeur Marcel Remy, chef du service d'Automatique de la Faculté Polytechnique de Mons, pour m'avoir accueilli dans son équipe, pour avoir partagé son grand savoir, offert ses conseils avisés quand j'en avais besoin et, enfin, pour avoir accepté de participer au jury de thèse en tant que secrétaire.

Toute ma reconnaissance va également à Madame le Professeur Anne-Lise Hantson que je remercie pour avoir accepté d'assurer la présidence du jury de thèse et pour m'avoir accueilli dans les locaux du service de Chimie et Biochimie Appliquées afin d'y mener des sessions expérimentales indispensables à la conclusion de ce travail.

Mes remerciements vont également:

- à Messieurs Philippe Dehottay et Olivier Laloux, chefs de service chez

GlaxoSmithKline (GSK) Biologicals, grâce à qui ce projet a pu être initié. L'expérience de Monsieur Dehottay m'a permis d'acquérir une vision très pragmatique du fonctionnement des bioprocédés, me permettant de diriger correctement mes recherches par rapport aux besoins réels des entreprises orientées vers les biotechnologies. J'en profite pour également remercier Sandrine Dessoy et Jean-Pierre Camelbeeck pour leur soutien et leurs conseils pratiques indispensables pendant les sessions expérimentales.

- à Messieurs les Professeurs Didier Dumur de l'Ecole Supérieure d'Electricité (SUPELEC) de Paris et Eugénio C. Ferreira de l'Université du Minho de Braga, pour avoir accepté de consacrer une partie de leur temps afin de participer à ce jury de thèse.
- à Messieurs les Professeurs Michel Perrier et Bala Srinivasan (Ecole Polytechnique de Montréal, Québec, Canada), Monsieur le Professeur Daniel F. Coutinho (Pontifícia Universidade do Rio Grande do Sul, PUCRS, Brésil), Monsieur le Professeur Lino O. Santos (Université de Coimbra, Portugal) et Madame le Professeur Isabel Rocha (Université du Minho de Braga, Portugal) pour leur précieuse collaboration à la réalisation de ce travail.

Il n'est possible de réaliser une thèse de doctorat que dans une atmosphère qui s'y prête correctement. Je n'oublie évidemment pas les gens qui, chaque jour, ont travaillé à l'instauration de cette atmosphère, certes, de travail, mais malgré tout et surtout exceptionnellement chaleureuse. Merci donc:

- à mes collègues (permanents ou temporaires) du service d'Automatique de la FPMs: Madame le Professeur Christine Renotte, Anne-Catherine, Véronique, Caroline, Francisca, Cristina, Ines, Clarisse, Ghizlane, Renato, Guillaume, Frédéric, Bob, Johan, Alexandre, Vincent, William, Armand, Carlos, Edmundo, Pedro, Pradeep, Yiqing, Ixbalank, Alexandru, Paul et Andrés.
- à mes collègues du service de Chimie et Biochimie Appliquées de la FPMs: Monsieur le Professeur Michel De Meyer, Magali, Christelle, Nathalie, Liza, Lionel, Henri, Michel et Amaury.
- à mes collègues du service de Chimie Générale et Biosystèmes de l'ULB: Aline, Nathalie, Anne, Xavier, Vincent et Jean-Louis.

Je me refuse à croire que la vie se résume au travail. De plus, l'équilibre mental nécessaire à la réussite professionnelle s'entretient bien souvent par l'intermédiaire d'autres facteurs qu'on jugera plus ou moins importants que le travail selon notre philosophie personnelle. Nous citerons parmi ces facteurs par exemple l'amitié et les hobbies. Etant dans l'impossibilité de citer les noms de toutes les personnes qui, de près ou de loin, rendent ma vie supportable voire parfois agréable, je remercierai juste vivement mes amis Confrères et surtout Amaury L., la personne la plus apte, à mon sens, à comprendre et respecter mes idées, bonnes ou mauvaises.

Je remercie évidemment toute ma formidable famille qui me témoigne énormément d'amour et d'intérêt. Je ne peux que me sentir honteux d'être trop souvent absent ou maladroit quand vient le moment de leur retourner ces témoignages. L'envie est toujours présente mais la manière manque.

Je terminerai ces remerciements en rendant hommage à mes parents. Je ne suis tout simplement pas grand chose sans leur intervention dans cette petite histoire. J'espère qu'ils verront à travers cette thèse de doctorat une sorte de concrétisation de tous les efforts qu'ils ont fournis pour m'éduquer et me catapulter le plus haut possible dans l'échelle sociale.

Introduction

Context and motivation

Monitoring and control systems, as scientific disciplines, are nowadays essential means for a lot of important applications. It is indeed inconceivable to build an aircraft system without incorporating several key robust controllers (autopilot, fuel balance, temperature and pressure control, airflow detectors, etc). In the biomedical field, surgicals, health-care systems, different laboratories like sleep laboratories, are more or less completely monitored or about to be. In the environmental context, low-energy house rhymes now with heating pump for temperature control. Computational, environmental and social progresses are then practically merged into many multidisciplinary techniques.

In the last decades, biology, agriculture, food science and medicine technologies have been gathered in a new science field recognized as "Biotechnology". Of course, human beings have always been dependent on chemical and biochemical processes to meet their needs. But health care has taken such an important place in everyone's life that the economic potentialities of the biotechnology market have pushed the industry, as for instance, food and biopharmaceuticals, to engage in a race at peak performance requiring more than the heuristics. Optimization of bioprocesses through monitoring and control is now the spearhead of many big industries for the next decades.

One of the fastest growing applications of biotechnology is the recombinant protein technology using microorganisms host strains like *Saccharomyces cerevisiae* (baker's yeast), *Escherichia coli* (bacteria) or animal cells. This technology allows the production of vaccines and different disease treatments (cancers, hormonal diseases, HIV, Malaria, etc). The social and economic factors are reaching a so important level that the scientific community of engineers (not only chemical and biochemical, but also automation and control engineers) is regularly consulted in order to optimize bioprocesses.

Bioprocess optimization is a delicate task as a strong knowledge of the cell physiological behavior is generally required. The interest is here focused on cell strains comparable to yeasts, bacteria and animal cells. Their main physiological feature resides in their primary metabolism or, more precisely, in their catabolism. This one is characterized by a limited energy production princi-

pally used for cell growth and division. The limitation comes itself from a limited capacity to oxidize the main nutrient, also called substrate and essential to growth: glucose. The excess part of this nutrient can follow another metabolic pathway more commonly known as fermentation, producing a side byproduct. For obvious reasons, literature tends to name this phenomenon "**Overflow Metabolism**" (Crabtree (1929), Deken (1966), Rocha (2003), Vemuri et al. (2006), Vemuri et al. (2007), Cappuyns et al. (2009)).

An optimization strategy relies on a control policy, which requires a dynamic model of the bioprocess. There exist different ways of modelling. The consideration of microscopic physical aspects (as, for instance, metabolic fluxes, see Stephanopoulos (1999)) leads to commonly called "white-box" models in opposition to "black-box" models where a mathematical map summarizes the process without real physical interpretation. Nevertheless, there remains a third way of modelling, generally describing macroscopic aspects of bioprocesses on the basis of components mass-balances equations, giving itself the name of "**Mechanistic Modelling**" (Bogaerts (1999), Bogaerts and Hanus (2002), Hulhoven et al. (2005), Bogaerts et al. (1999), Grosfils et al. (2007)).

Mechanistic models are widely used in bioprocess modelling mainly because of their lower degree of complexity (in comparison with microscopic models) allowing an easier control design. Moreover, when some key-components must be controlled but remain unmeasurable (generally for technical reasons as, for instance, the absence of specific probes), estimators can be build on the basis of mathematical mechanistic models and are therefore called "**Observers**" (Bogaerts and Vande Wouwer (2003)). The corresponding mathematical sensor is then called "**Software sensor**" in opposition to physical hardware sensors.

From this on, a control design must be chosen, taking the plant particularities into account:

- What is the plant optimum?
- Which state variables should be controlled?
- Are the controlled variables measurable?
- If not, is there a way to correctly estimate or observe them?
- Is a suboptimal solution more practical?
- Should the controller have a certain complexity degree? Is the complexity degree a source of limitation?

Unfortunately, accurate estimations of model parameters may be difficult to obtain. Measurement noise and parameter variations are classical sources of uncertainty which can severely degrade the predictive capability of a model with respect to the real process. Alternative solutions may be proposed in terms of state estimation as, for instance, the use of black-box models using more basic and "easy-to-get" signals while, from a control point of view, robust controller designs can be employed to overcome the problem of uncertainties.

In order to have a good practical knowledge about bioprocesses, it is sometimes preferable to extend its own experience until the actual construction of

a real culture plant. This work (and, therefore, its author) is intended to be as pragmatic and practical as possible, pointing out that theory which deals with bioprocess control becomes a must and an unavoidable source of knowledge when a full experimental feedback is taken into account. What a better feedback than its own practical experience?

The major contributions of this work are therefore:

- In state estimation:
  - An unusual and cheap way to estimate process key-variables using black-box models and especially **Artificial Neural Networks**, on the basis of industrial experimental data sets.
- In bioprocess control:
  - An original design of extremum-seeking control for fed-batch cultures.
  - Robust control designs using suboptimal but very efficient and practical strategies.
  - Experimental applications of a robust controller at laboratory and industrial scales.
- In bioprocess operation (experimental work):
  - Design, monitoring and control of an *Escherichia coli* (bacteria) laboratory pilot plant.

Outline

This work is divided in four parts.
Part one is composed of an introductive chapter describing microorganisms culture conditions and the phenomenon called **Overflow Metabolism**.
Part two is dedicated to general fed-batch culture monitoring and divided in 2 chapters. Chapter 2 presents a review of bioprocess modelling and observation, while chapter 3 contrasts two different techniques of state estimation illustrated by simulated and experimental results.
Part three reviews different existing control techniques and proposes original applications to fed-batch cultures of microorganisms. Chapter 4 is dedicated to an original design of extremum-seeking control, chapter 5 discusses the applicability of two linearizing control techniques and presents experimental applications of an improved RST controller to laboratory and industrial scale bioreactors.
Part four is composed of a chapter describing the experimental design and monitoring of a real bacteria pilot plant, and ends with a last chapter drawing general conclusions and perspectives of this work.

List of Publications

Book Chapters

L. Dewasme, Ph. Bogaerts, A. Vande Wouwer. **Monitoring of Bioprocesses: Mechanistic and Data-Driven Approaches** from the collective book, "Computational Intelligent Techniques for Bioprocess Modelling, Supervision and Control" in the Series *Studies in Computational Intelligence*, SCI 218, pp. 57-97, Springer-Verlag, Berlin Heidelberg, Germany, 2009.

Journal Papers

L. Dewasme, A. Richelle, P. Dehottay, P. Georges, M. Remy, Ph. Bogaerts, A. Vande Wouwer. **Linear Robust Control of *S. cerevisiae* Fed-batch Cultures at Different Scales**. *Biochemical Engineering Journal*, available on-line at doi:10.1016/j.bej.2009. 10.001 since 5 October 2009.

Proceedings

L. Dewasme, A. Vande Wouwer, S. Dessoy, P. Dehottay, X. Hulhoven, Ph. Bogaerts. **Experimental Study of Neural Network Software Sensors in Yeast and Bacteria Fed-batch Processes**. *10th IFAC Symposium on Computer Applications in Biotechnology (CAB)*, Cancun, Mexico, 2007.

L. Dewasme, F. Renard, A. Vande Wouwer. **Experimental Investigations of a Robust Control Strategy Applied to Cultures of *S. cerevisiae***. *European Control Conference (ECC)*, Kos, Greece, 2007.

L. Dewasme, A. Vande Wouwer. **Adaptive Extremum-Seeking Control Applied to Productivity Optimization in Yeast Fed-batch Cultures**. *17th World IFAC Congress*, Seoul, South Korea, 2008.

L. Dewasme, A. Vande Wouwer, M. Perrier. **Adaptive Extremum-seeking Control of Yeast Fed-batch Cultures**. *10th International Chemical and Biological Engineering Conference (CHEMPOR)*, Braga, Portugal, 2008.

L. Dewasme, X. Hulhoven, A. Vande Wouwer. **Scaling-up Control of Yeast Fed-batch Cultures**. *10th International Chemical and Biological Engineering Conference (CHEMPOR)*, Braga, Portugal, 2008.

L. Dewasme, A. Vande Wouwer, B. Srinivasan, M. Perrier. **Adaptive Extremum-seeking Control of Fed-batch Cultures of Microorganisms Exhibiting Overflow Metabolism**. *International Symposium on Advanced Control of Chemical Processes (ADCHEM)*, Istanbul, Turkey, 2009.

D. Coutinho, L. Dewasme, A. Vande Wouwer. **Robust Control of Yeast Fed-Batch Cultures to Productivity Enhancement**. *International Symposium on Advanced Control of Chemical Processes (ADCHEM)*, Istanbul, Turkey, 2009.

L. Dewasme, D. Coutinho, A. Vande Wouwer. **Linearizing Control of Yeast and Bacteria Fed-batch Cultures: A Comparison of Adaptive and Robust Strategies**. Accepted for the *7th International Conference on Informatics in Con-*

trol, Automation and Robotics (ICINCO), Madeira, Portugal, 2010.

L. O. Santos, L. Dewasme, A. Vande Wouwer. **Nonlinear Model predictive Control of Fed-batch Cultures of *E. coli*: Performance and Robustness Analysis**. Accepted for the *8th IFAC Symposium on Nonlinear Control Systems (NOLCOS)*, Bologna, Italy, 2010.

Conferences with Abstracts

L. Dewasme, A. Vande Wouwer, X. Hulhoven, Ph. Bogaerts. **NN-based Software Sensors in Yeast and Bacteria Fed-Batch Processes**. *26th Benelux Meeting on Systems and Control*, Lommel, Belgium, 2007.

L. Dewasme, F. Renard, A. Vande Wouwer. **Productivity Optimization of Cultures of *S. cerevisiae* through a Robust Control Strategy**. *26th Benelux Meeting on Systems and Control*, Lommel, Belgium, 2007.

L. Dewasme, F. Renard, A. Vande Wouwer. **Productivity Optimization of Yeast Fed-batch Cultures Using an Extremum-seeking Strategy**. *27th Benelux Meeting on Systems and Control*, Heeze, The Nederlands, 2008.

L. Dewasme, A. Vande Wouwer, B. Srinivasan, M. Perrier. **Adaptive Extremum-seeking Control of Fed-batch Cultures of Micro-organisms Exhibiting Overflow Metabolism**. *28th Benelux Meeting on Systems and Control*, Spa, Belgium, 2009.

L. Dewasme, D. Coutinho, A. Vande Wouwer. **Robust Linearizing Control of Yeast and Bacteria Fed-batch Cultures**. *29th Benelux Meeting on Systems and Control*, Heeze, The Nederlands, 2010.

Contents

I Overflow Metabolism **22**

1 Cultivating Microorganisms: Metabolism and Operating Modes **23**

1.1 Primary metabolism 23

1.2 Glycolysis and Krebs cycle: the oxidation pathway 25

1.3 Overflow metabolism: the fermentative pathway 26

1.4 Microorganisms culture modes of operation 27

1.5 Conclusion 31

II Monitoring of Fed-batch Cultures **33**

2 Mechanistic versus Black-box Approaches **34**

2.1 Introduction 34

2.2 A brief overview of bioprocess modelling 35

2.2.1 Mechanistic model of *S. cerevisiae* fed-batch cultures . . . 41

2.2.2 Mechanistic model of *E. coli* fed-batch cultures 43

2.3 Observability 45

2.4 Bioprocess state estimation 46

2.4.1 State observers 46

2.4.2 Classical state estimation method 47

2.5 Conclusion 63

3 Data-driven Approach **65**

3.1 Introduction 65

3.2 Input/output selection and measurements data analysis 65

3.3 Linear versus nonlinear black-box model 68

3.3.1 Linear strategy - Partial Least Squares regression (*PLS*) . 69
3.3.2 A nonlinear alternative: *PCA* and *Artificial Neural Network* (*ANN*) . . . 70
3.3.3 Comparison of the two approaches: Linear versus nonlinear modelling . . . 74
3.4 Monitoring of *E. coli* fed-batch cultures . . . 76
3.5 Monitoring of *S. cerevisiae* fed-batch cultures . . . 79
3.5.1 RBF-ANN software sensor potentiality in simultaneous estimations of different key-components . . . 80
3.6 Conclusion . . . 82

III Optimizing Productivity of Fed-batch Cultures 83

4 Real-Time Optimization of Fed-batch Cultures 84
4.1 Control objectives . . . 84
4.2 A brief review of real-time optimization . . . 86
4.2.1 Optimization criterion . . . 87
4.3 Model-free extremum-seeking . . . 89
4.3.1 Main principle . . . 89
4.3.2 Extremum-seeking through a bank of filters . . . 90
4.3.3 Extremum-seeking through a RLS scheme . . . 95
4.3.4 Controller design . . . 98
4.4 Simulation results . . . 99
4.4.1 Application of the bank of filters technique . . . 99
4.4.2 Application of the RLS technique . . . 102
4.5 Sensitivity analysis . . . 104
4.5.1 Sensitivity of the bank of filters strategy . . . 105
4.5.2 Sensitivity of the RLS strategy . . . 106
4.6 Model based vs model-free strategies . . . 108
4.6.1 An adaptive model-based extremum-seeking strategy . 108
4.6.2 A particular model-based extremum-seeking design for yeast fed-batch cultures . . . 111
4.7 Conclusion . . . 117

5 A Practical Suboptimal Strategy 119
5.1 Introduction . . . 119
5.2 Linearizing control: a comparison of adaptive and robust strategies . . . 120

5.2.1 A classical adaptive strategy 122
5.2.2 A robust strategy 123
5.2.3 Numerical results 125
5.2.4 Conclusion 127
5.3 Linear robust control 131
5.3.1 Model linearization 131
5.3.2 Controller design 134
5.4 Simulation results: application of the RST controller 136
5.4.1 Controller performance 136
5.4.2 Controller improvements considering a delayed output and probe dynamics 137
5.4.3 Robustness against measurement noise and model uncertainties 139
5.5 Experimental validations of the RST controller at different scales 142
5.5.1 Control interface 142
5.5.2 Laboratory-scale results 143
5.5.3 Industrial-scale results 147
5.6 Conclusion 149

IV Development of an Experimental Fed-batch Pilot Plant 150

6 Monitoring and Control of a Bacteria Fed-batch Pilot Plant 151
6.1 Materials and methods 151
6.1.1 Bioreactor setup 151
6.1.2 Media preparation and composition 152
6.1.3 Biomass measurement 152
6.1.4 Glucose measurement 153
6.1.5 Off-line acetate measurement 153
6.1.6 On-line acetate measurement 153
6.1.7 On-line gas measurement 158
6.2 Identification of a partial respiro-fermentative model 159
6.2.1 Model simplifications 159
6.2.2 Experimental scheme 160
6.3 Culture optimization 168
6.3.1 Simulation results 169
6.3.2 Experimental results 171

7 Perspectives and General Conclusions 174
7.1 Conclusions 174
7.2 Perspectives 175
7.2.1 Sensors 175
7.2.2 Control 176

List of Figures

1.1 Schematic view of the cells primary metabolism. 24
1.2 First part of the catabolism: Glycolysis and Krebs cycle 25
1.3 Sartorius Biostat B+ bioreactor. 29
1.4 Example of chemostat (courtesy of INRIA laboratories, Villefranche, France). 29
1.5 General schematic representation of the considered fed-batch bioreactor. 30

2.1 Evolution of 5 Monod laws where the saturation constant K_S is varying from $0,1\ g/l$ (in blue) to $0,5\ g/l$ (in green) 38
2.2 Evolution of an inhibited Monod law where the byproduct P is linearly increasing from 0 to $10\ g/l$ 38
2.3 Schematic representation of the simplified kinetic model using k_{os} as a global yield coefficient between the substrate and the oxygen consumptions 39
2.4 Illustration of Sonnleitner's bottleneck assumption for cells limited respiratory capacity 40
2.5 First simulated experiment 51
2.6 Reaction rates of the first simulated experiment 52
2.7 Second simulated experiment 52
2.8 Reaction rates of the second simulated experiment 53
2.9 Third simulated experiment 53
2.10 Reaction rates of the third simulated experiment 54
2.11 Fourth simulated experiment 55
2.12 Reaction rates of the fourth simulated experiment 55
2.13 Application of the *EKF* to the *E. Coli* model (2.6) using the parameter identification results 57

2.14 Application of the *EKF* to the *E. Coli* model (2.6) with bad initial estimations 58
2.15 Application of the *EKF* to the *E. Coli* model (2.6) with bad initial estimations - evolution of the "observability measure" 59
2.16 Application of the asymptotic observer to the *E. Coli* model (2.6) with bad initial estimations 60
2.17 Application of the asymptotic observer to the *E. Coli* model (2.6) with bad initial estimations - Evolution of the observation error on X 60
2.18 Application of the asymptotic observer to the *E. Coli* model (2.6) in order to estimate the substrate and the acetate concentrations 61

3.1 Typically available measurements 66
3.2 Example of a PCA performed on two normalized measured signals 67
3.3 Linear software sensor structure: PLS 69
3.4 Nonlinear software sensor structure: PCA and $RBF - ANN$ . . 72
3.5 Parameter identification scheme of the $RBF - ANN$ structure . 73
3.6 Biomass estimation in a culture of *S. cerevisiae* 74
3.7 Biomass estimation in $20 - l$ scale fed-batch culture of *E. coli* (expression of RP_1) 77
3.8 Biomass estimation in $150 - l$ scale fed-batch culture of *E. coli* (expression of RP_1) 77
3.9 Biomass estimation in $20 - l$ scale fed-batch culture of *E. coli* (expression of RP_2 when trained with RP_1) 78
3.10 Biomass estimation in $150 - l$ scale fed-batch culture of *E. coli* (expression of RP_2 when trained with RP_1) 78
3.11 Ethanol estimation in $15 - l$ scale fed-batch culture of *S. cerevisiae* 80
3.12 Glucose estimation in $15 - l$ scale fed-batch culture of *S. cerevisiae* 81
3.13 Simultaneous estimations of biomass, glucose and ethanol concentrations in $15 - l$ scale fed-batch culture of *S. cerevisiae* 81
3.14 Simultaneous estimations of key-components in $15 - l$ scale fed-batch culture of *S. cerevisiae* with PLS 82

4.1 Simulation of a fed-batch process controlled at a constant S_{sp} value 86
4.2 Critical substrate level (S_{crit}), separating the two regimes, as a function of the respiratory capacity (r_O) 88
4.3 Extremum-seeking scheme integrated to the bioreactor plant . . 89
4.4 Reaction rates and optimization criteria as a function of S 90
4.5 Extremum-seeking scheme with a bank of filters 91

4.6 DFT of the input signal y in a simulated case of yeast fed-batch culture. 93
4.7 DFT of the high-pass filter output signal $y - \eta$ in a simulated case of yeast fed-batch culture 93
4.8 DFT of the low-pass filter output signal ξ in a simulated case of yeast fed-batch culture 93
4.9 DFT of the integrator output signal $\hat{\theta} = S_{sp}$ in a simulated case of yeast fed-batch culture 94
4.10 Zoom on the optimum of Fig. 4.4 95
4.11 Extremum-seeking scheme with RLS 96
4.12 Biomass (X), substrate (S in blue and S_{sp} in red), and ethanol (E) concentrations evolutions when no respiratory capacity inhibition is considered 99
4.13 Convergence of the optimization criterion y to the optimum when no respiratory capacity inhibition is considered 100
4.14 Biomass (X), substrate (S in blue and S_{sp} in red), and ethanol (E) concentrations evolutions when inhibition is considered 101
4.15 Convergence of the optimization criterion y to the optimum when inhibition is considered 101
4.16 Biomass (X), substrate (S in blue and S_{sp} in red), and ethanol (E) concentrations evolutions with RLS when no inhibition is considered 102
4.17 Convergence of the optimization criterion y to the optimum with RLS when inhibition is not considered 103
4.18 Biomass (X), substrate (S in blue and S_{sp} in red), and ethanol (E) concentrations evolutions with RLS when inhibition is considered 103
4.19 Convergence of the optimization criterion y with RLS when inhibition is considered 104
4.20 Histogram of the productivity levels provided by 100 runs using the bank of filters extremum-seeking strategy with a random parameter uncertainty normally distributed with zero mean and 5% standard deviation 105
4.21 Biomass (X), substrate (S in blue and S_{sp} in red), ethanol (E) and oxygen (O) concentrations evolutions when applying noise on the input variables of the bank of filters strategy 106
4.22 Convergence of the optimization criterion y to the optimum when applying noise on the input variables of the bank of filters strategy. The arrows and ellispes indicate the extremum move due to the ethanol-inhibited respiratory capacity 107
4.23 Histogram of the productivity levels provided by 100 runs using the *RLS* extremum-seeking strategy with a random parameter uncertainty normally distributed with zero mean and 5% standard deviation 107

4.24 Biomass (X), substrate (S in blue and S_{sp} in red), ethanol (E) and oxygen (O) concentrations evolutions when applying noise on the input variables of the RLS strategy 108

4.25 Convergence of the optimization criterion y to the optimum when applying noise on the input variables of the RLS strategy. The arrows and ellipses indicate the extremum-zone move due to the ethanol-inhibited respiratory capacity 109

4.26 Haldane kinetic law 110

4.27 Simulation results of the model-based extremum-seeking strategy applied to microbial growth: biomass concentration, substrate concentration, feed flow rate and specific growth rate evolutions 112

4.28 Simulation results of the model-based extremum-seeking strategy applied to microbial growth: evolutions of the adapted parameters θ_μ, θ_S and θ_I 112

4.29 Linear approximation of $S_{crit} = f(r_O)$ 113

4.30 Substrate (S, S_{sp} and S_{crit}), biomass (X) and ethanol (E) concentrations evolutions. 116

4.31 Feed rate (F_{in}, α and ν parameters, and respiratory capacity (r_o) evolutions. 116

4.32 Representation of the algorithm convergence through the evolution of S_{crit} as a function of r_O 117

4.33 S_{crit} as a function of r_O (in green) and reduced approximation (in blue) 117

4.34 Biomass (X), Substrate (S, $\bar{S}_{crit} = S_{sp}$ and S_{crit}), and ethanol (E) concentrations evolutions 118

5.1 Linearizing control scheme. 121

5.2 Yeast cultures – ethanol concentration and feed rate when the controller is designed using a plain linearizing control approach (no adaptation and no robustification) in the presence of modeling errors. 126

5.3 Yeast cultures – biomass and ethanol concentrations, and feed rate – robust control strategy – results of 5 runs with random parameter variations and a noise standard deviation of ± 0.1 $[g/l]$. 127

5.4 Yeast cultures – ν adaptation and biomass concentration – adaptive control strategy – no measurement noise. 128

5.5 Yeast cultures – ethanol concentration and feed flow rate – adaptive control strategy – no measurement noise. 128

5.6 Yeast cultures – ν adaptation and biomass concentration – adaptive control strategy – noise standard deviation of ± 0.05 $[g/l]$. . 129

5.7 Yeast cultures – ethanol concentration and feed flow rate – adaptive control strategy – noise standard deviation of ± 0.05 $[g/l]$. . 129

5.8 Bacteria cultures – biomass and acetate concentrations, and feed rate – robust control strategy – results of 5 runs with random parameter variations and a noise standard deviation of $\pm 0.1\ [g/l]$.130

5.9 Bacteria cultures – ν adaptation and biomass concentration – adaptive control strategy – noise standard deviation of $\pm 0.05\ [g/l]$.130

5.10 Bacteria cultures – acetate concentration and feed flow rate – adaptive control strategy – noise standard deviation of $\pm 0.05\ [g/l]$.131

5.11 Closed-loop control of the bioreactor model. B, A, R, S and T are polynomials in backward-shift operator q^{-1} 135

5.12 Robust behavior analysis of the proposed controller in the Black-Nichols diagram 137

5.13 Simulation results with the RST controller defined in (5.39), (5.40), (5.42), (5.44) and (5.45) 138

5.14 Simulation results with the RST controller defined in (5.39), (5.40), (5.42), (5.44) and (5.45), when presented with a process incorporating a non-modeled delay of $12min$ 138

5.15 Robust behavior analysis of the improved controller in the Black-Nichols diagram 139

5.16 Simulation results with the RST controller defined in (5.39), (5.40), (5.42), (5.44) and (5.45), when presented with a process incorporating a modeled delay of $12min$ 140

5.17 Influence of the noise on the measured ethanol concentration with a non-robust RST controller $A_O = 1$ 141

5.18 Influence of the noise on the measured ethanol concentration with a robust RST controller $A_O = 1 - 0.7q^{-1}$ 142

5.19 Experimental results of the ethanol regulation applied to laboratory-scale fed-batch cultures of *S. cerevisiae*. Evolution of the ethanol probe measurement E around $E_{ref} = 1\ g/l$, the feed flow rate Fin expressed in % of the maximal pump speed and the parameter γ, image of the cells growth rate. 143

5.20 Experimental results of the ethanol regulation applied to laboratory-scale fed-batch cultures of *S. cerevisiae*. Evolution of the biomass, glucose and ethanol concentrations 144

5.21 Experimental results of the ethanol regulation applied to laboratory-scale fed-batch cultures of *S. cerevisiae*. Evolution of the growth rate μ and the parameter γ 145

5.22 Experimental results of the ethanol regulation applied to laboratory-scale fed-batch cultures of *S. cerevisiae*. Evolution of the dissolved oxygen (circles) and the stirrer speed (squares) respectively in percents of the phase saturation concentration and the maximum speed. 146

5.23 Experimental results of the ethanol regulation applied to laboratory-scale fed-batch cultures of *S. cerevisiae*. Evolution of the ethanol probe measurement E around $E_{ref} = 1\ g/l$ (when $E_0 > E_{ref}$), the feed flow rate F_{in} expressed in % of the maximal pump speed and the parameter γ, image of the cells growth rate 148

5.24 Experimental runs of industrial-scale fed-batch cultures of *S. cerevisiae* 148

5.25 Experimental results of the ethanol regulation applied to industrial-scale fed-batch cultures of *S. cerevisiae* 149

6.1 Calibration of the biomass concentration based on cell dry weight 152

6.2 Biomass measurements 153

6.3 Acetate measurement assembly based on conductivity 154

6.4 A-sep gas diffusion cell 155

6.5 Calibration of the acetate measurements using conductimetry . 156

6.6 Determination of the measurement system time constant 157

6.7 Validation of the acetate concentration estimation by conductimetry in real operating conditions 158

6.8 First semi fed-batch experiment 162

6.9 Second semi fed-batch experiment 163

6.10 Third semi fed-batch experiment 164

6.11 First direct validation of model (6.11) 166

6.12 Second direct validation of model (6.11) 167

6.13 Cross-validation of model (6.11) 167

6.14 Validation of model (6.16) 169

6.15 Simulation of the RST controller applied to *E.coli* model (6.11) with a large measurement delay (4 T_s). Evolution of the acetate concentration, the feed rate and γ 170

6.16 Simulation of the RST controller applied to *E.coli* model identified in (6.11) with a large measurement delay (4 T_s). Evolution of the biomass, glucose and acetate concentrations 170

6.17 Simulation of the RST controller applied to *E.coli* model (6.11) with a large measurement delay (4 T_s). Evolution of the corrected open-loop function in the Black-Nichols diagram 171

6.18 Experimental results of the RST controller applied to the *E.coli* pilot plant. First experiment 172

6.19 Experimental results of the RST controller applied to the *E.coli* pilot plant. Second experiment 173

6.20 Experimental results of the RST controller applied to the *E.coli* pilot plant. Third experiment 173

7.1 Off-line experimental results of the ANN applied to the *E.coli* pilot plant data. First direct validation 176
7.2 Off-line experimental results of the ANN applied to the *E.coli* pilot plant data. Second direct validation 177
7.3 Off-line experimental results of the ANN applied to the *E.coli* pilot plant data. Third direct validation 177
7.4 Off-line experimental results of the ANN applied to the *E.coli* pilot plant data. First cross-validation 178
7.5 Off-line experimental results of the ANN applied to the *E.coli* pilot plant data. Second cross-validation 178

List of Tables

2.1 Yield coefficients values of Sonnleitner and Käppeli *S. cerevisiae* model 42
2.2 Kinetic coefficients values of Sonnleitner and Käppeli *S. cerevisiae* model 42
2.3 Yield coefficients values of Rocha's *E.coli* model 44
2.4 Kinetic coefficients values of Rocha's *E.coli* model 44
2.5 Yield coefficients values of mechanistic model of *E. coli* 54
2.6 Kinetic coefficients values of mechanistic model of *E. coli* 56

3.1 Score variances and explanations for the specific example illustrated in Fig. 3.1 68
3.2 Loadings of the measurement signals (illustrated in Fig. 3.1) in each principal direction 68
3.3 Score explanations of 4 yeast fed-batch cultures data sets 75
3.4 Average error values for the different possible numbers of scores (inputs to the ANN) 75
3.5 Classification of the data sets in function of the recombinant protein, the scale and the type of validation 76

4.1 Variation of the estimation mean error with respect to the dither signal frequency ω (inhibition effect included in the model) . . 101
4.2 Variation of the estimation mean error with respect to the dither signal amplitude A (inhibition effect included in the model) . . 102
4.3 Variation of the estimation mean error with respect to the dither signal frequency ω (inhibition effect included in the model) . . 104
4.4 Variation of the estimation mean error with respect to the dither signal amplitude A (inhibition effect included in the model) . . 105
4.5 Tuning parameter values. 115

5.1 Order evaluation of each term of (5.30) 133
5.2 Parameters of the linear discrete-time model (5.38) 134

6.1 Cross-validation results of the second order regression law for the estimation of acetate concentration by conductivity 156
6.2 Off-line measurements of the first experiment. 162
6.3 Off-line measurements of the second experiment. 163
6.4 Off-line measurements of the third experiment. 164
6.5 Identified parameter values of model 6.11 168
6.6 Initial and operating conditions of the three experiments. 171

Part I

Overflow Metabolism

Chapter 1

Cultivating Microorganisms: Metabolism and Operating Modes

1.1 Primary metabolism

The finality of cells primary metabolism is to ensure their growth through the achievement of the cellular division. This primary metabolism is divided in 3 main parts (see Fig. 1.1): the catabolism (i.e., the energy production), the anabolism (i.e., energy consumption to produce amino-acids) and macromolecules synthesis (i.e., amino-acids and proteins production leading to cellular division).

In this work, our interest is focused on cells catabolism, presenting the following main pathways:

- The glycolysis which is a series of degradation reactions of the glucose (the main substrate) taking place in the cytoplasm and leading to a final product called pyruvate.
- The Krebs cycle, also called the tricarboxylic acids (*TCA*) cycle or citric acids cycle, which takes place inside the mitochondrions and uses pyruvate to product the cells energy units (Adenosine triphosphate or *ATP*) and reduced cofactors (typically $NADH$ and $FADH$).
- The electron transport, still taking place in mitochondrions and producing *ATP* from the reduced cofactors.
- The fermentative pathway which, in oxygen limitation, produces typical products like lactate or ethanol from pyruvate in the cytoplasm.

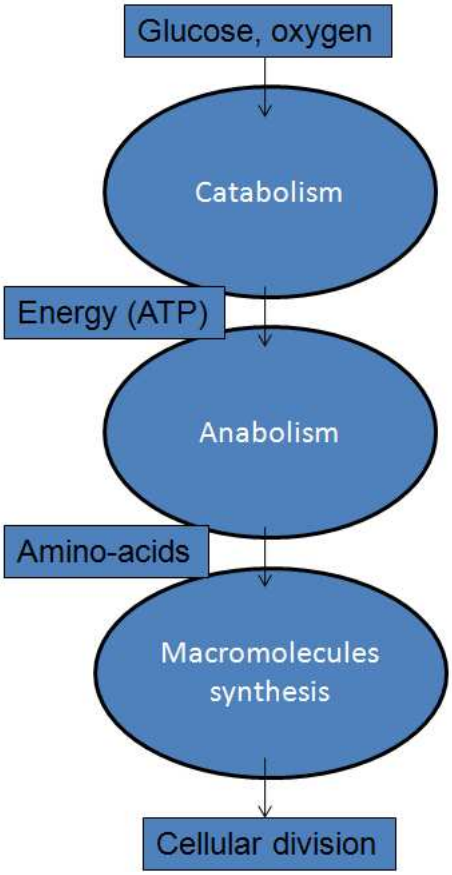

Figure 1.1: Schematic view of the cells primary metabolism.

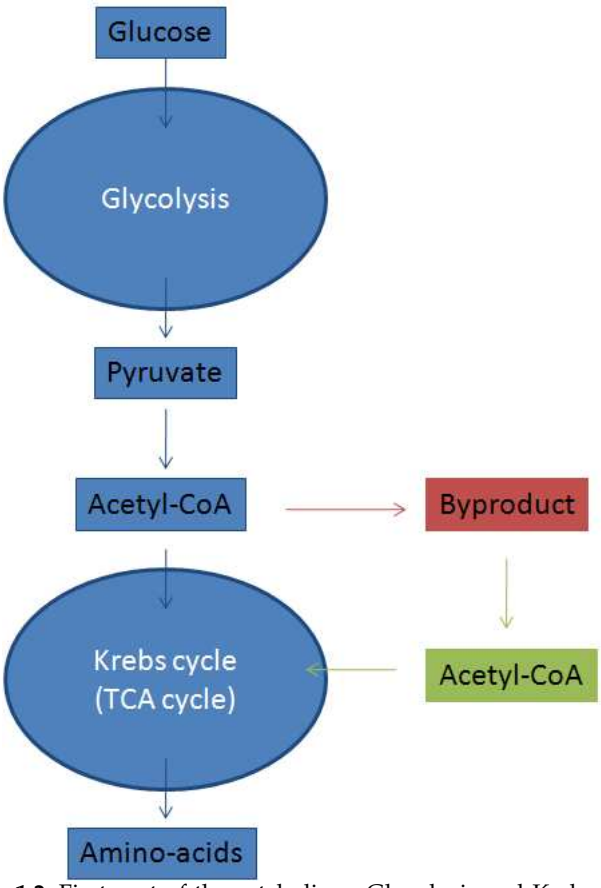

Figure 1.2: First part of the catabolism: Glycolysis and Krebs cycle. In blue and green: oxidation pathways respectively due to glucose and byproducts oxidation. In red: fermentative pathways.

1.2 Glycolysis and Krebs cycle: the oxidation pathway

The catabolism starts through the glycolysis reactions which allow the production of ATP and $NADH$ which will be used further on in the anabolism. The following pseudo-reaction summarizes the series of reactions represented in Fig. 1.2:

$$1\ Glucose + 2\ NAD^{+} \rightarrow 2\ ATP + 2\ NADH + 2\ Pyruvate \tag{1.1}$$

Fig. 1.2 shows that pyruvate is the source of the next metabolic pathway. Indeed, Acetyl-Coenzyme A ($Acetyl - CoA$) molecules previously synthesized from pyruvate molecules enter the Krebs cycle or TCA cycle and produce new ATP and $NADH$ molecules following the second pseudo-reaction:

$$1\,Acetyl-CoA+3\,NAD^{+}\rightarrow 3\,NADH+1\,ATP+1\,HS-CoA+2\,CO_2 \quad (1.2)$$

where $HS-CoA$ is the symbolic representation of the coenzyme A ($HS-$ is the "thiol" function which is the reactive part of the coenzyme A).

A general balance pseudo-reaction taking the previous reactions into account can be formulated as:

$$Glucose+O_2\rightarrow 6\,CO_2+6\,H_2O+Energy \quad (1.3)$$

Acetyl-CoA appears as the key-product in the realization of the Krebs cycle. When the cell oxidative capacity is not fully used by the glycolysis, if any other available byproduct is likely to be degraded to Acetyl-CoA, these new molecules will enter the Krebs cycle (1.2) until its capacity to accept new molecules is totally saturated (i.e., the oxidative capacity is completely exploited). A new pseudo-reaction comparable to (1.3) can be written for this particular case as:

$$Byproduct+O_2\rightarrow CO_2+H_2O \quad (1.4)$$

However, note that glycolysis is still the priority oxidation channel. Byproducts like ethanol, methanol, acetate, lactate, etc. only play a role of substitute substrate source.

1.3 Overflow metabolism: the fermentative pathway

Glucose is thus the main substrate source, necessary to the cells growth. From this on, it would be legitimate to imagine that more glucose, i.e. a higher glucose consumption rate, would increase the cells growth and that the more there is glucose, the better the growth is going to be. On the other hand, one can hardly imagine an infinitely high growth rate. Actually, another substrate is limiting the cells growth: the oxygen. The fermentation pathway classically happens when oxygen is limiting the substrate oxidation (however, note that we define this phenomenon as a simple limitation of oxygen and not real anaerobic conditions). In this case, Acetyl-CoA (synthesized from pyruvate) does not enter the Krebs cycle but follows an alternative pathway leading to byproducts synthesis like ethanol, acetate, lactate, formate, etc (see Fig. 1.2). Note that several micro-organisms have their own fermentative pathways. Several explanations of this switching mechanism have been proposed in the literature (like in Vemuri et al. (2007)) but this remains not well understood. The fermentative pathway can be summarized by the following pseudo-reaction:

$$Glucose+O_2\rightarrow 2\,byproduct+2\,CO_2+2\,ATP+2\,H_2O \quad (1.5)$$

This phenomenon testifies of the strong link existing between what is called glucose "overflow" or *Overflow Metabolism* or "short Crabtree effect" (Crabtree

(1929)), inducing a critical substrate concentration level or a critical substrate consumption rate, and the oxygen limitation.

However, this byproduct formation is generally inhibitive for the oxidative capacity of the cells, slowing down the growth (at low byproduct concentrations) or sometimes totally inhibiting it at high byproduct concentrations. As this byproduct formation is itself depending on the oxidative capacity of the cells, it is not difficult to understand that the cell environment is playing a key-role in the well-behave of a culture. The principal environment, where the cells are growing, is generally a tank filled with medium rich in vitamines, glucose, glycerol, different minerals or any other components necessary to a proper culture development. This special tank, in which cells culture are performed, is called a bioreactor. Starting from this initial equipment, different designs and modes of operation are possible and presented in the next section.

1.4 Microorganisms culture modes of operation

The design of a bioreactor and the choice of a culture mode of operation are difficult tasks as they are generally functions of the microorganism strain, the product of interest, or simply the available means. The culture conditions may radically change with the bioreactor size, shape (i.e., geometry), the presence of stirring impellers (existing in different types and generally used in order to homogeneously distribute the cells inside the bioreactor and provide a minimum of oxygenation) and their rotation speed, the injected air flow rate (also used for cell oxygenation) and its composition (O_2, CO_2, N_2), the temperature, the pH (acidity), the culture medium composition, the feed medium composition. On the basis of the previous remark, 3 main stirred-tank bioreactor culture modes are distinguished taking account of the culture broth inflows and outflows: batch, fed-batch and continuous.

The **batch** mode corresponds to a culture operated without feed broth addition or subtraction (note that sampling is not considered as a real subtraction): $\forall t,\ F_{in}(t) = F_{out}(t) = 0$ where t represents the culture time, F_{in} the inlet feed rate and F_{out} the outlet flow rate. In this case, cells are inoculated in the bioreactor vessel containing an initial quantity of medium which will not be altered by external feeding additions. Nevertheless, base or antifoam additions are sometimes necessary to preserve a good cellular (i.e., pH) or operating (i.e., foam can cause bioreactor overflows) environment. However, these additions are generally negligible in comparison with the medium volume so that the main feature of the batch mode is an assumed constant medium volume ($\forall t \geq t_0,\ V(t) = V(t_0)$ where t_0 is the initial time).

The **fed-batch** culture is operated when there is feed addition ($\forall t,\ F_{in} \geq 0$ where F_{in} can be seen as the resulting inlet feed rate if several flows are distinguished) generally all along the cells growth until the end of the process (i.e., when quality and quantity conditions are respected or when mechanical limitations as, for instance, the maximum volume, are reached). As no subtraction

is performed ($\forall t,\ F_{out}(t) = 0$), the main feature of this mode is a never decreasing medium volume ($\forall t \geq t_0,\ V(t) \geq V(t_0)$). An example of batch or fed-batch bioreactor is provided in Fig. 1.3.

Continuous reactor conditions imply cultures operated with continuous addition and subtraction flowing streams ($\forall t,\ F_{in}(t) \geq 0,\ F_{out}(t) \geq 0$, where, once again, $F_{out}(t)$ can be seen as the resulting outlet rate if several outputs are considered). So, adjusting the different inflow and outflow rates, no conclusion can be made on the instantaneous volume as if $F_{in}(t) > F_{out}(t),\ V(t^+) > V(t)$, where t^+ represents a small moment after t, while if $F_{in}(t) < F_{out}(t),\ V(t^+) < V(t)$ and if $F_{in}(t) = F_{out}(t),\ V(t^+) = V(t)$. A well-known example of continuous bioreactor is the chemostat (from "chemical static environment", see Fig. 1.4) in which the volume is generally kept constant by adapting the inflow and outflow rates. The main encountered problem is to find the optimal operating conditions (generally represented by a static continuous mode of operation, i.e., constant inflow and outflow rates values) maximizing the cells growth. Note that there exists a variation of the continuous mode: the perfused mode. In this particular case, the outflow rate is filtered (using an acoustic filter) in order to send the biomass back in the reactor so that only the medium is renewed.

Summarizing these last comments, the 3 bioreactor operating modes are, neglecting the time variable, mathematically expressed as:

- **Batch mode**: $F_{in} = F_{out} = 0$ and $V = Constant$.
- **Fed-batch mode**: $F_{in} \geq 0$, $F_{out} = 0$ and $V \geq V_0$ ($V_0 = V(t_0)$).
- **Continuous mode**: $F_{in} \geq 0$ and $F_{out} \geq 0$.

Continuous and fed-batch cultures are often performed for food and pharmaceutical applications. For instance, several experimental applications presented in this work will consider fed-batch bioprocesses aiming at maximizing the cell productivity for vaccines production.

A general fed-batch bioreactor scheme is represented in Fig. 1.5. From several measurements (not represented in the picture for the sake of clarity as they can be numerous) taken by different probes, a general monitoring control unit typically regulates important basic factors as, for instance, the dissolved oxygen in the liquid medium phase (also called "pO_2", a relative measurement of the oxygen concentration with respect to the concentration at saturation in the liquid phase and, for this reason, generally expressed in %) by controlling the motor imposing the rotational stirrer speed and, if necessary, by supplying air flow (which can be of different quality going from ambiant air to dry air or enriched in O_2) sent through the sparger situated at the bottom of the bioreactor vessel.

In most cases, pH is also regulated as cells strains can often grow in more or less neutral acidity conditions (i.e., between pH going from 5 to 8). To this end, base and acid tanks are prepared and connected to the bioreactor vessel. The monitoring unit receives the pH measurement (the availability of a pH probe is basic and included in any commercialized fermenter) and calculates, by means

Figure 1.3: Sartorius Biostat B+ bioreactor.

Figure 1.4: Example of chemostat (courtesy of INRIA laboratories, Villefranche, France).

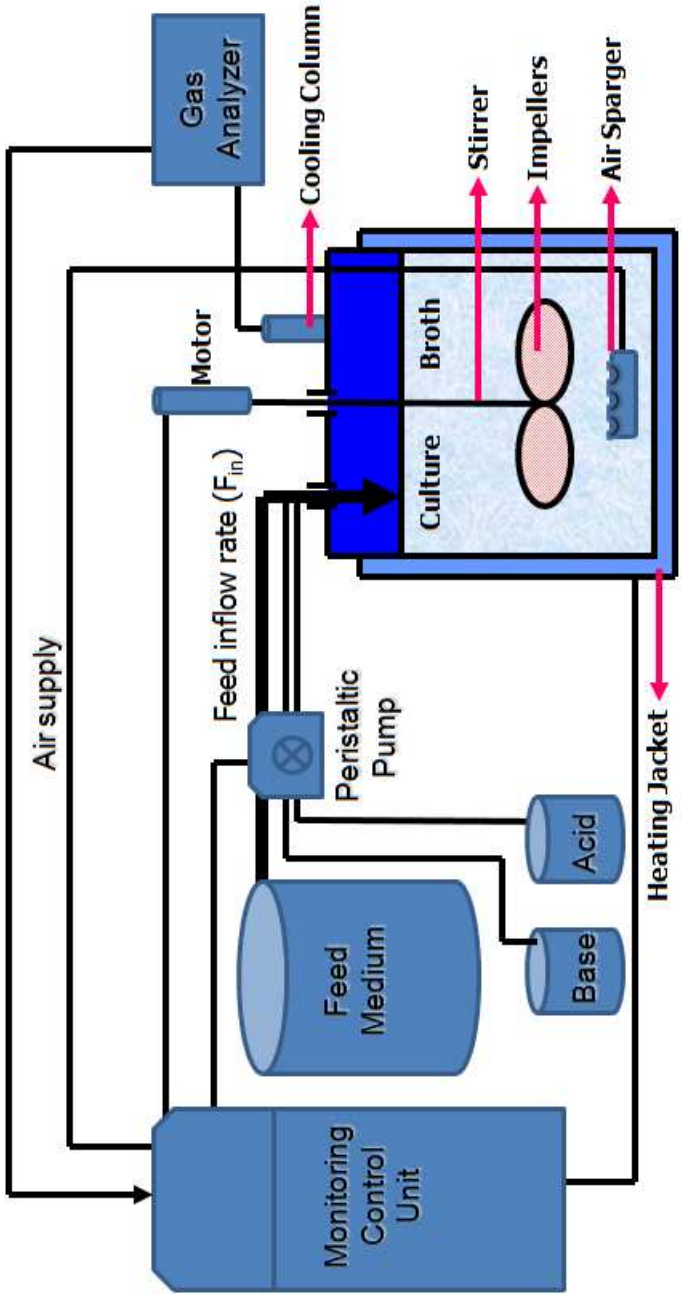

Figure 1.5: General schematic representation of the considered fed-batch bioreactor.

of a classical controller so as P, PI or PID, an input sent to the peristaltic pump in order to impose a certain base or acid flow rate. Only one pump is represented in Fig. 1.5, once again, for the sake of clarity but it is evident that each drawn tank requires its own pump. These pumps are also sometimes integrated to the monitoring control unit as in Fig. 1.3.

The temperature also needs to be controlled at a sufficient (and not too high) level. To this end, a heating jacket filled with heated water is controlled by the monitoring unit to regulate the bioreactor temperature (for instance bacteria and yeasts are growing between 30 and 37^0C).
In fed-batch bioprocesses, the inlet feed flow rate is controlled all along the culture time, requiring a new peristaltic pump in order to add the feed medium to the culture broth. Different control techniques can be used for this purpose. Open-loop techniques consist in imposing pre-registered pump inputs varying with time whatever the evolution of the operating conditions can be. Closed-loop techniques, on the other hand, use different measurements (or information about the operating conditions) to adapt the pump inputs, for instance, in order to maximize a specific feature so as biomass concentration or another metabolite concentration.

Finally, outlet gas coming from the vessel goes through a cooling column after which a gas analyzer (note that this equipment is more optional and expensive) can be placed to measure molar fraction of O_2 and CO_2 in the outlet gas. Combined to the molar fraction of O_2 and CO_2 in the inlet gas (air flow) sent into the culture medium through the sparger, a gas analyzer provides a convenient way to calculate the cells oxygen uptake rate (OUR) and carbon dioxide-exchange rate (CER). These latter signals are very informative about the culture operating conditions. Indeed, the respiratory quotient (RQ), which is the ratio of the produced carbon dioxide moles over the consumed oxygen moles, can indicate through which pathway the cells are evolving. For instance, if $RQ \leq 1$, the cells are evolving in the oxidative pathway (the oxidation is more important than the carbon dioxide production) while, if $RQ >> 1$, the cells are evolving through the fermentative pathway (the carbon dioxide production is far more important than the oxygen consumption).

1.5 Conclusion

Starting from cell primary metabolism, this section aims at reviewing how microorganisms host strains can be cultivated on the basis of a priori metabolic and heuristic knowledge. The attention is first focused on the cell catabolism and, more accurately, on the glycolysis, the Krebs cycle and the fermentation. On the basis of those principal metabolic pathways, consequent basic culture structure, equipment and classical operating conditions are presented, highlighting a special type of bioprocess widely used in different food or pharmaceutical industrial applications, which is called fed-batch culture. In the following chapters, the attention will be focused on all the means that are necessary to optimize fed-batch cultures of microorganisms exhibiting overflow

metabolism. Nevertheless, a mathematical optimization requires a mathematical expression of the purposes. A prior unavoidable step is then to mathematically describe the system. The next part of this work aims then at first macroscopically modelling the process.

Part II

Monitoring of Fed-batch Cultures

Chapter 2

Mechanistic versus Black-box Approaches

2.1 Introduction

Modelling of bioprocesses requires a complete monitoring of the fed-batch bioreactor plant described in chapter 1 but also off-line measurements of the model key macroscopic components (biomass, substrates, byproducts). Moreover, in order to optimize this bioprocess, several on-line measurements can be of a great interest. Monitoring of bioprocesses becomes then a particularly delicate task because on-line hardware sensors measuring the concentrations of the key culture components are expensive (in terms of acquisition and maintenance costs), are not always available (for instance, it is difficult to measure the low concentration levels of substrate in yeast or bacteria cultures, or to measure some product concentration such as acetate), and have stringent operational constraints (sterilization, sampling, etc). Hence, it is of significant interest to develop software sensors, which make use of available information sources, e.g., a mathematical process model and available on-line measurements. In this chapter, attention is focused on these soft sensor techniques, distinguishing mechanistic and data-driven modelling approaches. On the one hand, the mechanistic approach - which will appear as an "expensive" but "comprehensive" approach - is based on the existence of a physical (biological) process model and some measurements of the main macroscopic biological variables. Mechanistic models have a biological interpretation, which can be quite useful in understanding the process behaviour, and have a predictive capability which can compensate for the lack of frequent measurements of the biological variables. However this approach suffers from the difficulty and costs associated with the model derivation (which requires process knowledge, collection of experimental data, parameter estimation and model validation), and the costs associated with the sensors measuring the biological variables. On the other hand, the main advantage of data-driven techniques - which will appear as "cheap" but "limited" techniques - is their simplicity of implementa-

tion based on inexpensive, basic on-line measurement signals. However, data-driven representations usually lack biological interpretability and may have limited predictive capability (extrapolation in the absence of measurement information). This chapter is organized as follows. The next section is devoted to bioprocess modelling following a mechanistic approach. In the third section, bioprocess models and sensors are exploited to design software sensors. The classical extended Kalman filter and asymptotic observer are then dealt with.

2.2 A brief overview of bioprocess modelling

Any mathematical operation used to extract information from physical measurements can be viewed as a software sensor. State or parameter estimation is then conceivable once one can mathematically model the interactions within a system. The modelling objective is to establish (possibly simple) mathematical relations between explicative variables and explained ones. These relations are not exclusive. Different modelling approaches can be considered, depending on the process characteristics ((non)linearity, structural or parametric time variation, different time scales, stochastic nature of the measured signals), and the operating conditions (batch, fed-batch or continuous, repetitive, open-loop or closed-loop, small or large scale). In the following, two approaches are distinguished, i.e., the mechanistic approach which makes use of the available a priori knowledge about the process and experimental data to derive a physically (biologically) inspired model, and the data-driven approach which establishes a black-box representation of the process using the observation of input-output data. The mechanistic approach is the most popular bioprocess modelling technique. For optimization, monitoring and control purposes, this approach is usually macroscopic in essence (as opposed to microscopic approaches, which are based on a detailed analysis of the cell metabolic network), i.e., it makes use of the concept of a macroscopic reaction scheme involving a few reactants, products and catalysts considered as macroscopic entities. These reactions are represented as follows (Bastin and Dochain (1990)):

$$\sum_{i \in R_r} k_{i,r}\, \xi_i \quad \stackrel{\varphi_r}{\rightarrow} \quad \sum_{j \in P_r} k_{j,r}\, \xi_j \qquad\qquad r \in [1, \ldots, n_\varphi] \tag{2.1}$$

where

- $k_{i,r}$ and $k_{j,r}$ are the pseudo-stoichiometric coefficients or yield coefficients. They are negative when they relate to a reactant and positive when they relate to a product.
- φ_r is the reaction rate of reaction r.
- ξ_i is the i^{th} macroscopic component (N macroscopic components are considered).
- $R_r(P_r)$ is the set of reactants (products) in reaction r.
- n_φ is the number of reactions.

It is important to note that these macro-reactions do not satisfy elementary mass balances, hence the name pseudo-stoichiometric coefficients for $k_{i,r}$ and $k_{j,r}$. Using macroscopic mass balances, a general differential state-space model can be obtained as follows:

$$\frac{d\xi(t)}{dt} = K\varphi(\xi, t) - D(t)\xi(t) + F(t) - Q(t) \tag{2.2}$$

where

- ξ is the vector of concentrations of the macroscopic components.
- K is the pseudo-stoichiometric matrix.
- φ is the vector of reaction rates.
- D is the dilution rate ($D(t) = \frac{F_{in}(t)}{V(t)}$ where F_{in} is the inlet flow rate and V the medium volume).
- F is the vector of feed rate of selected components ($F_j = D(t)\xi_{in,j}(t)$ if the component is diluted in the feed stream, or $F_j = F_j(t)$ if the component is introduced in the culture in gaseous form) and Q is the vector of outflow rates of the considered components in gaseous form.

Establishing this kind of dynamic model requires the determination of a general reaction scheme, the selection of an appropriate kinetic model structure and a parameter identification procedure. The quality of the resulting model will of course depend on the information content of the experimental data at hand, as well as on an appropriate choice of the model structure. For these reasons, bioprocess models are usually uncertain (structural and parametric uncertainties), and while they offer an interesting insight into the system under consideration, they do not always predict the behaviour of the real system in a wide range of operating conditions. An appealing alternative to bypass the tedious identification steps required by the mechanistic approach is the data-driven black-box approach which considers the system only through the evolution of its inputs and outputs. A significant advantage of black-box models are their ability to exploit information contained in every available measurement. While the mechanistic approach requires off-line measurements of the component concentrations for model identification and on-line measurements of some of these components for state estimation, data-driven techniques allow information to be retrieved from signals as diverse as pH, dissolved oxygen, pressure, stirrer speed (signals which would be quite difficult to include in a reasonably complex mechanistic representation of the process). A classical example of black-box model is the function generated by an *Artificial Neural Network* (*ANN*), which defines a static map, model or function of the inputs. Different *ANN* architectures can be selected, differing in the number of layers and the type of nonlinear activation functions (sigmoids, Gaussian, etc). More details on these alternative structures will be given in the following.

In this chapter, we first consider a generic mechanistic model that would, in principle, allow the representation of the culture of different strains presenting an overflow metabolism (yeasts, bacteria, animal cells, etc).

This model describes therefore the cell catabolism through the following three main reactions, reminding the previously presented pseudo-reactions (1.3), (1.5) and (1.4):

$$\text{Substrate oxidation :} \quad k_{S1}\mathrm{S} + k_{O1}\,\mathrm{O} \overset{r_1 X}{\rightarrow} k_{X1}\,\mathrm{X} + k_{C1}\,\mathrm{C} \tag{2.3a}$$

$$\text{Substrate fermentation :} \quad k_{S2}\mathrm{S} + k_{O2}\,\mathrm{O} \overset{r_2 X}{\rightarrow} k_{X2}\,\mathrm{X} + k_{P2}\,\mathrm{P} + k_{C2}\,\mathrm{C} \tag{2.3b}$$

$$\text{Byproduct oxidation :} \quad k_{P3}\mathrm{P} + k_{O3}\,\mathrm{O} \overset{r_3 X}{\rightarrow} k_{X3}\,\mathrm{X} + k_{C3}\,\mathrm{C} \tag{2.3c}$$

where X, S, P, O and C are, respectively, the concentration in the culture medium of biomass, substrate (typically glucose), byproduct (i.e. ethanol or methanol in yeast cultures, acetate in bacteria cultures or lactate in animal cells cultures), dissolved oxygen and carbon dioxide. $k_{\xi i}$ ($i = 1, 2, 3$, $\xi = \mathrm{X}, \mathrm{S}, \mathrm{P}, \mathrm{O}, \mathrm{C}$) are the yield coefficients and r_1, r_2 and r_3 are the nonlinear specific consumption rates given by:

$$r_1 = \frac{\min\left(r_S, r_{S_{crit}}\right)}{k_{S1}} \tag{2.4a}$$

$$r_2 = \frac{\max\left(0, r_S - r_{S_{crit}}\right)}{k_{S2}} \tag{2.4b}$$

$$r_3 = \frac{\max\left(0, \frac{k_{os}(r_{S_{crit}} - r_S)}{k_{op}} \frac{P}{P+K_P}\right)}{k_{P3}} \tag{2.4c}$$

Note that these specific consumption rates are divided, for each reaction, by the corresponding substrate yield coefficient (k_{S1} and k_{S2} for the main substrate, as generally glucose, in the first two reactions and k_{P3} for the substitute carbon source, the byproduct, in the third reaction) in order to normalize the consumption mechanism with respect to the substrate source. For instance, the substrate consumption rate of the first reaction is $k_{S1}r_1$ which is equal to r_S or $r_{S_{crit}}$ if the oxidative capacity is completely exploited, while the corresponding biomass growth rate is $k_{X1}r_1$ which is respectively equal to $\frac{k_{X1}}{k_{S1}}r_S$ or $\frac{k_{X1}}{k_{S1}}r_{S_{crit}}$. The yield coefficient ratio $\frac{k_{X1}}{k_{S1}}$ illustrates this normalization of the growth rate with respect to the substrate consumption. The kinetic terms associated with the substrate consumption r_S and the critical substrate consumption $r_{S_{crit}}$ (function of the cells oxidative or respiratory capacity r_O) are given by:

$$r_S = \mu_S \frac{\mathrm{S}}{\mathrm{S} + K_S} \tag{2.5a}$$

$$r_{S_{crit}} = \frac{r_O}{k_{os}} = \frac{\mu_O}{k_{os}} \frac{\mathrm{O}}{\mathrm{O} + K_O} \frac{Ki_P}{Ki_P + P} \tag{2.5b}$$

These expressions take the classical form of Monod laws where μ_S and $\frac{\mu_O}{k_{os}}$ are the maximal values of, respectively, r_S and $r_{S_{crit}}$, K_S and K_O are the saturation constants of the corresponding expressions, and Ki_P is the inhibition constant. As a numerical exercise, Fig. 2.1 shows the evolution of such laws for instance, for a possible substrate consumption law where $\mu = \mu_S \frac{S}{S+K_S}$ with $\mu_S = 1\ g/g/h$ and $K_S = 0,1 - 0,2 - 0,3 - 0,4 - 0,5\ g/l$. Note that half the

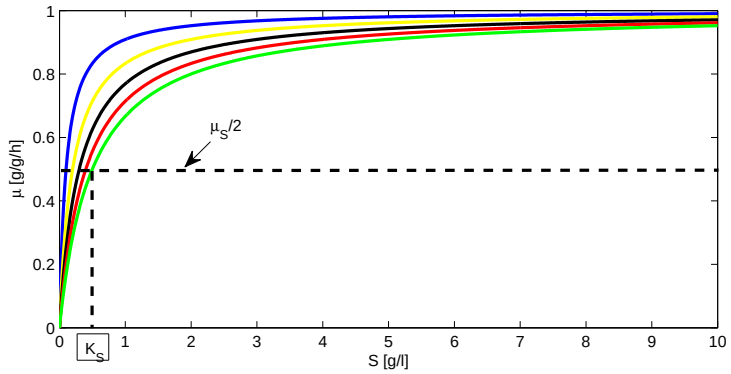

Figure 2.1: Evolution of 5 Monod laws where the saturation constant K_S is varying from $0,1\ g/l$ (in blue) to $0,5\ g/l$ (in green).

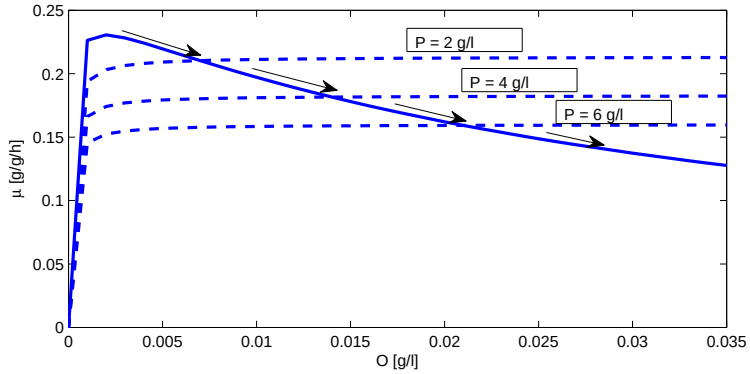

Figure 2.2: Evolution of an inhibited Monod law where the byproduct P is linearly increasing from 0 to 10 g/l. Dashed lines: evolutions of the same law for fixed concentrations of $P = 2 - 4 - 6\ g/l$.

maximum value of μ is reached when $S = K_S$. Of course, all these curves are converging to the same value: μ_S. Fig. 2.2 shows the evolution of another Monod expression like (2.5b) where inhibition of the oxidation capacity by another byproduct P is considered as in $\mu = \mu_O \frac{O}{O+K_O} \frac{Ki_P}{Ki_P+P}$ (as O is increasing from 0 to $0,007\ g/l$, P is linearly increasing from 0 to 10 g/l). This time, $\mu_O = 0.256\ g/g/h$, $K_O = 0.0001\ g/l$ and $Ki_P = 10\ g/l$. The dashed lines show the laws where $P = 2 - 4 - 6\ g/l$.

k_{os} and k_{op} represent the coefficients characterizing respectively the yield between the oxygen and substrate consumptions, and the yield between the byproduct and oxygen consumptions. In order to illustrate the role of k_{os} and k_{op}, consider for instance the oxygen consumed in the first two reactions (2.3a) and (2.3b). As shown by Fig. 2.3, a certain substrate quantity equal to $k_{S1}r_1$ is oxidized using an equivalent oxygen quantity $k_{O1}r_{O1} = k_{S1}r_1$ where r_{O1} can be seen as the oxygen consumption rate in the first reaction. In a similar way, the equivalent substrate and oxygen quantities required by the second reaction

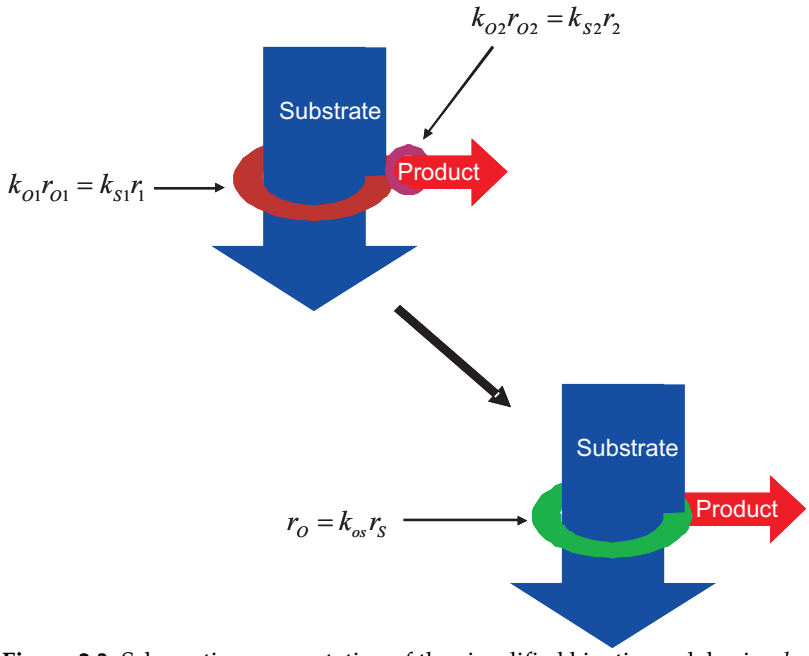

Figure 2.3: Schematic representation of the simplified kinetic model using k_{os} as a global yield coefficient between the substrate and the oxygen consumptions

are equal and respectively defined as $k_{S2}r_2$ and $k_{O2}r_{O2}$ where r_{O2} is the oxygen consumption rate in the second reaction. In order to globally compare r_S to r_O, a general yield coefficient k_{os} summarizing the general ratio between substrate and oxygen consumptions in the two reactions is chosen so that $r_O = k_{os}r_S$. The introduction of k_{op} in the model follows therefore the same reasoning for the byproduct. Nevertheless, note that for particular cells which don't need oxygen in (2.3b), k_{os} is sometimes summarized to k_{O1} and, for analogous reasons, k_{op} to k_{O3}. As the aim is to provide an as general as possible representation of overflow metabolism, this general writing is conserved in the following chapters.

Kinetic model (2.4) is based on Sonnleitner's bottleneck assumption (Sonnleitner and Käppeli (1986)) which was applied to a yeast strain *Saccharomyces cerevisiae* (Figure 2.4). Following sections 1.2 and 1.3, the cells are likely to change their metabolism because of their limited oxidative capacity (i.e., the limited capacity of the TCA cycle to accept Acetyl-CoA molecules as depicted in 1.3). When the substrate is in excess (concentration $S > S_{crit}$ and the glucose consumption rate $r_S > r_{S_{crit}}$), the cells produce a byproduct P through the fermentative pathway, and the culture is said in (respiro-) fermentative (RF) regime. On the other hand, when the substrate becomes limiting (concentration $S < S_{crit}$ and the glucose consumption rate $r_S < r_{S_{crit}}$), the available substrate (typically glucose), and possibly the byproduct P (as a substitute carbon source), if present in the culture medium, are oxidized. The culture is then said in respirative (R) regime.

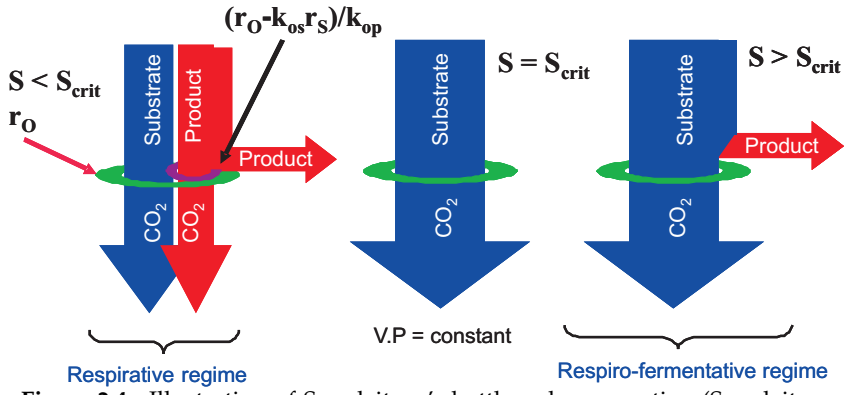

Figure 2.4: Illustration of Sonnleitner's bottleneck assumption (Sonnleitner and Käppeli (1986)) for cells limited respiratory capacity.

Following (2.2), component-wise mass balances give the following differential equations:

$$\frac{dX}{dt} = (k_{X1}r_1 + k_{X2}r_2 + k_{X3}r_3)X - DX \tag{2.6a}$$
$$\frac{dS}{dt} = -(k_{S1}r_1 + k_{S2}r_2)X + DS_{in} - DS \tag{2.6b}$$
$$\frac{dP}{dt} = (k_{P2}r_2 - k_{P3}r_3)X - DP \tag{2.6c}$$
$$\frac{dO}{dt} = -(k_{O1}r_1 + k_{O2}r_2 + k_{O3}r_3)X - DO + OTR \tag{2.6d}$$
$$\frac{dC}{dt} = (k_{C1}r_1 + k_{C2}r_2 + k_{C3}r_3)X - DC - CTR \tag{2.6e}$$
$$\frac{dV}{dt} = F_{in} \tag{2.6f}$$

where S_{in} is the substrate concentration in the feed, F_{in} is the inlet feed rate, V is the culture medium volume and D is the dilution rate ($D = F_{in}/V$). OTR and CTR represent respectively the oxygen transfer rate from the gas phase to the liquid phase and the carbon transfer rate from the liquid phase to the gas phase. Classical models of OTR and CTR are given by:

$$OTR = k_L a_O(O_{sat} - O) \tag{2.7a}$$
$$CTR = k_L a_C(C - C_{sat}) \tag{2.7b}$$

where $k_L a_O$ and $k_L a_C$ are respectively the volumetric transfer coefficients of O and C and, O_{sat} and C_{sat} are respectively the dissolved oxygen and carbon dioxide concentrations at saturation.

For illustration purposes, yeasts and bacteria model taken from the literature are compared to the general mechanistic model proposed in (2.4), (2.5) and (2.6) in the following sections 2.2.1 and 2.2.2.

2.2.1 Mechanistic model of *S. cerevisiae* fed-batch cultures

The yeast catabolism can be described using reaction scheme (2.3) where $k_{O2} = 0$, $k_{os} = k_{O1}$ and $k_{op} = k_{O3}$ (Renard (2006), Sonnleitner and Käppeli (1986)). Indeed, the fermentative pathway (1.5) often occurs, for yeast, independently of the oxygen conditions (i.e., in aerobic and anaerobic conditions) and produces ethanol as byproduct.

Summarizing these last remarks, reaction scheme (2.3) becomes:

$$\text{Substrate oxidation :} \quad \mathrm{S} + k_{O1}\,\mathrm{O} \overset{r_1 X}{\rightarrow} k_{X1}\,\mathrm{X} + k_{C1}\,\mathrm{C} \tag{2.8a}$$

$$\text{Substrate fermentation :} \ \mathrm{S} \overset{r_2 X}{\rightarrow} k_{X2}\,\mathrm{X} + k_{P2}\,\mathrm{E} + k_{C2}\,\mathrm{C} \tag{2.8b}$$

$$\text{Ethanol oxidation :} \quad \mathrm{E} + k_{O3}\,\mathrm{O} \overset{r_3 X}{\rightarrow} k_{X3}\,\mathrm{X} + k_{C3}\,\mathrm{C} \tag{2.8c}$$

where E is the ethanol concentration. The configuration of the yield coefficients is of course conventional. In the first two reactions (2.8a) and (2.8b), the yield coefficients are normalized with respect to the substrate concentration and in the third one (2.8c), they are normalized with respect to the ethanol concentration. Other formulations could be proposed as, for instance, a general normalization with respect to the biomass concentration, but this would require proportional modifications of the whole kinetic model.

The growth rates r_1, r_2 and r_3 are given by:

$$r_1 = \min\left(r_S, \frac{r_O}{k_{O1}}\right) \tag{2.9}$$

$$r_2 = \max\left(0, r_S - \frac{r_O}{k_{O1}}\right) \tag{2.10}$$

$$r_3 = \max\left(0, \frac{(r_O - k_{O1} r_S)}{k_{O3}} \frac{E}{E + K_E}\right) \tag{2.11}$$

where the respiratory or oxidative capacity $r_O = k_{O1}\, r_{S_{crit}}$ is given by:

$$r_O = \mu_O \frac{\mathrm{O}}{\mathrm{O} + K_O} \frac{Ki_E}{Ki_E + E} \tag{2.12}$$

All the yield and kinetic coefficients values are provided in Tables 2.1 and 2.2. Note that the original Sonnleitner and Käppeli's model does not take a possible inhibition of the respiratory capacity by ethanol into account. This assumption can indeed be acceptable when the ethanol concentration is relatively low (the order of Ki_E being $O(10^1)$), which is the case in many applications where the main objective is to limit the fermentation and to maximize the biomass growth. However, ethanol concentrations around 1 or 2 g/l can already significantly inhibit the cells growth (Pham (1999)) so that the consideration of an inhibitive term in (2.12) should not be neglected.

The differential system based on the main components mass balances is now:

Table 2.1: Yield coefficients values of Sonnleitner and Käppeli for *S. cerevisiae* model (Sonnleitner and Käppeli (1986))

Yield coefficients	Values	Units
k_{X1}	0,49	$g\ of\ X/g\ of\ S$
k_{X2}	0,05	$g\ of\ X/g\ of\ S$
k_{X3}	0,72	$g\ of\ X/g\ of\ E$
k_{S1}	1	
k_{S2}	1	
k_{P2}	0,48	$g\ of\ E/g\ of\ S$
k_{P3}	1	
k_{O1}	0,3968	$g\ of\ O_2/g\ of\ S$
k_{O2}	0	
k_{O3}	1,104	$g\ of\ O_2/g\ of\ E$
k_{C1}	0,5897	$g\ of\ CO_2/g\ of\ S$
k_{C2}	0,4621	$g\ of\ CO_2/g\ of\ S$
k_{C3}	0,6249	$g\ of\ CO_2/g\ of\ E$

Table 2.2: Kinetic coefficients values of Sonnleitner and Käppeli for the *S. cerevisiae* model (Sonnleitner and Käppeli (1986))

Kinetic coefficients	Values	Units
μ_O	0,256	$g\ of\ O_2/g\ of\ X\ /h$
μ_S	3,5	$g\ of\ S/g\ of\ X\ /h$
K_O	0,0001	$g\ of\ O_2/l$
K_S	0,1	$g\ of\ S/l$
K_E	0,1	$g\ of\ E/l$
Ki_E	10	$g\ of\ E/l$

$$\frac{dX}{dt} = (k_{X1}r_1 + k_{X2}r_2 + k_{X3}r_3)X - DX \tag{2.13a}$$

$$\frac{dS}{dt} = -(r_1 + r_2)X + DS_{in} - DS \tag{2.13b}$$

$$\frac{dE}{dt} = (k_{P2}r_2 - r_3)X - DE \tag{2.13c}$$

$$\frac{dO}{dt} = -(k_{O1}r_1 + k_{O3}r_3)X - DO + OTR \tag{2.13d}$$

$$\frac{dC}{dt} = (k_{C1}r_1 + k_{C2}r_2 + k_{C3}r_3)X - DC - CTR \tag{2.13e}$$

$$\frac{dV}{dt} = F_{in} \tag{2.13f}$$

All along this work, this *S. cerevisiae* model will be considered to represent yeast cultures.

2.2.2 Mechanistic model of *E. coli* fed-batch cultures

E.coli is a very important bacteria host strain abundantly used in biopharmaceutical industries for different purposes like vaccine production through biomass growth (Rocha (2003), Hulhoven et al. (2006)). The bacteria catabolism is just differing from the yeast's in the sense where acetate, the main byproduct of the fermentative pathway, can only be produced in the presence of oxygen (Rocha (2003)). If oxygen is missing, the fermentative pathway may occur but leads to formate or lactate productions.

In this case, k_{O2} is then different from 0 and the reaction scheme is as follows:

$$\text{Substrate oxidation :} \quad k_{S1}\,\mathrm{S} + k_{O1}\,\mathrm{O} \overset{r_1 X}{\rightarrow} \mathrm{X} + k_{C1}\,\mathrm{C} \tag{2.14a}$$

$$\text{Substrate fermentation :} \quad k_{S2}\,\mathrm{S} + k_{O2}\,\mathrm{O} \overset{r_2 X}{\rightarrow} \mathrm{X} + k_{P2}\,\mathrm{A} + k_{C2}\,\mathrm{C} \tag{2.14b}$$

$$\text{Ethanol oxidation :} \quad k_{P3}\,\mathrm{A} + k_{O3}\,\mathrm{O} \overset{r_3 X}{\rightarrow} \mathrm{X} + k_{C3}\,\mathrm{C} \tag{2.14c}$$

where A is the acetate concentration. Following the same remark as in section 2.2.1 for reaction scheme (2.8), it should be noticed that this new reaction scheme is entirely normalized with respect to biomass (following Rocha (2003)). Once again, a new kinetic coefficient normalization could be performed with a new yield coefficients formulation for comparison purposes but this is the matter of subsequent chapters.

The growth rates r_1, r_2 and r_3 are given by:

$$r_1 = \frac{\min\left(r_S, \frac{r_O}{k_{os}}\right)}{k_{S1}} \tag{2.15}$$

$$r_2 = \frac{\max\left(0, r_S - \frac{r_O}{k_{os}}\right)}{k_{S2}} \tag{2.16}$$

$$r_3 = \frac{\max\left(0, \frac{(r_O - r_S k_{os})}{k_{op}} \frac{A}{A+K_A}\right)}{k_{P3}} \tag{2.17}$$

where the respiratory or oxidative capacity $r_O = k_{os}\, r_{S_{crit}}$ is given by:

$$r_O = \mu_O \frac{\mathrm{O}}{\mathrm{O} + K_O} \frac{Ki_A}{Ki_A + A} \tag{2.18}$$

The differential system based on the main components mass balances is now:

Table 2.3: Yield coefficients values of Rocha's *E.coli* model (Rocha (2003))

Yield coefficients	Values	Units
k_{X1}	1	
k_{X2}	1	
k_{X3}	1	
k_{S1}	0,316	$g\ of\ S/g\ of\ X$
k_{S2}	0,04	$g\ of\ S/g\ of\ X$
k_{P2}	0,157	$g\ of\ A/g\ of\ X$
k_{P3}	0,432	$g\ of\ A/g\ of\ X$
k_{O1}	0,339	$g\ of\ O_2/g\ of\ X$
k_{O2}	0,471	$g\ of\ O_2/g\ of\ X$
k_{O3}	0,955	$g\ of\ O_2/g\ of\ X$
k_{C1}	0,405	$g\ of\ CO_2/g\ of\ X$
k_{C2}	0,754	$g\ of\ CO_2/g\ of\ X$
k_{C3}	1,03	$g\ of\ CO_2/g\ of\ X$
k_{os}	2,02	$g\ of\ O_2/g\ of\ X$
k_{op}	1,996	$g\ of\ O_2/g\ of\ X$

Table 2.4: Kinetic coefficients values of Rocha's *E.coli* model (Rocha (2003))

Kinetic coefficients	Values	Units
μ_O	0,7218	$g\ of\ O_2/g\ of\ X\ /h$
μ_S	1,832	$g\ of\ S/g\ of\ X\ /h$
K_O	0,0001	$g\ of\ O_2/l$
K_S	0,1428	$g\ of\ S/l$
K_A	0,5236	$g\ of\ A/l$
Ki_A	6,952	$g\ of\ A/l$

$$\frac{dX}{dt} = (r_1 + r_2 + r_3)X - DX \tag{2.19a}$$

$$\frac{dS}{dt} = -(k_{S1}r_1 + k_{S2}r_2)X + DS_{in} - DS \tag{2.19b}$$

$$\frac{dA}{dt} = (k_{P2}r_2 - k_{P3}r_3)X - DA \tag{2.19c}$$

$$\frac{dO}{dt} = -(k_{O1}r_1 + k_{O2}r_2 + k_{O3}r_3)X - DO + OTR \tag{2.19d}$$

$$\frac{dC}{dt} = (k_{C1}r_1 + k_{C2}r_2 + k_{C3}r_3)X - DC - CTR \tag{2.19e}$$

$$\frac{dV}{dt} = F_{in} \tag{2.19f}$$

2.3 Observability

Observability is a structural system property that relates to the possibility of estimating the system state on the basis of the available measurement information. If the system under consideration is nonlinear (which is almost always the case in bioprocess applications), observability depends on the system inputs and can be defined as:

Definition. A system is observable if

$$\begin{gathered}\forall t_0, \exists t_1 < \infty | y\left(t; t_0, \xi(0), u(t)\right) = y\left(t; t_0, \xi'(0), u(t)\right), \\ \forall u(t), t_0 < t < t_1 \Rightarrow \xi(0) = \xi'(0).\end{gathered} \tag{2.20}$$

In other words, a system is observable if two identical output trajectories y (function of time t, the initial states $\xi(0)$ and of the input command $u(t)$) over a given finite time horizon implies the equality of the initial states $\xi(0)$ and $\xi'(0)$.

A closer look at observability is provided by canonical observability forms as introduced in Gauthier and Kupka (1994) and Zeitz (1984), which allow the determination of observability for nonlinear systems (such as biological systems) if they can be put in the following form:

$$\begin{gathered}\forall i \in \{1, \ldots, q\}, x_i \in \Re^{n_i}, n_1 \geq n_2 \geq \ldots \geq n_q, \\ \textstyle\sum_{1 \leq i \leq q} n_i = n \\ \dot{x} = \begin{cases} \dot{x_1} = f_1(x_1, x_2) \\ \dot{x_2} = f_2(x_1, x_2, x_3) \\ \vdots \\ \dot{x_{q-1}} = f_{q-1}(x_1, \ldots, x_q) \\ \dot{x_q} = f_q(x_1, \ldots, x_q) \end{cases} \\ y = x_1\end{gathered} \tag{2.21}$$

where x is the state vector, y the vector of measured states, f_i a partition of the nonlinear state equations, q the number of partitions. (2.22) is also called a *Lower Hessenberg System*, i.e., a system where $\frac{\partial f_i}{\partial x_j} = 0$ with $j > i + 1$. This definition simply says that the Jacobian of $\dot{x}$ is a *Lower Hessenberg Matrix*. To assess if the system is observable, the bioprocess model (2.2) - or (2.6) in the particular case of bacteria culture - must be put in the form of (2.22) by defining an appropriate partition, and the following condition must be checked:

$$rank \frac{\partial f_i}{\partial x_{i+1}} = n_{i+1} \quad \forall i \in \{1, \ldots, q-1\} \tag{2.22}$$

(2.22) and (2.22) simply translate the fact that a partition of states x_{i+1} is only observable if any perturbation of these states propagates to partition x_i.

2.4 Bioprocess state estimation

2.4.1 State observers

Starting from (2.2), one defines a general state observer as follows:

$$\frac{d\hat{\xi}(t)}{dt} = K\varphi(\hat{\xi},t) - D(t)\hat{\xi}(t) + F(t) - Q(t) + \Omega(\hat{\xi})\,(y-\hat{y}) \tag{2.23a}$$

$$y = L\xi = \xi_1 \tag{2.23b}$$

where $\hat{\xi}$ is the on-line estimate of ξ, $\Omega(\hat{\xi})$ is the gain matrix depending on $\hat{\xi}$, L is an elementary matrix that selects the measured components of ξ (ξ_1 represents the vector of measured components). The only difference between (2.2) and (2.23a) lies in the additional term proportional to the observation error of the measured part of the state $(\xi_1 - \hat{\xi}_1)$. (2.23a) becomes identical to (2.2) when the estimation is perfect. It is now up to the user to find acceptable designs of $\Omega(\hat{\xi})$ such that a fast decay of the observation error is achieved. Omitting the dependence on time t for the sake of clarity, the observation error dynamics corresponds to:

$$\frac{d\left(\xi-\hat{\xi}\right)}{dt} = K\left(\varphi(\xi) - \varphi(\hat{\xi})\right)\right) - D\left(\xi-\hat{\xi}\right) + \Omega(\hat{\xi})L\left(\xi-\hat{\xi}\right) \tag{2.24}$$

where $\left(\xi-\hat{\xi}\right) = 0$ appears as an equilibrium point. A practical way to design $\Omega(\hat{\xi})$ is to consider the linearized approximation of model (2.24) as follows:

$$\frac{d\left(\xi-\hat{\xi}\right)}{dt} = \left(A(\hat{\xi}) - \Omega(\hat{\xi})L\right)\left(\xi-\hat{\xi}\right) \tag{2.25}$$

with

$$A(\hat{\xi}) = K\left[\frac{\partial\varphi(\xi)}{\partial\xi}\right]_{\xi=\hat{\xi}} - DI_N \tag{2.26}$$

where I_N is the square identity matrix of dimension NxN. The problem is then reduced to an arbitrary choice of the eigenvalues of the matrix $\left(A(\hat{\xi}) - \Omega(\hat{\xi})L\right)$ fixing the rate of convergence of the observation error to zero. The convergence is ensured if (Vidyasagar (1978)):

- $\left(A(\hat{\xi}) - \Omega(\hat{\xi})L\right)$ is continuously differentiable,
- $\left(A(\hat{\xi}) - \Omega(\hat{\xi})L\right)$ is bounded,
- The real parts of all the eigenvalues of $\left(A(\hat{\xi}) - \Omega(\hat{\xi})L\right)$ are negative.

The solution of (2.25) takes then an exponential form so that the convergence is said to be exponential. From this, it follows that the system is exponentially observable and (2.23a) is an exponential observer. Sometimes, the design of (2.25)

does not allow a free assignment of the eigenvalues (i.e., a free design of the dynamics) but leads to a system converging asymptotically to the equilibrium point $\left(\xi - \hat{\xi}\right) = 0$. Actually, this means that the system (2.25) is still converging but not over a finite time. Such observers are called asymptotic observers.

In the next sections, a few popular state estimation techniques are presented (for more details and techniques see Bastin and Dochain (1990), Bogaerts and Vande Wouwer (2003) and Goffaux and Vande Wouwer (2005)). Their application to a mechanistic model of culture of micro-organisms with an overflow metabolism (e.g. yeasts or bacteria cultures) is investigated in order to discuss the advantages and also the possible limitations of general mechanistic model-based observers.

2.4.2 Classical state estimation method

An Example of Exponential Observer: the Kalman Filter

The Kalman filter (Gelb (1974)), which is by far the most popular state estimation technique used for bioprocess monitoring, is an exponential observer that minimizes the variance of the estimation error. It was first developed in a linear framework before being extended to the nonlinear case. Consider the following nonlinear system derived from (2.2):

$$\frac{d\xi_1}{dt} = K_1\varphi(\xi) - D\xi + D\xi_1^{in} + \eta_1(t); \quad \xi_1(0) = \xi_{1,0} \tag{2.27a}$$

$$\frac{d\xi_2}{dt} = K_2\varphi(\xi) - D\xi + D\xi_2^{in} + \eta_2(t); \quad \xi_2(0) = \xi_{2,0} \tag{2.27b}$$

$$y = L\xi + \epsilon(t) = \xi_1 + \epsilon(t) \tag{2.27c}$$

where ξ_1 represents the vector of measured states while ξ_2 represents the unmeasured states that complete the partition of ξ. ξ^{in} is the vector of states contained in the inlet flows. $\epsilon(t)$ is the measurement noise, whereas $\eta(t) = [\eta_1(t)\ \eta_2(t)]^T$ is the model noise (both assumed white and normally distributed with zero mean). Assuming that this system is exponentially observable, the *Extended Kalman Filter* (*EKF*) is based on a first-order linearization of the process model along the estimated trajectory

$$\frac{d\hat{\xi}}{dt} = K\varphi(\hat{\xi}) - D\hat{\xi} + D\xi^{in} + \Omega(\hat{\xi})(y - L\hat{\xi}); \quad \hat{\xi}(0) = \hat{\xi}_0 \tag{2.28a}$$

$$\frac{dP}{dt} = A(\hat{\xi})P + PA(\hat{\xi})^T - PL^T R_\epsilon^{-1} LP + R_\eta; \quad P(0) = P_0 \tag{2.28b}$$

$$\Omega(\hat{\xi}) = PL^T R_\epsilon^{-1} \tag{2.28c}$$

where Ω is the observer error gain, P is the solution of the *Riccati equation* (2.28b), R_η is the covariance matrix of the state (or model) noise, R_ϵ is the covariance matrix of the measurement noise and A is the linear transition matrix

computed along the estimated trajectory. The previous formulation (2.28) provides time-continuous estimations from time-continuous measurements. In practice however, concentrations of the main species are generally measured at discrete times only and with relatively low sampling frequencies (the measurements are sometimes collected at different rates, i.e., resulting in an asynchronous measurement configuration). The corresponding formulation is the *continuous-discrete EKF* where continuous estimations are provided from discrete measurements

$$y = L\xi(t_k) + \epsilon(t_k) \tag{2.29}$$

where $\epsilon(t_k)$, the measurement noise at time t_k is a normally distributed white noise with zero mean and covariance matrix $R_\epsilon(t_k)$.

The algorithm now proceeds in two steps: a prediction step (corresponding to the time period between two measurement times) and a correction step occurring each time a new measurement is available. The first step (prediction between t_k and t_{k+1}) corresponds to:

$$\frac{d\xi(t)}{dt} = K\varphi(\xi(t), t) - D\xi(t) + D\xi^{in}; \quad \xi(t_k) = \xi(t_k^+), t_k^+ \leq t < t_{k+1}^- \tag{2.30a}$$

$$\frac{dP(t)}{dt} = A(\xi(t))P(t) + P(t)A(\xi(t))^T + R_\eta; \quad P(t_k) = P(t_k^+), t_k^+ \leq t < t_{k+1}^- \tag{2.30b}$$

The correction step occurring at time t_{k+1} corresponds to:

$$\Omega(\xi(t_{k+1})) = P(t_{k+1}^-)L^T \left[LP(t_{k+1}^-)L^T + R_\epsilon(t_{k+1})\right]^{-1} \tag{2.31a}$$

$$\xi(t_{k+1}^+) = \xi(t_{k+1}^-) + \Omega(\xi(t_{k+1})) \left(y(t_{k+1}) - L\xi(t_{k+1}^-)\right) \tag{2.31b}$$

$$P(t_{k+1}^+) = P(t_{k+1}^-) - \Omega(\xi(t_{k+1}))LP(t_{k+1}^-) \tag{2.31c}$$

with t_{k+1}^- and t_{k+1}^+ characterizing respectively the values before and after correction. The Kalman filter is an optimal exponential observer in the sense that it minimizes asymptotically the mean square estimation error. Unfortunately, the extension to nonlinear systems is realized through a linearization along the estimated trajectory. The *EKF* is no longer optimal and can sometimes lead to biased estimates or, in the worst case of bad initial conditions, to convergence problems. The Kalman filter, as well as most of the exponential observers, relies on the availability of an accurate process model. This prerequisite is far from being satisfied in many bioprocess applications, where the models are usually uncertain. It is therefore of interest to look for more robust alternatives, which justifies the following approach.

Asymptotic Observer

Even if uncertainties are always hanging over all the parameters of a bioprocess model, their impact is more concentrated on the kinetic terms which are generally badly known. In the context of bioprocess applications, the observers that allow to asymptotically reconstruct unknown states when the kinetics are unknown are called *asymptotic observers*. The asymptotic convergence requires that the yield coefficients are known and the number of measured state variables is equal to or larger than the rank p of the yield matrix K (Bastin and Dochain (1990)).

A partition of the yield matrix (K_a, K_b) is first selected so that the (pxM) submatrix K_a is a full row rank submatrix (i.e., so that the rank of K_a is equal to p). Then, there exists a state transformation

$$z = C\xi_a + \xi_b \tag{2.32}$$

where the $(N-p)xp$ matrix C is the unique solution of

$$CK_a + K_b = 0 \tag{2.33}$$

so that

$$\frac{dz}{dt} = -Dz + C(F_a - Q_a) + (F_b - Q_b) \tag{2.34}$$

Under these conditions, the dynamics of z is independant of the kinetics. If a partition induced by the measured and unmeasured states is now considered, i.e., K_1, K_2 corresponding to (ξ_1,ξ_2), the auxiliary vector z can be defined accordingly

$$z = A_1\xi_1 + A_2\xi_2 \tag{2.35}$$

with appropriate definitions of the $(N-p)xq$ matrix A_1 and $(N-p)x(N-q)$ matrix A_2. In this latter case, the asymptotic observer structure is as follows:

$$\frac{d\hat{z}}{dt} = -D\hat{z} + A_1(F_1 - Q_1) + A_2(F_2 - Q_2) \tag{2.36a}$$

$$\hat{\xi_2} = A_2^+(\hat{z} - A_1\xi_1) \tag{2.36b}$$

where A_2^+ is a left pseudo inverse of A_2. The convergence of such an observer is unfortunately ensured only if the dilution rate is persistently exciting. This is confirmed by the dynamics of the estimation error:

$$\frac{d(\xi_2 - \hat{\xi_2})}{dt} = -D(\xi_2 - \hat{\xi_2}) \tag{2.37}$$

Hence, in a bioprocess monitoring application, the convergence is ensured only if the culture is operated in fed-batch or continuous conditions while, for batch

processes, any initial error will last over the batch duration. The main drawback of this class of observer is therefore that the convergence is completely determined by the operating conditions.

Application of Observers to an Identified Mechanistic Model of E. coli

A simplified version of the *E. coli* model of section 2.2.2 (i.e., considering $k_{os} = k_{O1}$, $k_{O2} = 0$ and $k_{op} = k_{P3}$) is now used in an illustrative example based on simulated data. The following simulations are therefore only aiming at showing the efficiency of the identification procedures from a mathematical point of view. However, from a biological point of view, it should be reminded that $k_{O2} = 0$ is not realistic for *E. coli* as acetate cannot be produced without oxygen (in anaerobic conditions, *E. coli* produces lactate instead of acetate).

First an experimental field (a set of experiments) is defined in order to estimate the model parameters, and assess model accuracy. Rigorously, the choice of this experimental field should rely on optimal experiment design as developed in Bernaerts et al. (2005) and Versyck et al. (1999). This theory is however not always applicable in practical situations, as it requires input signals that are difficult to achieve in practice (very high or very low concentrations, for instance), or even sometimes not feasible due to the complexity of the model. Here, operating conditions are chosen based on process knowledge, so as to highlight the influence of the several parameters.

The identification procedure is subdivided into two steps, the first one being devoted to the pseudo-stoichiometry (or yield coefficients), and the second one to the kinetics, through a decoupling technique based on a state transformation (analog to (2.32) used in the asymptotic observer; see Bastin and Dochain (1990) for more details). The system described by expressions (2.32) and (2.34) is nonlinearly parametrized by the yield coefficients k_i but linearly parametrized by the elements of matrix C. Combinations of the yield coefficients become linearly identifiable independently of the kinetics by a linear regression technique and each k_i value can be recovered following (2.33) as long as K_a is full rank and invertible. This identification procedure is called $C - identifiability$ (from matrix C in (2.32)).

A necessary and sufficient condition of C-identifiability is (Chen and Bastin (1996)):

k^j being the vector of unknown yield coefficients of the j^{th} column of K, k^j is C-identifiable if and only if there exists at least one non singular partition of $K = \begin{bmatrix} K_a \\ K_b \end{bmatrix}$ where K_a is full rank and does not contain any element of k^j.

For being applicable, this procedure requires that the reaction scheme is C-identifiable, which is not the case of the reaction scheme (2.14), even with $k_{O2} = 0$. To alleviate this problem, it is required to introduce three additional constraints between the stoichiometric coefficients (one by reaction, which are indeed easy to determine as the ratio of consumed and produced moles of certain components like oxygen-carbon (2.3a), acetate-carbon (2.3b) and again oxygen-carbon (2.3c), are known). In the first step, the experimental field con-

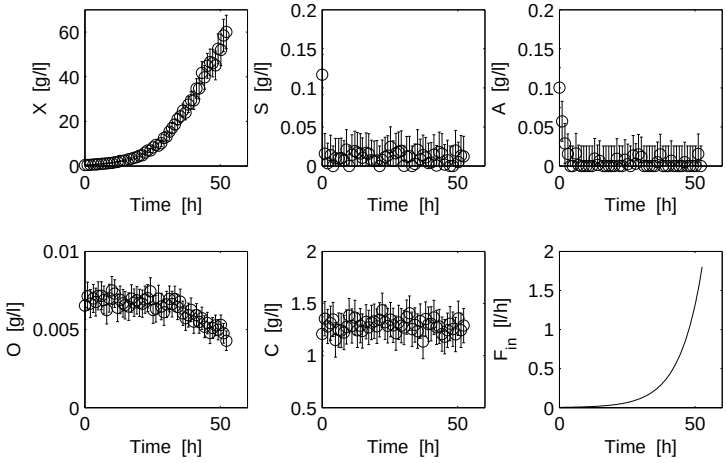

Figure 2.5: First simulated experiment - A batch phase is achieved until S, the substrate concentration (initially chosen around $0.1g/l$), decreases to $0.01g/l$. Then, a fed-batch phase starts and the feed flow rate is calculated so that S is maintained at $0.01g/l$. The culture ends when the feed medium (its capacity is estimated to $15kg$) is exhausted. The cells evolve most of the time in the respirative regime

sists of three simulations. The first one forces the cells to evolve, most of the time, through the respirative pathway (see Figs. 2.5, 2.6). The second one does as well through the respiro-fermentative pathway (see Figs. 2.7, 2.8). However, it should be noticed that such acetate levels (see 2.7) are generally not biologically acceptable and lead to biomass death. In realistic conditions, the maximum feed rate should be chosen lower. The third experiment reproduces operating conditions in the neighbourhood of the optimum (see Figs. 2.9 and 2.10). It is important to notice that white noise is added to the samples in order to provide realistic measurement conditions (with zero mean and a relative standard deviation of 5 %). The sampling period is chosen equal to 1 hour.

Table 2.5 gives values of the yield coefficients found in the literature and already exposed in section 2.2.2 (considered here as "theoretical" values) and the result of the first identification step based on the previously-defined experimental field. This procedure consists in an identification of the stoichiometric coefficients independently of the kinetics (Bastin and Dochain (1990)).

The maximum deviation from a reference value is 6.9% and the mean value of the error is 3.2%. The results of the identification of the yield coefficients can therefore be considered as quite good. Based on these results, the second identification step is carried out for the kinetic parameters (see Figs. 2.11 and 2.12). Instead of using the data coming from the previous experiments, a fourth one is achieved in order to put in evidence the influence of some kinetic parameters. For instance, an acetate concentration evolving between 0 and $3g/l$ provides a better identification of Ki_A and K_A.

The kinetic values are listed in Table 2.6. In contrast with the previous step, the

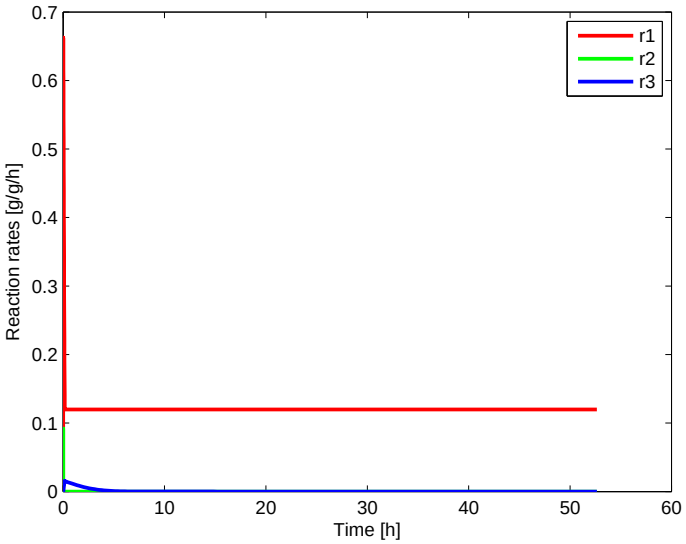

Figure 2.6: First simulated experiment - Reaction rates

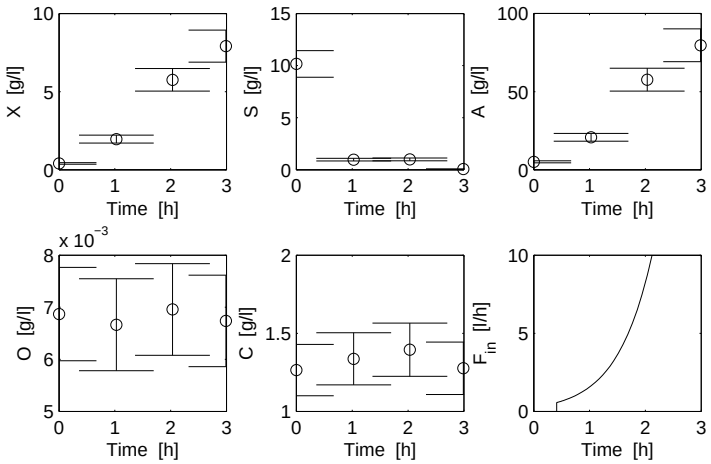

Figure 2.7: Second simulated experiment - A batch phase is achieved until S, initialized around $10g/l$, decreases to $1g/l$. Then, a fed-batch phase starts and the feed flow rate is calculated so that S is maintained at $1g/l$. The culture ends when the feed medium (its capacity is estimated to $15kg$) is exhausted. Note that the feed flow rate saturates at $10l/h$. This value is considered as the maximum pump speed. After 2 hours, the feed flow rate saturates and the injected quantity of substrate becomes insufficient to maintain S at $1g/l$

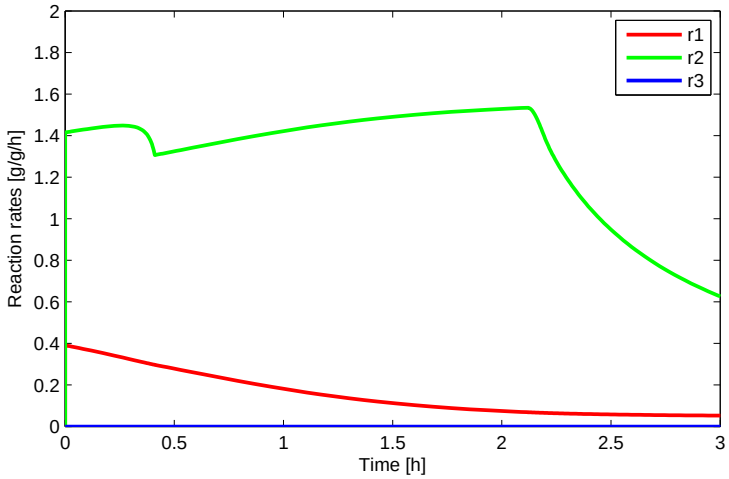

Figure 2.8: Second simulated experiment - Reaction rates

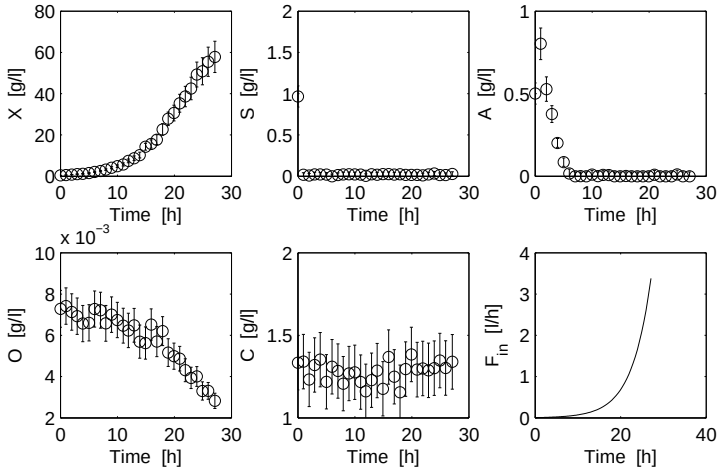

Figure 2.9: Third simulated experiment - A batch phase is achieved until S, the substrate concentration (initially chosen around $1 g/l$), decreases to $0.02 g/l$. Then, a fed-batch phase starts and the feed flow rate is calculated so that S is maintained at $0.02 g/l$. The culture ends when the feed medium (its capacity is estimated to $15 kg$) is exhausted. The cells evolve in the neighbourhood of the optimal operating conditions. Note how fast the cells grow as compared to the previous experiments (the same concentration is reached within 25 hours instead of more than 50)

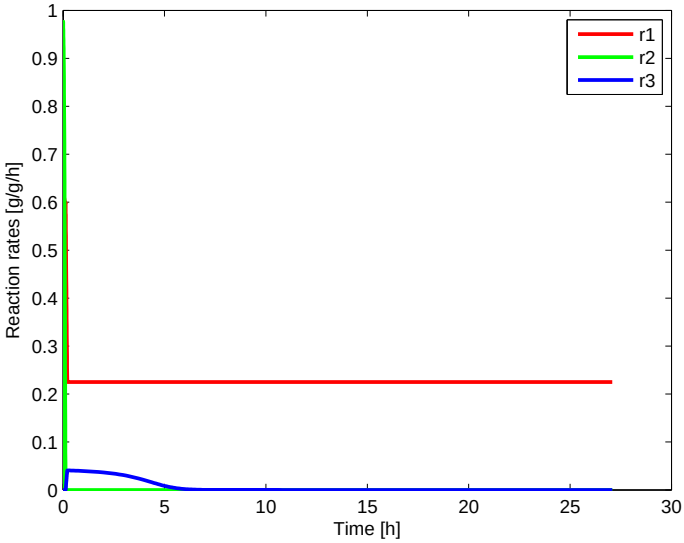

Figure 2.10: Third simulated experiment - Reaction rates

Table 2.5: Yield coefficients values of mechanistic model of *E. coli*

Yield coefficient	Exact value	Identified value
k_{S1}	3.164	3.211
k_{S2}	25.22	23.911
k_{P2}	10.9	10.247
k_{P3}	6.382	6.35
k_{O1}	1.074	1.088
k_{O3}	6.098	6.207
k_{C1}	1.283	1.3
k_{C2}	19.1	17.872
k_{C3}	6.576	6.694

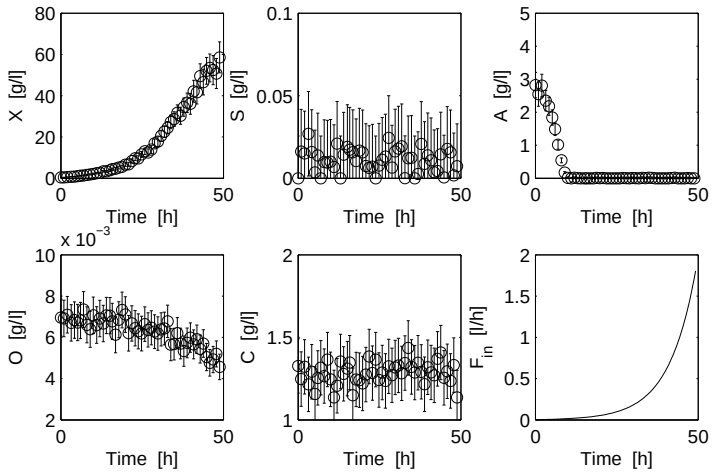

Figure 2.11: Fourth simulated experiment - A fed-batch phase is directly started and the feed flow rate is calculated so that S is maintained at $0.01 g/l$ (i.e., as low as possible). The culture ends when the feed medium (its capacity is estimated to $15 kg$) is exhausted or if the sum of the reaction rates is close to zero. The cells evolve most of the time in the respirative regime

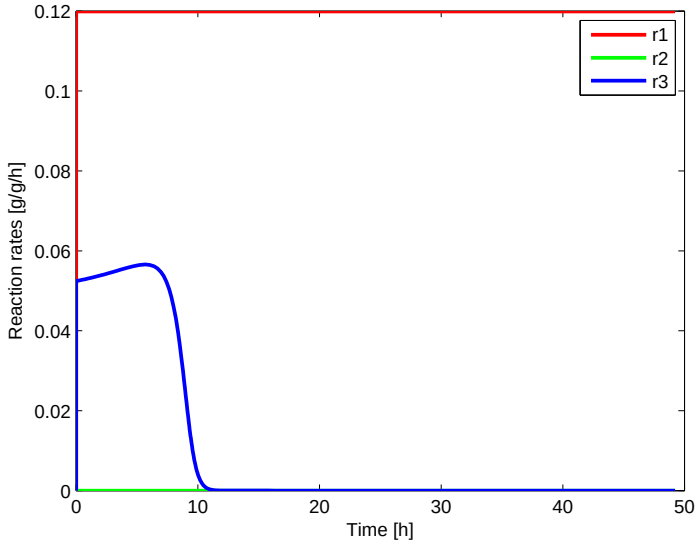

Figure 2.12: Fourth simulated experiment - Reaction rates

Table 2.6: Kinetic coefficients values of mechanistic model of *E. coli*

Kinetic coefficient	Exact value	Initial value	Identified value
K_S	0.14	0.1	0.11
μ_S	1.832	1	1.54
μ_O	0.72	1	0.68
Ki_A	7	10	7.66
K_A	0.5	1	0.48

minimization of a cost function measuring the deviation between the model prediction and the measured outputs is a nonconvex problem, which usually requires some form of multistart strategy and the selection of an appropriate local (or global) optimizer. Here, for the sake of simplicity, only one starting point is considered, which is chosen far enough from the exact values but allows a satisfactory parameter estimation.

These latter results show that the identification of the kinetic coefficients is more delicate and that experimental data used for identification must be chosen with care, whenever possible. The identified parameters present significant errors from 5 to more than 20%. Based on the identified model and a few online measurements, an EKF can, in principle, be designed. Fig. 2.13 shows a simulation of the continuous-discrete *EKF* applied to the full model (2.6) (the confidence in the model is represented by $R_\eta = \begin{bmatrix} 10^{-2} & 0 & 0 & 0 & 0 \\ 0 & 10^{-2} & 0 & 0 & 0 \\ 0 & 0 & 10^{-2} & 0 & 0 \\ 0 & 0 & 0 & 10^{-2} & 0 \\ 0 & 0 & 0 & 0 & 10^{-2} \end{bmatrix}$). The case where S, O and C are measured (using a white noise with respective standard deviations of $\sigma_S = 10^{-2}$, $\sigma_O = 10^{-4}$ and $\sigma_C = 10^{-3}$ so that $R_\epsilon = \begin{bmatrix} \sigma_S^2 & 0 & 0 \\ 0 & \sigma_O^2 & 0 \\ 0 & 0 & \sigma_C^2 \end{bmatrix}$) while X and A are estimated is considered. These results correspond to the ideal case where the initial conditions are perfectly known (diagonal terms of P_0 can be small as in $P_0 = \begin{bmatrix} 1 & 0 & 0 & 0 & 0 \\ 0 & 1 & 0 & 0 & 0 \\ 0 & 0 & 1 & 0 & 0 \\ 0 & 0 & 0 & 1 & 0 \\ 0 & 0 & 0 & 0 & 1 \end{bmatrix}$). However, after 10 hours, the Kalman observer trajectory diverges from the exact simulated model demonstrating a lack of robustness to modelling errors.

In a more realistic situation, errors on the initial states have to be taken into account. Fig. 2.14 shows the results of the application of the EKF to model (2.6) using an exact predictive model (the confidence in the model is now

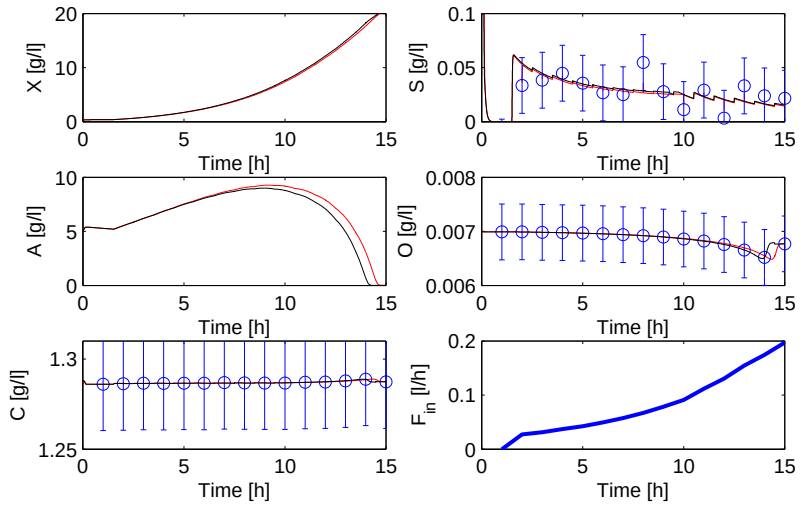

Figure 2.13: Application of the *EKF* to the *E. Coli* model (2.6) using the parameter identification results - black line: exact simulated model; red-line: *EKF* estimations; circles: simulated measurements (the sampling period is 1 hour)

$R_\eta = \begin{bmatrix} 10^{-8} & 0 & 0 & 0 & 0 \\ 0 & 10^{-8} & 0 & 0 & 0 \\ 0 & 0 & 10^{-8} & 0 & 0 \\ 0 & 0 & 0 & 10^{-8} & 0 \\ 0 & 0 & 0 & 0 & 10^{-8} \end{bmatrix}$ while R_ϵ remains unchanged) but starting from erroneous initial states (this is taken into account in $P_0 = \begin{bmatrix} 10^3 & 0 & 0 & 0 & 0 \\ 0 & 10^3 & 0 & 0 & 0 \\ 0 & 0 & 10^3 & 0 & 0 \\ 0 & 0 & 0 & 10^3 & 0 \\ 0 & 0 & 0 & 0 & 10^3 \end{bmatrix}$). The *EKF* provides very bad estimates and is obviously unable to provide enough correction from the on-line measurements. This latter observation is to be related with observability problems.

A study of the practical observability is now proposed, on the basis of the canonical form (2.22) of model (2.6), considering partitions $x_1 = [S, O, C]$ and $x_2 = [X, A]$. Following (2.22), we obtain:

$$\frac{\partial f_1}{\partial x_2} = \begin{bmatrix} -k_{S1}r_1 - k_{S2}r_2 & -X\left(k_{S1}\frac{\partial r_1}{\partial A} + k_{S2}\frac{\partial r_2}{\partial A}\right) \\ -k_{O1}r_1 - k_{O3}r_3 & -X\left(k_{O1}\frac{\partial r_1}{\partial A} + k_{O3}\frac{\partial r_3}{\partial A}\right) \\ k_{C1}r_1 + k_{C2}r_2 + k_{C3}r_3 & X\left(k_{C1}\frac{\partial r_1}{\partial A} + k_{C2}\frac{\partial r_2}{\partial A} + k_{C3}\frac{\partial r_3}{\partial A}\right) \end{bmatrix} \tag{2.38}$$

$$rank\frac{\partial f_1}{\partial x_2} = n_2 = 2 \tag{2.39}$$

Obviously, condition (2.22) only holds if S, A and X are different from 0. Even

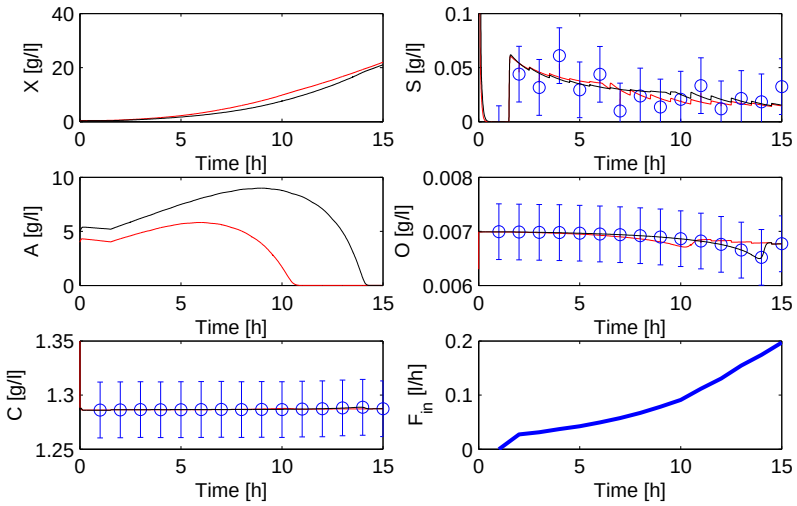

Figure 2.14: Application of the *EKF* to the *E. Coli* model (2.6) using the parameter identification results - black line: exact simulated model; red-line: *EKF* estimations; circles: simulated measurements (the sampling period is 1 hour)

if the acetate concentration is vanishing after 15 hours (see Fig. 2.13 and Fig. 2.14), global observability is thus verified between 0 and 15 hours. It can be shown that even if this test is successful, it only implies theoretical observability. To assess practical observability, Bogaerts and Vande Wouwer (2004) have proposed a measure of observability based on square matrices M_i:

$$M_i(\xi, D) = \left(\frac{\partial f_i}{\partial \xi i + 1}\right)^T \left(\frac{\partial f_i}{\partial \xi i + 1}\right) \tag{2.40}$$

with $i = 1, \ldots, q-1$

$$F_{obs} = \sum_{k=1}^{N} \sum_{i=1}^{q-1} \sqrt{cond\left(M_i(\xi(t_k), D(t_k))\right)} \tag{2.41}$$

where "cond" represents the condition number of the matrix, i.e., the ratio of its largest to its smallest eigenvalue and t_k are the discrete measurement times.

Fig. 2.15 shows the evolution of this criterion in the same situation as Fig. 2.14. The initial value is very high ($O(10^8)$) and increases gradually with time inducing that the M_i matrices are ill-conditioned and the *EKF* is unable to provide enough correction to the non measured states using information from the measured ones (which is related to the lack of sensitivity quantified by the M_i matrices in (2.41)).

An asymptotic observer is now designed in order to eliminate the uncertain kinetic model and to estimate in a more robust way the biomass and acetate concentrations. The states and yield matrix partitions are:

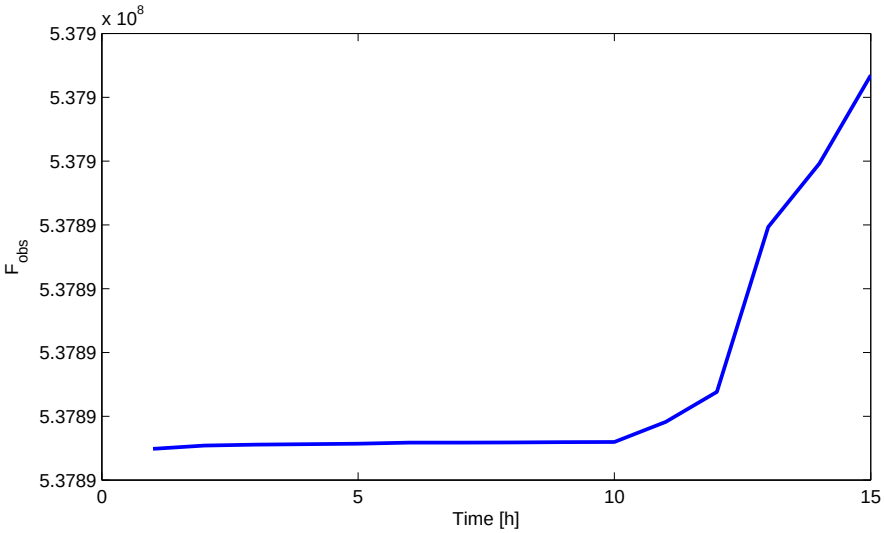

Figure 2.15: Application of the *EKF* to the *E. Coli* model (2.6) with bad initial estimations - evolution of the "observability measure" (the sampling period is 1 hour)

$$\xi_1 = \begin{bmatrix} S \\ O \\ C \end{bmatrix} \quad and \quad K_1 = \begin{bmatrix} -k_{S1} & -k_{S2} & 0 \\ -k_{O1} & 0 & -k_{O3} \\ k_{C1} & k_{C2} & k_{C3} \end{bmatrix} \tag{2.42}$$

$$\xi_2 = \begin{bmatrix} X \\ A \end{bmatrix} \quad and \quad K_2 = \begin{bmatrix} 1 & 1 & 1 \\ 0 & k_{P2} & -k_{P3} \end{bmatrix} \tag{2.43}$$

and the observer equations are given by:

$$\begin{bmatrix} \dot{z_1} \\ \dot{z_2} \end{bmatrix} = -D \begin{bmatrix} z_1 \\ z_2 \end{bmatrix} + C \begin{bmatrix} DS_{in} \\ OTR \\ CTR \end{bmatrix} \tag{2.44}$$

$$\begin{bmatrix} \hat{X} \\ \hat{A} \end{bmatrix} = \begin{bmatrix} z_1 \\ z_2 \end{bmatrix} - C \begin{bmatrix} S \\ O \\ C \end{bmatrix} \tag{2.45}$$

Fig. 2.16 shows the results of the application of the asymptotic observer, as defined in (2.44) and (2.45), using the same initial errors on X and A as in Fig. 2.15. The estimates seem to slowly converge to the right trajectories. Nevertheless, Fig. 2.17 also shows that the evolution of the estimation error on X is not vanishing.

To stress the fact that the latter results are not an isolated case, we now consider the observation of the substrate and acetate concentrations on the basis of biomass, oxygen and carbon dioxyde measurements, which will lead to even more severe state estimation problems, as will be clear in the following. The states and yield matrix partitions are now:

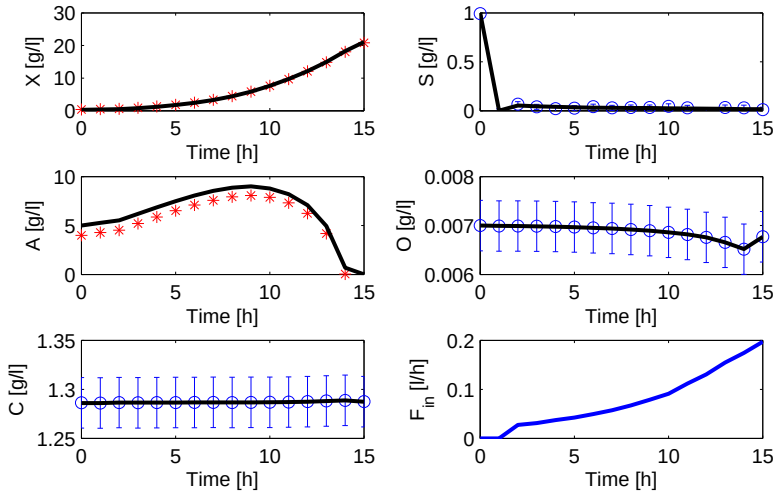

Figure 2.16: Application of the asymptotic observer to the *E. Coli* model (2.6) with bad initial estimations - black line: exact simulated model; red stars: asymptotic observer estimations; circles: simulated measurements (the sampling period is 1 hour)

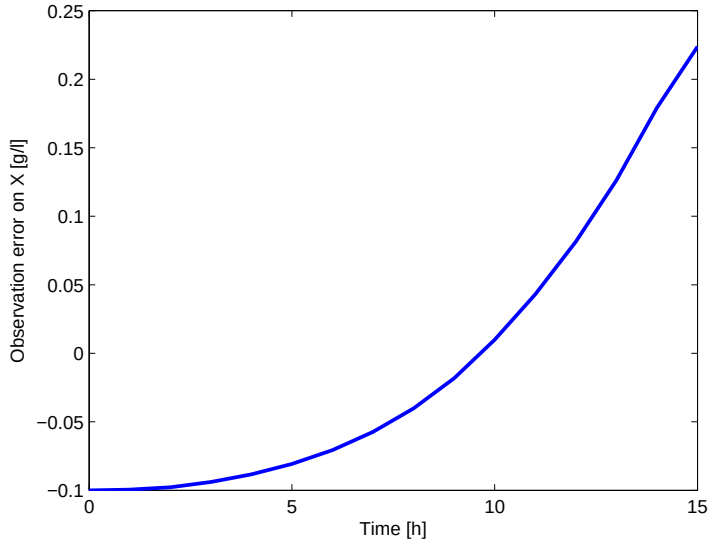

Figure 2.17: Application of the asymptotic observer to the *E. Coli* model (2.6) with bad initial estimations - Evolution of the observation error on X

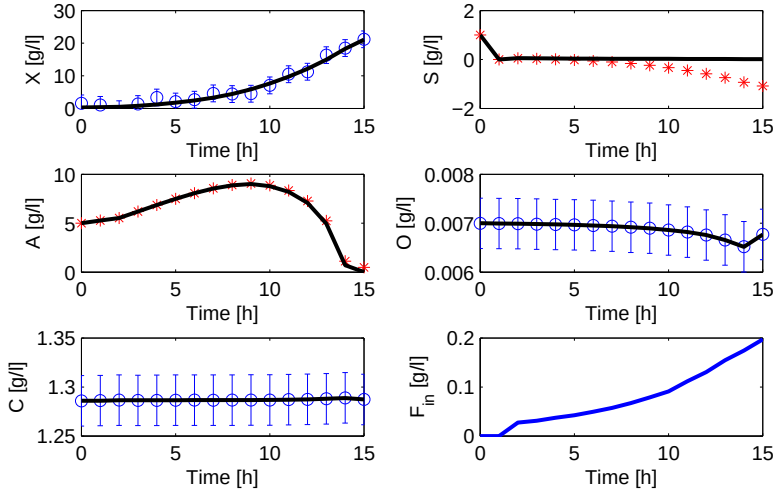

Figure 2.18: Application of the asymptotic observer to the *E. Coli* model (2.6) in order to estimate the substrate and the acetate concentrations - black line: exact simulated model; red stars: asymptotic observer estimations; circles: simulated measurements (the sampling period is 1 hour)

$$\xi_1 = \begin{bmatrix} X \\ O \\ C \end{bmatrix} \quad and \quad K_1 = \begin{bmatrix} 1 & 1 & 1 \\ -k_{O1} & 0 & -k_{O3} \\ k_{C1} & k_{C2} & k_{C3} \end{bmatrix} \tag{2.46}$$

$$\xi_2 = \begin{bmatrix} S \\ A \end{bmatrix} \quad and \quad K_2 = \begin{bmatrix} -k_{S1} & -k_{S2} & 0 \\ 0 & k_{P2} & -k_{P3} \end{bmatrix} \tag{2.47}$$

and the observer equations are given by:

$$\begin{bmatrix} \dot{z_1} \\ \dot{z_2} \end{bmatrix} = -D \begin{bmatrix} z_1 \\ z_2 \end{bmatrix} + C \begin{bmatrix} DS_{in} \\ OTR \\ CTR \end{bmatrix} \tag{2.48}$$

$$\begin{bmatrix} \hat{S} \\ \hat{A} \end{bmatrix} = \begin{bmatrix} z_1 \\ z_2 \end{bmatrix} - C \begin{bmatrix} X \\ O \\ C \end{bmatrix} \tag{2.49}$$

Fig. 2.18 shows the estimation results where the substrate estimate is not bounded to zero in order to illustrate the dramatically-increasing divergence of the observer (note that the real trajectory is very close but not equal to zero and is, of course, positive).

The explanation of this phenomenon is that even though the asymptotic observer is insensitive to the kinetic parameters, it can be quite sensitive to small errors in the pseudo-stoichiometric coefficients as shown by the following developments. From (2.49), the expressions of the estimated states are obtained:

$$\begin{aligned}\hat{S} = z_1 &+ \frac{(k_{S1}k_{C2}k_{O3} + k_{S2}(k_{C2} - k_{C3}))X}{k_{O1}(k_{C3} - k_{C2}) + k_{O3}(k_{C2} - k_{C1})} \\ &+ \frac{(k_{S1}(k_{O1}k_{C3} - k_{O3}k_{C1}) + k_{S2}(k_{C3} - k_{C1}))O}{k_{O1}(k_{C3} - k_{C2}) + k_{O3}(k_{C2} - k_{C1})} \\ &+ \frac{(k_{S2}(k_{C1} - k_{C2}) - k_{S1}k_{O1}k_{C2})C}{k_{O1}(k_{C3} - k_{C2}) + k_{O3}(k_{C2} - k_{C1})} \qquad (2.50a) \\ \hat{A} = z_2 &+ \frac{(k_{P2}(k_{C2} - k_{C3}) + k_{P3}k_{O3})X}{k_{O1}(k_{C3} - k_{C2}) + k_{O3}(k_{C2} - k_{C1})} \\ &+ \frac{(k_{P2}(k_{C3} - k_{C1}) - k_{P3}(k_{O3} - k_{O1}))O}{k_{O1}(k_{C3} - k_{C2}) + k_{O3}(k_{C2} - k_{C1})} \\ &+ \frac{(k_{P2}(k_{C1} - k_{C2}) - k_{P3}k_{O1})C}{k_{O1}(k_{C3} - k_{C2}) + k_{O3}(k_{C2} - k_{C1})} \qquad (2.50b)\end{aligned}$$

Some combinations of the yield coefficients can have a significant impact on the accuracy of the estimated states. Consider the sensitivity matrix:

$$\begin{aligned}\left(\frac{\partial \hat{S}}{\partial k_i}\right) &= \begin{pmatrix} \frac{\partial \hat{S}}{\partial k_{S1}} & \frac{\partial \hat{S}}{\partial k_{S2}} & \frac{\partial \hat{S}}{\partial k_{P2}} \\ \frac{\partial \hat{S}}{\partial k_{P3}} & \frac{\partial \hat{S}}{\partial k_{Q1}} & \frac{\partial \hat{S}}{\partial k_{Q3}} \\ \frac{\partial \hat{S}}{\partial k_{C1}} & \frac{\partial \hat{S}}{\partial k_{C2}} & \frac{\partial \hat{S}}{\partial k_{C3}} \end{pmatrix} \\ &= \begin{pmatrix} 1.22X - 0.008O - 0.22C & -0.13X + 0.06O - 0.19C & 0 \\ 0 & 0.95X - 0.4O - 1.35C & -0.71X - 0.3O + 1.1C \\ 0.46X - 0.38O - 0.08C & -0.08X - 0.07O - 0.02C & -0.35X + 0.29O + 0.06C \end{pmatrix} \qquad (2.51)\end{aligned}$$

and in particular, the expression of the sensitivity with respect to k_{S1}. When the culture starts, the biomass concentration X is very low so that its impact on the estimated state is negligible. On the other hand, when the culture has been running for hours, the biomass concentration is of the order of 10 to $100 g/l$. This means that a small error on k_{S1} will lead to a variation of the estimate proportional to 1, 22x10 or approximately 12 times the initial error. If the error on k_{S1} is around 1% of its theoretical value, the observer is likely to produce an estimation error of 12% from the correct value, which cannot always be tolerated (for instance, substrate concentrations are generally low in *E. coli* applications, in order to avoid an accumulation of acetate which is an inhibitory product for the cells growth). Consider now that the culture reaches biomass concentrations around $100 g/l$, the consequence of a small error on a yield coefficient has a larger effect on the estimated states as the estimation error reaches 100%. This observation does not hold for the oxygen concentration as its values cannot exceed $0.007 g/l$, the concentration at saturation, but it holds for the carbon dioxide in the sensitivities with respect to k_{O1} and k_{O3}, as the concentration at saturation is $1.293 g/l$. An intuitive way to alleviate this high sensitivity is

to separate the model in two submodels depending on the metabolic pathway (Bastin and Dochain (1990)). Indeed, this allows the estimation of 3 states on the basis of only 2 measured ones and the biomass terms in (2.50) disappear so that we can expect less sensitivity problems. In this case, the partitions of the yield matrix of the two submodels are:

For the respirative pathway:

$$K_1^R = \begin{bmatrix} -k_{O1} & -k_{O3} \\ k_{C1} & k_{C3} \end{bmatrix} \quad and \quad K_2^R = \begin{bmatrix} 1 & 1 \\ -k_{S1} & 0 \\ 0 & -k_{P3} \end{bmatrix} \tag{2.52}$$

For the respiro-fermentative pathway:

$$K_1^{RF} = \begin{bmatrix} -k_{O1} & 0 \\ k_{C1} & k_{C2} \end{bmatrix} \quad and \quad K_2^{RF} = \begin{bmatrix} 1 & 1 \\ -k_{S1} & -k_{S2} \\ 0 & k_{P2} \end{bmatrix} \tag{2.53}$$

For instance, the sensitivities of the estimated substrate concentration with respect to k_{O1} become for each pathway:

$$\left(\frac{\partial \hat{S}}{\partial k_{O1}} \right)_R = 237O + 46.1C \tag{2.54a}$$

$$\left(\frac{\partial \hat{S}}{\partial k_{O1}} \right)_{RF} = 2.74O - 0.19C \tag{2.54b}$$

Unfortunately, the terms involving the oxygen and carbon dioxide concentrations in (2.54a) and (2.54b) are relatively large so that no real improvement is provided. Even if the respiro-fermentative pathway does not seem to be sensitive to small errors on k_{O1}, the other pathway does. In fact, the bypass of the biomass concentration measurement transfers the sensitivity to the oxygen and carbon dioxide terms. As a conclusion, bioprocess modelling and identification are delicate tasks, and uncertainties on the pseudo-stoichiometric and kinetic parameters are almost unavoidable. Standard observers such as the extended Kalman filter and the asymptotic observer are affected to some extent by these uncertainties and of course also by practical observability. More robust state estimation techniques have been proposed, which can alleviate these problems. However, these techniques are beyond the scope of this chapter, and in the continuation of this text, attention is focused on data-driven techniques.

2.5 Conclusion

In this chapter, a generic macroscopic model of fed-batch cultures of microorganisms exhibiting overflow metabolism is first described and illustrated with in-the-literature-already existing models of *S. cerevisiae* (yeast strain) and *E. coli*

(bacteria strain). Unfortunately, several states are generally not available on-line, limiting their exploitation in a possible control scheme aiming at optimizing the process. In order to alleviate this problem, bioprocess state estimation is then introduced by the definition of observability, a model feature which is necessary to reconstruct on-line unmeasurable states. Classical state estimators, and more particularly the Extended Kalman Filter (*EKF*) and the asymptotic observer (*AO*), are presented and applied to a simplified model of *E. coli*. Their practical limitations in realistic simulated conditions are also discussed, concluding that the main drawbacks of observers based on mechanistic models are their high sensitivity to model uncertainties (focusing on the kinetics for the *EKF* and the stoichiometry for the *AO*) but also the time-varying degree of observability which can sometimes be unsufficient to ensure a correct convergence of the estimates.

Chapter 3

Data-driven Approach

3.1 Introduction

The previous chapter presents the potential of classical mechanistic model-based observers. Even though a wide range of state estimation algorithms are readily available, their practical use remains relatively limited. The main reasons previously exposed are: (a) many state estimation algorithms require a dynamic model of the bioprocess, involving a macroscopic reaction scheme and kinetics, which are difficult to accurately establish from prior process knowledge and available measurement data; (b) state estimation algorithms usually rely on some hardware sensors, which are expensive and not always fully reliable; (c) manual operation has a long history in the bioprocess industry and advanced monitoring and control are currently emerging techniques. It appears legitimate to propose to investigate, in the following sections, the use of simple estimation algorithms based on black-box models and standard industrial measurement signals, such as those related to pH, temperature, pressure and dissolved oxygen concentration, as suggested in previous studies (see, e.g., Karim et al. (1997), Hulhoven et al. (2006) and Dewasme et al. (2007b)). In the next sections, designs of software sensors based on partial least squares and neural network techniques are presented. Simulation and real-life experimental data are then used to assess the applicability and performance of the several methods.

3.2 Input/output selection and measurements data analysis

It is difficult to establish a mechanistic model linking the abovementioned basic measurements to the main macroscopic species concentrations (biomass, substrate and metabolic products). This, of course, motivates a black-box strategy but also raises the question of which of the available signals could be informative for establishing a black-box model. Indeed, some signals could carry

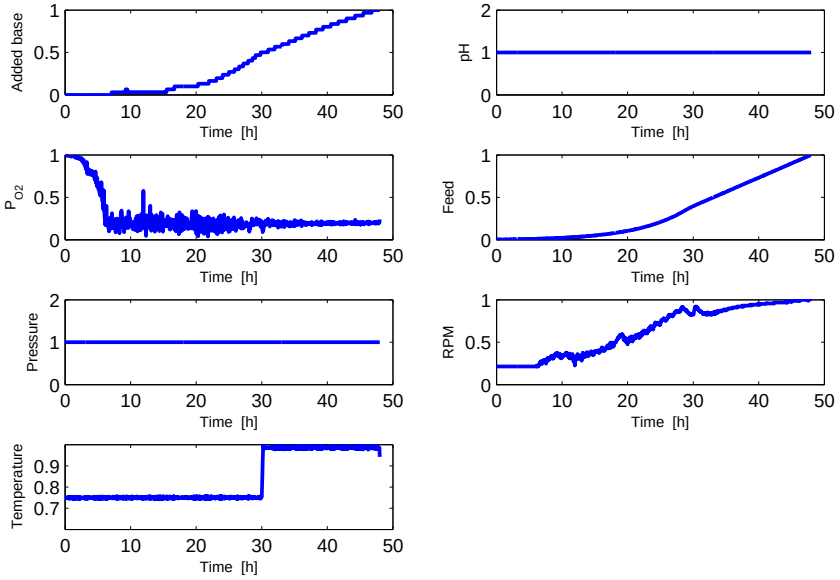

Figure 3.1: Typically available measurements: added base weight, pH, dissolved oxygen ($PO2$), added feed weight, pressure, stirring speed (RPM) and temperature

very little or redundant information and play a detrimental role in a learning procedure. That is why the information content of the available measurement signals is first assessed before being used as inputs to a black-box structure reproducing some selected outputs (i.e., some of the macroscopic species concentrations). A way of assessing the information content of the inputs is through *Principal Component Analysis* (Geladi and Kowalski (1986)). For illustration purpose, we consider the cultures of genetically manipulated strains of *S. cerevisiae* and *E. coli* growing in different-scale bioreactors. In standard operations, several regulation loops are active, including temperature, dissolved oxygen, pH (usually by base addition), air flow, pressure and stirring (in order to avoid oxygen limitation). Typical available measurements are represented in Fig. 3.1. All of them are normalized for the sake of confidentiality.

Whereas the aim of the regulation loops is to maintain the process variables constant, useful dynamic information can be extracted from the actuator signals. For instance, pH is maintained constant via the addition of a certain quantity of base, whose evolution is informative of the culture evolution. In order to assess the correlation and the redundancy existing between the different signals, principal component analysis (PCA) is used in order to construct new signals, which are linear combinations of the normalized original ones. This analysis aims at describing a maximum of the data dispersion with a minimum of components. A new representation of the data matrix is obtained through a so-called "score matrix" T:

$$T_{nxa} = X_{nxm} P_{mxa} \tag{3.1}$$

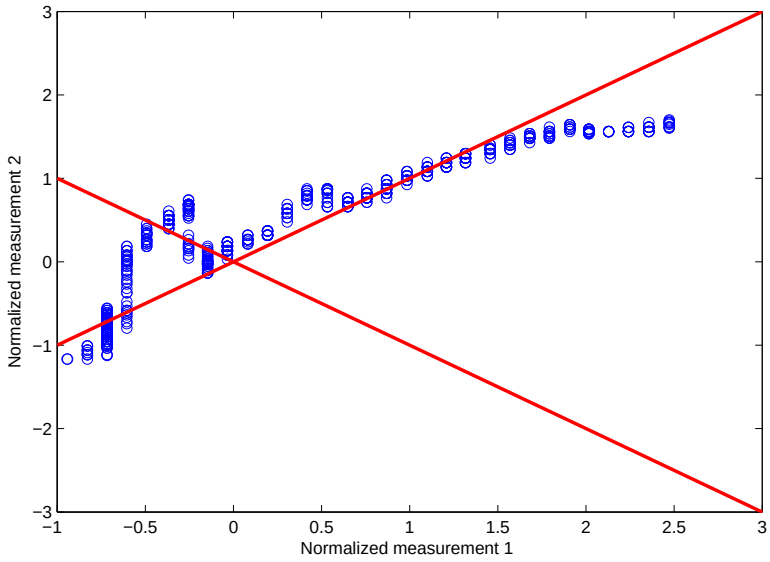

Figure 3.2: Example of a PCA performed on two normalized measured signals. The principal directions are represented by the red lines

where X is the initial data matrix of dimension nxm with n and m being respectively the number of measurements and the number of signals. P is the orthogonal loading matrix ($PP' = I$) of dimension mxa where a is the number of considered scores or components. Geometrically, it consists in finding a space representation spreading as much as possible the cloud of data points in each new axis direction. Fig. 3.2 gives an idea of what can be these new directions for a specific example where two normalized measurements are considered. The score matrix provided by the principal component analysis is $P = \begin{pmatrix} 0.7071 & -0.7071 \\ 0.7071 & 0.7071 \end{pmatrix}$. The cloud of points can then be represented in a new space defined by the red lines (which, as a matter of fact, correspond to the bisectors of the previous axes).

A nonlinear iterative partial least squares algorithm ($NIPALS$) is used in order to build the scores in the sense that it calculates the first score t_1 (the first column of T) and the corresponding loadings vector p_1 from X before subtracting their product to obtain the residual as follows:

- X is projected onto t_1 (set as a column of X) to find the corresponding loading p_1: $p_1 = \frac{Xt_1}{t_1^T t_1}$;
- The loading vector is then normalized: $p_1 = p_1(p_1^T p_1)^{-0.5}$;
- X is projected onto p_1 to find the corresponding score vector t_1: $t_1 = \frac{Xp_1}{p_1^T p_1}$;
- The first principal component is removed from X: $e = X - t_1 p_1^T$

Table 3.1: Score variances and explanations for the specific example illustrated in Fig. 3.1

	Variances	Explanation(%)
t_1	3.544	50.627
t_2	1.37	19.564
t_3	0.989	14.132
t_4	0.887	12.675
t_5	0.160	2.298
t_6	0.048	0.679
t_7	0.002	0.026

Table 3.2: Loadings of the measurement signals (illustrated in Fig. 3.1) in each principal direction

	t_1	t_2	t_3	t_4	t_5	t_6	t_7
Base	0.495	0.263	-0.152	0.055	-0.256	-0.169	0.752
pH	-0.196	0.742	-0.206	-0.1265	0.562	-0.19	-0.015
PO2	-0.429	0.429	-0.12	-0.098	-0.625	0.466	0.007
Feed	0.487	0.279	-0.153	0.06	-0.367	-0.319	-0.65
Pressure	-0.009	-0.32	-0.787	-0.526	0.007	-0.016	-0.003
RPM	0.514	0.09	-0.081	0.039	0.302	0.785	-0.109
Temperature	0.177	0.081	0.52	-0.83	-0.046	-0.013	0.002

The next scores and loadings are obtained iteratively following the same operation on each residual e. As an illustration, Tab. 3.1 gives the variances of the scores t_i (i.e., the eigenvalues of the covariance matrix of the measurement data) and also the percentage of the total variance explained by each score (for the specific example illustrated in Fig. 3.1). The loadings of the same normalized measurements signals are listed in Tab. 3.2 for each score. The stirrer speed (RPM for rotation per minute), the added base weight (*Base*), the added feed weight (*Feed*), and the dissolved oxygen ($PO2$) have the largest weights in the first principal component. Hence, as this component seems to be the most informative (see Tab. 3.1), these signals apparently convey more information than the others.

In this example, the notion of data compression is well illustrated as the first 4 scores contain more than 95 percents of the measurement information. Therefore, these 4 signals could be used as inputs to a software sensor if this analysis carries over all data sets.

3.3 Linear versus nonlinear black-box model

Even though a mechanistic bioprocess model is usually nonlinear (the nonlinearity stems from the kinetics), the relation between selected measurement inputs (elementary signals such as RPM, base weight, feed rate and $PO2$) and

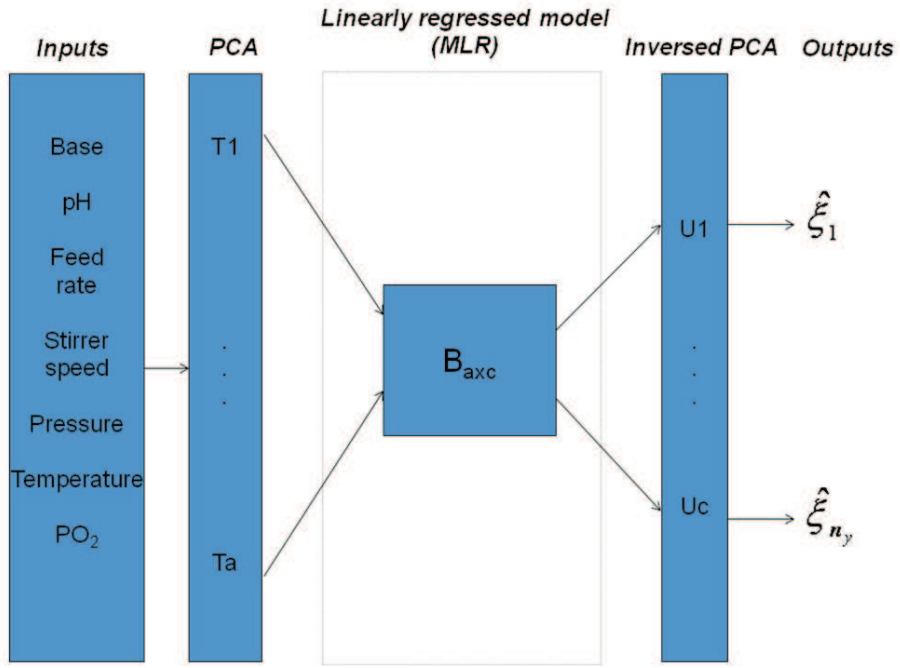

Figure 3.3: Linear software sensor structure: PLS.

outputs (some component concentrations), could incidentally be linear. Before embarking in the construction of a nonlinear black-box model (which is more complex to identify than a linear one), it is therefore of interest to evaluate the linear/nonlinear character of this relationship and to select the best model. In this section, two classical black-box modelling strategies are applied to bioprocesses and compared. Both of them are built using input and/or output variables represented by their scores matrix as mentioned in the previous section. The first one leads to a linear representation whereas the second is a nonlinear approach.

3.3.1 Linear strategy - Partial Least Squares regression (PLS)

This first strategy (Geladi and Kowalski (1986)) is an extension of the multiple linear regression (MLR) using the properties of the $NIPALS$ algorithm through 2 PCA on the input and output data. This strategy is decomposed in 3 relations (2 outer (PCA) and 1 inner linear regression (LR) relations, see Fig. 3.3): One can build the score matrix of the input (X) and output (Y) data matrix:

$$T_{nxa} = X_{nxn_x} P_{n_x xa} + E_{nxa} \tag{3.2a}$$
$$U_{nxc} = Y_{nxn_y} Q_{n_y xc} + F_{nxc} \tag{3.2b}$$

where T and U are respectively the nxn_x input and nxn_y output score matrix (considering n different measurements for n_x input and n_y output signals), P

and Q the loadings matrix (considering again limited numbers $a \leq n_x$ and $c \leq n_y$ of components) and E and F the residuals matrices depending on the number of selected components or scores columns (remind that if the number of components is equal to the number of input signals, $E = F = 0$). The third relation is a simple linear regression between the input and output scores following:

$$U_{nxc} = T_{nxa}B_{axc} + G_{nxc} \tag{3.3}$$

where B is the regression coefficient matrix and G a new residual matrix.

Note that an intermediate algorithm exists and is called *Principal Components Regression* (PCR). The main difference between PCR and PLS lies in the way the factor scores are extracted. Indeed, the PCR only uses the covariance structure of the input variables while PLS uses the covariance structure of the input and output variables. As it is known that bioprocesses present different element concentrations correlated as it appears in (2.6), using the covariance structure of the input and output variables should be preferable.

3.3.2 A nonlinear alternative: PCA and *Artificial Neural Network* (ANN)

The previous input-output representation is by essence linear. To describe the behaviour of a bioprocess, it might be necessary to include some nonlinearity in the model representation. Attention is now focused on feed-forward multilayer perceptrons or radial basis function networks, which are universal approximators. Standard feedforward NNs define a static map between a selected number of inputs (denoted $y(t)$, as they represent the measurement information coming from the bioprocess) and outputs (denoted $\hat{\xi}(t)$, as they correspond to estimates of component concentrations)

$$\hat{\xi}(t) = f(y(t)) \tag{3.4}$$

One of the most common NN architectures in system modelling is the perceptron (Rosenblatt (1958)). A perceptron consists in an on/off static function (called activation function or decision function) delivering a binary output. The sum of a linear combination of the inputs weighted by synaptic weights is compared to a threshold separating the activation and inactivation zones:

$$\hat{\xi}_i = f(x_i) = \begin{cases} 0 : x_i < 0 \\ 1 : x_i > 0 \end{cases} \tag{3.5}$$

where

- $x_i = \sum_j w_{ij} y_j$ is the input of the i^{th} neuron.
- w_{ij} corresponds to the weight linking the j^{th} input to the i^{th} neuron.
- y_j and $\hat{\xi}_i$ are respectively the input and output vectors.

This is the simplest neural network structure recalling the first mathematical model of neuron proposed by McCulloch and Pitts (1943). There exists a learning rule developed by Rosenblatt and ensured to converge (i.e., to provide weight values that enable the recognition of each class corresponding to the binary values 0 and 1) if the related data are linearly separable (Minsky and Papert (1969)). Networks of perceptrons may then be built using multiple layers structures where all the neurons outputs depend only on the inputs from the previous layer and do not interact with the same-layer neurons. These structures are called *Multilayer Perceptrons* (*MLP*). This time, the nonlinearity used in the activation function is continuous (for instance, a sigmoid function) and we distinguish the first and the last layers, respectively called input and output layers, from the intermediate layers also called the hidden layers. Actually, only the first and the last layers input and output are available from an external point of view. The multilayer perceptron learning phase is performed by calculating a least square error criterion first applied to the output layer:

$$E = \frac{1}{2} \sum_{i=1}^{K} \left(\hat{\xi}_i(X) - \xi_i \right)^2 \tag{3.6}$$

where

- K is the number of neurons of the output layer.
- $\hat{\xi}_i$ are the outputs.
- ξ_i are the desired outputs.
- X is the input vector of the output layer neurons.

and by propagating this error back to the previous layers in order to update the weights as follows:

$$w_{l,ij}(k+1) = w_{l,ij}(k) - \alpha \left(\frac{\partial E}{\partial w_{l,ij}} \right)_{l-1} \tag{3.7}$$

where

- $w_{l,ij}$ corresponds to the weight linking the j_{th} input to the i^{th} neuron of the l^{th} layer.
- α is a strictly positive tuning parameter called the learning rate.
- $\left(\frac{\partial E}{\partial w_{l,ij}} \right)_{l-1}$ is the first derivative of the error calculated for the $l-1$ layer with respect to $w_{l,ij}$.

For obvious reasons linked to its principle, this learning algorithm is called the *Backpropagation Algorithm* (Werbos (1974)). This kind of network is abundantly used in biomedical applications and particularly in speech processing and handwritten pattern recognition (Gosselin (1996a), Gosselin (1996b), Morgan and Bourlard (1995) and Bourlard (1992)).

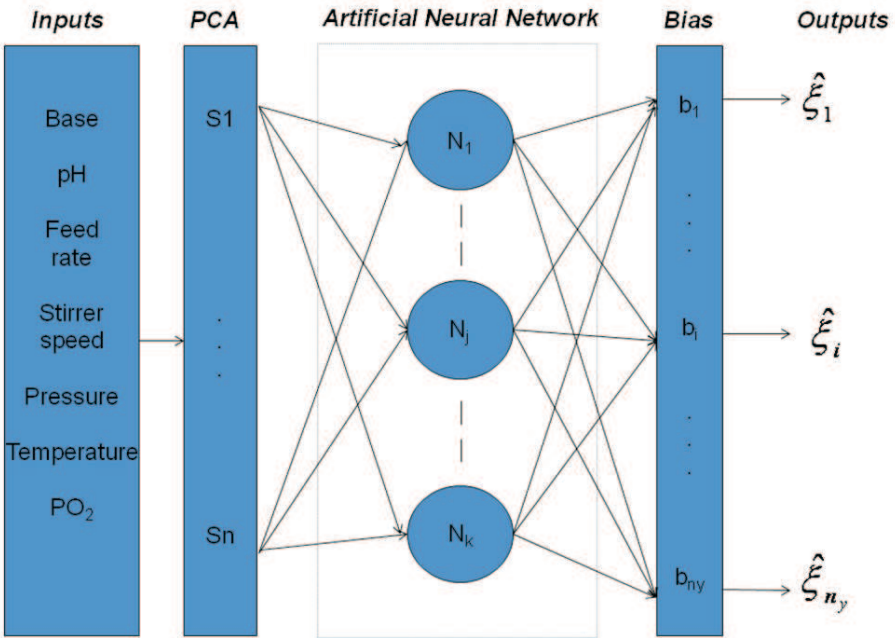

Figure 3.4: Nonlinear software sensor structure: PCA and $RBF - ANN$

Another classical neural network structure is the *Radial Basis Function* network, which has proved quite useful in modelling bioprocesses (Vande Wouwer et al. (2004)). This structure differs from the last one by the activation principle and the learning rules. This network (Fig. 3.4) delivers outputs calculated by a continuous mathematical expression of the form:

$$\hat{\xi}_i(t) = \sum_{j=1}^{k} w_{ij} e^{\frac{-\left\|y(t)-c_j\right\|^2}{r_j^2}} + b_i \quad i = 1 \ldots n_y \tag{3.8}$$

where

- y is the input of length n_y;
- $\hat{\xi}_i$ is the i^{th} component of the output vector;
- k is the number of neurons in the hidden layer;
- w_{ij} are the weights linking the neurons to the outputs;
- c_j are the centers;
- r_j are the radii (i.e., the average spherical distance from the center);
- b_i are the biases.

The learning procedure of this network is divided in several learning steps (see Fig. 3.5). The number of neurons k is taken large enough so as to be able to

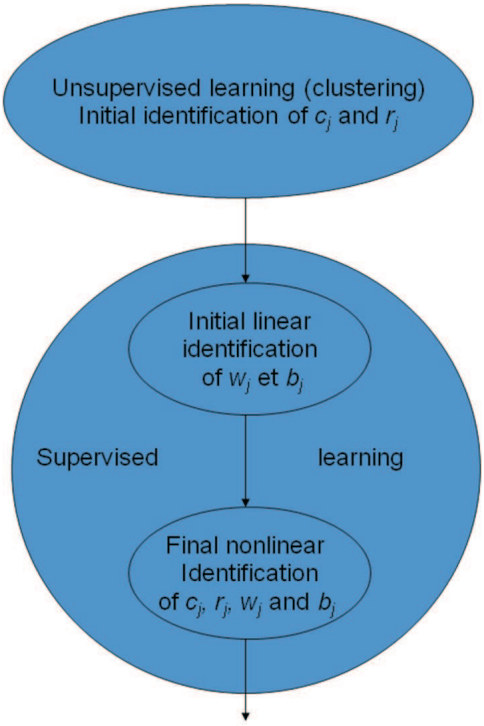

Figure 3.5: Parameter identification scheme of the $RBF - ANN$ structure

reproduce the desired input-output behaviour, but small enough so as to avoid overparametrization and lack of generalization (to data sets not considered in the identification phase).

A 3-steps learning procedure is used (as in Vande Wouwer et al. (2004), see Fig. 3.5): The first step is an unsupervised learning phase in which the first estimates of the centers and the radii are obtained by a $k - means$ clustering algorithm. These first estimates allow the NN outputs to cover the experimental field. The second step is a supervised learning phase consisting in an initial linear identification of the weights and biases by minimization of a quadratic cost function. Finally, a last nonlinear identification of all the parameters is achieved starting from the values obtained in the previous steps and minimizing a Gauss-Markov criterion taking the measurement errors into account:

$$\theta^T = \left[w^T b^T r^T c^T\right] = min_\theta \frac{1}{2} \sum_{i=1}^{N} \left(\xi_i - \hat{\xi}_i(\theta)\right)^T Q_i^{-1} \left(\xi_i - \hat{\xi}_i(\theta)\right) \qquad (3.9)$$

where

- ξ_i are the measured output values;
- Q_i is the error covariance matrix on the measured outputs;
- $\hat{\xi}_i$ are the estimated outputs based on θ.

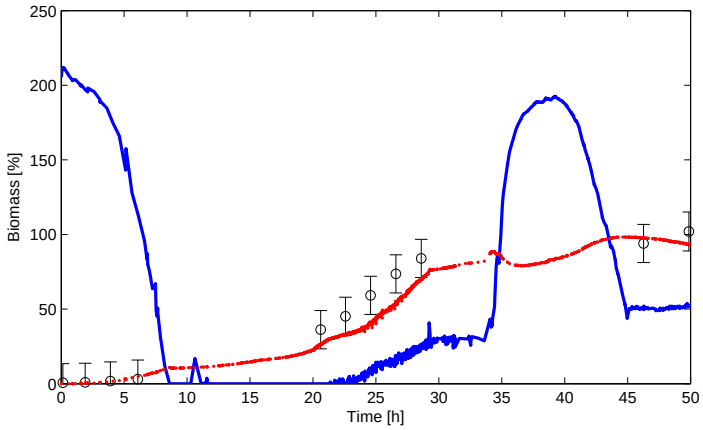

Figure 3.6: Biomass estimation in a culture of *S. cerevisiae*. Red line: output of the $RBF-ANN$ nonlinear model; blue line: output of the PCR linear model; circles: real off-line measurements

3.3.3 Comparison of the two approaches: Linear versus nonlinear modelling

To compare the performance of the two proposed methods, a large panel of experimental data collected from different bioreactors operated with different strains at different scales is available. This large data set will ensure the pertinence and the generality of the results. As a start, four data sets corresponding to fed-batch cultures of *S. cerevisiae* (yeast strain) operated in a laboratory-scale bioreactor are considered. Among the 4 data sets, two are used to identify the black-box model while the two others are used to perform cross-validation tests. Our goal is to estimate the biomass concentration all along the cultures based on four available measurements (chosen as the most informative signals: base addition, feed flow rate, stirrer speed and dissolved oxygen concentration). As only one variable need to be estimated, a PCR is used instead of a PLS for the linear approach while a $RBF-ANN$ is used for the nonlinear approach. Fig. 3.6 shows the evolution of the estimated biomass concentration during one of the two latter experiments (cross-validation). Recall that the standard input signals, on which a PCA is achieved, are provided at a high sampling rate and thus provide a frequent biomass estimation which can be very useful for process monitoring.

For the sake of confidentiality, all the experimental results are normalized. Unfortunately, only the nonlinear model seems to reproduce satisfactorily the biomass concentration evolution. This can be explained by the probable existence of nonlinearities in the relation between the chosen input variables and the biomass concentration. 3 neurons are sufficient to deal with these nonlinearities. Note that 3 neurons already represent 12 parameters (4 radii, 4 centers, 3 weights and 1 bias) to identify if 4 inputs and only 1 output are considered. One must be conscious that the number of parameters increases to 16 for 2 outputs instead of 1, to 20 for 3 outputs and so on. Only three of the four available scores have been used for producing the previous results as it has been ob-

Table 3.3: Score explanations of 4 yeast fed-batch cultures data sets

Explanation(%)	Set1	Set2	Set3	Set4
$S1$	84.0197	83.2870	83.8876	84.4641
$S2$	14.4769	14.9386	14.3560	13.7753
$S3$	1.4563	1.7236	1.6982	1.7162
$S4$	0.0471	0.0508	0.0582	0.0443

Table 3.4: Average error values for the different possible numbers of scores (inputs to the ANN)

Number of scores	$E_m(\%)$
1	6.65
2	4.52
3	2
4	3.5

served that the addition of the fourth one is useless (reducing the number of parameters to 10). The best way to understand this observation and justify our choice is to analyse the table of explanation for each score (Tab. 3.3).

It appears that more than 95% of the variance information is contained in the first two scores. Anyway, before drawing too early conclusions from this table, we also assess the quality of the NN prediction using different numbers of scores through a criterion calculating an average error:

$$E_m = \left(\frac{1}{N} \sum_{i=1}^{N} (\xi_i - \hat{\xi}_i)^2 \right)^{\frac{1}{2}} \tag{3.10}$$

where

- N is the number of experimental biomass concentration measurements;
- ξ is the biomass measurement vector;
- $\hat{\xi}$ is the biomass estimate vector.

Tab. 3.4 shows the value of this criterion for different numbers of scores. As expected from Tab. 3.3, the projection in only one principal direction of the data space is sufficient to ensure good results. Nevertheless, the minimum is observed for three scores. As this number of inputs corresponds to a reasonable number of parameters (3 radii, 3 centers, 3 weights and 1 bias if only one output is considered), this input structure is selected for the next experimental evaluations.

Table 3.5: Classification of the data sets in function of the recombinant protein, the scale and the type of validation

Scale/ Recombinant protein	RP_1	
	Direct validation	Cross-validation
20l	4	2
150l	0	1

Scale/ Recombinant protein	RP_2	
	Direct validation	Cross-validation
20l	0	8
150l	0	1

3.4 Monitoring of *E. coli* fed-batch cultures

Genetically modified strains of *E. coli*, which are commonly used in biopharmaceutical industries to express recombinant proteins and to produce vaccines, are now considered. For these bacteria strains, 16 data sets are available, which correspond to the expression of two different recombinant proteins RP_1 (for 7 of them) and RP_2 (for 9 of them), as well as two different bioreactor scales (20l and 150l). See Tab. 3.5 for a description of the experimental field. Fig. 3.7 shows the time-evolution of the three input signals (scores) and the estimation of the biomass concentration by a $RBF - ANN$ trained with 4 data sets corresponding to fed-batch cultures of bacteria in $20 - l$ bioreactor where RP_1 is expressed. Actually, 3 data sets are used in cross-validation tests and Fig. 3.7 shows one of them. For the represented test, the average error is 1.32%. Fig. 3.8 shows the results of the cross-validation test on the 7^{th} data set corresponding to a $150 - l$ scale bioreactor. Again, note that the ANN parameters are not modified in between these tests, which constitutes challenging cross-validation tests. The overall average error amounts to only 1.95%, testifying of the good quality of the results.

The ANN software sensor is then tested with the 9 remaining experiments, where RP_2 is expressed. Fig. 3.9 shows that the ANN software sensor reproduces again very satisfactorily the evolution of the biomass concentration, the type of protein expressed having little influence on the performance. Moreover, as depicted in Fig. 3.10, the performance of the ANN is also independent of the bioreactor scale for the strain expressing RP_2. Note that genetic modifications have significant influence on the cell metabolism. Therefore, the use of a mechanistic model requires a new identification of the parameters whereas the ANN software sensor is still performing well without any parameter reidentification. The ANN software sensor appears then as a powerful tool in terms of flexibility and robustness.

For the data sets of the strain expressing RP_2 when the ANN sensor is trained with the four data sets corresponding to RP_1, the overall average error only amounts to 4.4%. This method has also been applied to other strains of *E. coli*

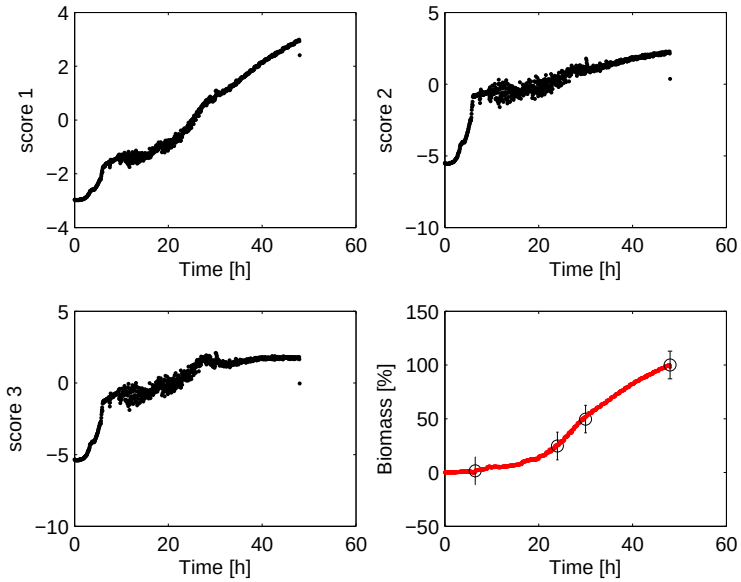

Figure 3.7: Biomass estimation in $20 - l$ scale fed-batch culture of *E. coli* (expression of RP_1)

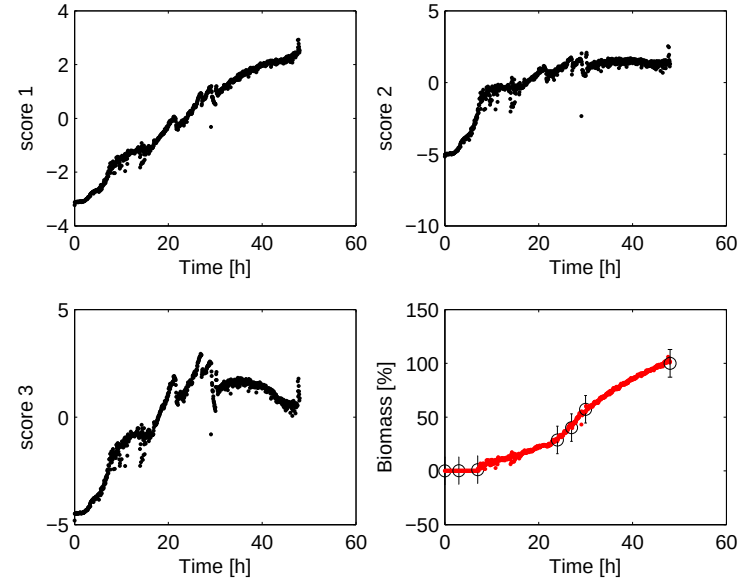

Figure 3.8: Biomass estimation in $150 - l$ scale fed-batch culture of *E. coli* (expression of RP_1)

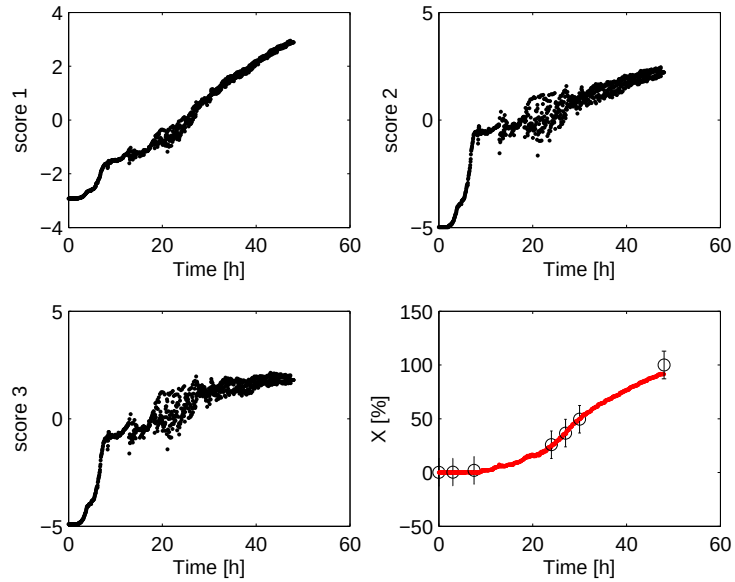

Figure 3.9: Biomass estimation in $20-l$ scale fed-batch culture of *E. coli* (expression of RP_2 when trained with RP_1)

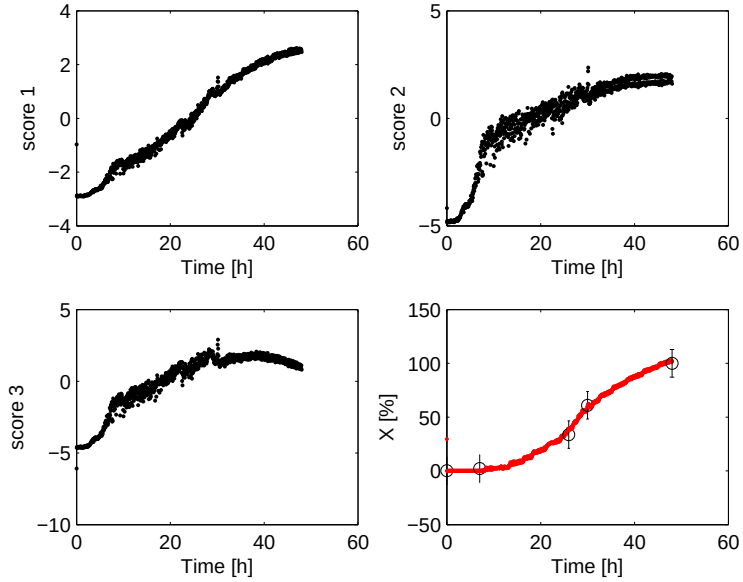

Figure 3.10: Biomass estimation in $150-l$ scale fed-batch culture of *E. coli* (expression of RP_2 when trained with RP_1)

evolving in different fed-batch processes after reidentification of the parameters. In all the cases, the ANN software sensor performs well, and provides a useful tool for on-line biomass monitoring. The proposed approach is therefore quite versatile and applicable to a broad range of bioprocesses (in some situations, other measurements signals - or additional measurement signals - have to be selected, this selection being achieved efficiently using PCA).

3.5 Monitoring of *S. cerevisiae* fed-batch cultures

The ANN software sensor is also able to estimate other key-component concentrations. First, the ethanol concentration, which is another key-component of yeast cultures, is considered. An overfeeding in glucose leads yeasts to switch from the respirative metabolism to the respiro-fermentative one, implying a production of ethanol by fermentation of the excess of glucose. It is common in industrial applications to avoid this accumulation of ethanol because it has an inhibiting influence on cell growth. As the industrial objective is generally to optimize the productivity, i.e. to maximize the production and to minimize the culture time, the ethanol concentration is always under supervision, requiring multiple off-line measurements and the time that it costs. Some hardware sensors are readily available but, unfortunately, they are still very expensive and all the laboratories cannot always afford such equipments. Moreover, on-line ethanol measurements are useful for optimizing control such as the robust RST controller presented in Valentinotti et al. (2003), Renard et al. (2006) and Dewasme et al. (2007a). This motivates the following assessment of the potentialities of the ANN software sensor in estimating other key-components like the overflow product. Again, the results presented in Fig. 3.11 are normalized for confidentiality reasons. The 5 data sets that will be used here come from a $15-l$ scale bioreactor. Two data sets were used for the learning phases and three in cross-validation. Note that the complexity of the structure is increased as the number of neurons amounts now to 4.

The impact of the noise corrupting the inputs appears clearly on the output between 40 and 50 hours of culture. Indeed, ethanol stays at a low level from the beginning to the end of the culture while some inputs are increasing and the noise that they imply grows as well. On the whole, the output mean value follows the off-line measurements. The average error confirms these observations as it amounts to 15% (recall that we deal with very low values), which is very satisfactory.
In many applications, product inhibition is not the main concern as long as the substrate concentration is limited (i.e. for instance in yeast cultures: no overflow, no fermentation). To ensure this last condition, glucose measurements are needed. As for the ethanol, off-line measurements of glucose means a consequent waste of time and monitoring of on-line glucose measurements can be an alternative when no ethanol measurement is available. The following results (using a structure of the same complexity, with 4 neurons, as for ethanol estimation) demonstrate the efficiency of the nonlinear software sensor applied to glucose estimation. The experiment is performed at glucose concentrations of an order of magnitude lower than ethanol concentrations. This explains the more significant impact of noise from 20 hours on to the end of the culture.

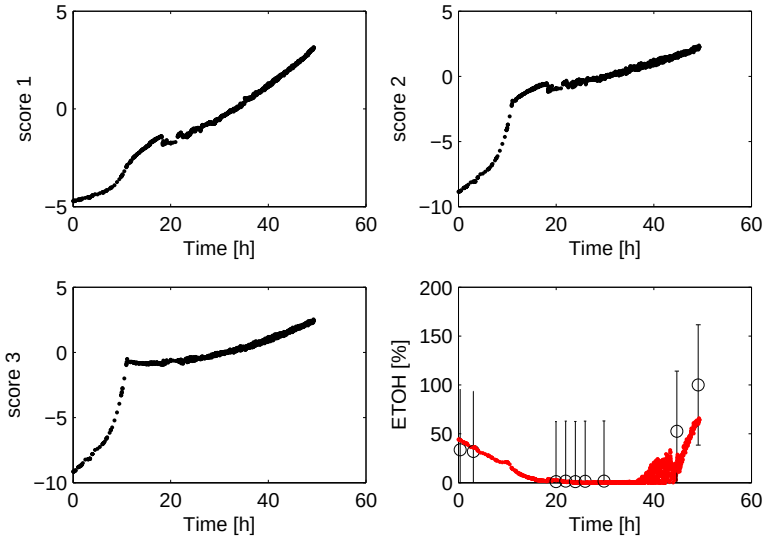

Figure 3.11: Ethanol estimation in $15-l$ scale fed-batch culture of *S. cerevisiae*

The average error on the 5 data sets is around 28%. Remember however that these cultures are operated at a very low glucose concentration level, necessarily leading to a poor estimation accuracy as it is typically the case with available hardware sensors. Therefore, the ANN software sensor needs a learning phase targeting the scale covered by the experimental field. See, for instance, the 7^{th} off-line measurement in Fig. 3.12, e.g., this point is actually beyond the experimental field so that the ANN calculates a trajectory which is more in accordance with the training data. Note that this deviation remains limited when working at low concentrations.

3.5.1 RBF-ANN software sensor potentiality in simultaneous estimations of different key-components

Now that the efficiency of the ANN in estimating key-components of interest is demonstrated, the possibility to estimate multiple outputs with only one $RBF-ANN$ structure is investigated as depicted in Fig. 3.13. To this end, the 5 same data sets are used and the new structure is trained with 3 scores using only 3 neurons to limit the number of parameters (which amounts now to 18) and the computational expense. As illustrated in Fig. 3.13: the level of the average error goes from "excellent" for the biomass concentration to "satisfactory" for the glucose and ethanol concentrations. A PLS algorithm is also considered but, again, a linear model seems inadequate for representing the link between the basic signals and the key-components, as observed in Fig. 3.14.

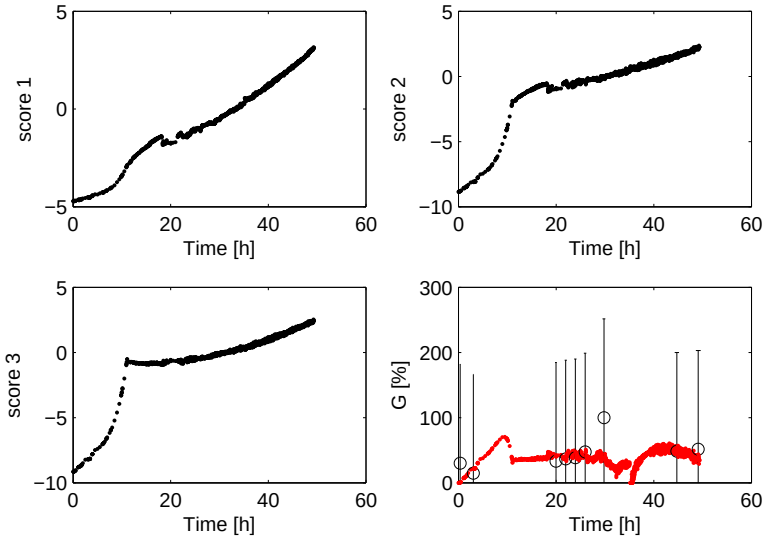

Figure 3.12: Glucose estimation in $15-l$ scale fed-batch culture of *S. cerevisiae*

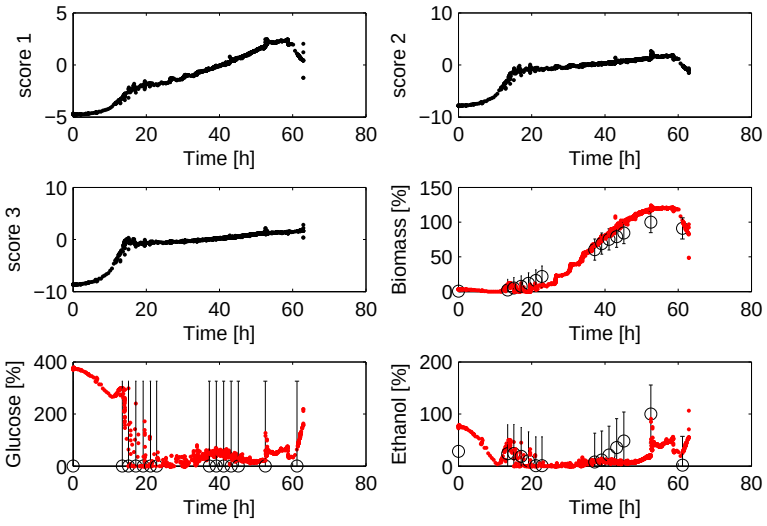

Figure 3.13: Simultaneous estimations of biomass, glucose and ethanol concentrations in $15-l$ scale fed-batch culture of *S. cerevisiae*

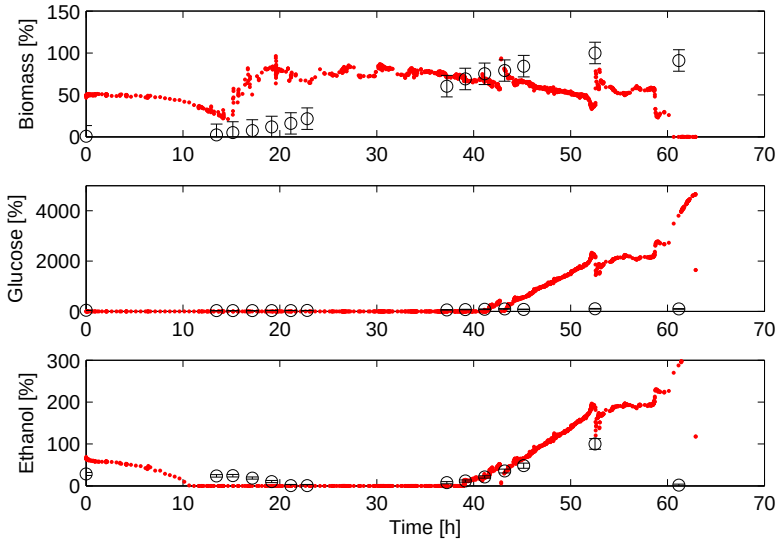

Figure 3.14: Simultaneous estimations of key-components in $15-l$ scale fed-batch culture of *S. cerevisiae* with *PLS*

3.6 Conclusion

Soft sensor techniques are particularly significant for monitoring bioprocesses, for which hardware sensors are expensive and delicate to use. Two main design approaches can be distinguished, based on the underlying model that is exploited. On the one hand, mechanistic models provide an interesting insight in the biological system, but require significant efforts for their derivation (measurements of component concentrations, careful design of experiments, parameter identification, model validation). On the basis of the dynamic model and a few on-line measurements, a wide range of observers can be designed, which provides time-continuous estimation of the component concentrations. Parameter uncertainties have to be dealt with adequately. On the other hand, data-driven techniques offer the possibility to exploit basic signals such as base addition, stirrer speed, etc, and to establish a map to some of the component concentrations of interest. In particular, principal component analysis can be used to select informative signals and artificial neural networks can be used to build the desired maps. These data-driven techniques have proved quite useful and effective in many real life applications, and some of them are discussed in this chapter.

Part III

Optimizing Productivity of Fed-batch Cultures

Chapter 4

Real-Time Optimization of Fed-batch Cultures

4.1 Control objectives

Industrial vaccine production is usually achieved using fed-batch cultures of genetically modified yeast or bacteria strains, which can express different kinds of recombinant proteins. From an operational point of view, it is necessary to determine an optimal feeding strategy (i.e. the time evolution of the input flow rate to the fed-batch culture) in order to maximize productivity. The main problem encountered comes from the metabolic changes of such strains in presence of feeding overflow. Indeed, during a culture, the cells strains are likely to change their metabolism because of their limited respiratory capacity. When the substrate is in excess (concentration $S > S_{crit}$), the cells produce a by-product through fermentation, and the culture is said in respiro-fermentative (RF) regime. The byproduct generally has a detrimental effect on the cells growth because it directly inhibits the cells respiratory capacity (Pham (1999)). On the other hand, when the substrate becomes limiting (concentration $S < S_{crit}$), the available substrate (typically glucose), and possibly the by-product (as a substitute carbon source), if present in the culture medium, are oxidized. The culture is then said in respirative (R) regime. Thus, the optimal operating conditions that maximize the biomass productivity are at the boundary of the two regimes. In these conditions, the fermentation and by-product oxidation rates are equal to zero and, from (2.4):

$$r_1 = min(r_S, r_{S_{crit}}) \tag{4.1a}$$

$$r_2 = max(0, r_S - r_{S_{crit}}) \tag{4.1b}$$

where

$$r_{S_{crit}} = \frac{r_O}{k_{os}} \tag{4.2a}$$

$$r_S = \frac{S}{S + K_S} \tag{4.2b}$$

$$r_O = \mu_O \frac{O}{O + K_O} \frac{Ki_P}{Ki_P + P} \tag{4.2c}$$

the following relations hold:

$$r_1 = r_S = r_{S_{crit}} = \frac{r_O}{k_{os}} \tag{4.3a}$$

$$r_2 = 0 \tag{4.3b}$$

Expression (4.2a) shows that the respiratory capacity has an influence on the critical substrate concentration level. For illustration purposes, Fig.4.1 shows a simulation of a fed-batch yeast culture where the substrate concentration in the culture medium is regulated around a constant theoretical set-point value $S_{sp} = 0.0226 g/l$. This constant value is based on the assumption that the respiratory capacity would not be influenced by the ethanol level ($r_O = \mu_O \frac{O}{O+K_O}$ so that, following (4.3a), $r_1 = r_{S_{crit}} = r_S$, $r_2 = 0$ and $S_{sp} = S_{crit}$). As this assumption is not correct in practice, ethanol is produced during the batch, thus inhibiting the respiratory capacity and affecting the optimal glucose level, and the biomass growth rate is lower than expected ($r_O = \mu_O \frac{O}{O+K_O} \frac{Ki_E}{Ki_E+E}$ so that, following (4.1), $r_1 = r_{S_{crit}} < r_S$, $r_2 \neq 0$ and $S_{sp} \neq S_{crit}$). A simple regulation strategy, i.e., a regulation that does not adapt the glucose setpoint according to the respiratory capacity variations, does not allow to avoid the production of ethanol, leading to a poor level of productivity (while, as demonstrated in the following, more than 80 g/l of biomass can be obtained within 30 h with glucose setpoint adaptation, only 30 g/l are obtained in Fig. 4.1).

Consequently, after a trivial mathematical manipulation of (4.3a) using the Monod law $r_S = \mu_S \frac{S}{S+K_S}$, a relation between the critical substrate concentration level and the cell respiratory capacity is obtained as:

$$S_{crit} = \frac{K_S r_O}{k_{os}\mu_S - r_O} \tag{4.4}$$

Fig. 4.2 shows a plot of this relation where the point $[0, 0]$ corresponds to a totally inhibited respiratory capacity, preventing any growth, and the point $[r_{O_{max}}, S_{crit_{max}}]$ corresponds to maximum productivity (i.e. absence of metabolite product in the culture medium and a sufficient level of oxygenation). Obviously, the presence of the byproduct in the culture medium can decrease the respiratory capacity and in turn the value of the critical substrate concentration. Moreover, the estimation of the critical substrate level S_{crit} requires additional measurements (P, O) and a perfect knowledge of K_S, k_{os}, μ_S, K_O, μ_O and Ki_P, which are generally uncertain.

In order to maintain the system at the edge between the respirative and respiro-fermentative regimes, it would be necessary to determine on-line an estimation

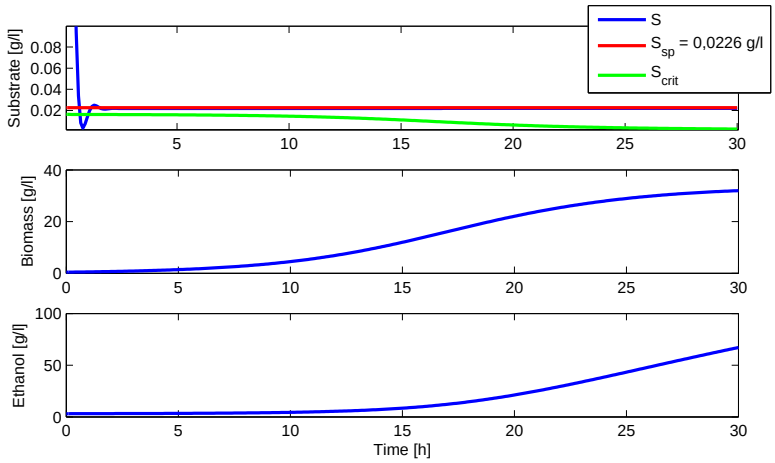

Figure 4.1: Simulation of a fed-batch process controlled at a constant S_{sp} value

of the biological threshold S_{crit} and to control the substrate concentration in the culture medium around a setpoint S_{sp} ideally equal to S_{crit} in order to reach the optimal operating conditions (Dewasme and Vande Wouwer (2008)). To this aim, a first intuitive strategy achieving a real-time optimization and called *extremum-seeking* is proposed and tested in simulated realistic conditions. Different forms of extremum-seeking facing the particular case of fed-batch bioprocesses of overflow metabolized cells are studied next.

4.2 A brief review of real-time optimization

Real-time optimization (*RTO*) is a general term used to characterize approaches that all aim at iteratively improving or optimizing process performances using plant data through different available state variable measurements. In this regard, Chachuat et al. (2009) proposes a review of the various existing *RTO* techniques using approaches based on adaptation strategy, feasibility and optimality. Three categories are defined:

- **Model parameter adaptation**, which is a standard approach using two-step-adaptation first, identifying model parameters and, then, optimizing the process (see Srinivasan and Bonvin (2002)).
- **Modifier adaptation**, which consists in adapting the cost function and the possible constraints in such a way that the cost function gradient and the values of the constraint gradients of the model match with those of the plant (in the literature, see Marchetti et al. (2009)).
- **Direct input adaptation**, which transforms the optimization problem into a feedback control problem through the constancy or invariance of measured variables at a certain level, itself enforcing optimal performances

(see Skogestad (2000), Ariyur and Krstic (2003), Titica et al. (2003a), Akesson (1999), Henes and Sonnleitner (2007)).

The latter category contains methods such as self-optimizing control (Skogestad (2000)), *NCO* tracking and extremum-seeking (Ariyur and Krstic (2003)) which will attract our attention in the following.

The first two extremum-seeking techniques that are studied in this work are non-model based or "model-free". The first one is related to the work of Blackman in the 60's, revisited and improved in Ariyur and Krstic (2003) while the second one is based on a simple recursive least squares technique (*RLS*). Note that a classical model-free extremum-seeking, using gradient descent, comparable to Ariyur and Krstic (2003), has already been applied succesfully to dynamic optimization of continuous bioprocesses in Wang et al. (1999). In Titica et al. (2003a) and Titica et al. (2003b), real-time optimization of fed-batch bioreactors via an original model-based extremum-seeking technique is considered. In these latter works, a kinetic model using classical Monod or Haldane laws is used, inducing the existence of a smooth cost function along which the search for the extremum is performed. Several other theoretical and applicative publications on real-time optimization using a gradient descent along a smooth cost function can also be cited as Tan et al. (2006), Tan et al. (2008), Tan et al. (2009), Chioua et al. (2008), Peters et al. (2007), Zhang et al. (2002), Zhang and Ordonez (2009) and Methekar et al. (2010). However, even in the most recent publications, convex or, at least, smooth cost function (i.e., existence of a steady-state where the cost function first derivative exists, is zero, and where its second derivative is always negative or positive) is one of the most recurrent assumptions. In this work, a fed-batch model based on a kinetic model commonly used in the literature (see Renard (2006), Rocha (2003), Sonnleitner and Käppeli (1986)) and presenting a discontinuous derivative at the extremum, is considered. The necessary condition of optimality (*NCO*) is then not fulfilled. To our knowledge, this case is not examined in the literature, which makes it original. Moreover, as suggested in the end of Titica et al. (2003a), varying oxidative capacity of the cells (due to simple oxygen limitation or byproduct inhibition) is also considered, forcing a kinetic change and, furthermore, a slow displacement of the extremum.

4.2.1 Optimization criterion

Optimal operating conditions are situated at the boundary of the oxidative and respiro-fermentative pathways (i.e., where the glucose concentration perfectly matches with S_{crit}). In this particular case, the oxidation of glucose is the only active reaction as no byproduct is produced nor consumed, inducing that r_2 and r_3 vanish. Moreover, when the glucose concentration reaches S_{crit}, r_1 is also maximized (see 4.3a). Maximizing the cells growth is therefore equivalent to maximize the substrate consumption rate and to minimize the fermentation rate (i.e., the simultaneous maximizations of the glucose consumption and the respiratory capacity). This can be formulated as follows:

$$\max_{S_{sp}} Y = \max_{S_{sp}} (\varphi_1 - \varphi_2) \tag{4.5}$$

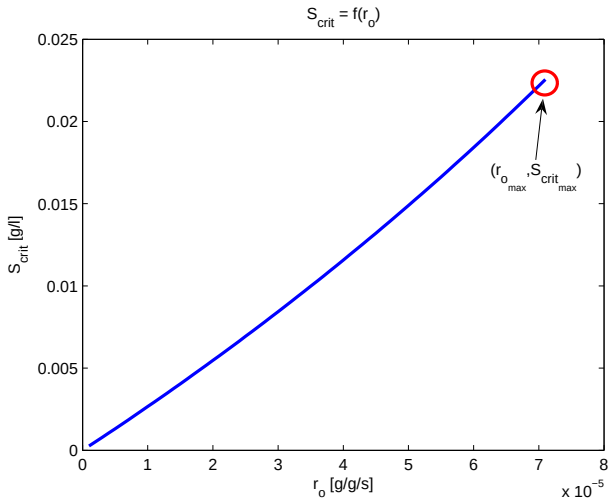

Figure 4.2: Critical substrate level (S_{crit}), separating the two regimes, as a function of the respiratory capacity (r_O)

where:

- Y is the assumed measurable cost function;
- φ_1 and φ_2 correspond to the reaction rates $r_1 X$ and $r_2 X$, respectively.

In order to estimate the cost function Y online, we use a pseudo-steady state assumption. Indeed, assuming that the variations of substrate, oxygen and carbon dioxyde concentrations are equal to zero, we obtain from (2.6b), (2.6d) and (2.6e):

$$D(S_{in} - S) = (k_{S1} r_1 + k_{S2} r_2) X \tag{4.6a}$$
$$-DO + OTR = (k_{O1} r_1 + k_{O2} r_2 + k_{O3} r_3) X \tag{4.6b}$$
$$DC + CTR = (k_{C1} r_1 + k_{C2} r_2 + k_{C3} r_3) X \tag{4.6c}$$

Dilution terms can be considered as negligible in comparison with OTR, CTR and DS_{in}. Replacing the reaction rates $r_i X$ by φ_i ($i = 1, 2, 3$), (4.6) can be written:

$$DS_{in} = k_{S1} \varphi_1 + k_{S2} \varphi_2 \tag{4.7a}$$
$$OTR = k_{O1} \varphi_1 + k_{O2} \varphi_2 + k_{O3} \varphi_3 \tag{4.7b}$$
$$CTR = k_{C1} \varphi_1 + k_{C2} \varphi_2 + k_{C3} \varphi_3 \tag{4.7c}$$

From this on, after some basic mathematical manipulations, it is possible to recover a measurable function y (see Fig. 4.3) of the yield coefficients, OTR, CTR and DS_{in}, proportional image of the assumed measurable cost function

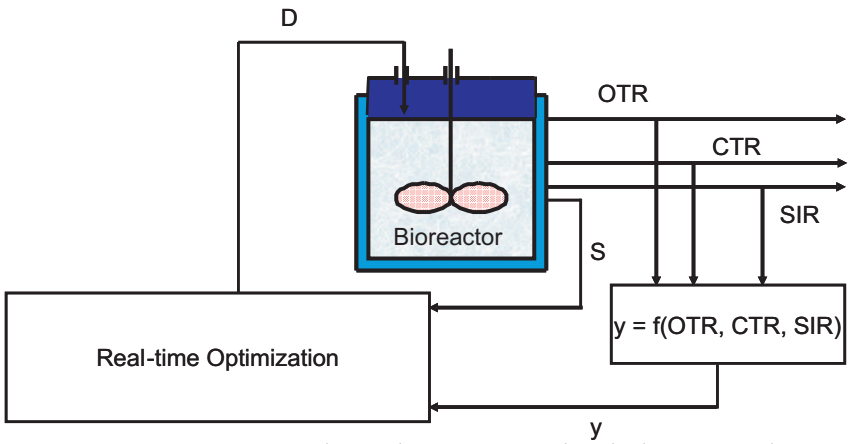

Figure 4.3: Extremum-seeking scheme integrated to the bioreactor plant

$Y = \varphi_1 - \varphi_2$. We decide to call DS_{in} the "substrate intake rate" (SIR) and we obtain:

$$Y = (\varphi_1 - \varphi_2) \propto y \tag{4.8a}$$

$$y = (k_{S1} + k_{S2})\, k_{C3}\, OTR - (k_{S1} + k_{S2})\, k_{O3}\, CTR + (k_{O3}k_{C2} - k_{O1}k_{C3} + k_{C1}k_{O3} - k_{O2}k_{C3})SIR \tag{4.8b}$$

This optimization criterion can thus be evaluated on the basis of 3 measurements (OTR, CTR and SIR) coupled to a sufficiently good identification of several yield coefficients (see Fig. 4.3). Fig. 4.4 shows the evolution of the reaction rates and $r_1 - r_2$ (with a magnifying scaling factor) as a function of the substrate concentration for a model of *S. cerevisiae* where the respiratory capacity is assumed to be constant (no oxygen limitation and no respiratory capacity inhibition by the byproduct). Indeed, the evolution of $r_1 - r_2$ is proportionnal to the criterion $\varphi_1 - \varphi_2$ by a X factor. Consequently, it is preferable to represent $r_1 - r_2$ at a fixed scale in order to study its main features. The optimum shown in Fig. 4.4 appears to be unique and defined as a cusp, i.e. the criterion is differentiable everywhere but at its optimum ($\frac{\partial(r1-r2)(S_{crit})}{\partial S}$ does not exist) and the convexity is switching before and after the optimum ($\frac{\partial^2(r1-r2)(S^-_{crit})}{\partial S^2} < 0$ and $\frac{\partial^2(r1-r2)(S^+_{crit})}{\partial S^2} > 0$).

4.3 Model-free extremum-seeking

4.3.1 Main principle

The objective of a general extremum-seeking strategy is to determine on-line unknown parameters (which, in this case, are reduced to one parameter $\theta = S_{sp}$, image of the critical substrate level) of a system (represented by the bioreactor in Fig. 4.3) by permanently estimating its gradient through the analysis

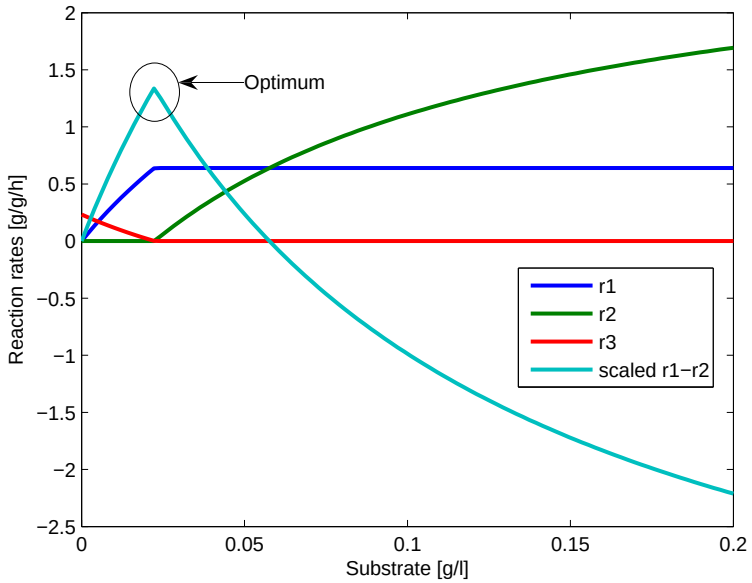

Figure 4.4: Reaction rates and optimization criteria as a function of S

of the measurement $Y = f(\theta)$, following the injection of a periodical excitation signal d (also called "dither signal", typically sinusoidal) in the controller delivering a certain dilution rate $D = \frac{F_{in}}{V}$.

Two adaptive model-free extremum-seeking techniques are proposed in the following.

4.3.2 Extremum-seeking through a bank of filters

The objective of the extremum-seeking strategy is to determine on-line the parameter $\hat{\theta}$ (which in this case represents the glucose concentration setpoint S_{sp} ideally equal to S_{crit}). The main principle of the bank of filters (i.e., the extremum-seeking scheme) technique is to isolate the information about the gradient in ξ. To this aim, as shown in Fig. 4.5, the system is first excited by a sinusoidal signal of the form $Asin(\omega t)$, disturbing its states and unknown physical quantities (as, for instance, in our case, S_{crit}) in order to recover information about their variations in y precisely at the frequency $\frac{\omega}{2\pi}$. Nevertheless, the assumed measurable signals composing y (i.e., OTR, CTR and SIR) may present a large panel of different mid-frequencies covering or hiding the information of interest at the frequency $\frac{\omega}{2\pi}$.

A signal processing represented by the bank of filters is therefore needed in order to recover the information of interest. The corresponding equations to

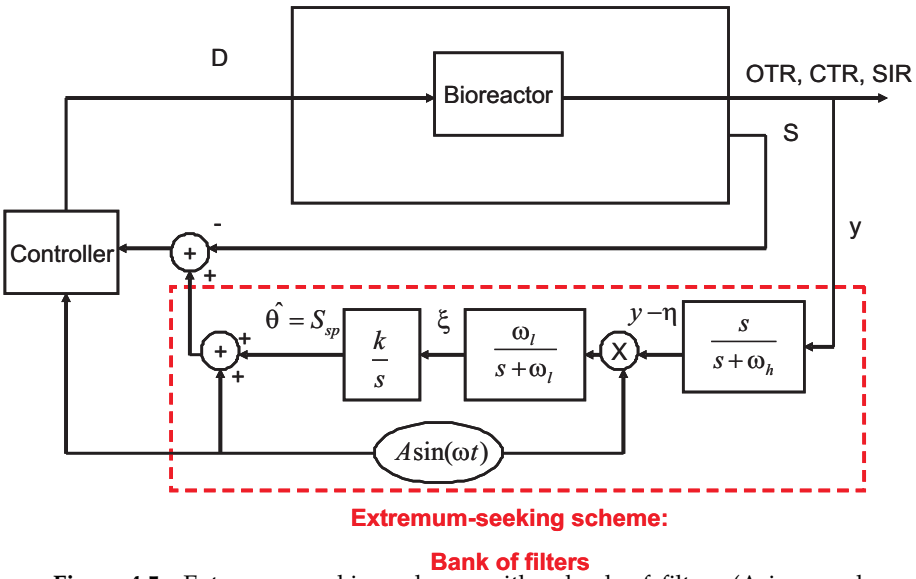

Figure 4.5: Extremum-seeking scheme with a bank of filters (Ariyur and Krstic (2003), Krstic and Wang (2000))

Figure 4.5 are (Ariyur and Krstic (2003), Krstic and Wang (2000)):

$$y = f(\hat{\theta} + Asin(\omega t)) \tag{4.9a}$$

$$\dot{\hat{\theta}} = k\xi \tag{4.9b}$$

$$\dot{\xi} = -\omega_l \xi + \omega_l (y - \eta) Asin(\omega t) \tag{4.9c}$$

$$\dot{\eta} = -\omega_h \eta + \omega_h y \tag{4.9d}$$

where:

- $y = y(\hat{\theta} + Asin(\omega t))$ is the measurable cost function;
- $\hat{\theta}$ is the estimation of the unknown parameter (in our case, $\hat{\theta} = \hat{S}_{sp}$);
- k is the gain of the integrator;
- $\xi (= \frac{1}{k}\frac{d\hat{\theta}}{dt})$ can be seen as the gradient estimation;
- ω_l is the cut-off frequency of the low-pass filter;
- ω_h is the cut-off frequency of the high-pass filter;
- η is an intermediate variable explaining the absence of the low frequencies rejected from y in $y - \eta$ by the high-pass filter;

The overall feedback system of Fig. 4.5 has then three time scales:

- fast - the plant with the stabilizing controller;
- medium - the periodic perturbation;

- slow - the filters (at least the high-pass filter as the low-pass filter is not always necessary and its cut-off frequency has more or less the same order as $\frac{\omega}{2\,\pi}$) in the extremum-seeking scheme.

The following didactic example, assuming a model of a yeast fed-batch culture, illustrates the operation from a frequential point of view:

- A first high-pass filter with a cut-off frequency $\omega_h = 0,1\ \omega$ is used in order to reject the non-informative continuous component of y. To illustrate this, the Discrete Fourier Transforms (DFT) of the input signal y and the high-pass filter output signal $y - \eta$ are respectively represented in Figs. 4.6 and 4.7. The absence of a significative continuous component can be observed in 4.7 as its magnitude is now equivalent to the mid-frequencies magnitudes (considered here as noise). Note that all the frequencies are normalized with respect to the sampling frequency $f_S = 8\frac{\omega}{2\pi}$.
- The output is then multiplied by the dither signal in order to be "demodulated". There exist now another continuous component inside the result of this demodulation accompanied by another informative frequency peak in $2\ \frac{\omega}{2\pi} = 0,25\ f_S$ hidden in the disturbing mid-frequencies peaks. Indeed, the demodulation acts as follows: $asin(\omega t)bsin(\omega t) = \frac{ab}{2}(1 - cos(2\omega t))$, showing the presence of a constant $\frac{ab}{2}$ (continuous component) and a component in 2ω.
- The second low-pass filter, which is not always necessary, is used in order to better isolate this new continuous component containing the information of interest and especially to attenuate the influence of the residual mid-frequencies signals and the second component of the demodulation in $2\ \omega$. The DFT of the low-pass filter output signal is represented in Fig. 4.8. Note that the second component of the demodulation is still present in $0,25 f_S$.
- This signal ξ is then filtered one last time by an integrator in order to attenuate the last "parasite" components and to recover the estimation of the unknown parameter from the integration of the continuous component appearing in Fig. 4.9.

Convergence of the bank of filters technique

As demonstrated in Krstic and Wang (2000), by choosing adequate values for all the parameters of the optimizing loop, a nonlinear system should exponentially converge to an $O(\omega + A)$-neighborhood of the optimum value θ^* (with ω and A as small positive constants) if the following assumptions are fulfilled:

Assumption 4.1 There exists an input $F_{in}(S, S_{sp}, t)$ that exponentially stabilizes the system $\dot{S} = f(S(t), F_{in}(t), t)$ to the equilibrium produced by S_{sp}: $\dot{S} = f(S_{sp}, F_{in}(t)) = 0$.

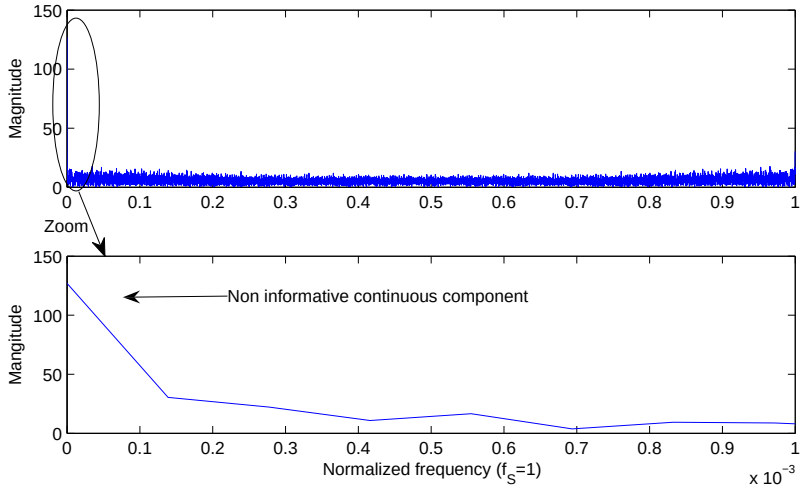

Figure 4.6: DFT of the input signal y in a simulated case of yeast fed-batch culture.

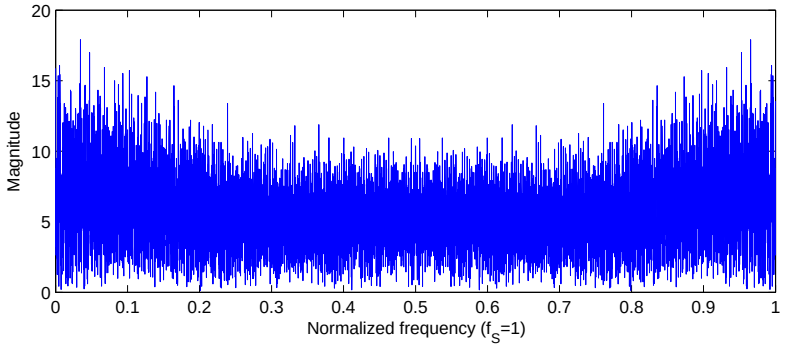

Figure 4.7: DFT of the high-pass filter output signal $y - \eta$ in a simulated case of yeast fed-batch culture

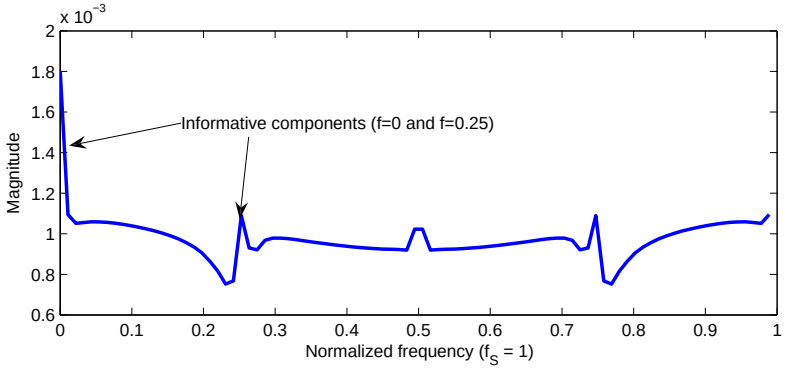

Figure 4.8: DFT of the low-pass filter output signal ξ in a simulated case of yeast fed-batch culture

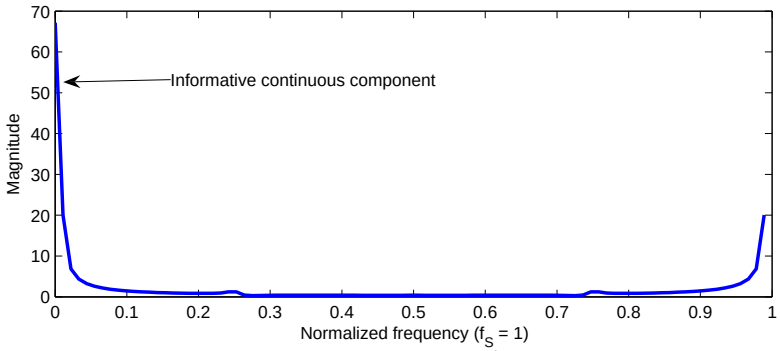

Figure 4.9: DFT of the integrator output signal $\hat{\theta} = S_{sp}$ in a simulated case of yeast fed-batch culture

Indeed, there exist many feed profiles $F_{in}(t)$, each of them stabilizing system (2.6b) to different $S = S_{sp}$, the ideal trajectory being the $F^*_{in}(t)$ stabilizing (2.6b) to the physical optimum $S = \theta^* = S_{crit}$.

The next assumption characterizes this optimum following the classical necessary condition of optimality (NCO) for a maximum:

Assumption 4.2 There exists $\theta^* = S_{crit} \in \Re$ such that:

$$\frac{\partial y}{\partial \theta^*} = 0 \tag{4.10a}$$

$$\frac{\partial^2 y}{\partial {\theta^*}^2} < 0 \tag{4.10b}$$

Looking at Fig. 4.4, it is obvious that Y (4.8a) has discontinuous derivatives around the extremum appearing here as a cusp so that assumption 4.2 is not verified. A rigorous proof of convergence is beyond the scope of this work, and a more practical approach will be followed. To explain, however, the good behaviour of the extremum-seeking scheme as depicted in Fig. 4.5, we propose now to divide the domain of criteria (4.8) into 2 regions limited, on the left side, by $[0\ S^-_{crit}]$ and, on the right side, by $[S^+_{crit}\ +\infty]$, such that:

$$r_1 - r_2 = \begin{cases} r_1 = \frac{\mu_S S}{S+K_S}\ if\ S \leq S^-_{crit} \\ r_{1_{max}} - r_2 = \frac{2r_O}{k_{OS}} - \frac{\mu_S S}{S+K_S}\ if\ S \geq S^+_{crit} \end{cases} \tag{4.11}$$

Considering that the oxygenation is perfect and that the by-product concentration is sufficiently low so that the respiratory capacity r_O is constant, we get:

$$(r_1 - r_2)' = \begin{cases} r_1' = \frac{\mu_S K_S}{(S+K_S)^2}\ if\ S \leq S^-_{crit} \\ (r_{1_{max}} - r_2)' = -\frac{\mu_S K_S}{(S+K_S)^2}\ if\ S \geq S^+_{crit} \end{cases} \tag{4.12}$$

By linearizing (4.11) around the optimum value, we see that the derivatives have opposite values. In the case of a cost function respecting the NCO, the convergence is ensured (pushing the gradient ξ to zero in average) in a $O(\omega +$

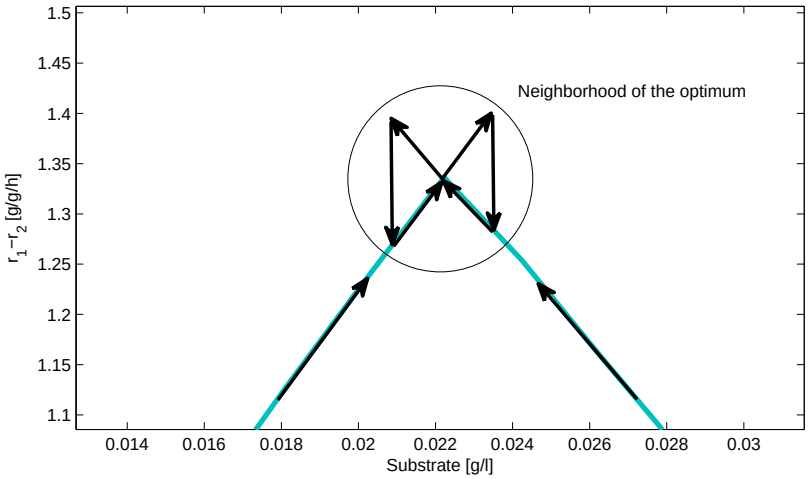

Figure 4.10: Zoom on the optimum of Fig. 4.4. The arrows indicate the direction of the algorithm displacement, following the sign of the gradient. The ellipse indicates the neighborhood in which the system will oscillate if the parameter values are adequately selected by trial and error.

A)-neighborhood of the optimum value, forcing ω and A to be chosen sufficiently small in order to reduce this neighborhood as much as possible. In the case of $r_1 - r_2$, the gradient is not pushed to zero (actually, (4.12) shows that it remains more or less constant) but its sign changes at S_{crit}. If the algorithm performs sufficiently small calculation steps, it will jump around the optimum and remain in a small neighborhood as shown by Fig. 4.10. The system is not converging in the sense of NCO but the correct direction towards the optimum, indicated by the gradient, ensures neverending oscillations in the neighborhood of the optimum (see Fig. 4.10). The only condition to obtain results comparable to Krstic and Wang (2000) is still to force ω and A to be sufficiently small but also to compromise k so as to ensure a fast convergence (which requires a large value of k), and to ensure a convergence in an acceptable neighborhood of the optimum (which requires a small k). Indeed, as the gradient is not converging to zero, (4.9b) shows that θ variations are now conditioned by k.

4.3.3 Extremum-seeking through a RLS scheme

This second technique presents a scheme somewhat equivalent to the previous one where the bank of filters is actually replaced by a continuous recursive least squares (RLS, Sastry and Bodson (1989), Aström and Wittenmark (1995)) scheme (see Figure 4.11). The following comments describe how it operates.

Considering Figs. 4.4 and 4.10, the cost function to the left and to the right of S_{crit} is approximated by two straight lines with opposite slopes (according to (4.12)). For the left part, any increase or decrease of S ($S = S_{sp}$ as the controller is assumed to be faster than the extremum-seeking scheme) corresponds to a

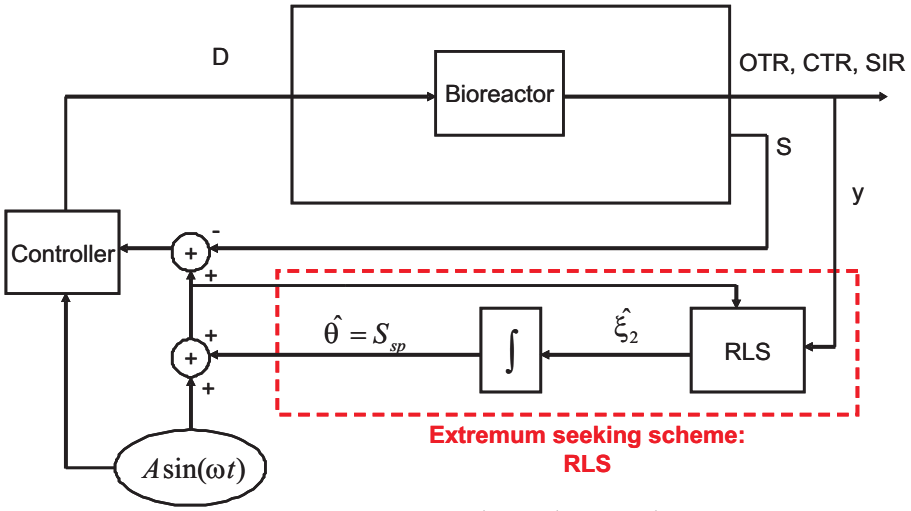

Figure 4.11: Extremum-seeking scheme with RLS.

respective increase or decrease of Y. On the other hand, for the right part, any increase or decrease of $S = S_{sp}$ corresponds to a respective decrease or increase of Y. Taking these last two remarks into account, the following relation holds:

$$Y \propto y = \xi_1 + \xi_2 S_{sp} \tag{4.13}$$

where ξ_1 and ξ_2 are the a priori unknown (as long as the model is also considered as unknown) coefficients of the first order relation linking y and S_{sp}. Finally, it appears clearly that the proportional coefficient ξ_2 always indicates the direction to follow in order to reach the optimum $S_{sp} = S_{crit}$. Therefore, ξ_2 can be seen as a gradient which, once pushed to zero in average (as the dither signal is still present), leads to the optimum. Rewriting relation (4.13) under a classical regressive form, we obtain:

$$y = \hat{\xi}\Phi^T \tag{4.14}$$

where:

- y is still the result of the 3 measurements (OTR, CTR and SIR) and, so, the vector of measurements;
- $\hat{\xi} = [\hat{\xi}_1\ \hat{\xi}_2]$ is the vector of estimated parameters;
- $\Phi = [1\ S_{sp}]$ is the regressor.

Real values of the parameters ξ_1 and ξ_2 can be identified through the continuous RLS scheme that follows:

$$e = y - \hat{\xi}\Phi^T \tag{4.15a}$$

$$\dot{\hat{\xi}} = KR^{-1}\Phi^T e \tag{4.15b}$$

$$\dot{R} = K(\Phi^T\Phi - \lambda R) \tag{4.15c}$$

where:

- K is the strictly positive and constant adaptation gain;
- R is the inversed covariance matrix acting as a directional adaptation gain;
- λ is a forgetting factor used in order to avoid a "covariance wind-up problem" due to the absence of bounds in R growth (if $\lambda = 0$, $\dot{R} \geq 0$ (Sastry and Bodson (1989))).

$\hat{\xi}_2$ can be considered as the gradient estimation. This one is pushed to zero in average using an integral control of the form:

$$\dot{\hat{S}}_{sp} = k_i \hat{\xi}_2 \tag{4.16}$$

Convergence of the RLS strategy

According to the literature (see Aström and Wittenmark (1995)), in order to converge towards the true sought value, that is, to converge to a true unique solution,

$$R(t) = \int_0^t e^{-\lambda(t-\tau)} \Phi^T(\tau)\Phi(\tau)d\tau \tag{4.17}$$

must always be invertible.

Considering the definition of Φ in (4.14), (4.17) becomes:

$$\begin{aligned} R(t) &= \int_0^t e^{-\lambda(t-\tau)} \begin{bmatrix} 1 & S_{sp}(\tau) \\ S_{sp}(\tau) & S_{sp}^2(\tau) \end{bmatrix} d\tau \\ &= \begin{bmatrix} \int_0^t e^{-\lambda(t-\tau)}d\tau & \int_0^t e^{-\lambda(t-\tau)}S_{sp}(\tau)d\tau \\ \int_0^t e^{-\lambda(t-\tau)}S_{sp}(\tau)d\tau & \int_0^t e^{-\lambda(t-\tau)}S_{sp}^2(\tau)d\tau \end{bmatrix} \end{aligned} \tag{4.18}$$

And it is now clear that if $d = 0$, i.e. $S_{sp}(\tau) \approx S_{sp}$ can be considered as constant, (4.18) becomes:

$$R(t) = (1 - e^{-\lambda t}) \begin{bmatrix} 1 & S_{sp} \\ S_{sp} & S_{sp}^2 \end{bmatrix} \tag{4.19}$$

and is not invertible, while if $d = Asin(\omega\tau)$, i.e. $S_{sp}(\tau) \approx S_{sp} + Asin(\omega\tau)$, (4.18) becomes:

$$R(t) = \begin{bmatrix} 1 - e^{-\lambda t} & 0 \\ 0 & (1 - e^{-\lambda t})(S_{sp}^2 + \frac{A^2}{2}) \end{bmatrix} \tag{4.20}$$

and is now invertible. The convergence of the RLS is thus ensured considering a sinusoïdal dither signal as depicted in Fig. 4.11.

4.3.4 Controller design

We derive adaptation and control laws from the consideration of a candidate Lyapunov function ensuring system stability. First, equation (2.6b) can be rewritten as follows:

$$\frac{dS}{dt} = -\nu X - D(S - S_{in}) \tag{4.21}$$

where $\nu = k_{S1}r_1 + k_{S2}r_2$ is considered as an unknown kinetic parameter.

Defining:

$$Z_S = \hat{S}_{sp} + d - S \tag{4.22}$$

the control error variable,

$$\tilde{\nu} = \nu - \hat{\nu} \tag{4.23}$$

the estimation error on ν, we consider the following Lyapunov function:

$$V = \frac{1}{2}Z_S^2 + \frac{1}{2\gamma}\tilde{\nu}^2 \tag{4.24}$$

where γ is a strictly positive tuning parameter.

A stabilizing controller is obtained if one can prove the strict negativity of the Lyapunov function derivative. Differentiating V and considering $\hat{S}_{sp}$ constant in order to decouple the control law from the extremum-seeking scheme (this can be done assuming that the controller converges significantly faster than the extremum-seeking scheme), we obtain:

$$\dot{V} = Z_S[\nu X + D(S - S_{in}) + \dot{d}] + \tilde{\nu}(-\frac{\dot{\hat{\nu}}}{\gamma}) \tag{4.25}$$

Replacing (4.22) and (4.23) in (4.24) and forcing $\dot{V}$ to be negative as in:

$$\dot{V} = -k_p Z_S^2 \tag{4.26}$$

where k_p is a strictly positive tuning parameter, we obtain:

$$-k_p Z_S = \hat{\nu} X + D(S - S_{in}) + \dot{d} \tag{4.27}$$

provided that:

$$\dot{\hat{\nu}} = -\gamma Z_S X \tag{4.28}$$

Finally, the stabilizing control law is given by:

$$D = \frac{[k_p Z_S + \dot{d} + \hat{\nu} X]}{S_{in} - S} \tag{4.29}$$

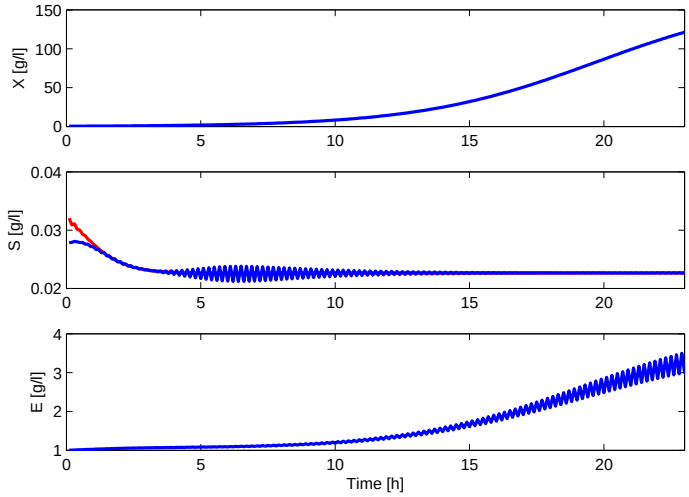

Figure 4.12: Biomass (X), substrate (S in blue and S_{sp} in red), and ethanol (E) concentrations evolutions when no respiratory capacity inhibition is considered

4.4 Simulation results

Coupling the controller (4.29) with the extremum-seeking schemes, we apply the complete loop to a small-scale simulated yeasts culture (typically $20l$ bioreactor) using model (4) with the kinetic relations (3). The initial and operating conditions are:

$X_0 = 0,4g/l$, $S_0 = 0,05g/l$, $E_0 = 1g/l$, $O_0 = O_{sat} = 0,035g/l$, $C_0 = C_{sat} = 1,286g/l$, $V_0 = 5l$ and $S_{in} = 350g/l$.

where E_0 is the initial concentration of ethanol (the yeast by-product). For the kinetic and yield parameter values, the reader is referred to Tables 2.1 and 2.2 in section 2.2.

4.4.1 Application of the bank of filters technique

The parameters of the extremum-seeking scheme and the controller (i.e., the tuning parameters) are defined, by trial and error, as follows:

$A = 0,007$, $\omega = \frac{2\pi}{0,2}h^{-1}$, $\omega_h = 0,05\omega$, $\omega_l = 1,5\omega$, $k = 100$ and $k_p = 100$.

Fig. 4.12 and 4.13 show the results when no inhibition from ethanol accumulation is considered in the reference model (that plays the role of real system). This seems to be realistic as the ethanol concentration is below $4g/l$.

However, inhibition is an important phenomenon that has to be taken into account. When included in our bioprocess model, the extremum-seeking results are as shown in Fig. 4.14 and 4.15. It is obvious that the biomass level that can be achieved is significantly affected by the presence of ethanol, despite the set-point adaptation. Note that these results are very satisfactory in view of the

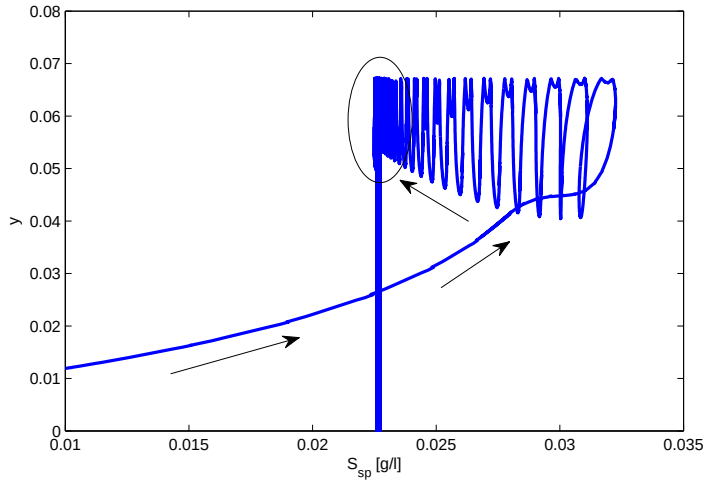

Figure 4.13: Convergence of the optimization criterion y to the optimum when no respiratory capacity inhibition is considered. The ellipse indicates the optimum-neighborhood

situation where a constant substrate concentration is regulated (see Fig. 4.1). Indeed, a small error on S_{sp} with respect to S_{crit} would lead to a dramatic accumulation or reconsumption of ethanol and biomass growth would probably be affected beyond model prediction. Moreover, the convergence rate is acceptable as S_{crit} is reached in both cases between 5 and $10h$ (to be compared with a typical batch duration of $24h$).

As it is explained in Ariyur and Krstic (2003) and Krstic and Wang (2000), the output error of the extremum-seeking algorithm achieves a local exponential convergence to an $O(A+\omega)$-neighborhood of the origin if it is assumed that we are operating around a point of zero slope. As observed in section 4.2.1 (and Fig. 4.4), the criterion doesn't present a point of zero slope as the function has discontinuous derivatives around the optimum. Despite this difficulty, we see that the algorithm converges well. However, there is clearly a source of bias in the set-point when oxygen limitations (for instance, due to a too small $k_L a_O$) and respiratory inhibition by ethanol are considered (see Fig. 4.14). Indeed, in this case, the optimum is decreasing with the respiratory capacity (as defined by (4.2c) and illustrated by Fig. 4.15). As the ethanol concentration grows, the respiratory capacity slightly decreases and, following (4.4), S_{crit} does so. To conclude this comment on estimation error, Tables 4.1 and 4.2 show the evolutions of the estimation mean errors with respect to the frequency ω when A is fixed to $0,007$ (Table 4.1) and the amplitude A when ω is fixed to $\frac{2\pi}{0,2}$ (Table 4.2).

It appears clearly from these last tables that the estimation error is decreasing as ω and A increase. More accurate studies of the estimation error are not developed in this work but are still the subject of further research.

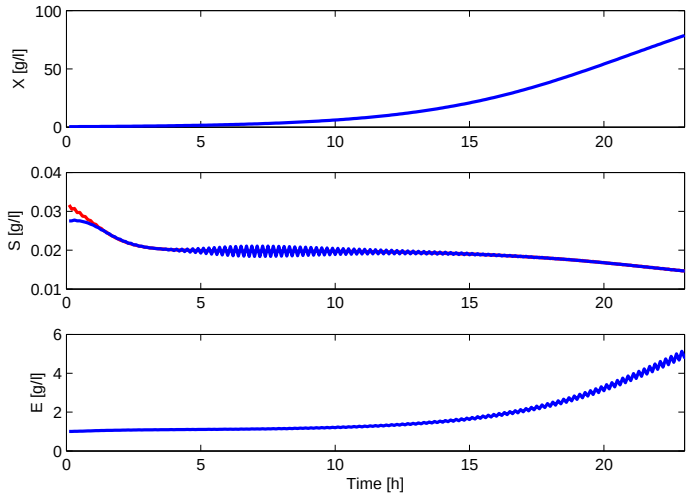

Figure 4.14: Biomass (X), substrate (S in blue and S_{sp} in red), and ethanol (E) concentrations evolutions when inhibition is considered

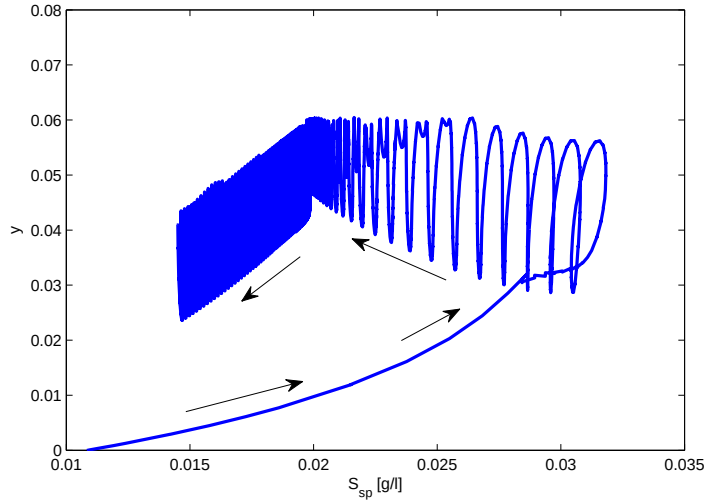

Figure 4.15: Convergence of the optimization criterion y to the optimum when inhibition is considered. The last arrow indicates the extremum move due to the ethanol-inhibited respiratory capacity

Table 4.1: Variation of the estimation mean error with respect to the dither signal frequency ω (inhibition effect included in the model)

ω	Estimation mean error $\lvert S_{sp} - S_{crit} \rvert$
$2\pi/0,2$	0,003
$2\pi/0,133$	0,0018
$2\pi/0,089$	0,0014
$2\pi/0,006$	0,0011
$2\pi/0,004$	0,0008

Table 4.2: Variation of the estimation mean error with respect to the dither signal amplitude A (inhibition effect included in the model)

A	Estimation mean error $\lvert S_{sp} - S_{crit} \rvert$
0,002	0,0267
0,004	0,0165
0,008	0,0025
0,016	0,0019
0,032	0,0014

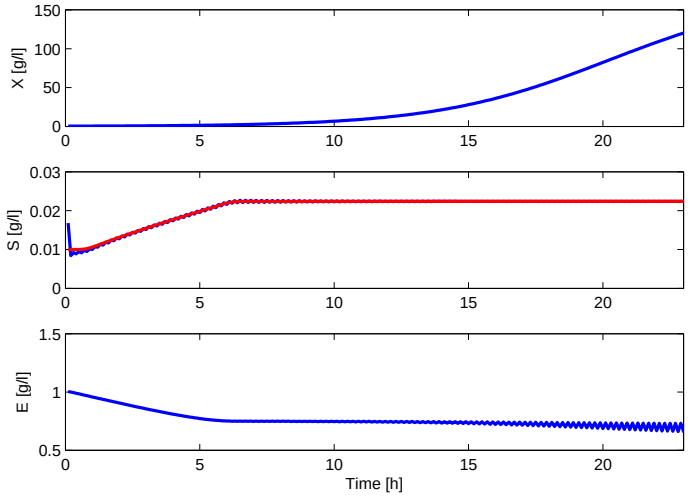

Figure 4.16: Biomass (X), substrate (S in blue and S_{sp} in red), and ethanol (E) concentrations evolutions with RLS when no inhibition is considered

4.4.2 Application of the RLS technique

The tuning parameters are defined as:

$A = 0,001, \omega = \frac{2\pi}{0,2}, k = 100, \lambda = 0,1, k_i = 0,01$ and $k_p = 100$.

The culture time is still fixed to $24h$. Fig. 4.16 and 4.17 show the results when no inhibition from ethanol accumulation is considered, and Fig. 4.18 and 4.19 when the inhibition term in (2.5b) is taken into account. In comparison with the bank of filters technique, the main observations are: (i) the convergence is clearly faster (smaller ethanol accumulation even with an initial condition on substrate 10 times higher than previously). (ii) the estimation error is smaller. When inhibition is considered as in Fig. 4.18, the expected set-point bias has less consequence on the estimation error. Note also that, in this application, the *RLS* algorithm is less computationally demanding, easier to tune than the bank of filters strategy and the convergence is achieved within the time interval of 5-10h which is quite acceptable.

Tables 4.3 and 4.4 show the evolutions of the estimation mean errors with re-

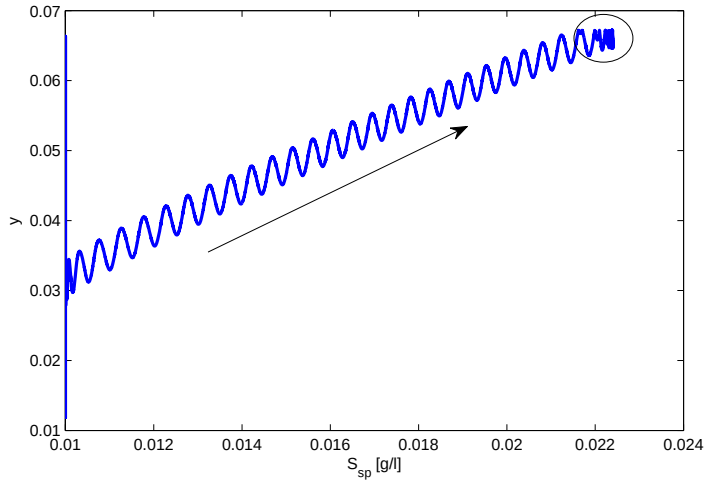

Figure 4.17: Convergence of the optimization criterion y to the optimum with RLS when inhibition is not considered

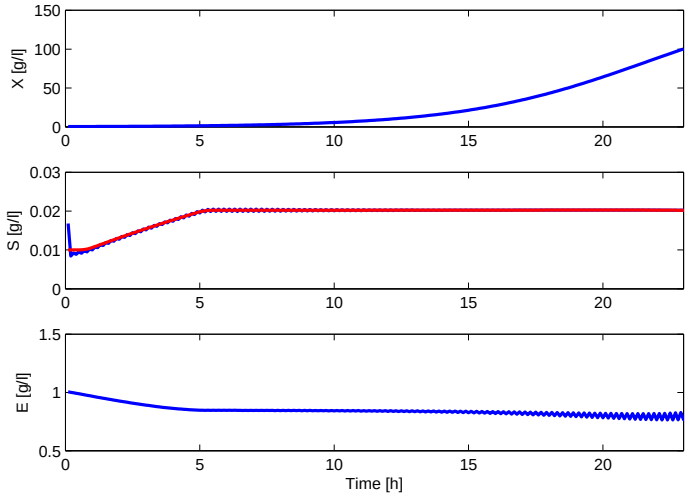

Figure 4.18: Biomass (X), substrate (S in blue and S_{sp} in red), and ethanol (E) concentrations evolutions with RLS when inhibition is considered

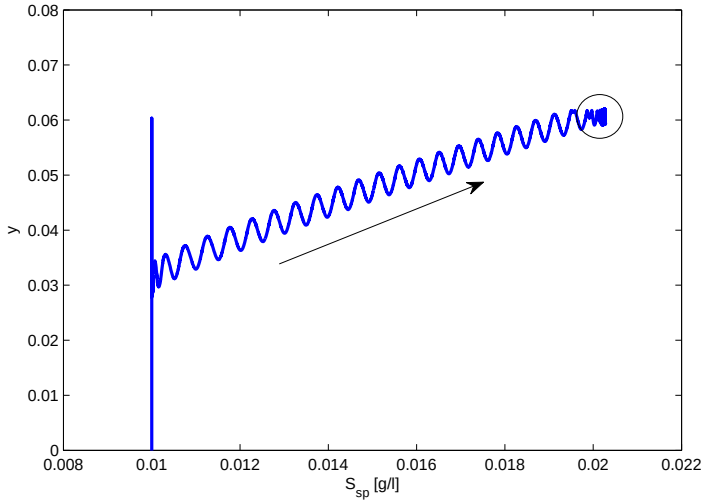

Figure 4.19: Convergence of the optimization criterion y with RLS when inhibition is considered

Table 4.3: Variation of the estimation mean error with respect to the dither signal frequency ω (inhibition effect included in the model)

ω	Estimation mean error $\lvert S_{sp} - S_{crit} \rvert$
$2\pi/0,2$	0,0011
$2\pi/0,133$	0,0012
$2\pi/0,089$	0,0014
$2\pi/0,006$	0,0018
$2\pi/0,004$	0,0029

spect to the frequency ω when A is fixed to $0,001$ (Table 4.3) and the amplitude A when ω is fixed to $\frac{2\pi}{0,2}$ (Table 4.4).

The *RLS* algorithm seems to be more sensitive to dither signal amplitude variations while the frequency seems less influent. However, note that for both techniques, A has to be kept sufficiently low for stability reasons (see section 4.3.2).

4.5 Sensitivity analysis

In this last section, a sensitivity analysis is performed first, with respect to parameter uncertainties and finally, with respect to possible noise disturbances on the input signals.

Concerning the first analysis, a random Monte-Carlo approach is applied to the k_i coefficients in (4.8). 100 runs are computed, in which a normally distributed random uncertainty error with zero mean and 5% standard deviation is applied. The results are presented, taking into account the productivity level

Table 4.4: Variation of the estimation mean error with respect to the dither signal amplitude A (inhibition effect included in the model)

A	Estimation mean error $\lvert S_{sp} - S_{crit} \rvert$
0,002	0,0007
0,004	0,0001
0,008	0,0002
0,016	0,0047
0,032	0,0084

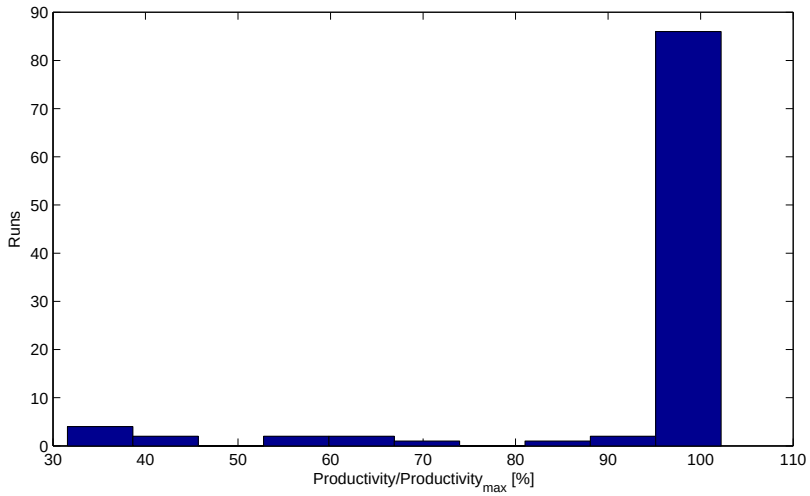

Figure 4.20: Histogram of the productivity levels provided by 100 runs using the bank of filters extremum-seeking strategy with a random parameter uncertainty normally distributed with zero mean and 5% standard deviation

defined as:

$$P_X = \frac{1}{t_f} \frac{V(t_f)X(t_f) - V_0X_0}{S_{in}(V(t_f) - V_0)} \tag{4.30}$$

where the 0 index represents the initial conditions and the batch time t_f is fixed to $23h$.

4.5.1 Sensitivity of the bank of filters strategy

Fig. 4.20 shows the histogram of the productivity levels provided by 100 runs of the bank of filters strategy. These levels are expressed in percentage with respect to the maximum level obtained with the true parameter values and which is $0,021$ g of biomass/g of feeding/h.

Obviously, 86% of the runs provide productivity levels comparable to the maximum (i.e., above 95% of the maximum obtained with perfect model values)

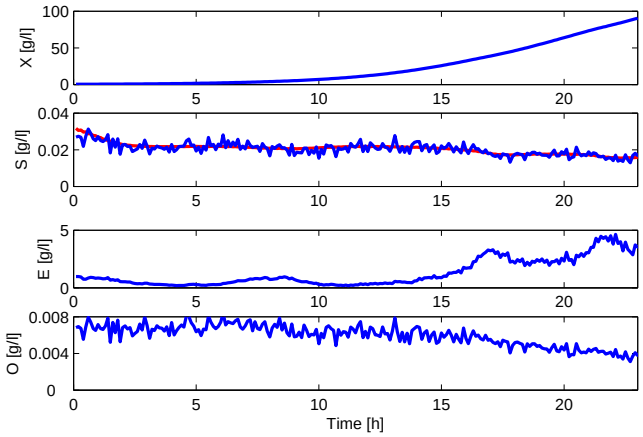

Figure 4.21: Biomass (X), substrate (S in blue and S_{sp} in red), ethanol (E) and oxygen (O) concentrations evolutions when applying noise on the input variables of the bank of filters strategy

leading to biomass concentrations included between 60 and $85 g/l$ and ethanol concentrations below $7 g/l$, which can be tolerated considering an inhibition constant (Ki_E similar to Ki_P in (2.5b)) of $10 g/l$ (see Pham (1999)). Unfortunately, 6% of the runs provide a very bad level due to an unlucky error combination of the stoichiometric parameters.

Concerning the sensitivity with respect to noise on the inputs (OTR, CTR and SIR), Fig. 4.21 and 4.22 respectively show the evolution of the main state variables and the convergence of the algorithm when a white noise of zero mean and 10% standard deviation is applied. Excepted the small decrease of the final biomass concentration, conclusions are equivalent to section 4.4. Nevertheless, the noise magnitude becomes critical once getting over 15% standard deviation and leads to dramatic ethanol concentrations which must be avoided.

4.5.2 Sensitivity of the RLS strategy

Based on the same initial and operating conditions, Fig. 4.23 shows that, regarding parameter uncertainties, the RLS strategy provides a more robust behaviour as 99% of the runs provide productivity levels comparable to the maximum (i.e., above 97% of the maximum productivity obtained with perfect model values) leading to biomass concentrations included between 60 and $110 g/l$ and ethanol concentrations below $2 g/l$. It also appears in Fig. 4.23 that the remaining run (the last percent) still provides a productivity level equal to 80% of the maximum (which, using the RLS strategy, is equal to $0,0222$ g of biomass/g of feeding/h).

Then, white noise with zero mean and 20% standard deviation (i.e., twice as much as the noise standard deviation applied to the bank of filters strategy) is applied to the input variables. From the obvious results shown in Fig. 4.24 and 4.25, it can be concluded that the RLS strategy definitely appears as not only more efficient but also more robust than the bank of filters for the considered

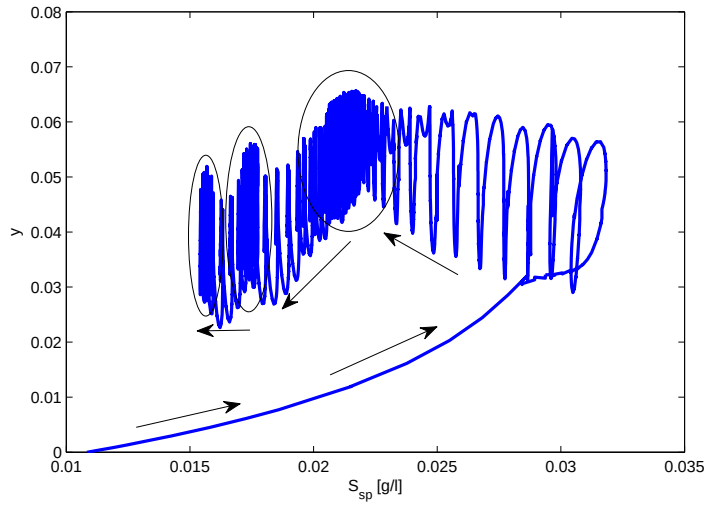

Figure 4.22: Convergence of the optimization criterion y to the optimum when applying noise on the input variables of the bank of filters strategy. The arrows and ellipses indicate the extremum move due to the ethanol-inhibited respiratory capacity

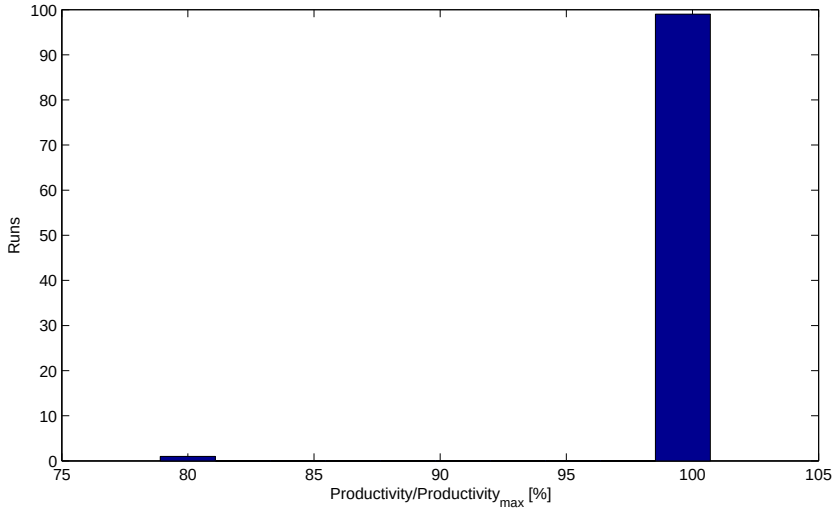

Figure 4.23: Histogram of the productivity levels provided by 100 runs using the *RLS* extremum-seeking strategy with a random parameter uncertainty normally distributed with zero mean and 5% standard deviation

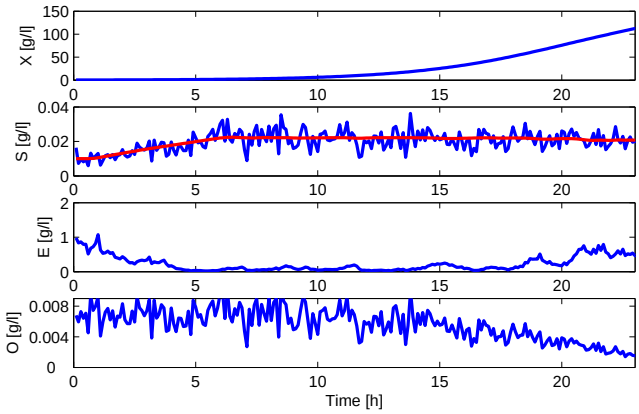

Figure 4.24: Biomass (X), substrate (S in blue and S_{sp} in red), ethanol (E) and oxygen (O) concentrations evolutions when applying noise on the input variables of the RLS strategy

application.

4.6 Model based vs model-free strategies

In this section, a model-based extremum-seeking strategy is presented. This technique lies on Lyapunov stability arguments, as depicted in the literature (see Titica et al. (2003a), Guay and Zhang (2003), Betancur et al. (2004), Marcos et al. (2004)). First, an introductive review of the method is achieved and illustrated by simulation results using a model of microbial growth as in Titica et al. (2003a). Then, an application of the method to the yeast model (2.13) is performed and ends this last section dedicated to extremum-seeking strategies.

4.6.1 An adaptive model-based extremum-seeking strategy

In the study of Titica et al. (2003a), the fed-batch microbial growth model presenting a gazeous by-product, is depicted by the following mass-balances:

$$\frac{dX}{dt} = \mu X - DX \tag{4.31a}$$

$$\frac{dS}{dt} = -k_1 \mu X + D(S - S_{in}) \tag{4.31b}$$

$$\phi_P = k_2 \mu X \tag{4.31c}$$

$$\frac{dV}{dt} = DV \tag{4.31d}$$

where the states X (g/l) and S (g/l) are respectively the biomass and substrate concentrations, μ (h^{-1}) is the specific growth rate, $D = \frac{F}{V}$ (h^{-1}) dilution rate,

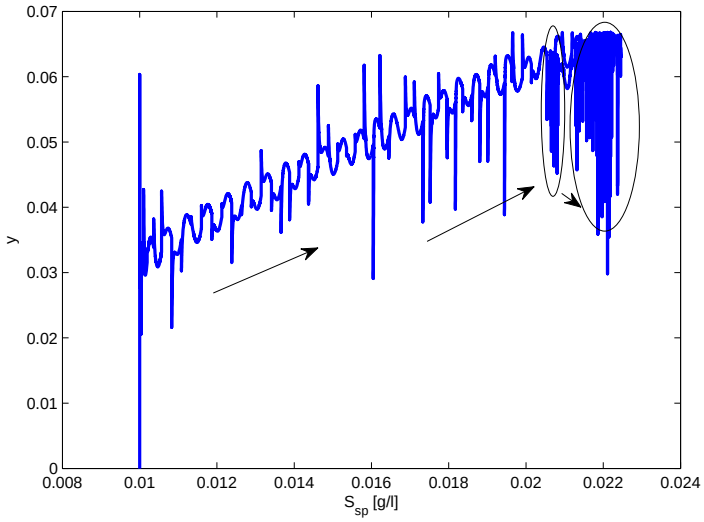

Figure 4.25: Convergence of the optimization criterion y to the optimum when applying noise on the input variables of the RLS strategy. The arrows and ellipses indicate the extremum-zone move due to the ethanol-inhibited respiratory capacity

$\phi_P(g/l/h)$ the by-product production rate, S_{in} the substrate concentration in the feed medium, $F(l/h)$ the inlet feed rate and $V(l)$ the culture medium volume.

The specific growth rate is approximated by a continuous Haldane law of the form:

$$\mu = \frac{\mu_0 S}{K_S + S + \frac{S^2}{K_I}} \tag{4.32}$$

where μ_0 is a constant linked to the maximum value of the specific growth rate μ^*, K_S the saturation constant and K_I the inhibition constant. Fig. 4.26 shows this typical fed-batch culture kinetic law when the cells growth rate present an inhibition on substrate. The maximum specific growth rate is reached if $S = S_{crit} = \sqrt{K_S K_I}$. Beyond this value, the specific growth rate enters in an inhibition zone and decreases as the substrate concentration increases.

Thus, in order to maximize the productivity, the substrate concentration should be controlled at the constant value S_{crit}. Unfortunately, K_S and K_I are generally unknown, so that an adaptive control algorithm based on an extremum-seeking strategy is proposed in order to recover S_{crit}. The controlled variable is, of course, still the dilution rate D. The following rewriting of the Haldane parameters is now proposed:

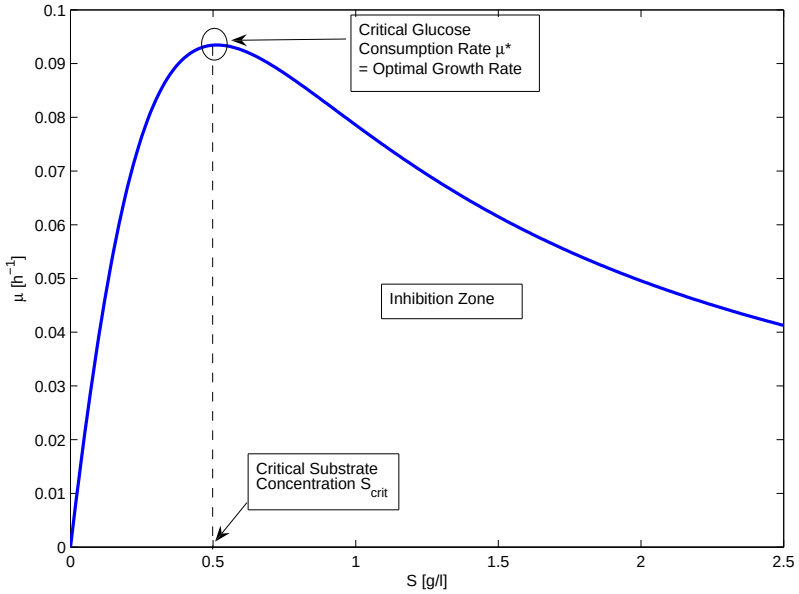

Figure 4.26: Haldane kinetic law

$$\theta_\mu = \frac{\mu_0}{K_S} \tag{4.33a}$$

$$\theta_S = \frac{1}{K_S} \tag{4.33b}$$

$$\theta_I = \frac{1}{K_S K_I} \tag{4.33c}$$

Practically, ϕ_P can't be measured but combining (4.31b) and (4.31c), an estimator of ϕ_P can be built as follows:

$$\begin{aligned} \frac{d\hat{\phi}_P}{dt} = & \frac{1-\hat{\theta}_I S^2}{S(1+\hat{\theta}_S S+\hat{\theta}_I S^2)} \left[D(S_i - S) - \theta_k \phi_P\right] \phi_P \\ & + \frac{\hat{\theta}_\mu S \phi_P}{1+\hat{\theta}_S+\hat{\theta}_I S^2} - D\phi_P + k_{\phi_P} e_{\phi_P} \end{aligned} \tag{4.34}$$

where $k_{\phi_P} > 0$, $e_{\phi_P} = \phi_P - \hat{\phi}_P$ and $\theta_k = \frac{k_1}{k_2}$ (which is known).

Following the definition (4.33c) of θ_I, the desired set-point can be expressed as $S_{crit} = \frac{1}{\sqrt{\hat{\theta}_I}}$. As this last parameter is unknown, a periodic dither signal $d(t)$ is added to the input signal in order to fill a persistent excitation condition (PE, see Titica et al. (2003a)) comparable to (4.17), ensuring that the adaptive scheme converges to the true sought value of $\hat{\theta}_I$ leading, finally, to the optimal biological value S_{crit}.

A control error variable Z_s comparable to (4.22) is now defined:

$$Z_s = S - \frac{1}{\sqrt{\hat{\theta}_I}} - d(t) \tag{4.35}$$

Reasoning as in (4.24) and (4.26), we obtain:

$$V = \frac{Z_s^2}{2} + \frac{1}{2}\left(\frac{\tilde{\theta}_\mu^2}{\gamma_\mu} + \frac{\tilde{\theta}_S^2}{\gamma_S} + \frac{\tilde{\theta}_I^2}{\gamma_I}\right) + \frac{e_{\phi_P}^2}{2}(1 + \theta_S S + \theta_I S^2) \tag{4.36}$$

The control law estabished by Titica et al. (2003a). is then:

$$D = \frac{1}{(S_{in} - S)}\left[-k_z Z_s + \theta_k \hat{\phi}_P + a - k_d d\right] \tag{4.37}$$

where k_z (k_p in (4.26)) is the proportionnal error gain and k_d a new tuning parameter of $d(t)$, defined as:

$$\dot{d}(t) = a(t) + \frac{1}{2}\hat{\theta}_I^{-\frac{3}{2}}\frac{d\hat{\theta}_I}{dt} - k_d d(t) \tag{4.38}$$

where $a(t)$ is called the "closed-loop" dither signal, the part of (4.38) that is designed by the user, while the remaining part corresponds to a mathematical exploitation leading to an input of the form of (4.37). The convergence analysis based on (4.36), using a judicious choice of the adaptive laws for θ_μ, θ_S and θ_I, are somewhat complex so that it is recommanded to consult Titica et al. (2003a) for further details.

Simulation results are presented in Fig. 4.27 and 4.28 where the kinetic parameters true values are:

$\mu_0 = 0.53h^{-1}$, $K_S = 1.2g/l$, $K_I = 0.22g/l$, $k_1 = 0.4$ et $k_2 = 1.0$.

Initial and operating conditions are:

$S_0 = 2.0g/l$, $X_0 = 7.2g/l$, $V_0 = 1.0l$ and $S_{in} = 20g/l$.

The chosen sampling period is $30min$, which taking into account the slow system dynamics, is acceptable. So is the convergence rate (within 5 and 10 h).

The main difference between this model and (2.13), excepted the continuous form of its kinetics, is the assumption of a perfect cell oxygenation without byproduct inhibition inducing the S_{crit} value, considered here as constant.

4.6.2 A particular model-based extremum-seeking design for yeast fed-batch cultures

Borrowing the last extremum-seeking structure from Titica et al. (2003a), another alternative than (4.8) to solve the problem of parameter uncertainties in

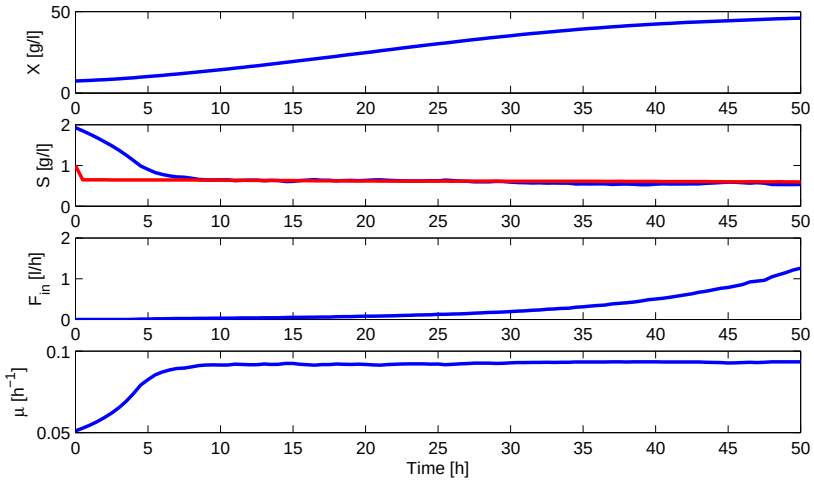

Figure 4.27: Simulation results of the model-based extremum-seeking strategy applied to microbial growth: biomass concentration, substrate concentration, feed flow rate and specific growth rate evolutions

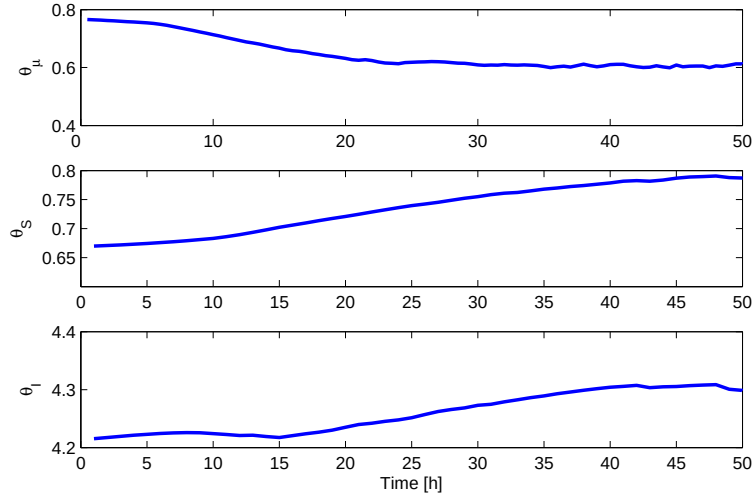

Figure 4.28: Simulation results of the model-based extremum-seeking strategy applied to microbial growth: evolutions of the adapted parameters θ_μ, θ_S and θ_I

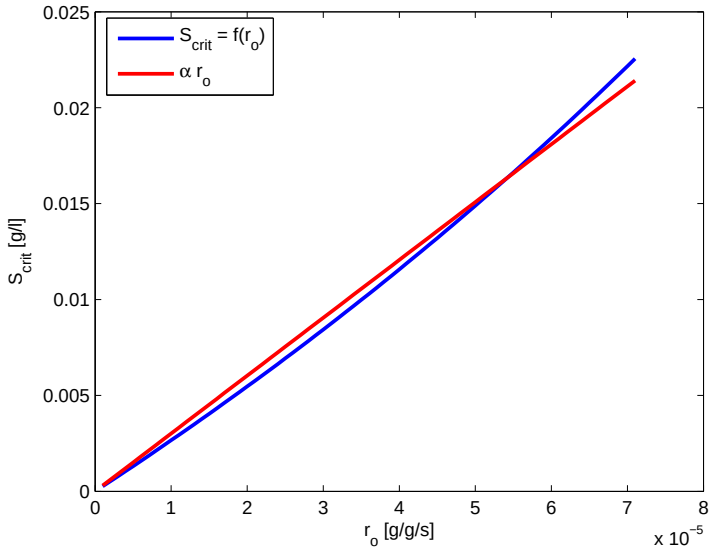

Figure 4.29: Linear approximation of $S_{crit} = f(r_O)$

(4.4) is now proposed, considering a state-dependent S_{crit} (i.e., a critical substrate concentration, function of the cells oxygenation as suggested in the perspectives of Titica et al. (2003a)). As the order of r_O is clearly smaller than $k_{os}\mu_S$ (for instance, in yeast culture, $r_{Omax} = \mu_O = O(10^{-1})$ and $k_{os}\mu_S = O(10^0)$), we propose to approximate (4.4) by the following expression:

$$S_{crit} \approx \frac{K_S}{k_{os}\mu_S} r_O = \alpha r_O \tag{4.39}$$

where α is a positive parameter which has to be adapted during the batch (as a modelling exercise, a residual mean error of 0.2% is obtained after a linear regression applied to (4.4) demonstrating the quality of a first-order approximation - see Fig. 4.29).

Redefining the control error variable as:

$$Z_S = k_p(S - S_{crit}) + k_i \int (S - S_{crit})dt - d \tag{4.40}$$

where k_p and k_i are positive tuning parameters,

$$\tilde{\nu} = \nu - \hat{\nu} \tag{4.41}$$

The estimation error on ν, and

$$\tilde{\alpha} = \alpha - \hat{\alpha} \tag{4.42}$$

the estimation error on α, we consider the following new Lyapunov function:

$$V = \frac{1}{2}Z_S^2 + \frac{1}{2\gamma}\tilde{v}^2 + \frac{1}{2\gamma_S}\tilde{\alpha}^2 \tag{4.43}$$

where γ and γ_S are strictly positive tuning parameters.

A stabilizing controller is obtained following the same steps going from (4.36) to (4.38), that is, forcing $\dot{V}$ to be negative as in:

$$\dot{V} = -k_z Z_S^2 \tag{4.44}$$

where k_z is a strictly positive tuning parameter. And so, provided that:

$$\dot{\hat{v}} = -\gamma k_p Z_S X \tag{4.45a}$$
$$\dot{\hat{\alpha}} = -\gamma_S Z_S (k_p \dot{r}_O + k_i r_O) \tag{4.45b}$$
$$\hat{S}_{crit} = \hat{\alpha} r_O \tag{4.45c}$$

Finally, the control law is given by:

$$D = \frac{\left[\frac{k_z Z_S - a + k_d d}{k_p} - \hat{v}X\right]}{S - S_{in}} \tag{4.46}$$

with a dither signal chosen as:

$$\dot{d} = a + k_i(S - \hat{\alpha} r_O) - k_p \hat{\alpha} \dot{r}_O - k_d d \tag{4.47}$$

where a is a closed-loop excitation signal and k_d is a new strictly positive parameter.

Simulation results of the application of the model-based extremum-seeking strategy to the yeast model

In this section, we apply the controller designed in section 4.6.2 to a simulated case-study corresponding to classical small-scale (20 l bioreactor) culture conditions. The initial and operational conditions are:

$X_0 = 0.4 g/l$, $S_0 = 0.5 g/l$, $E_0 = 3 g/l$, $O_0 = O_{sat} = 0.007 g/l$, $C_0 = C_{sat} = 1.286 g/l$, $V_0 = 6.8 l$, $S_{in} = 350 g/l$

For the kinetic and yield parameter values, the reader is referred to section 2.2.

The selection of an appropriate dither signal is based on a persistent excitation (PE) condition (Guay and Zhang (2003), Marcos et al. (2004), Adetola and Guay (2006)) which, once fulfilled, ensures the asymptotic convergence of the parameter estimates.

The excitation signal is here chosen as a simple sum of sinusoidal signals of the form:

Parameter	Value	Unit
γ_S	10	/
γ	10^{-7}	/
k_p	15	/
k_i	0.004	/
k_z	0.0015 X	/
k_d	0.01	/
ω_i	$\frac{2\pi\ i}{4000}$	rad/s

Table 4.5: Tuning parameter values.

$$a = \sum_{i=1}^{5} A_i sin(\omega_i\ t) \tag{4.48}$$

where A_i are normally distributed random numbers contained in $[-5\ 10^{-4}, 5\ 10^{-4}]$ and ω_i are the pulsations.

The initial substrate and ethanol concentrations are chosen at high values, so as to challenge (in a difficult situation) the controller convergence speed. Figures 4.30, 4.31 and 4.32 present the simulation results. The substrate concentration evolution (Figure 4.30) shows that the presence of ethanol at the beginning of the batch causes a decrease of the critical substrate concentration level. An adaptation of this critical substrate concentration is then needed so as to avoid an increased production of ethanol (due to the excess of substrate) and a serious inhibition of cell growth. At the end of the batch, ethanol is almost completely consumed so that the system is driven close to the optimum (see Figure 4.32). Figure 4.31 also shows the evolution of the feed rate F_{in}. $\hat{v}$ converges to its true value, so as $\hat{\alpha}$ through a judicious choice of the value of γ_S (see Table 4.5) as the convergence is generally very slow. The productivity is quite satisfactory as more than $150 g/l$ of biomass are obtained within less than 40 hours, despite the high initial concentrations in substrate and ethanol.

The main drawback of this control strategy is the delicate choice of the tuning parameters, depending on the initial and operating conditions. This problem originates in the presence of the error control variable Z_S as a factor in (4.45b). If the substrate concentration quickly converges to its setpoint, i.e. the controller works efficiently and Z_S vanishes, the convergence of α is significantly affected. In turn, if the critical substrate level is overestimated, the control action can lead to the production of ethanol, and as a consequence, the inhibition of the respiratory capacity and a further decrease of the critical substrate level. With a bad choice of the tuning parameters, the biomass growth can therefore be seriously inhibited.

A simple way round this problem is to systematically underestimate the critical substrate level. This can be achieved by considering a lower linear approximation, i.e. a linear function below the real curve $S_{crit}(r_O)$ in the classical operating area (very low values of r_O are never reached in a controlled process). For instance, if we impose the point $(\mu_O, 0.02)$ to belong to this approximation (cfr Figure 4.33), the adaptation law of α is now the following one:

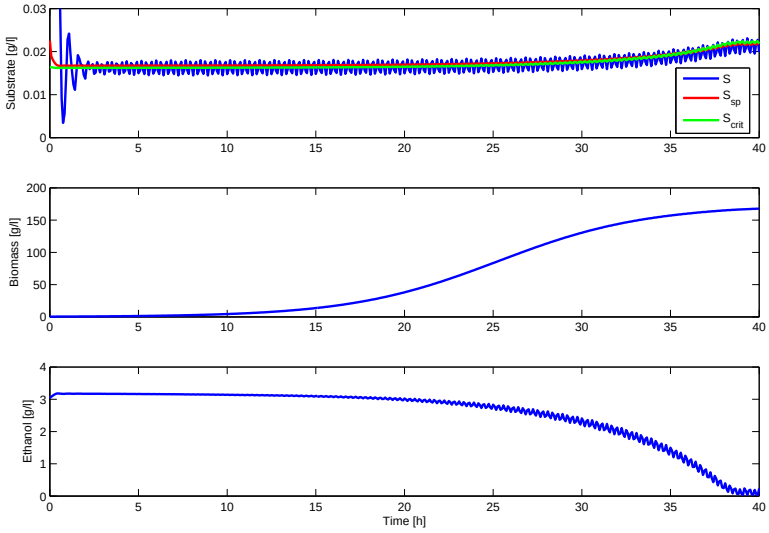

Figure 4.30: Substrate (S, S_{sp} and S_{crit}), biomass (X) and ethanol (E) concentrations evolutions

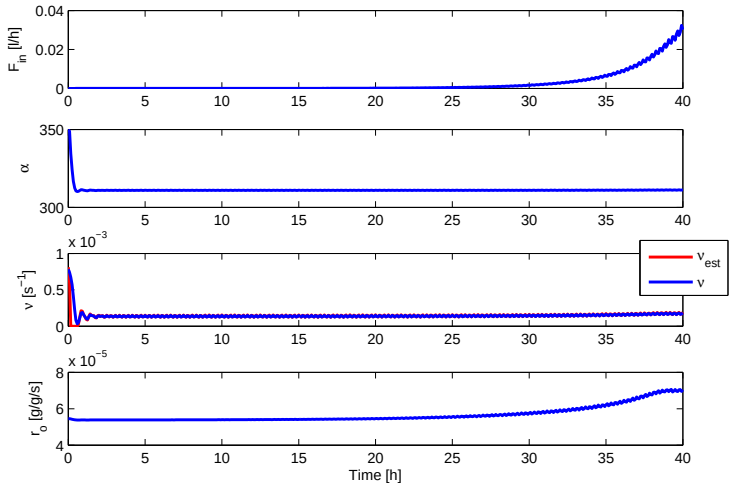

Figure 4.31: Feed rate (F_{in}, α and ν parameters, and respiratory capacity (r_o) evolutions.

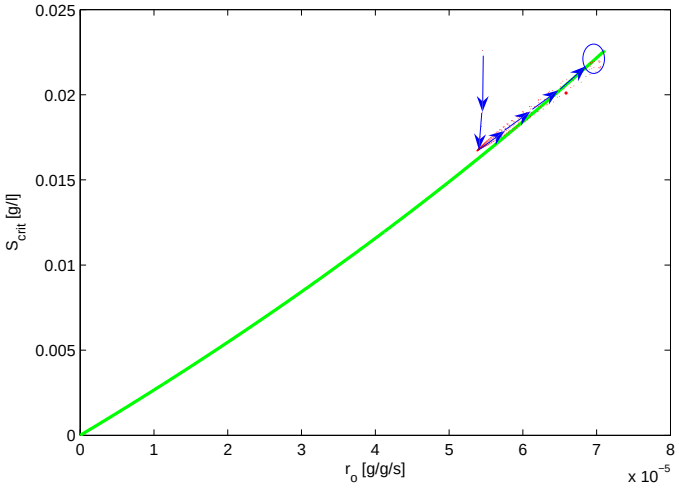

Figure 4.32: Representation of the algorithm convergence through the evolution of S_{crit} as a function of r_O

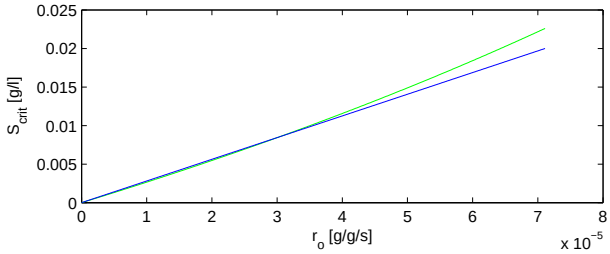

Figure 4.33: S_{crit} as a function of r_O (in green) and reduced approximation (in blue).

$$\bar{S}_{crit} = \bar{\alpha} r_O \tag{4.49}$$

where $\bar{S}_{crit}$ and $\bar{\alpha}$ are the lower values of S_{crit} and α. α is thus equal to $\frac{0.02}{\mu_O}$.

Figure 4.34 shows simulation results using this modified strategy. The performance is now much more robust to the initial and operating conditions. The dither signal is simplified in $a = Asin(\omega\, t)$ since ν is now the only parameter to be estimated ($A = 0.0005$ and $\omega = \frac{2\pi}{1000}$).

4.7 Conclusion

The high productivity of fed-batch cultures using genetically modified strains exhibiting overflow metabolism relies on a double condition: an optimal feeding strategy and the implied limitation of the inhibiting by-product formation. To this end, an adaptive controller using two different non-model based extremum-seeking strategies is designed for a general case of overflow metabolized strain and is applied to the particular case of *S. cerevisiae*. The tracking of

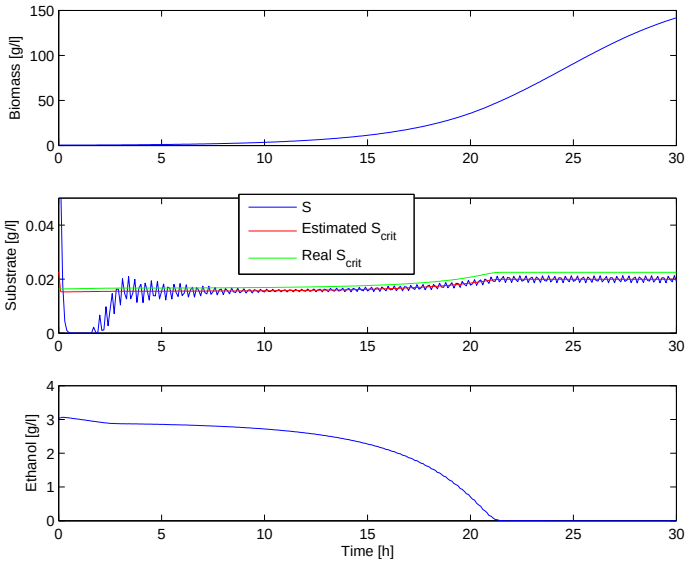

Figure 4.34: Biomass (X), Substrate (S, $\bar{S}_{crit}$ and S_{crit}), and ethanol (E) concentrations evolutions

the critical substrate level, representing the optimum, is correctly performed by both extremum-seeking techniques, limiting the ethanol accumulation despite the considerations of an ethanol-inhibited respiratory capacity and discontinuous derivatives around the optimum. Moreover, the recursive least squares strategy shows better performances and robustness facing parameter uncertainties and noise disturbances.
A model-based extremum-seeking strategy is then designed. Based on Lyapunov stability arguments, original adaptation laws are derived to estimate on-line unknown kinetic parameters. Finally, a simplified strategy is proposed, which provides a more robust estimation of the critical substrate level. Unfortunately, even if the substrate critical level can be estimated through (4.4) with the oxygen and byproduct measurements, the substrate concentration measurement is a difficult task as the order of concentration levels (for instance, $O(10^{-2}) to O(10^{-1}) g/l$ for *S. cerevisiae* and *E. coli*) are below or, at least, sometimes judged too close to the resolution of currently available probes ($O(10^{-1})$). Therefore, extremum-seeking strategies appear as a very helpful tool if the practical conditions allow an accurate output measurement or observation, which is not always the case. An alternative solution must then be elaborated in the worst case of insufficient output measurement (or observation) accuracy. This solution is part of this work and is the next chapter topic.

Chapter 5

A Practical Suboptimal Strategy

5.1 Introduction

In this section, the attention is focused on the consequences of practical limitations as explained in section (4.7). Indeed, expensive cost of hardware probes, possible inaccuracy of those ones or even software probes (for instance, with respect to the measurement order) or, simply, their inexistence (due to unfeasibility), may lead the practician to reconsider a bit lower the real process maximum yield. Non-modeled or neglected biological phenomenons are also sometimes acting in this direction. For instance, some genetically modified cells strains may be less tolerant than others to metabolic switches which must therefore be limited, making strategies like extremum-seeking dangerous for their well-behave. However, in this particular case, a theoretically suboptimal but still efficient strategy can be elaborated on the basis of a control structure taking the following main observations into account:

- The most evident choice of a manipulated variable in a fed-batch system is the feed flow rate F_{in}. Considering that we are looking for the simplest way of modeling the bioreactor, we assume that F_{in} appears as the sole input of the system.
- As explained in Valentinotti et al. (2003), the maximum of productivity is obtained at the edge between the respirative and respiro-fermentative regimes, where the quantity of byproduct is constant and equal to zero ($VP = 0$, see Fig. 2.4). Unfortunately, evaluating accurately the volume is a difficult task as it depends on the inlet and outlet flows including F_{in} but also the added base quantity for pH control and several gas flow rates. Moreover, maintaining the quantity of by-product constant in a fed-batch process means that the by-product concentration has to decrease while the volume increases. So, even if the volume is correctly measured, VP

becomes unmeasurable once P reaches the sensitivity level of the by-product probe. For those practical limitations, a sub-optimal strategy is elaborated through the control of the by-product concentration around a low value depending on the sensitivity of commercially available probes (for instance, a general order for ethanol probe is $0.1g/l$), and requiring only an estimation of the volume by integration of the feed rate.

The basic principle of the controller is thus to regulate the by-product at a constant low setpoint, leading to a self-optimizing control in the sense of Skogestad (2004) and ensuring that the culture operates in the respiro-fermentative regime, close to the biological optimum, i.e., close to the edge with the respirative regime.

After those observations, the control framework must be chosen in accordance with the process requirements in terms of adaptation and/or robustness. For instance, linear control framework generally makes the design of robust controllers easier than in a nonlinear framework.

Although the first part of the following section is devoted to a linearizing control strategy offering an original robust gain design using *LMIs* (Coutinho et al. (2008)), the second part of this section is therefore devoted to the design of an original robust linear *RST* controller (Valentinotti et al. (2004), Renard and Wouwer (2008)) using the observer polynomial.

5.2 Linearizing control: a comparison of adaptive and robust strategies

Even if its name does not suggest it, the linearizing control strategy is indeed an adaptive nonlinear strategy which is widely applied to bioprocesses (Bastin and Dochain (1990)). However, linearizing control requires the knowledge of an accurate model, and on-line parametric adaptation is usually implemented so as to ensure performance. Whereas parametric adaptation is a simple approach, it does not guarantee stability in the presence of unmodeled dynamics. Chen et al. (1995) and Pomerleau (1990) demonstrated its usefulness in an industrial application context of yeast fed-batch cultures. Their respective algorithms are based on the alleviation of time-varying model uncertainties (especially kinetic uncertainties) by the use of a few state measurements and judicious parameter adaptation schemes related to Lyapunov stability theory. In this study, another approach is also considered, which is based on nonlinear robust control and the used of Linear Matrix Inequalities (LMIs) to design the free linear dynamics so as to ensure robust stability and performance. A comparison of the adaptive and robust control approaches is provided in terms of implementation, and simulation tests show the respective advantages and limitations of both strategies.

The component-wise mass balances of reaction scheme (2.3) lead to the following state-space representation

$$\dot{x} = Kr(x)X + Ax - ux + B(u) \tag{5.1}$$

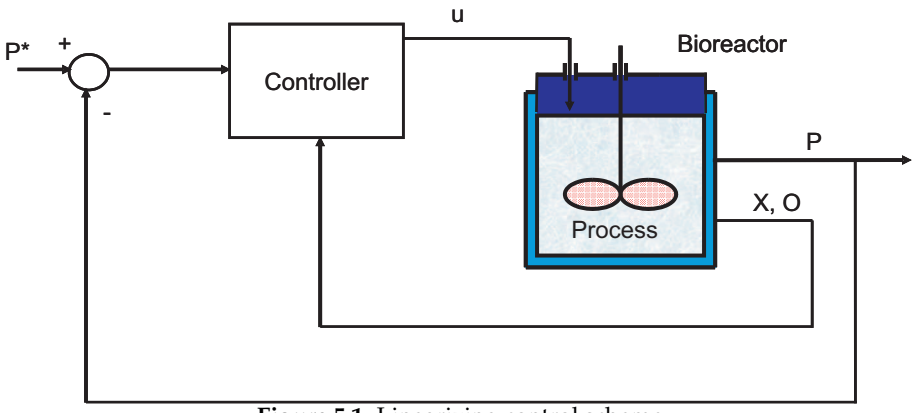

Figure 5.1: Linearizing control scheme.

where $x = [\ X \quad S \quad P \quad O \quad C \quad V\ ]'$ is the state vector, $r(x) = [\ r_1 \quad r_2 \quad r_3\ ]'$ is the vector of reaction rates, and $u = D = F_{in}/V$ is the control input (the dilution rate). The matrices K and A, and the vector function $B(\cdot)$ are given by:

$$K = \begin{bmatrix} k_{X1} & k_{X2} & k_{X3} \\ -k_{S1} & -k_{S2} & 0 \\ 0 & k_{P2} & -k_{P3} \\ -k_{O1} & -k_{O2} & -k_{O3} \\ k_{C1} & k_{C2} & k_{C3} \\ 0 & 0 & 0 \end{bmatrix}, \; B(u) = \begin{bmatrix} 0 \\ S_{in}\, u \\ 0 \\ k_L a_O\, O_{sat} \\ k_L a_C\, C_{sat} \\ 0 \end{bmatrix}, \tag{5.2}$$

$$A = \begin{bmatrix} 0_{3\times3} & 0_{3\times2} & 0_{3\times1} \\ 0_{2\times2} & -[k_L a_O\ k_L a_C]\ I_{2\times2} & 0_{2\times2} \\ 0_{1\times3} & 0_{1\times2} & 0 \end{bmatrix},$$

A feedback linearizing controller is illustrated in Figure 5.1. In a first step, this controller is derived assuming a perfect process knowledge. The basic idea is to derive a nonlinear controller, which allows a linearization of the process behavior (Chen et al. (1995), Pomerleau (1990)).

As the theoretical value of S_{crit} is very small (below 0.1 g/l) and assuming a quasi-steady state of S (i.e. considering that there is no accumulation of glucose when operating the bioreactor in the neighborhood of the optimal operating conditions), the small quantity of substrate VS is almost instantaneously consumed by the cells ($\frac{d(VS)}{dt} \approx 0$ and $S \approx 0$) and (2.6b) becomes:

$$r_2 X = -\frac{k_{S1} r_1 X + S_{in} u}{k_{S2}} \tag{5.3}$$

where r_1 and r_2 are nonlinear functions of S, P and O as given by (2.4a-2.4b).

Replacing $r_2 X$ by (5.3) in the mass balance equation for P (2.6c), we obtain:

$$\dot{P} = -\frac{k_{P2} k_{S1}}{k_{S2}} r_1 X - k_{P3} r_3 X - u\left(P - \frac{k_{P2}}{k_{S2}} S_{in}\right) \tag{5.4}$$

A first-order linear reference model is imposed:

$$\frac{d(P^* - P)}{dt} = -\lambda(P^* - P)\,, \; \lambda > 0 \tag{5.5}$$

and a constant setpoint is considered so that:

$$\frac{dP}{dt} = \lambda(P^* - P)\ ,\ \lambda > 0 \tag{5.6}$$

Equating (5.6) and (5.4), the following control law is obtained:

$$F_{in} = V\frac{\lambda(P^* - P) + (\frac{k_{P2}k_{S1}}{k_{S2}}r_1 + k_{P3}r_3)X}{\frac{k_{P2}}{k_{S2}}S_{in} - P} \tag{5.7}$$

where $\frac{k_{P2}k_{S1}}{k_{S2}}r_1$ and $k_{P3}r_3$, the kinetic expressions, contain several uncertain parameters.

5.2.1 A classical adaptive strategy

In Chen et al. (1995), the parameter uncertainties are handled using an on-line estimation of the kinetic term $\frac{k_{P2}k_{S1}}{k_{S2}}r_1 + k_{P3}r_3$ in the linearizing control law (5.7). In this study, the biomass concentration X is supposed to be measured using a probe (for instance an optical density probe or a conductance probe, which are nowadays widely available but still expensive. However, note that software sensors as described in chapters 2 and 3 could also be used), whereas in Chen et al. (1995), an asymptotic observer is used to estimate this component concentration. The following adaptive scheme is therefore a simplified version of the original algorithm.

$$F_{in} = V\frac{\lambda(P^* - P) + \hat{\nu}X}{\frac{k_{P2}}{k_{S2}}S_{in} - P} \tag{5.8}$$

A direct adaptive scheme as described in Bastin and Dochain (1990) is used. Consider the following Lyapunov function candidate:

$$V(t) = \frac{1}{2}\left(\tilde{P}^2 + \frac{\tilde{\nu}^2}{\gamma}\right) \tag{5.9}$$

where $\tilde{P} = P^* - P$, $\tilde{\nu} = \nu - \hat{\nu}$ and γ is a strictly positive scalar. The specific growth rates r_1 and r_3 (and, of course, the pseudo-stoichiometric coefficients k_{P2}, k_{S1}, k_{S2} and k_{P3}) are assumed to be constant so that ν variations are negligible ($\frac{d\nu}{dt} = 0$).

Using the Lyapunov stability theory, the time derivative of the Lyapunov candidate function should be negative for the closed-loop system to be stable:

$$\frac{dV}{dt} = \frac{d\tilde{P}}{dt}\tilde{P} + \tilde{\nu}\frac{d\tilde{\nu}}{dt}\frac{1}{\gamma} \tag{5.10}$$

Considering (5.6) and a possible parameter mismatch ($\hat{\nu} \neq \nu$):

$$\frac{d\tilde{P}}{dt} = -\lambda\tilde{P} - \tilde{\nu}X \tag{5.11}$$

so that (5.10) becomes:

$$\frac{dV}{dt} = -\lambda \tilde{P}^2 - \tilde{P}\tilde{\nu}X - \tilde{\nu}\frac{d\hat{\nu}}{dt}\frac{1}{\gamma} \tag{5.12}$$

Choosing the following ν adaptive law cancels the second and the third terms:

$$\frac{d\hat{\nu}}{dt} = \gamma X \tilde{P} \tag{5.13}$$

5.2.2 A robust strategy

Structural and parametric uncertainties can be lumped into a global parametric error:

$$\delta = \bar{\nu} - \nu \tag{5.14}$$

where δ is a nonlinear function of (S, P, O) representing possible inexact cancelations of nonlinear terms due to model uncertainties and $\bar{\nu}$ represents the hypothetical exact unknown value. Rewriting the kinetic term in (5.8) using the new expression taken from (5.14), we obtain:

$$u = F_{in} = V\frac{\lambda(P^* - P) + \bar{\nu}X - \delta X}{\frac{k_{P2}}{k_{S2}}S_{in} - P} \tag{5.15}$$

which corresponds to the perturbed reference system:

$$\dot{P} = \lambda(P^* - P) - \delta X \tag{5.16}$$

Borrowing the ideas of the Quasi-LPV approach (Leith and Leithead (2000)), we bound the time-varying parameter δ which is supposed to belong to a known set $\Delta := \{\delta : \underline{\delta} \leq \delta \leq \overline{\delta}\}$ with $\underline{\delta}$ and $\overline{\delta}$ respectively representing the minimal and maximal admissible uncertainties.

The parameter λ is designed to ensure some robustness and tracking performance to the overall closed-loop system, which is modeled as follows:

$$\mathcal{M} : \left\{ \begin{array}{rcl} \dot{P} & = & -\lambda z - \delta X \\ z & = & P^* - P \end{array} \right. \tag{5.17}$$

where $z = P^* - P$ is the performance output.

Let $w = \left[\begin{array}{cc} P^* & X \end{array} \right]' \subset \mathcal{L}_{2,[0,T]}$ be the disturbance input to the system $\mathcal{M}$, $a(\lambda, \delta) = \left[\begin{array}{cc} \lambda & -\delta \end{array} \right]$ and $c = \left[\begin{array}{cc} 1 & 0 \end{array} \right]$. The closed-loop system (5.17) can be rewritten:

$$\mathcal{M} : \left\{ \begin{array}{rcl} \dot{P} & = & -\lambda P + a(\lambda, \delta)w \\ z & = & -P + c\,w\,,\ \delta \in \Delta \end{array} \right. \tag{5.18}$$

Consider the finite horizon (for instance, between the instant 0 and the time T) $\mathcal{L}_2$-gain of system $\mathcal{M}$ (Green and Limebeer (1994)), representing the worst-case of the ratio of $\|z\|_{2,[0,T]}$ (i.e., the finite horizon 2-norm of the tracking error) and $\|w\|_{2,[0,T]}$ (i.e., the finite horizon 2-norm of the disturbance input), which is defined as:

$$\|\mathcal{M}_{wz}\|_{\infty,[0,T]} = \sup_{\delta \in \Delta, 0 \neq w \subset \mathcal{L}_{2,[0,T]}} \frac{\|z\|_{2,[0,T]}}{\|w\|_{2,[0,T]}} \tag{5.19}$$

Thus, the parameter λ is designed based on the $\mathcal{H}_\infty$ control theory (Green and Limebeer (1994),Skogestad and Postlethwaite (2001)). Let $\alpha > 0$ be an upper limiting of $\|\mathcal{M}_{wz}\|_{\infty,[0,T]}$. Thus, the problem is to find α such that:

$$\min_{\lambda,\delta\in\Delta} \alpha : \|\mathcal{M}_{wz}\|_{\infty,[0,T]} \leq \alpha \tag{5.20}$$

while ensuring the robust stability of system (5.18).

This optimization problem can be written in terms of linear matrix inequalities (*LMIs*) and solved using readily available toolboxes, e.g., SeDuMi (Sturm et al. (2006)) can be applied to solve the problem. These constraints can be easily obtained via a quadratic Lyapunov function (Boyd et al. (1994)):

$$V(P) = P'QP = QP^2 \tag{5.21}$$

where Q is a stricly positive symetric matrix (i.e., $Q = Q' \succ 0$) and " ′ " corresponds to the transposition matrix operation.

The minimization in (5.20) is then equivalent to:

$$\min\ \alpha\ :\ V(P) \succ 0\ ,\ \dot{V}(P) + \frac{1}{\alpha} z'z - \alpha w'w \prec 0 \tag{5.22}$$

where, using (5.18) and (5.21), the time derivative of $V(P)$ is given by:

$$\begin{aligned} \dot{V}(P) &= \dot{P}'QP + P'Q\dot{P} \\ &= (-\lambda P + aw)'QP + P'Q(-\lambda P + aw) \\ &= -\lambda P'QP + (aw)'QP - \lambda P'QP + P'Qaw \\ &= -2\lambda P'QP + a'w'QP + P'Qaw \end{aligned} \tag{5.23}$$

Using (5.23) in (5.22), the following expression is obtained:

$$\begin{bmatrix} P \\ w \end{bmatrix}' \begin{bmatrix} -2m & Qa \\ a'Q & -\alpha I_{n_w} \end{bmatrix} \begin{bmatrix} P \\ w \end{bmatrix} - \frac{1}{\alpha} zz' \prec 0 \tag{5.24}$$

where $m = \lambda Q$ and I_{n_w} is the unity matrix of dimension $n_w \times n_w$ and n_w is the dimension of w.

Now, consider the following lemma (*Schur Complement*):

Lemma 1. The following matrix inequalities are equivalent

$$\begin{aligned} &(i) && T > 0, R - ST^{-1}S' \succ 0 \\ &(ii) && R > 0, T - S'R^{-1}S \succ 0 \\ &(iii) && \begin{bmatrix} R & S \\ S' & T \end{bmatrix} \succ 0 \end{aligned}$$

Hence, using the expression of z, a and c in (5.18) and Lemma 1, the optimization problem in (5.20) can be written as follows:

$$\begin{aligned} &\min_{Q,m} \alpha\ :\ \alpha > 0\ ,\ Q = Q' > 0\ \text{ and} \\ &\begin{bmatrix} -2m & m & -\delta Q & -1 \\ m & -\alpha & 0 & 1 \\ -\delta Q & 0 & -\alpha & 0 \\ -1 & 1 & 0 & -\alpha \end{bmatrix} \prec 0 \end{aligned} \tag{5.25}$$

If there exists a feasible solution to the above optimization problem for all δ evaluated at the vertices of Δ, then (5.20) is satisfied and $\lambda = mQ^{-1}$.

Note that this method is likely to be conservative, as the parameter δ has to bound the nonlinearities of the inexactly cancelation terms. Less conservative results can be obtained by considering the approach of Coutinho et al. (2008) to deal with the nonlinearities at the cost of a larger computational effort.

5.2.3 Numerical results

In this section, for comparing the adaptive and robust linearizing control strategies, several numerical simulations considering small-scale bacteria and yeast cultures (respectively in 5 and 20 l bioreactors) are performed. The first simulation set is dedicated to yeast cultures with initial and operating conditions: $X_0 = 0.4g/l$, $S_0 = 0.5g/l$, $E_0 = 0.8g/l$, $O_0 = O_{sat} = 0.007g/l$, $C_0 = C_{sat} = 1.286g/l$, $V_0 = 6.8l$, $S_{in} = 350g/l$. The second simulation set is dedicated to bacteria cultures with initial and operating conditions: $X_0 = 0.4g/l$, $S_0 = 0.05g/l$, $A_0 = 0.8g/l$, $O_0 = O_{sat} = 0.007g/l$, $C_0 = C_{sat} = 1.286g/l$, $V_0 = 3.5l$, $S_{in} = 250g/l$

The values of all model parameters are listed in Tables 2.1, 2.2, 2.3 and 2.4. Note that, for yeast cultures, coefficients k_{os} and k_{op} are simply replaced by k_{O1} and k_{O3} while $k_{O2} = 0$, in accordance with the model of sonnleitner1986. For the bacteria model, parameters values are taken from Rocha (2003) and slightly modified to adapt the yield coefficient normalization to the proposed reaction scheme (2.3) and kinetic model (with a slight difference in the formulation of r_3).

The state variables are assumed available (i.e., measured) online for feedback. The adaptive and robust linearizing feedback controllers proposed in section 5.2 aim at tracking the byproduct set-point (E^* and $A^* = 1\ g/l$) which is chosen sufficiently low so as to stay in the neighborhood of the optimal trajectory but also sufficiently high to avoid probe sensitivity limitations. In this setup, a noisy byproduct measurement is considered.

To design the parameter λ in (5.16) via the optimization problem (5.20), the parameters K_S, K_P, K_O, K_{i_p} and μ_S, μ_O are assumed to be respectively varying of $\pm 100\%$ and $\pm 15\%$ from their nominal values (which are acceptable variations with respect to a realistic identification as performed in chapter 2). Simulating the operating conditions of the control strategy in (5.15), we may infer that $\underline{\delta} = 0\ s^{-1}$ and $\overline{\delta} = 0.5/3600\ s^{-1}$ for yeast cultures, and $\underline{\delta} = 0\ s^{-1}$ and $\overline{\delta} = 0.1/3600\ s^{-1}$ for bacteria cultures (these values are chosen following previous observations of the simulated model). In light of (5.18) and (5.20), these constraints yield for yeasts and bacteria, respectively to $\lambda = 0.0056$ and $\lambda = 0.0046$.

Concerning the adaptive control law, $\lambda = 1$ and $\gamma = 0.05$ for yeast cultures while $\lambda = 2$ and $\gamma = 0.25$ for bacteria cultures. Note also that the sampling period is chosen equal to $0.1\ h$.

Before discussing the results of the proposed methods, it is interesting to observe the performance of a plain linearizing controller, i.e. without adaptation or robustification, applied to the yeast process in the presence of modeling er-

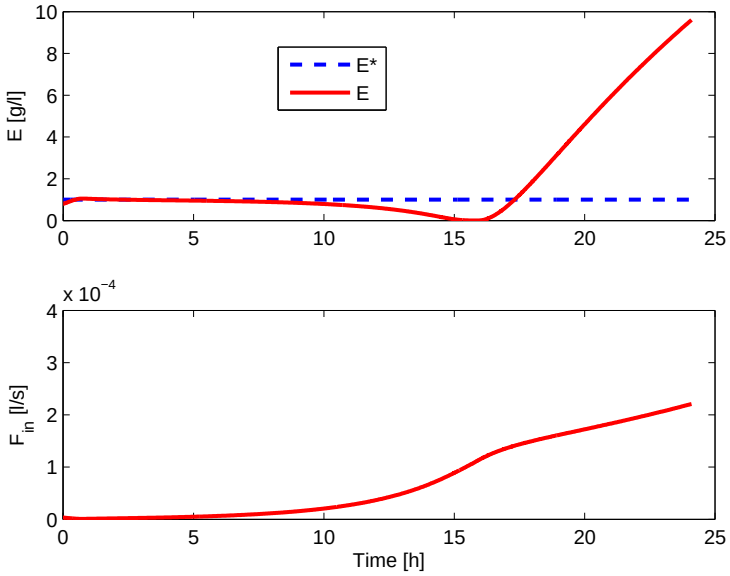

Figure 5.2: Yeast cultures – ethanol concentration and feed rate when the controller is designed using a plain linearizing control approach (no adaptation and no robustification) in the presence of modeling errors.

rors. For instance, consider the situation where the user selects a relatively high gain $\lambda = 1$, and $\hat{v}$ is fixed to $k_{P2}/2$. Figure 5.2 illustrates the consequences of such choices. Even if the controller behaves correctly during the first hours, the divergence of the ethanol signal during the last hours will impact the quality of the culture.

Figure 5.3 shows now the closed-loop response of biomass X, ethanol E concentrations, and the inlet feed rate F_{in}, for five different values of the kinetic parameters (which were randomly chosen) in yeast cultures under a robust control strategy. In all simulation runs, a white noise is added to the ethanol concentration measurement with a standard deviation of ± 0.1 $[g/l]$ and the culture is considered as always evolving in the optimal operating conditions in which $r_1 = \frac{r_O}{k_{os}}$ and $r_3 = 0$ so that the hypothetical parameter $\bar{v}$ in (5.15) is taken as

$$\bar{v} = \frac{k_{P2}\tilde{k}_{S1}}{k_{S2}} r_1 + k_{P3}\tilde{r}_3 \approx \frac{\frac{k_{P2}k_{S1}}{k_{S2}} r_O}{k_{os}} \tag{5.26}$$

Figure 5.3 shows that during the start-up phase, F_{in} saturates to 0, leading to an ethanol overshoot (see Figure 5.3). The different curves are more or less undistinguishable (the same noise signal is applied during the 5 runs) except in the last hours where the consequences of model errors appear. Nevertheless, these results are very satisfactory as model errors have a negligible influence.

Figures 5.4 and 5.5 show the results of a simulation performed with the same

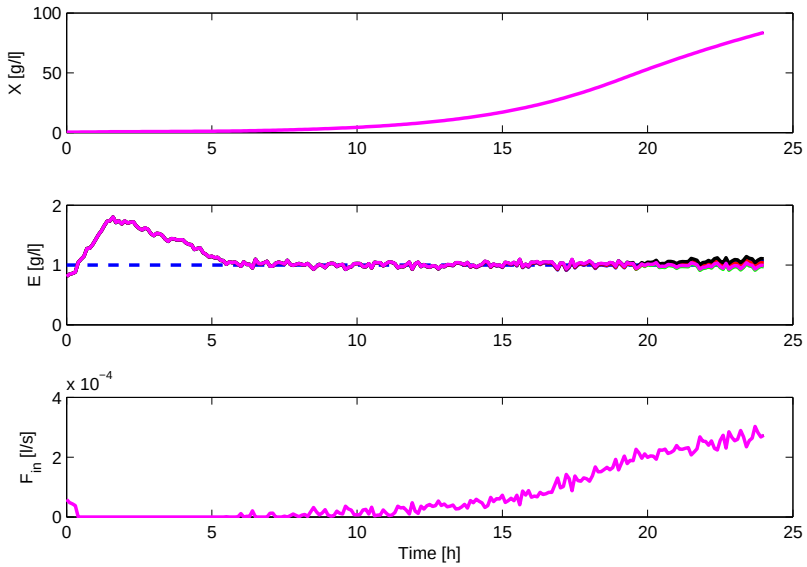

Figure 5.3: Yeast cultures – biomass and ethanol concentrations, and feed rate – robust control strategy – results of 5 runs with random parameter variations and a noise standard deviation of $\pm 0.1\ [g/l]$.

initial and operating conditions with the adaptive strategy, in the ideal case where there is no measurement noise, whereas Figures 5.6 and 5.7 correspond to a noise standard deviation of $\pm 0.05\ [g/l]$ added to the ethanol concentration measurements. Due to sensitivity problems of the adaptive law, higher noise levels usually lead to computational failures. When the parameter adaptation performs well, the productivity of the adaptive and robust strategies is more or less the same, i.e., a biomass concentration of approximately 80 g/l is obtained within 24 hours.

Figure 5.8 shows the closed-loop response of biomass X, acetate A concentrations, and inlet feed rate F_{in}, for five different values of the kinetic parameters which are randomly chosen, in the bacteria cultures under a robust control strategy. Figures 5.9 and 5.10 show similar simulation runs with the adaptive strategy. The same comments concerning the noise sensitivity apply.

Note that the productivity is lower in the bacteria cultures (for biological and operating reasons, bacteria strains lead to reaction rates and, therefore, growth rates that are smaller than yeast reaction rates). However, from a control point of view, results are sactisfactory in both cases.

5.2.4 Conclusion

Linearizing control is a powerful approach to the control of fed-batch bioprocesses. In most applications reported in the literature, on-line parameter adaptation is proposed in order to ensure the control performance despite modeling uncertainties. On-line parameter adaptation is however sensitive to mea-

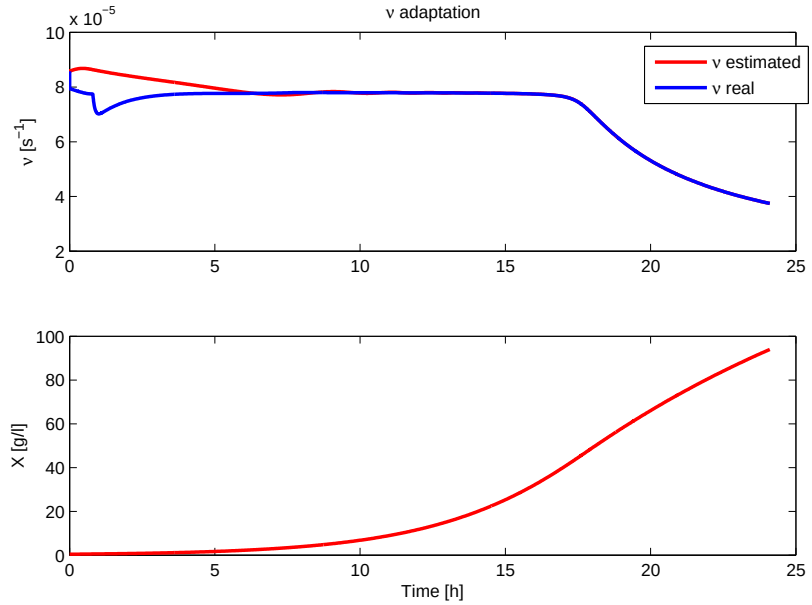

Figure 5.4: Yeast cultures – ν adaptation and biomass concentration – adaptive control strategy – no measurement noise.

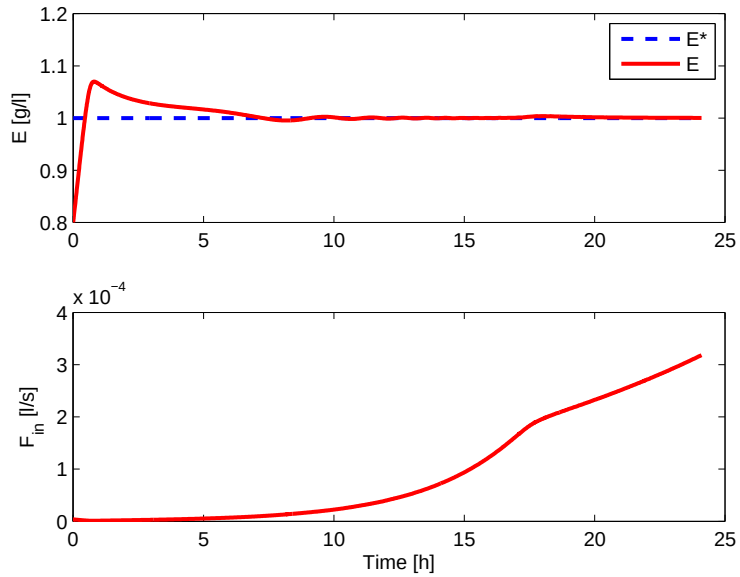

Figure 5.5: Yeast cultures – ethanol concentration and feed flow rate – adaptive control strategy – no measurement noise.

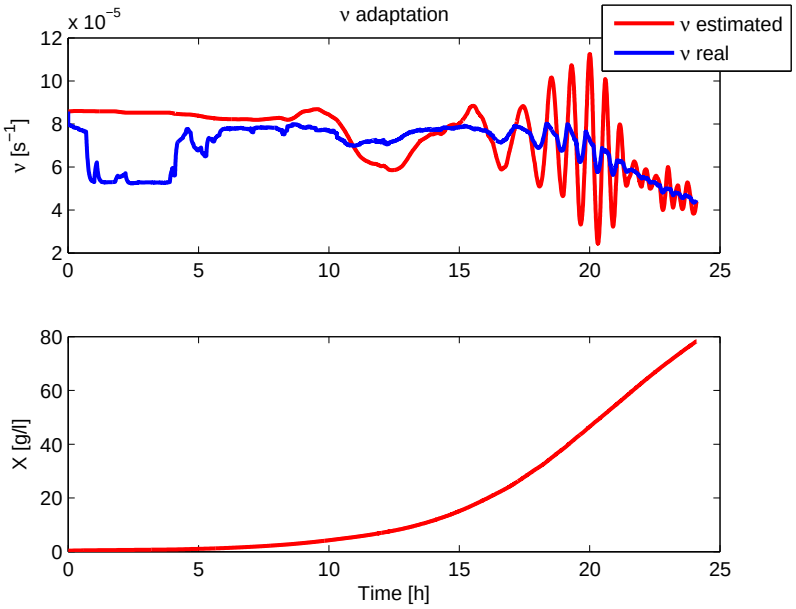

Figure 5.6: Yeast cultures – ν adaptation and biomass concentration – adaptive control strategy – noise standard deviation of $\pm 0.05\ [g/l]$.

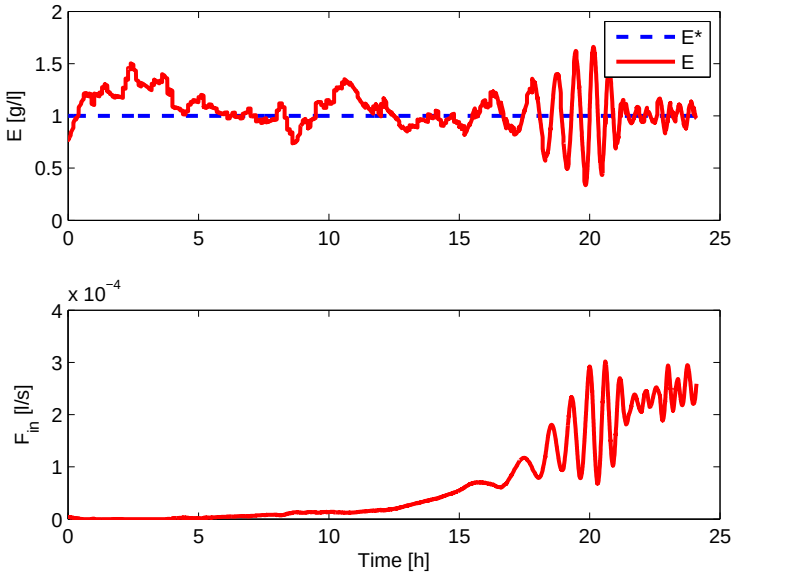

Figure 5.7: Yeast cultures – ethanol concentration and feed flow rate – adaptive control strategy – noise standard deviation of $\pm 0.05\ [g/l]$.

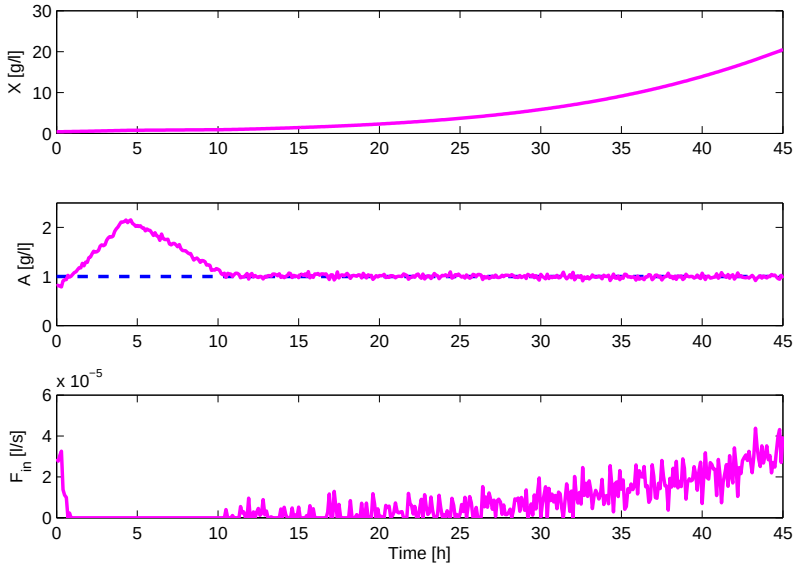

Figure 5.8: Bacteria cultures – biomass and acetate concentrations, and feed rate – robust control strategy – results of 5 runs with random parameter variations and a noise standard deviation of $\pm 0.1\ [g/l]$.

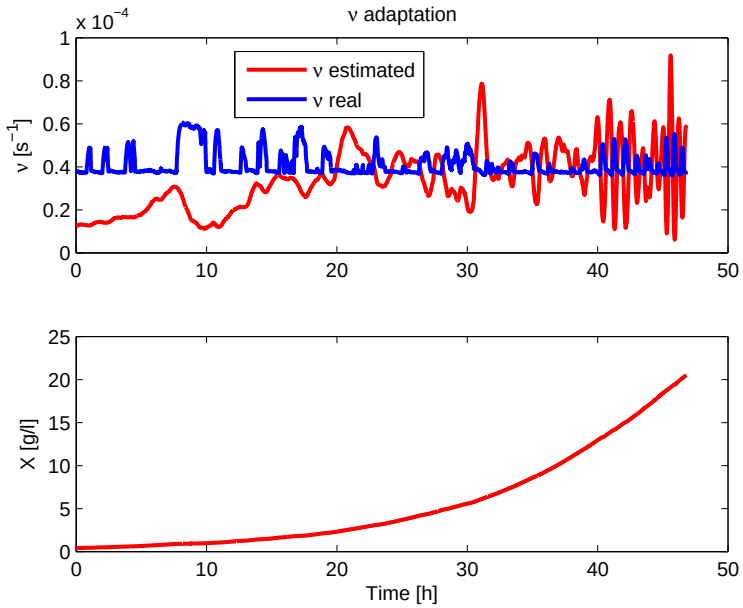

Figure 5.9: Bacteria cultures – ν adaptation and biomass concentration – adaptive control strategy – noise standard deviation of $\pm 0.05\ [g/l]$.

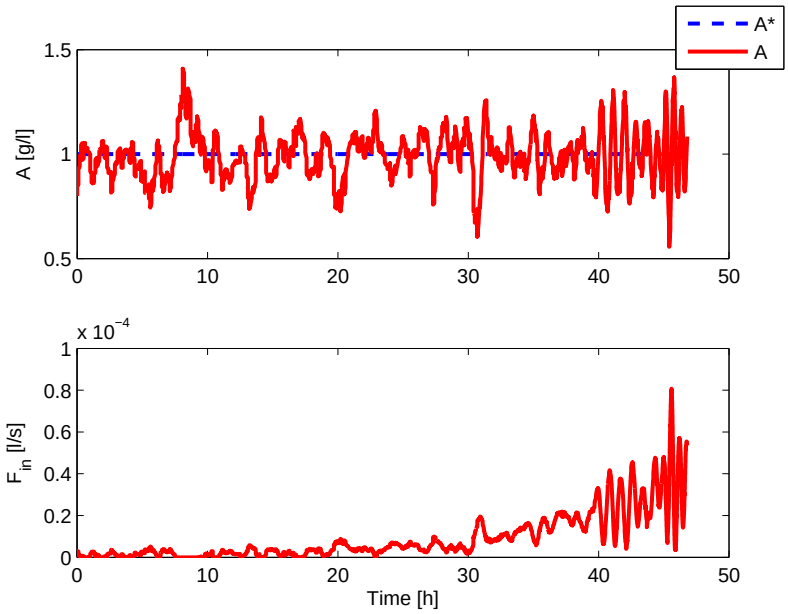

Figure 5.10: Bacteria cultures – acetate concentration and feed flow rate – adaptive control strategy – noise standard deviation of $\pm 0.05\ [g/l]$.

surement noise, and requires some kind of tuning. On the other hand, robust control provides an easy design procedure, based on well established computational procedures using the LMI formalism. Large parametric and structural uncertainties, as well as measurement noise levels can be dealt with.

5.3 Linear robust control

5.3.1 Model linearization

Expressions (2.4) and (2.5) recall that model (2.6) is highly nonlinear in the macroscopic key components. The linear controller design requires a linearization along the proposed suboptimal trajectory (i.e., where $E_{ref} = 1\ g/l$). As proposed in Renard et al. (2006), two partial linear models representing each regime, respectively, can be derived and have the interesting property that they share the same structure.

The following linearization is first performed considering respiro-fermentative culture conditions ($S > S_{crit}$, $r_3 = 0$). Substrate consumption represents one of the fastest dynamics of the system.

Starting from the simplification in (2.6b), (5.3) and (2.6c), related to the byproduct mass balance, are combined to give:

$$\frac{dP}{dt} = \frac{F_{in}}{V}\left(\frac{k_{P2}}{k_{S2}} S_{in} - P\right) - \frac{k_{P2} k_{S1}}{k_{S2}} r_1 X \tag{5.27}$$

This equation can be linearized along a nominal trajectory defined by $P^*(t)$, $F_{in}^*(t)$, $V^*(t)$, $X^*(t)$ and $O^*(t)$. As long as the process is operated in the neighborhood of this trajectory, $P^*(t)$ can be considered as a constant variable P_{ref}, the control set point (or reference), while $F_{in}^*(t)$ and $V^*(t)$, respectively corresponding to the necessary feed-rate and the related volume ($\frac{dV^*(t)}{dt} = F_{in}^*(t)$, see (6f)) to maintain P at P_{ref} , are linked by the following relation:

$$F_{in}^* = \frac{V^*}{\frac{k_{P2}}{k_{S2}} S_{in} - P^*} \frac{k_{P2} k_{S1}}{k_{S2}} r_1^* X^* \tag{5.28}$$

Setting:

$$\begin{array}{c} P = P^* + \delta P \\ F_{in} = F_{in}^* + \delta F_{in} \\ V = V^* + \delta V \\ X = X^* + \delta X \\ O = O^* + \delta O \end{array} \tag{5.29}$$

where δ denotes a very small variation, a first-order Taylor series development can be achieved:

$$\begin{aligned} \frac{d\delta P}{dt} = \; & \frac{\frac{k_{P2}}{k_{S2}} S_{in} - P^*}{V^*} \delta F_{in} - \frac{F_{in}^*}{V^*} \delta P - \frac{F_{in}^*}{V^*} \frac{\frac{k_{P2}}{k_{S2}} S_{in} - P^*}{V^*} \delta V - \frac{k_{P2} k_{S1}}{k_{S2}} X^* \frac{\partial r_1^*}{\partial O} \delta O \\ & - \frac{k_{P2} k_{S1}}{k_{S2}} r_1^* \delta X \end{aligned} \tag{5.30}$$

Along the nominal trajectory, it is assumed that the process is operated not far from the optimal conditions (i.e., close to the edge of the two regimes) so that $r_1^* \approx \frac{r_O}{k_{os}}$. Moreover, when the oxygenation is not limiting and the ethanol quantity is not sufficient to significatively inhibit the respiratory capacity (i.e., (2.5b) with $K_O << O$ and $K_{i_p} >> P$), the following simplification holds:

$$r_1^* \approx \frac{r_{Omax}}{k_{os}} = \frac{\mu_O}{k_{os}} \rightarrow \frac{\partial r_1^*}{\partial O} \approx 0 \tag{5.31}$$

Now, considering (5.28) and 5.31, (5.30) can be written as follows:

$$\begin{aligned} \frac{d\delta P}{dt} = \; & \frac{\frac{k_{P2}}{k_{S2}} S_i n - P^*}{V^*} \delta F_{in} - \frac{X^*}{\frac{k_{P2}}{k_{S2}} S_{in} - P^*} \frac{k_{P2} k_{S1}}{k_{S2}} r_1^* \delta P - \frac{X^*}{V^*} \frac{k_{P2} k_{S1}}{k_{S2}} r_1^* \delta V \\ & - \frac{k_{P2} k_{S1}}{k_{S2}} r_1^* \delta X \end{aligned} \tag{5.32}$$

From the contributions brought by δF_{in}, δP, δV and δX, using constant values of P^* and r_1^*, different values of V^* and X^* going from the start to the end of, for instance, a $20 - l$ yeast culture (note that this assumption is still correct for bacteria cultures) and considering realistic operating parameters, the order of magnitude of the "δF_{in} term" is always significantly larger than the others as shown in Table 5.1.

Table 5.1: Order evaluation of each term of (5.30)

	Culture start	Culture end
$\frac{\frac{k_{P2}}{k_{S2}}S_{in}-P^*}{V^*}$	$O(10^1)$	$O(10^1)$
$\frac{X^*\frac{k_{P2}k_{S1}}{k_{S2}}r_1^*}{\frac{k_{P2}}{k_{S2}}S_{in}-P^*}$	$O(10^{-3})$	$O(10^{-1})$
$\frac{X^*\frac{k_{P2}k_{S1}}{k_{S2}}r_1^*}{V^*}$	$O(10^{-2})$	$O(10^0)$
$\frac{k_{P2}k_{S1}}{k_{S2}}r_1^*$	$O(10^{-1})$	$O(10^{-1})$

From this on, it is legitimate to neglect these latter contributions and to consider the following model in variations:

$$\frac{d\delta P}{dt} = \frac{\frac{k_{P2}}{k_{S2}}S_{in} - P^*}{V^*}\delta F_{in} \tag{5.33}$$

Moreover, defining the biomass specific growth rate $k_{X1}r_1 + k_{X2}r_2 + k_{X3}r_3$ as μ, (2.6a) is written:

$$\frac{d(VX)}{dt} = \mu VX \tag{5.34}$$

By integrating (5.34) over the culture period, we obtain the evolution of the biomass quantity along the nominal trajectory (where, from (5.31), $\mu^* \approx k_{X1}r_1^*$ can also be considered as constant):

$$V^*X^* = V_0X_0exp(\mu^* t) \tag{5.35}$$

Replacing δP and δF_{in} respectively by $P - P^*$ and $F_{in} - F_{in}^*$ in (5.33) and taking into account (5.28) and (5.35), the linear model between the measured state P and the input F_{in} is obtained:

$$\frac{dP}{dt} = \frac{\frac{k_{P2}}{k_{S2}}S_{in} - P^*}{V^*}(F_{in} - d_X) \tag{5.36}$$

where:

$$d_X = \frac{\frac{k_{P2}k_{S1}}{k_{S2}}r_1^*}{\frac{k_{P2}}{k_{S2}}S_{in} - P^*}V_0X_0exp(\mu^* t) \tag{5.37}$$

Finally, a discrete-time transfer function linking the ethanol concentration to the feed rate can be obtained for the respiro-fermentative regime on the basis of (5.37) and, using similar developments, also for the respirative regime. A general discrete-time model representing both regimes can be described by:

Table 5.2: Parameters of the linear discrete-time model (5.38)

Parameter	RF regime	R regime
b	$T_S \frac{\frac{k_{P2}}{k_{S2}} S_{in} - P}{V}$	$T_S \frac{\frac{k_{os}}{k_{op}} S_{in} - P}{V}$
c	$\frac{\frac{k_{P2} k_{S1}}{k_{S2}} r_1}{\frac{k_{P2}}{k_{S2}} S_{in} - P} V_0 X_0$	$\frac{\frac{r_{Omax}}{k_{op}}}{\frac{k_{os}}{k_{op}} S_{in} - P} V_0 X_0$
γ	$exp(\mu T_S)$	$exp(\mu T_S)$

$$P(k) = \frac{bq^{-1}}{1 - q^{-1}} (F_{in}(k) - d_X(k)) \tag{5.38a}$$

$$d_X(k) = \frac{c}{1 - \gamma q^{-1}} \delta(k) \tag{5.38b}$$

where q^{-1} is the backward shift operator ($x(k-1) = q^{-1}x(k)$), the parameters b and c are functions of the operating regime and d_X is seen as the perturbation representing the cells growth (γ is an image of the cells growth rate). All the parameter expressions are listed in Table 5.2 where T_S represents the sampling period.

5.3.2 Controller design

For the sake of clarity, we call B the polynomial bq^{-1}, A the polynomial $1 - q^{-1}$, C the polynomial c and D_X the polynomial $1 - \gamma q^{-1}$.

Potentialities of application of conventional PID controllers are unfortunately limited since the biomass grows exponentially. Indeed, (5.38) shows that the unstable disturbance, which is an image of the biomass growth, needs to be rejected. In Axelsson (1989), Axelsson et al. (1988) and Axelsson (1988), the tuning of a PID controller regulating the ethanol concentration is investigated. Despite the integral part of the controller, an exponentially growing error is observed, showing that this type of controllers is inappropriate. Moreover, the derivative action, which usually improves the stability margin, has bad robustness with respect to the process parameters (Axelsson (1988)).

Consequently, an adaptive RST controller based on the internal model principle in order to reject the unstable disturbance is chosen. A great advantage of this kind of controllers is presented in the following design method using a pole placement procedure which allows to easily impose the tracking behaviour independently of the robustness performance.

The two-degree-of-freedom RST controller, applied to the linearized model of the bioreactor (see Fig. 5.11), is designed to control the ethanol concentration at E_{ref} and reject the disturbance d_X.

The control law can be written as:

$$R(q^{-1}) F_{in}(k) = -S(q^{-1}) P(k) + T(q^{-1}) P_{ref} \tag{5.39}$$

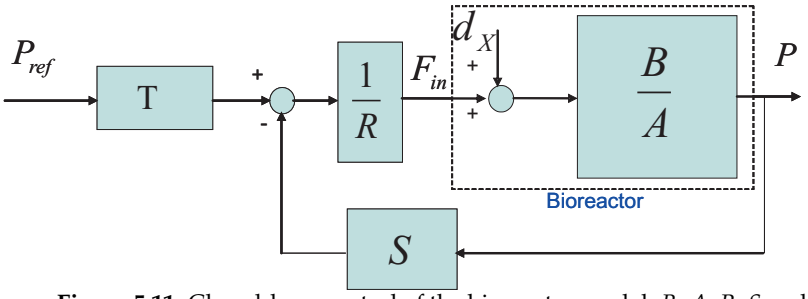

Figure 5.11: Closed-loop control of the bioreactor model. B, A, R, S and T are polynomials in backward-shift operator q^{-1}

and, omitting the backward-shift operator, the closed-loop equation takes the form

$$P(k) = \frac{BT}{AR + BS} P_{ref} + \frac{BR}{AR + BS} d_X(k) \tag{5.40}$$

The RST controller polynomials are then computed using a pole-placement procedure (Astrom and Wittenmark (1997), Landau (1998)), in which the reference model is given by:

$$H_m(q^{-1}) = \frac{B(q^{-1})A_m(1)}{B(1)A_m(q^{-1})} \tag{5.41}$$

where A_m is chosen to tune the tracking performance and, $A_m(1)$ and $B(1)$ are respectively the static gains of the polynomials A_m and B. R and S are found by solving a diophantine equation of the form:

$$AR + BS = A_O A_m \tag{5.42}$$

where A_O is the observer polynomial, which can be selected independently of A_m so as to confer some robustness to the controller.

Following the internal model principle (Francis and Wonham (1975)), the unstable pole γ of the disturbance d_X should be included into the R polynomial (i.e, D_X is a factor of R). This disturbance will be canceled out if a correct estimation of the parameter γ is available, for instance through a Recursive Least Squares algorithm (Astrom and Wittenmark (1997)). Indeed, after the initial time, (5.38b) can be written as:

$$d_X(k) - \gamma d_X(k-1) = 0 \tag{5.43}$$

By replacing the closed-loop transfer function denominator and R by their new expressions and the disturbance d_X by (5.38b), we obtain:

$$P(k) = \frac{BT}{A_O A_m} P_{ref}(k) + \frac{BD_X R'}{A_O A_m} \frac{c}{D_X} \delta(k) \tag{5.44}$$

It appears that the disturbance is compensated and T is only chosen to ensure the setpoint tracking:

$$T = A_O \frac{A_m(1)}{B(1)} \tag{5.45}$$

5.4 Simulation results: application of the RST controller

5.4.1 Controller performance

The first simulation run illustrates the byproduct regulation based on the linearized model (5.38), theoretical parameter values taken from Sonnleitner's yeast kinetic model (Sonnleitner and Käppeli (1986)) and the RST controller defined in (5.39) and applied in closed-loop as in (5.40). An initial ethanol concentration of 0.8 g/l is chosen so that the process has to operate in the respiro-fermentative regime (this point will be detailed in section 5.5), and the only yield coefficients whose knowledge is a priori required, are k_{S1}, k_{S2} and k_{P2} (see (2.6) and Table 5.2). Initial and operating conditions are chosen as follows: $k_L a_O = k_L a_C = 300h^{-1}$ (note that these values only aim at representing a case where the oxygenation is not limited. In practical conditions, $k_L a_O$ and $k_L a_C$ have different values); $S_{in} = 350g/l$; $X_0 = 0.4g/l$; $S_0 = 0.012g/l$; $E_0 = 0.8g/l$; $O_0 = 100\% = 0.007\ g/l$; $T_S = 6min$. The biological reactions occur on such a time scale that a sampling period of $6min$ is acceptable. A first-order tracking behavior with a time constant of $1h$ can be selected, which corresponds to $A_m = 1 - 0.9q^{-1}$.

The tuning of the observer polynomial A_0 is generally achieved by loopshaping, i.e., by modifying the shape of the corrected open-loop transfer function in a Black-Nichols diagram (Fig. 5.12).

Following the general Nyquist theorem transposed to this diagram, the stability of the closed-loop system is verified if the corrected open-loop curve surrounds the point $(0, -180)$ by the right side (i.e, the curve cuts the phase axis on the right side of $(0, -180)$). Three margins are defined (see Fig. 5.12) : an upper gain margin (OB), a lower gain margin (OC) and a phase margin (OD). Stability robustness can then be analyzed through these criterions, defining an ellipsoïd area that the curve should not enter. Actually, an equivalent mathematical expression can be stated through the moduli of the direct and complementary sensitivity functions. Ensuring a modulus lower than $6dB$ for the direct sensitivity function ($\sigma_d = \frac{AR}{AR+BS}$) and lower than 3 dB for the complementary sensitivity function ($\sigma_c = \frac{BS}{AR+BS}$) provides a good stability robustness. This analysis (Renard and Wouwer (2008)) leads to the conclusion that while those last criteria are not respected without robustification ($A_O = 1$), a first order observer polynomial ($A_O = 1 - a_1 q^{-1}$) is indeed sufficient to ensure a good robustification. The value $a_1 = 0.7$ is obtained by trial and error and ensures a comfortable gain margin at high frequencies, corresponding to the frequency range of the neglected glucose dynamics (2.6b).

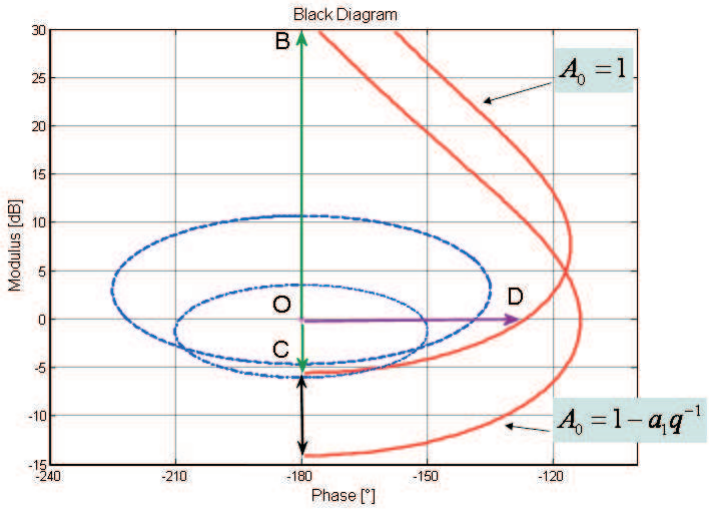

Figure 5.12: Robust behavior analysis of the proposed controller in the Black-Nichols diagram. Upper and lower gain margins are represented by the *OB* and *OC* arrows and the phase margin by the *OD* arrow.

The tracking performance is tested in Fig. 5.13 where the reference, initially set to $1g/l$ is changed to $2g/l$. As E reaches the previous set-point within $4h$ from the start, the new set-point is also reached after $4h$. This last observation is expected as A_m is chosen in order to impose a time constant of $1h$.

5.4.2 Controller improvements considering a delayed output and probe dynamics

Experimentally, it is sometimes observed that the ethanol signal does not respond instantaneously to feed variations so that a latency phase, estimated between 6 and $12min$, has to be taken into account in model (5.38a). Chosing a sampling period of $6min$, this latency phase correspond then to 1 or 2 sampling periods.

A second test considers the performance of the same controller of Fig. 5.13 when facing a process model incorporating a delay of $12min$. In this case, the regulation is not designed taking this delay into account and it can be observed on Fig. 5.14 that the tracking performance is affected by oscillations. Note that initial and operating conditions remain unchanged.

Taking the time delay into account, the discrete model becomes:

$$P(k) = \frac{bq^{-3}}{1-q^{-1}}(F_{in}(k) - d_X(k)) \tag{5.46}$$

necessitating the use of a second order observer polynomial
$A_O = (1-0.85q^{-1})(1-0.15q^{-1})$, following the same analysis as the one shown by Fig. 5.12 (see Fig. 5.15).

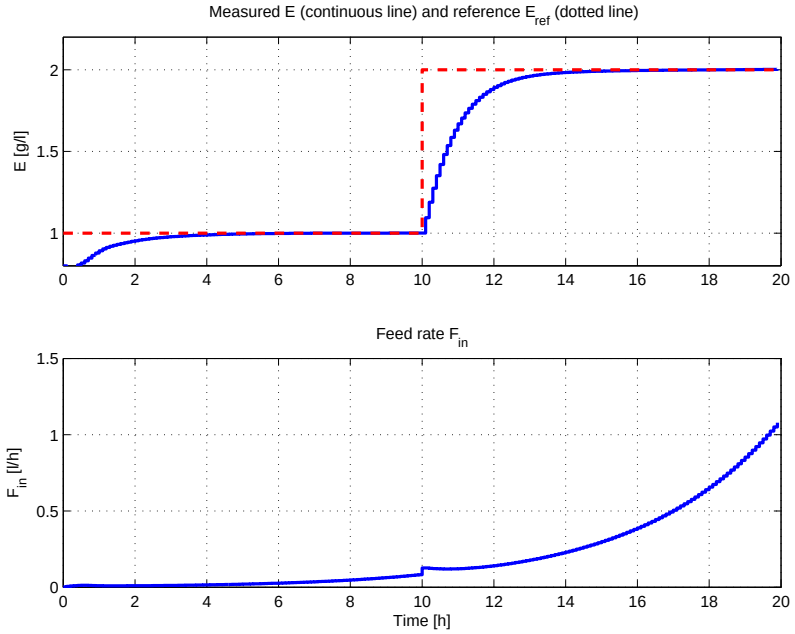

Figure 5.13: Simulation results with the *RST* controller defined in (5.39), (5.40), (5.42), (5.44) and (5.45). Evolution of the ethanol concentration and the feed flow rate.

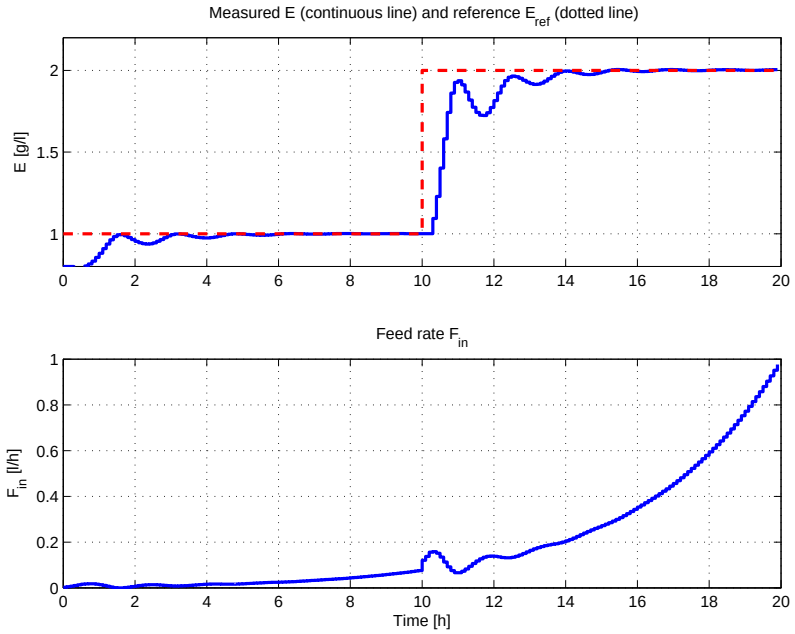

Figure 5.14: Simulation results with the *RST* controller defined in (5.39), (5.40), (5.42), (5.44) and (5.45), when presented with a process incorporating a non-modeled delay of $12min$. Evolution of the ethanol concentration and the feed flow rate.

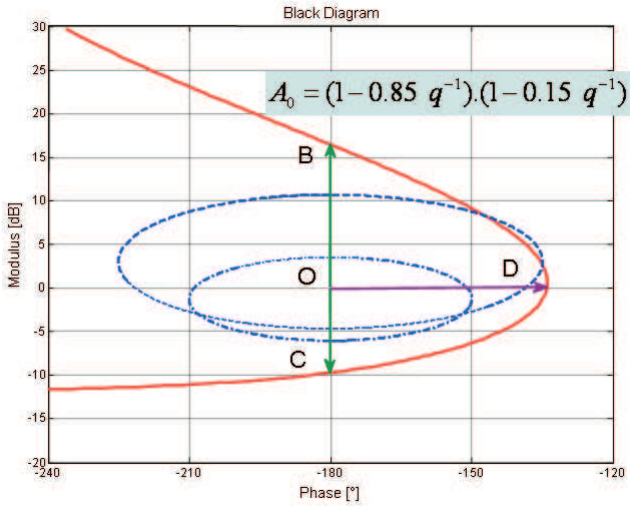

Figure 5.15: Robust behavior analysis of the improved controller in the Black-Nichols diagram.

Note that with a relatively large sampling time, the probe dynamics can generally be neglected. However, reducing the sampling period can be interesting to improve the performance of the recursive least squares algorithm and, in turn, the disturbance rejection. Modeling the ethanol probe dynamics can be achieved by a first-order transfer function with a time constant T_{mes} (generally in a range from 1 to 3 min). Including this second refinement in (5.46), the discrete model becomes:

$$P(k) = \frac{bq^{-3}((T_S + T_{mes}(\nu - 1)) + (T_{mes} - \nu(T_S + T_{mes}))q^{-1})}{(1 - q^{-1})(1 - \nu q^{-1})}(F_{in}(k) - d_X(k)) \tag{5.47}$$

where $\nu = exp(\frac{T_S}{T_{mes}})$

Nevertheless, these performance improvements, inducing a reduction of the sampling period, can be detrimental to the system in terms of stability robustness as the delay, estimated in sampling periods, dramatically increases. Consequently, (5.46) will be prefered to (5.47) and only a 2-sampling-period delay is taken into account. The sampling period must then be carefully chosen to estimate correctly the delay in a minimum of sampling periods. Still using the same initial and operating conditions as in Fig. 5.13, we obtain the results shown in Fig. 5.16 where the oscillations vanish and the tracking performance is better.

5.4.3 Robustness against measurement noise and model uncertainties

In the first hours of culture, when the biomass concentration is very low, the cells are likely to alternatively switch between the two metabolic pathways,

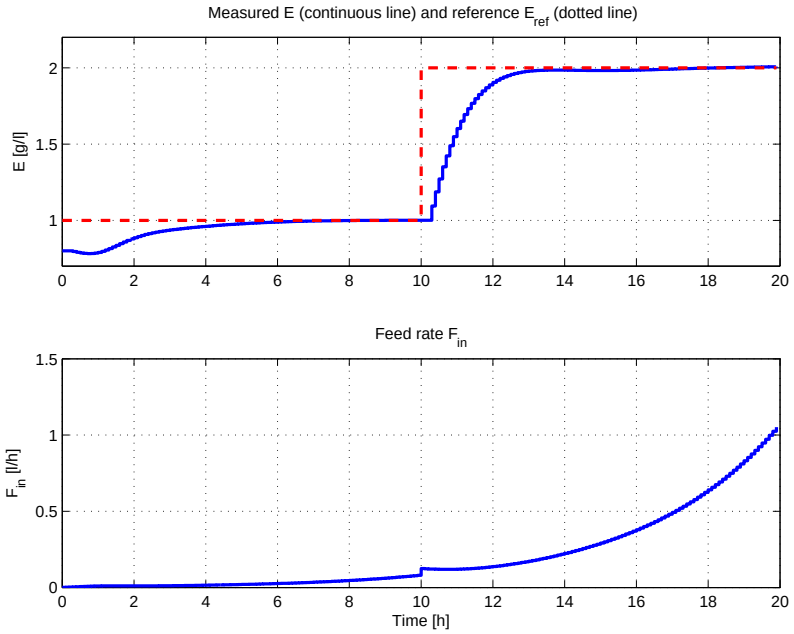

Figure 5.16: Simulation results with the *RST* controller defined in (5.39), (5.40), (5.42), (5.44) and (5.45), when presented with a process incorporating a modeled delay of $12min$. Evolution of the ethanol concentration and the feed flow rate.

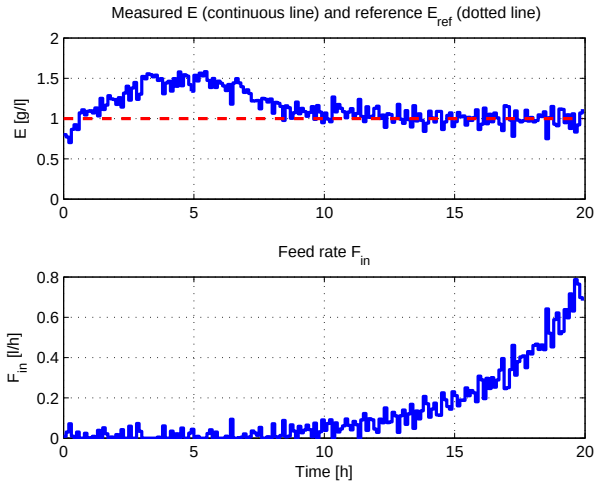

Figure 5.17: Influence of the noise on the measured ethanol concentration with a non-robust RST controller $A_O = 1$.

leading to hard sollicitations and saturations (to 0 when the controller calculates negative feed rates) of the input actuator (i.e., the feed pump). Indeed, the quasi-steady state assumption of the substrate concentration (5.3) is generally verified during the cells exponential growth in the neighborhood of the optimal operating conditions but not in the starting transient period. The best way to illustrate this idea is to challenge the controller in the presence of measurement noise as achieved in section 5.2.3, amplifying the saturation effect.

Fig. 5.17 shows a new simulation where a white noise ($\sigma^2 = 0.005g^2/l^2$) is added to the ethanol concentration measurements and where no robustification by the observer polynomial is considered ($A_O = 1$). Starting with the same initial conditions as in Fig. 5.13, 5.14 and 5.16, the set-point is now kept at $1g/l$ during $20h$ in order to observe the large divergence that occurs during the first $10h$, consequence of the multiple actuator saturations generated by the noise.

On the other hand, Fig. 5.18 shows the same simulation with the robustified controller of Fig. 5.13 ($A_O = 1 - 0.7q^{-1}$). It appears clearly that the noise on the input F_{in} is attenuated, limiting the actuator saturations and the divergence of the ethanol concentration overshoot. The same observations can be made with the robustified controller of Fig. 5.16 in the presence of delay.

The only a priori knowledge on the system is the yield coefficient values k_{S1}, k_{S2} and k_{P2} in the RF regime and the ratio $\frac{k_{os}}{k_{op}}$ in the R regime (see Table 5.2). Considering that the order of the products $\frac{k_{P2}}{k_{S2}}S_{in}$ and $\frac{k_{os}}{k_{op}}S_{in}$ are generally higher than E (i.e., P), uncertainties on these last products have a proportionnal influence on the gain b. Finally, simulations presenting absolute errors going from 50% to 100% of the theoretical values of $\frac{k_{P2}}{k_{S2}}S_{in}$ and $\frac{k_{os}}{k_{op}}S_{in}$ produce similar results to Fig. 5.13, 5.16 and 5.18 (where the controller is robustified) which are not reproduced. In summary, once the controller is robustified by the observer

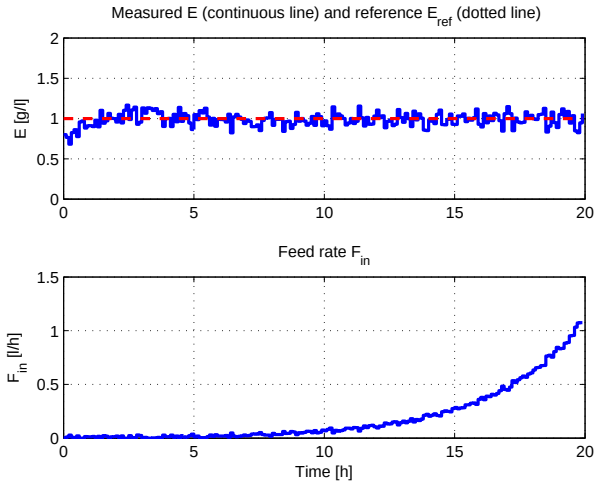

Figure 5.18: Influence of the noise on the measured ethanol concentration with a robust RST controller $A_O = 1 - 0.7q^{-1}$.

polynomial, very large intervals of model uncertainties are tolerated thanks to the increased stability margin (see Fig. 5.12 and 5.15).

5.5 Experimental validations of the RST controller at different scales

Experimental investigation of the *RST* control scheme to fed-batch cultures of *S. cerevisiae* is performed with laboratory-scale and industrial-scale bioreactors. For all these experimental tests, only a 2-sampling-period delay is taken into account. Indeed, a sampling period of 6 *min* appears sufficient to ensure good control performance so that the ethanol probe dynamics is neglected. Consequently, model (5.46) is used in the following.

5.5.1 Control interface

The on-line ethanol concentration measured by a *Frings* probe is acquired through the Ethernet network and transfered into a $LabVIEW^{TM}$ (National Instruments, USA) virtual instrument (*.vi*) where the controller is implemented in a block diagram and supervised through the corresponding front control panel. Every six minutes (which correspond to the sampling period), the feed-rate is updated by the controller on the basis of the process value (the ethanol measurement), and converted into the corresponding percentage of the maximum speed of an ISMATEC peristaltic pump.

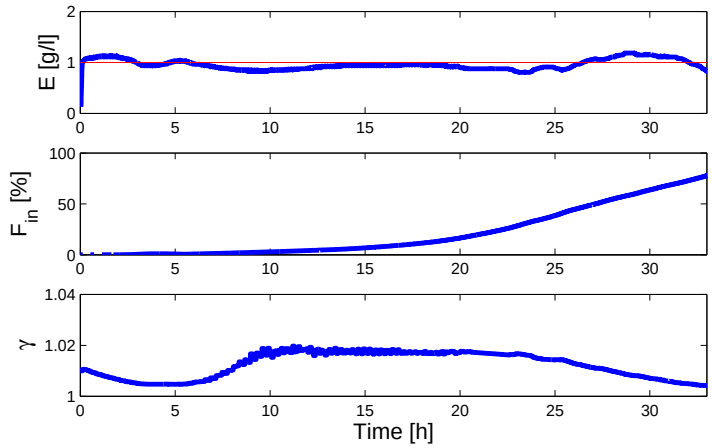

Figure 5.19: Experimental results of the ethanol regulation applied to laboratory-scale fed-batch cultures of *S. cerevisiae*. Evolution of the ethanol probe measurement E around $E_{ref} = 1\ g/l$, the feed flow rate Fin expressed in % of the maximal pump speed and the parameter γ, image of the cells growth rate.

5.5.2 Laboratory-scale results

Fig. 5.19 shows a typical run with a regulation of the ethanol at 1 g/l.

Fig. 5.20 shows the biomass, substrate (glucose) and ethanol off-line concentrations (circles)and a spline interpolation of these measurements (stars, sampled every hour) providing an image of the evolution of these key components when no off-line measurement is available (typically during the evening and the night). Note also that a slight off-set between the off-line measurements obtained by HPLC and the online ethanol probe measurements (delivered every 2 seconds and so, almost appearing as a continuous blue line) is increasing with time but does not really affect the controller performance as both concentrations are approximately constant.

In Fig. 5.21, the measured cell growth rate μ and the corresponding γ are calculated using a discrete approximation of the form:

$$\mu \approx \frac{X(k+1) - X(k)}{X(k) T_{S_{ext}}} \tag{5.48}$$

$$\gamma \approx exp\left(\frac{X(k+1) - X(k)}{X(k) T_{S_{ext}}} T_S\right) \tag{5.49}$$

where T_S is the controller sampling period and $T_{S_{ext}}$ is the resampling period after interpolation of the experimental data.

The least squares estimate (sampled every 5 minutes) needs 10 hours to converge to the real value of γ and is almost perfectly maintained during the 15 following hours until the "culture end phase", characterized by an important decrease of γ, starts.

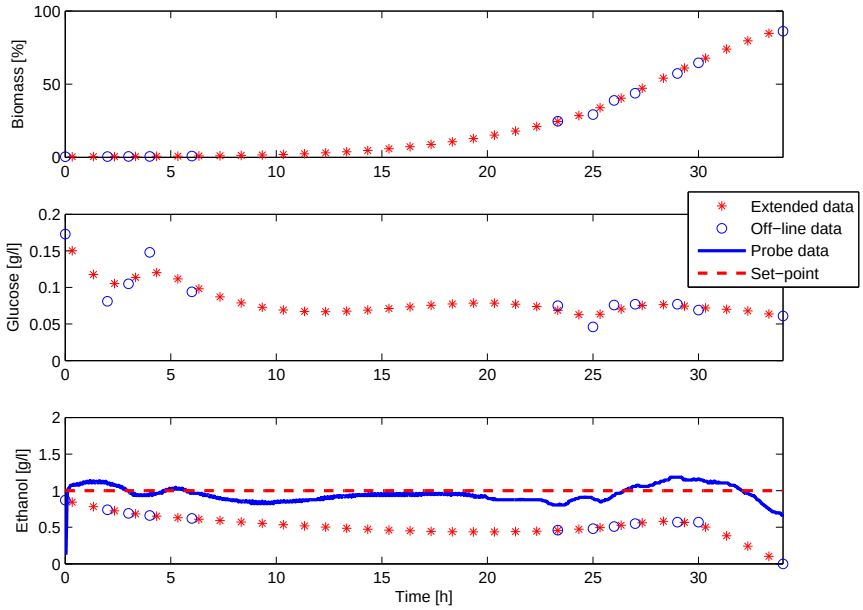

Figure 5.20: Experimental results of the ethanol regulation applied to laboratory-scale fed-batch cultures of *S. cerevisiae*. Evolution of the biomass, glucose and ethanol concentrations (off-line measurements are represented by circles and the spline interpolation by stars). The continuous line represents the ethanol probe measurement and the dashed line the ethanol concentration set-point.

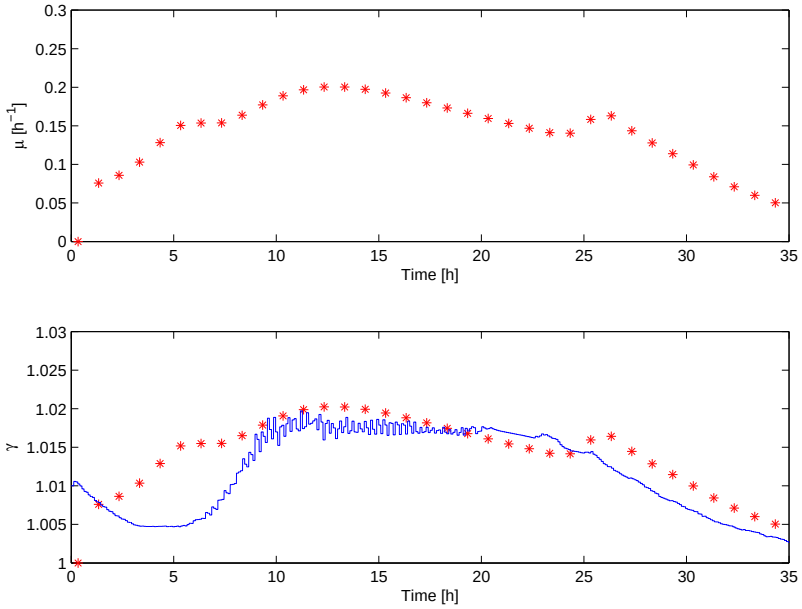

Figure 5.21: Experimental results of the ethanol regulation applied to laboratory-scale fed-batch cultures of *S. cerevisiae*. Evolution of the growth rate μ and the parameter γ (stars), both based on the spline interpolation of the off-line biomass measurements, and estimated γ (continuous line).

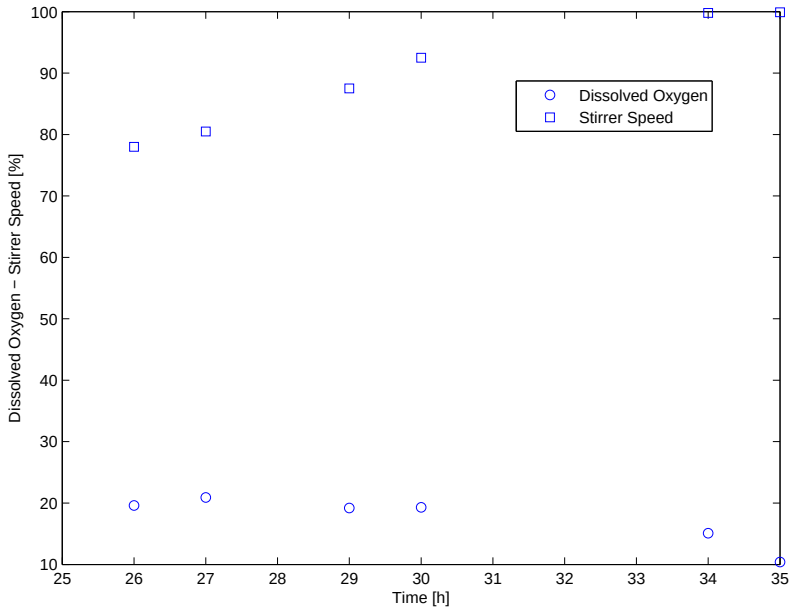

Figure 5.22: Experimental results of the ethanol regulation applied to laboratory-scale fed-batch cultures of *S. cerevisiae*. Evolution of the dissolved oxygen (circles) and the stirrer speed (squares) respectively in percents of the phase saturation concentration and the maximum speed.

Consequently, the ethanol concentration stays around the reference value of 1 g/l during the first 10 hours and, when the estimate of the cells growth rate converges, the regulation becomes more accurate (as the disturbance, which represents the substrate demand for cell growth, can be almost exactly compensated). This demonstrates the efficiency of the controller, which is able to reject an unstable time-varying exponential disturbance. After 20 h, the ethanol concentration deviates slightly from the setpoint. This can be explained by an apparent decrease of the cell growth as reflected by the estimated value of γ. This limitation phenomenon can be due to a lack of oxygenation (see Fig. 5.22) in the last hours, resulting from an unsufficient air flow following a saturation of the stirrer speed to its maximum value.

Nevertheless, the encountered metabolic changes are robustly limited by the controller which prevents the sudden ethanol increase. Note that the culture was stopped before the controller manages to reset more accurately the ethanol concentration at 1 g/l. Anyway, other results presented in the next figures better illustrate this missing part.

Initial process conditions play an important role in terms of productivity. As the controller only regulates the ethanol concentration around the setpoint E_{ref} (which is chosen by the user), and as the initial ethanol concentration in the culture medium (E_0) depends on the residual concentration at the end of the

preculture (which is a priori unknown), the initial difference between the set point and the initial concentration can be crucial for the culture time.

Moreover, the ethanol concentration in the feed medium (E_{in}) plays also a determinant biological role. Indeed, it is possible to force the cells to evolve through a preselected pathway by adjusting the ethanol concentration (E_{in}) in the feed medium (note that in this work, E_{in} is always equal to zero). When $E_{in} < E_{ref}$, the controller constrains the cells to evolve in the respiro-fermentative pathway (as ethanol is always produced to cancel the dilution effects and maintain the concentration around E_{ref}) while when $E_{in} > E_{ref}$, the cells are constrained to evolve in the respirative pathway (as ethanol is never produced and only consumed).

If the ethanol set point is chosen so that $E_{ref} > E_0$, the cells are evolving through the respiro-fermentative pathway during the first hours (as the controller constrains the cells to produce ethanol in order to reach the set point), which is beneficial as the cells are driven through the same pathway in the future growth conditions (indeed, $E_{in} < E_{ref}$). On the other hand, if E_{ref} is chosen so that $E_{ref} < E_0$, the cells are evolving through the respirative pathway during the first hours as ethanol has to be consumed until E reaches E_{ref} (note that at this moment, $F_{in} = 0$).

The bad resulting consequences are (1) a waste of time induced by the growth on ethanol which is very slow in comparison with the growth on glucose and (2) a latency which is experimentally observed when the cells are switching from the respirative to the respiro-fermentative pathway (this is actually the case here, as $E_{in} < E_{ref}$). In Fig. 5.23, the waste of time can be estimated to about 10 to 15 hours as the final batch time is 50 hours (instead of 35 hours, resulting in a decreased productivity). Note that the oxygen limitation discussed in Fig. 5.22 is still present (see the small deviation between 30 and 40 hours on Fig. 5.23).

5.5.3 Industrial-scale results

Industrial-scale fermentation is generally so costly that biotechnological industries establish some very strict security norms that should never be overridden. An open-loop protocol is generally defined. The same feeding profile optimized through previous runs (their number and so, the efficiency of the method, being limited by the financial provisions) is imposed, as a recipe based on heuristics, for each run of the production campaign. For confidentiality reasons, the operating conditions of these experiments cannot be detailed.

Fig. 5.24 shows two different experiments realized in open-loop (the principal constraints being the security norms and a limited accumulation of ethanol) and with closed-loop control on ethanol. The aim of each run is to reach a fixed biomass concentration (represented in % for confidentiality reasons). Obviously, 30 hours are spared in the second case, leading to a productivity improvement estimated to 40%.

On-line results obtained with the controller are presented in Fig. 5.25. The only scaling parameter that has been adapted from the laboratory-scale control settings is the initial volume (remember that V is used to adapt the gain in the

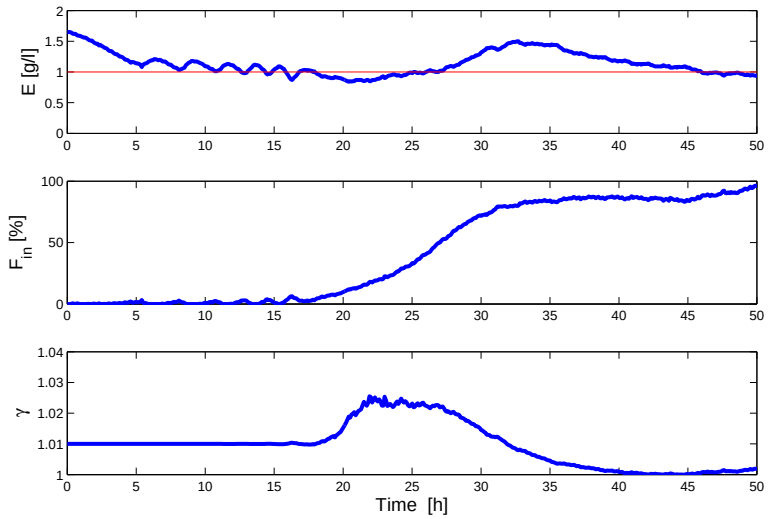

Figure 5.23: Experimental results of the ethanol regulation applied to laboratory-scale fed-batch cultures of *S. cerevisiae*. Evolution of the ethanol probe measurement E around $E_{ref} = 1\ g/l$ (when $E_0 > E_{ref}$), the feed flow rate F_{in} expressed in % of the maximal pump speed and the parameter γ, image of the cells growth rate.

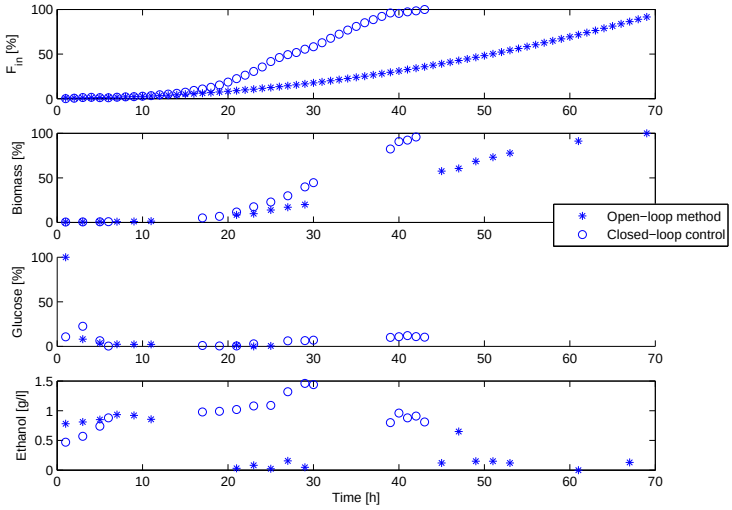

Figure 5.24: Experimental runs of industrial-scale fed-batch cultures of *S. cerevisiae*. Stars: experimental realization of a recipe based on heuristics. Circles: experimental application of the ethanol controller to the same process. Evolution of the feed rate and biomass, glucose and ethanol concentrations.

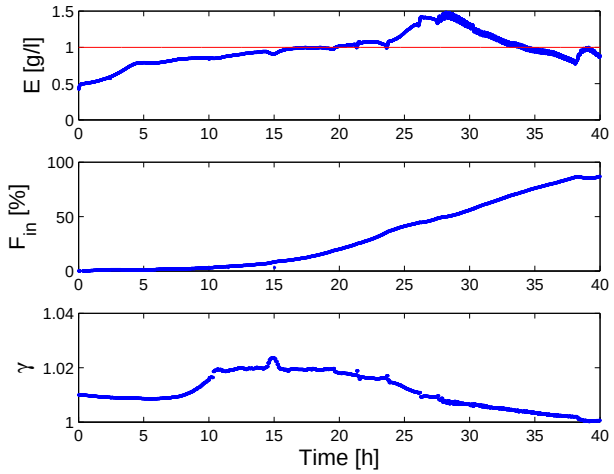

Figure 5.25: Experimental results of the ethanol regulation applied to industrial-scale fed-batch cultures of *S. cerevisiae*. Evolution of the ethanol concentration E around $E_{ref} = 1\ g/l$, the feed flow rate Fin expressed in % of the maximal pump speed and the parameter γ, image of the cells growth rate.

expression of b, see Table 5.2). The observations are very similar to those made at laboratory-scale except for a more important noise magnitude observed on the ethanol signal. An explanation to this phenomenon is that whereas the probe, and particularly its size, remain unchanged, the noise disturbances due to the stirring increase with the scale.

5.6 Conclusion

Based on quasi-steady state assumptions and model linearization, a RST controller is designed to regulate the ethanol concentration at an imposed setpoint. This design is based on a pole placement procedure (for setpoint tracking) and the selection of an observer polynomial (for loop robustification), which can be achieved very easily and independently. The controller requires the online adaptation of the varying cells growth rate, considered as an unstable exponential disturbance to be rejected, justifying the non-applicability of controllers such as PID. The estimation of the unstable pole is achieved through a simple recursive least squares algorithm. The influence of latency phases and sensor dynamics can also be taken into account. Robustness against measurement noise and model uncertainties can also be easily handled. In all the experimental validations, the controller performed well independently of the bioreactor scale, demonstrating its reliability under various conditions. As compared to conventional open-loop operation in industrial productions and previous experimental results using closed-loop PID-like control, the application of the presented particular closed-loop control can ensure a robust ongoing control all along the culture and leads to very significant productivity gain.

Part IV

Development of an Experimental Fed-batch Pilot Plant

Chapter 6

Monitoring and Control of a Bacteria Fed-batch Pilot Plant

In this chapter, an experimental setup is described, which will serve as a platform for elaborating and testing dynamic models, monitoring and control algorithms. Starting from a Biostat B+ bioreactor from Sartorius-Stedim, a wild-type strain of *E. coli* is cultivated first in batch operating conditions in order to identify a macroscopic model of this particular bioprocess and then in fed-batch conditions in order to develop and apply several monitoring and control tools. The real-time control systems aim at optimizing the biomass productivity (i.e., maximizing the biomass concentration within an acceptable and optimal culture time) using different instrumentation going from original hardware probe assemblies to software sensors as well as control techniques already presented in Part III.

6.1 Materials and methods

6.1.1 Bioreactor setup

Fermentations of a wild-type strain (*B*) of *E. coli* (B-11303, ATCC) are performed in a 5 l compact laboratory scale bioreactor (Biostat B+ - Sartorius, see Fig. 1.3) with a configuration comparable to Fig. 1.5. pH is regulated at 7 thanks to a PI controller (directly incorporated into the basic monitoring unit called Digital Fermenter Control or *DFC*, delivered with the vessel) injecting $NaOH$ 2 M (base) and H_3PO_4 0.5 M (acid). Oxygenation conditions are regulated through dissolved oxygen control by a 2-stage cascade controller (also provided in the *DFC*) acting first on the stirrer speed (from 200 to 1500 RPM) and, in case of stirrer saturation, on the aeration system supplying air flow (from 0.3 to 20 l/min). The temperature is controlled by the *DFC* at 37^oC using a heating water jacket.

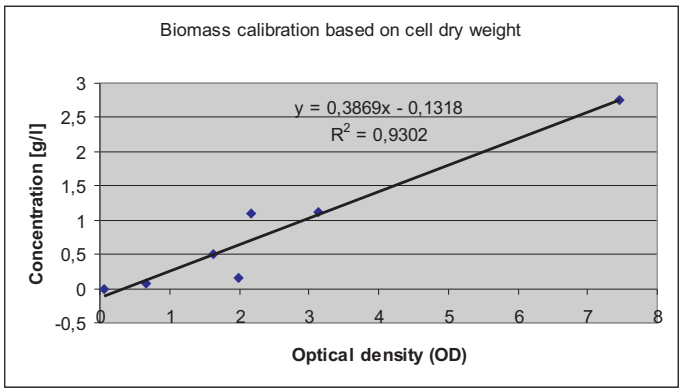

Figure 6.1: Calibration of the biomass concentration based on cell dry weight.

6.1.2 Media preparation and composition

The preculture, culture and feeding media are prepared in accordance with the recipes of Rocha (2003). The general culture medium used in all of the following experimental results is of the following composition: 1 to 5 g/l of glucose (depending on the application), 6 g/l of Na_2HPO_4, 3 g/l of KH_2PO_4, 1 g/l of NH_4Cl, 0.5 g/l of $NaCl$, 0.12 g/l of $MgSO_4.7H_2O$ and 0.34 g/l of *thiamin*. Note that the culture medium used in Rocha (2003) is completed with $CaCl_2.2H_2O$, *kanamicin*, trace metals solution and vitamin solution but these are not considered as necessary in the following experiments. The preculture is realized in 2 erlenmeyers, each of them containing 500 ml of medium inoculated after 24 h in the bioreactor already filled with 2 l of medium so that a starting batch phase is always performed in a volume of 3 l before any addition of feeding. The feeding medium is composed of 200 g/l of glucose, 10 g/l of NH_4Cl and 4 g/l of $MgSO_4.7H_2O$.

6.1.3 Biomass measurement

Off-line biomass measurement is performed thanks to a *Shimadzu* $UV-VIS$ *mini spectrophotometer* measuring the optical density (OD) at 560 nm. A calibration of the biomass concentration from the optical density using the cell dry weight was determined so that one OD unit is equal to 0.38 g/l of biomass (see Fig. 6.1). On-line biomass measurement is also available through the use of the turbidity measurement system *Fundalux II* (also from Sartorius) also delivering an OD measurement. Another on-line measurement can be performed using a *FOGALE* biomass probe detecting only living biomass through a conductance measurement. For illustration purpose, a comparison of punctual biomass measurements is provided in Fig. 6.2. Obviously, the optical density goes on increasing after 3 h while the living biomass is maintained constant before decreasing (i.e., before dying). This third method offers thus a practical way to detect biomass death (i.e., a misfunctioning culture).

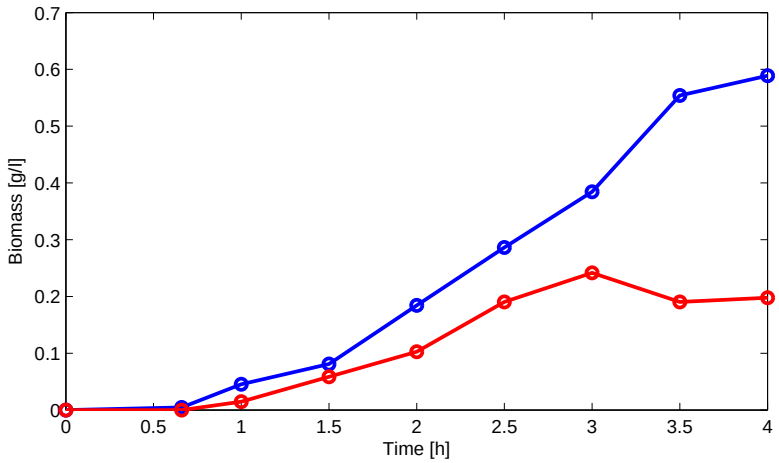

Figure 6.2: Biomass measurements. In blue: biomass concentration based on *OD* measurements. In red: living biomass concentration.

6.1.4 Glucose measurement

Off-line glucose measurements are performed by a Process Trace enzymatic system. Note that on-line measurements can also be achieved through the same system using a dialysis probe or a microfiltration probe. However, the highest sensitivity of available measurement kits is 0.01 g/l. Unfortunately, the level of the critical glucose concentration is, of course, a priori unknown but is in the range of this highest sensitivity. This measurement is then very useful in batch operating conditions where glucose concentrations are sufficiently high but more delicate to use in fed-batch conditions where the glucose concentration is too small to allow an accurate measurement.

6.1.5 Off-line acetate measurement

Off-line acetate measurements can be achieved by an *Alliance* HPLC (*Waters*, USA) using a 3 μm *Atlantis* C18 column (4, 6x150 mm, *Waters*, USA) at 30^oC and a *UV detector* 486 (*Waters*, USA) set at 210 nm in isocratic mode with a NaH_2PO_4 20 mM solution as mobile phase (using a flow rate of $0,5$ ml/min). To ensure reproducibility and stability of the measurement, the samples are buffered in the mobile phase prior to injection. For comparison purposes, an acetic acid kit purchased from *Megazyme* (Ireland) is also used.

6.1.6 On-line acetate measurement

An in-house experimental setup has been designed to measure on-line the acetate concentration (see Fig. 6.3). A Process Trace microfiltration probe is first used to get the supernatant of the filtration of the culture broth. The filtration rate is set at 35 ml/h by a peristaltic Ismatec pump (this rate is voluntarily

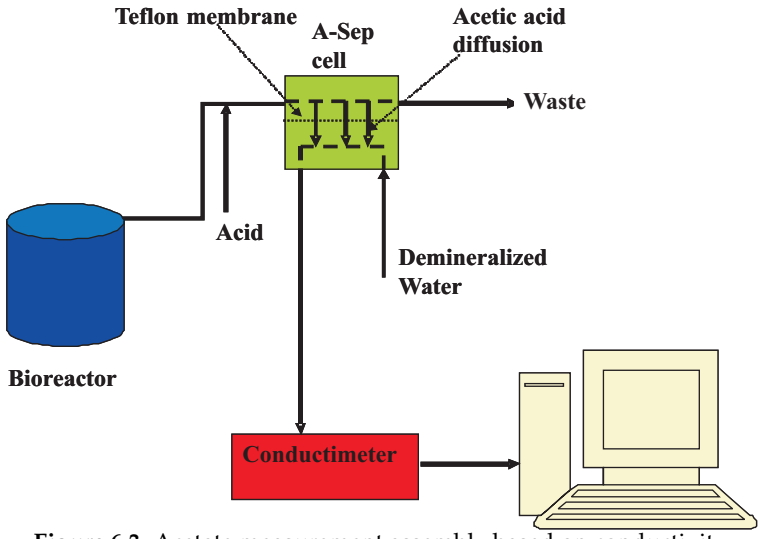

Figure 6.3: Acetate measurement assembly based on conductivity.

chosen at a low level as the whole quantity of the supernatant is not reintegrated in the culture medium and goes to waste). This supernatant is mixed with sulfuric acid (100 g/l), generating acetic acid (in order to allow a perfect acidification, the pipe driver makes several nodes before entering the next part of the assembly). A gas diffusion cell built from a modified $A-Sep$ ($Applitek$) cell is traversed by counter-current streams (as represented in Figs. 6.3 and 6.4) along a Teflon membrane through which acetic acid gaz diffuses from the supernatant to a demineralized water flow. Fig. 6.4 shows a description of the $A-sep$ cell and particularly of the inner part composed of slopes allowing a sufficiently long transit time to enhance a good gas diffusion through the teflon membrane. A conductimeter probe provided by *Consort* (Belgium) allows then the data recording of the conductivity variation, function of the acetic acid (and so, acetate) concentration in the outlet flow, on a computer through a $RS-232$ acquisition *Visual Basic* software.

Conductimeter calibration and validations

Determination of the conductivity-concentration relation is performed using sodium acetate solutions as standards in water and culture medium. This relation is determined in a $0-2,5\ g/l$ range as this should approximately be the level of acetate concentrations during a fed-batch culture. Moreover, higher ranges of acetate concentrations are a priori not of our concern as the cell respiratory capacity would be too inhibited and lead to poor productivity. Considering a second order relation, the calibration leads to the following results:

$$A = 0.001x^2 + 0.0014x - 0.0068 \tag{6.1}$$

where:

- x is the conductivity $[\mu S/cm]$ (S is here used for *Siemens*)

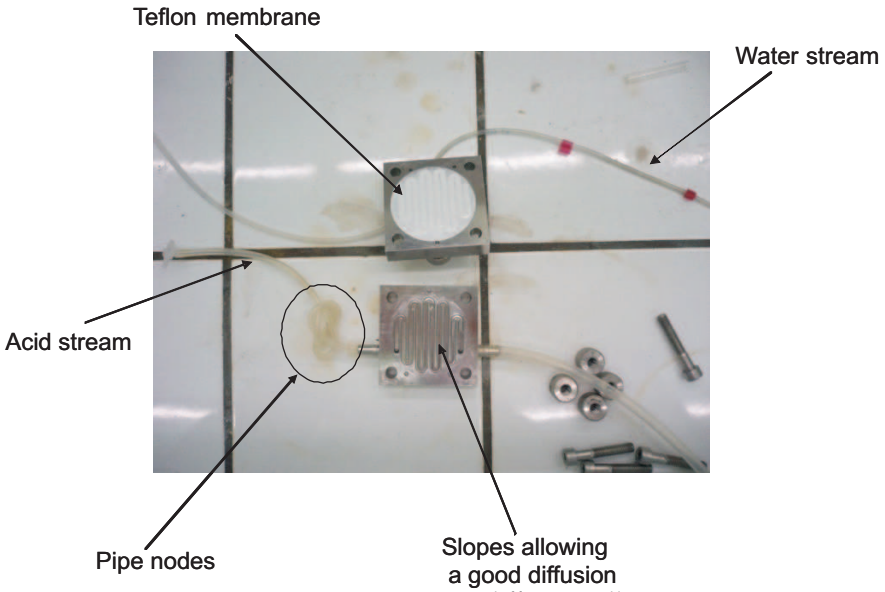

Figure 6.4: A-sep gas diffusion cell.

- A is the acetate concentration $[g/l]$

This regression is represented in Fig. 6.5.

The correlation coefficient R is 0.9995 for a second degree polynomial regression. A cross-validation of this calibration curve is achieved for assessing reproducibility and robustness of the set-up. Some parameters can indeed cause variability, as for instance the medium composition, the temperature, the acidity, the presence of CO_2, etc. Table 6.1 shows the root-mean-square error of prediction ($RMSEP$, which is a common tool for estimating the efficiency of a calibration) on the estimation for a cross-validation in culture medium, following two previous calibrations in water. $RMSEP$ is defined as:

$$RMSEP = \sqrt{\frac{1}{N}\sum_{i=1}^{N}(y_i - \hat{y}_i)^2} \tag{6.2}$$

where N is the number of samples in the cross-validation set and $\hat{y}_i$ the estimate of y_i by the calibration law.

As shown in Table 6.1, the disturbance effect (coming from the probe sensitivity, the temperature, the acidity or the presence of CO_2) on the measurements is clearly present but limited as the general $RMSEP$ is $0,24\ g/l$, which allows this method to be acceptable for a robust acetate concentration control. These cross-validation results are also represented in Fig. 6.5. Note that demineralized water and medium conductivities have the same value around $2,75\ \mu S/cm$, demonstrating the negligible influence of the medium components on the conductivity measurement.

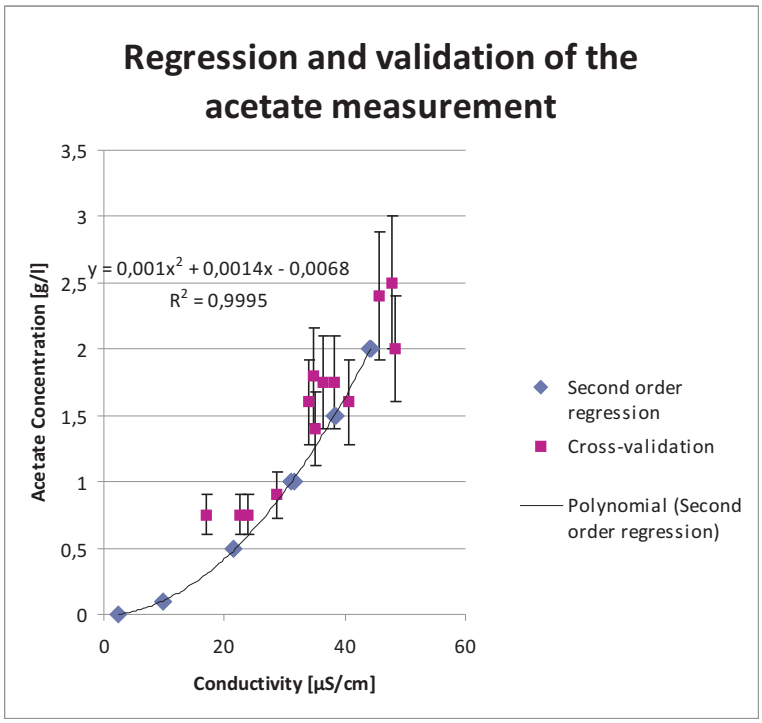

Figure 6.5: Calibration of the acetate measurements using conductimetry.

Table 6.1: Cross-validation results of the second order regression law for the estimation of acetate concentration by conductivity.

$Concentration[g/l]$	$Conductivity[\mu S/cm]$	$Estimation[g/l]$	$RMSEP[g/l]$
0,75	22,5	0,523	0,227
1,75	36,4	1,355	0,395
0,75	24	0,594	0,156
1,75	38,2	1,491	0,259
1,6	33,9	1,177	0,423
1,4	35	1,254	0,146
0,9	28,7	0,846	0,054
0,75	17	0,3	0,45
1,8	34,9	1,247	0,553
1,6	40,7	1,691	0,091
2,5	47,9	2,336	0,164
2,4	45,7	2,128	0,272
2	48,2	2,365	0,365

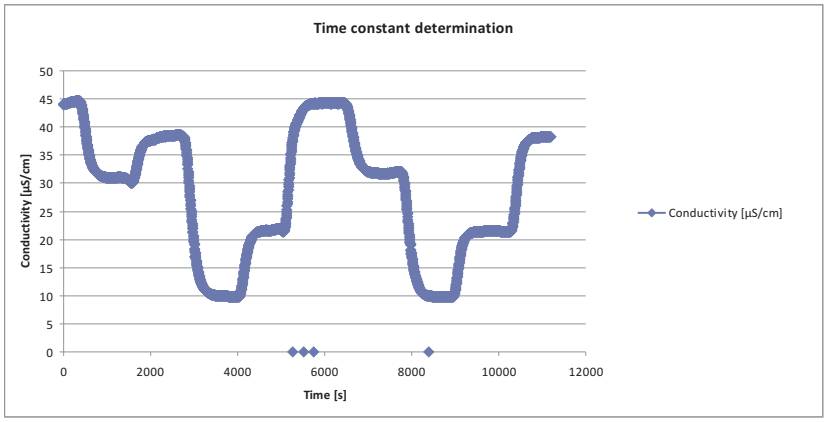

Figure 6.6: Determination of the measurement system time constant.

Estimation of the acetate measurement system time constant

In order to estimate the whole measurement system time constant, different steps in acetate concentration are achieved to challenge the conductimeter response (see Fig. 6.6).

Considering that the conductimeter probe is converging like a first order linear time-invariant system (LTI), the mean response time T_c (i.e., for LTI systems, 5 T_c is the time needed to reach 99% of the steady-state value) is estimated to 3 min. Moreover, the sampling time for acetate concentration measurement is fixed to 6 s.

The main drawback of this method is the variation of the reactor volume due to the continuous supernatant sampling. The pump flow rate is set between 10 ml/h and 20 ml/h to compromise a sufficiently fast communication of acetate concentration variations and a sufficiently low bioreactor volume variation (the length of the fed-batch culture being the main decision criteria for the applied flow rate).

Validation in real culture conditions: results and discussion

The system is now used to follow in real-time the acetate level during a real bacteria fermentation. Samples are taken every 30 min and off-line measurements are performed using HPLC and enzymatic kit analysis. Fig. 6.7 shows the evolution of the conductivity-based, HPLC and enzymatic measurements during 6h of fermentation conducted on *E. coli*.

The experience is performed in three steps (neglecting the preculture phase).

- First, a batch phase is operated in a culture medium with a sufficiently large initial glucose concentration to allow the acetate concentration to increase to a significant concentration level.
- Then, when glucose is exhausted, the cells oxidize the remaining acetate

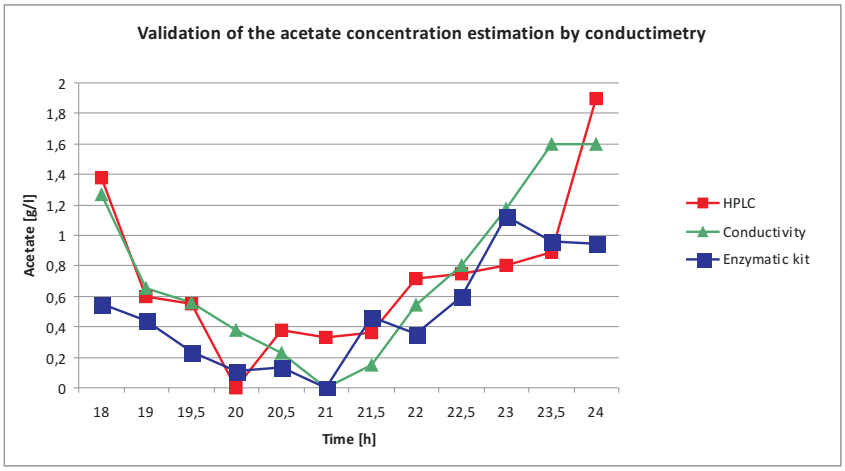

Figure 6.7: Validation of the acetate concentration estimation by conductimetry in real operating conditions; red squares: HPLC measurements; green triangles: conductivity-based measurements (at off-line measurements times); purple crosses: enzymatic measurements.

(i.e., the last carbon source) so that, between 17 h and 21 h, the acetate concentration is in the range of the conductimeter calibration ($0 - 2,5\ g/l$).

- Finally, between 21 h and 24 h, a short fed-batch phase where the feeding rate is provided by adjusting manually the pump speed, is performed. Cells switch then in the respiro-fermentative regime and acetate is produced.

In conclusion, the conductivity-based measurement of the acetate concentration shows good accordance with the HPLC and enzymatic measurements. Note that these 6 hours are chosen as the acetate concentration is varying in the range in which the conductimeter calibration is performed (i.e., decreasing and increasing between 0 and $2,5\ g/l$).

6.1.7 On-line gas measurement

Molar fractions of O_2 and CO_2 in the outlet gas are available thanks to gas analysis using a $DUET - gas\ analyser$ from $System - C - Industry$. As explained in Rocha (2003), OTR and CTR can be measured from the knowledge of molar fractions of O_2, CO_2 and N_2 in the outlet gas, the volume and the inlet air flow. Indeed, using the ideal gas law, assuming that temperature and pressure are the same for the inlet and outlet gas, that no nitrogen is consumed and a quasi steady-state of oxygen in the gas phase (i.e., no dramatic change in oxygen), the following relation holds (Rocha (2003)):

$$OTR = \frac{Air_{in} M_{O_2}}{V} (O_{2_{in}} - O_{2_{out}}) \tag{6.3}$$

where:

- Air_{in} is the volumetric air inflow rate;
- M_{O_2} is the molar mass of oxygen;
- V is the medium volume;
- $O_{2_{in}}$ is the molar fraction of O_2 in the inlet gas;
- $O_{2_{out}}$ is the molar fraction of O_2 in the outlet gas (measured by the gas analyser).

Similarly, the CTR can be estimated by the following expression:

$$CTR = \frac{Air_{in} M_{CO_2}}{V}(CO_{2_{in}} - CO_{2_{out}}) \tag{6.4}$$

where:

- M_{CO_2} is the molar mass of carbon dioxide;
- $CO_{2_{in}}$ is the molar fraction of CO_2 in the inlet gas;
- $CO_{2_{out}}$ is the molar fraction of CO_2 in the outlet gas (measured by the gas analyser).

In the next experimental applications, the inlet air flow is chosen equal to $1\ l/min$ and $O_{2_{in}}$ and $CO_{2_{in}}$ are measured in the outlet gas before starting the culture.

6.2 Identification of a partial respiro-fermentative model

6.2.1 Model simplifications

In order to gain a priori knowledge about this particular bioprocess, before applying any observation or control technique (indeed, strategies presented in Part III generally require a minimum of a priori knowledge about the process), a simple experimental model identification exercise is performed. Starting from the general model presented in chapter 2, a simplified reaction scheme taking only the respiro-fermentative pathway into account (i.e., oxidation and fermentation of glucose) and considering that oxygen conditions are not limiting the cells growth is imagined as follows:

$$\text{Substrate oxidation :} \quad k_{S1}\mathrm{S} + k_{O1}\mathrm{O} \overset{r_1 X}{\rightarrow} k_{X1}\,\mathrm{X} \tag{6.5a}$$

$$\text{Substrate fermentation :} \quad k_{S2}\mathrm{S} + k_{O2}\mathrm{O} \overset{r_2 X}{\rightarrow} k_{X2}\,\mathrm{X} + k_{P2}\,\mathrm{P} \tag{6.5b}$$

The specific growth rates are:

$$r_1 = \frac{\min\left(r_S, r_{S_{crit}}\right)}{k_{S1}} \tag{6.6}$$

$$r_2 = \frac{\max\left(0, r_S - r_{S_{crit}}\right)}{k_{S2}} \tag{6.7}$$

In the proposed situation, as the oxygen is assumed not to be limiting, K_O is also neglected in (2.5b) and, finally, $r_{S_{crit}} = \frac{\mu_O}{k_{os}} \frac{\mathrm{O}}{\mathrm{O}+K_O} \frac{Ki_P}{Ki_P+P} \approx \frac{\mu_O}{k_{os}} \frac{Ki_P}{Ki_P+P}$. The kinetic terms associated with the substrate consumption r_S and the critical substrate consumption $r_{S_{crit}}$ are:

$$r_S = \mu_S \frac{\mathrm{S}}{\mathrm{S}+K_S} \tag{6.8a}$$

$$r_{S_{crit}} = \frac{r_O}{k_{os}} \approx \frac{\mu_O}{k_{os}} \frac{Ki_P}{Ki_P+P} \tag{6.8b}$$

Therefore, assuming the existence of the fermentation reaction and taking (6.8) into account, the specific growth rates take the following forms:

$$r_1 = \frac{r_{S_{crit}}}{k_{S1}} \tag{6.9}$$

$$r_2 = \frac{r_S - r_{S_{crit}}}{k_{S2}} \tag{6.10}$$

Finally, normalizing the yield coefficients with respect to the substrate ($k_{S1} = k_{S2} = 1$), the simplified reaction scheme gives the following component-wise mass balances differential equation system:

$$\frac{dX}{dt} = (k_{X1} r_{S_{crit}} + k_{X2}(r_S - r_{S_{crit}}))X - DX \tag{6.11a}$$

$$\frac{dS}{dt} = -r_S X - D(S - S_{in}) \tag{6.11b}$$

$$\frac{dA}{dt} = k_{P2}(r_S - r_{S_{crit}})X - DA \tag{6.11c}$$

$$\frac{dO}{dt} = -k_{O1}\frac{\mu_O}{k_{os}} - k_{O2}(\mu_S - \frac{\mu_O}{k_{os}})X - DO + OTR \tag{6.11d}$$

6.2.2 Experimental scheme

Three semi fed-batch (a batch phase followed by a fed-batch phase) experiments are performed. For each run, biomass, glucose and acetate are measured

off-line. The biomass concentration is obtained through the OD measurement, the glucose through the *Process TRACE* enzymatic measurement and acetate through HPLC measurement. As shown in Figs. 6.8, 6.9 and 6.10, and Tables 6.2, 6.3 and 6.4, the initial concentrations are not necessarily identical from one experiment to another.

The identification is achieved through the following steps:

- Using two biomass, substrate and acetate data sets:
  - The identification of k_{X1}, k_{X2}, k_{P2}, μ_S and $\frac{\mu_O}{k_{os}}$ is achieved on the basis of the batch phases only (K_S and Ki_P can therefore be neglected as, in batch mode, the glucose concentration is assumed to be much larger than the saturation constant K_S of (2.5a) so that $\mu_S \frac{S}{S+K_S} \approx \mu_S$ and, moreover, assuming that the byproduct concentration is smaller than Ki_P, $r_{S_{crit}} \approx \frac{\mu_O}{k_{os}}$).
  - Using the corresponding fed-batch phases, a new identification of the previously determined parameters coupled to K_S and Ki_P is performed (using the previous values as starting point so as to alleviate local minima).
- Using the remaining biomass, substrate and acetate data set, a cross validation is performed.
- Using one oxygen data set (for the 3 experiments, only 2 oxygen data sets are available), k_{O1} and k_{O2} are obtained on the basis of the previously identified parameters.
- Using the second oxygen data set, a cross-validation of these last two parameters is performed.

Table 6.2: Off-line measurements of the first experiment.

Time (h)	Biomass (OD)	Biomass (g/l)	Glucose (g/l)	Acetate (g/l)
0	0,24	0,093	3,8	0,16
1,5	0,829	0,321	3,784	0,29
2	1,05	0,406	3,724	0,4183
3	2	0,774	3,523	0,985
4	2,335	0,904	3,212	1,99
5	3,103	1,201	2,793	2,855
5,66	3,438	1,33	2,489	3,427
22,5	8,772	3,395	0,423	0,446
24	8,37	3,239	0,227	0,421
26	9,15	3,541	0,109	0,508

$PO_2(\%)$	OTR (g/l/h)	CTR (g/l/h)	Added base (ml)
84	0	0	0
33	0,0952	0,0357	4
28	0,143	0,064	7
29,2	0,19	0,186	14
30,2	0,238	0,257	23
29,7	0,238	0,279	30
29,7	0,238	0,279	35
30,5	0,143	0,329	148
29,6	0,19	0,329	164
30,4	0,238	0,486	189

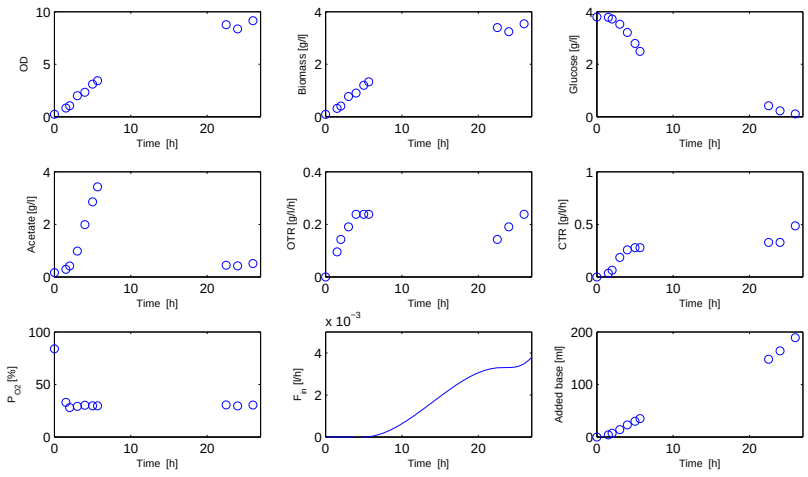

Figure 6.8: First semi fed-batch experiment. The fed-batch phase is started after 6 *h*. Bubbles: off-line measurements. Solid line: imposed feeding profile.

Table 6.3: Off-line measurements of the second experiment.

Time (h)	Biomass (OD)	Biomass (g/l)	Glucose (g/l)	Acetate (g/l)
0	0,504	0,195	3,541	1,075
3,4	2,52	0,975	2,089	3,75
4,4	3,44	1,331	0,754	3,629
5,4	3,68	1,424	0,112	4,101
6,4	4,5	1,741	0,161	4,192
21,75	9,219	3,568	0,107	7,597
22,75	10,766	4,166	0,108	7,914
24	11,5	4,45	0,104	12,626
25,75	10,896	4,217	0,108	12,784
27,5	13,38	5,178	0,108	11,852
28,5	13,277	5,138	0,114	12,225

$PO_2(\%)$	OTR (g/l/h)	CTR (g/l/h)	Added base (ml)
72	0	0	0
29,6	0,381	0,5	27
29,2	0,238	0,4	33
29,5	0,286	0,457	40
29,1	0,286	0,407	45
29,4	0,429	0,564	157
29,5	0,429	0,557	169
29,5	0,524	0,643	186
29,5	0,476	0,6	208
29,5	0,524	0,629	238
30	0,524	0,629	258

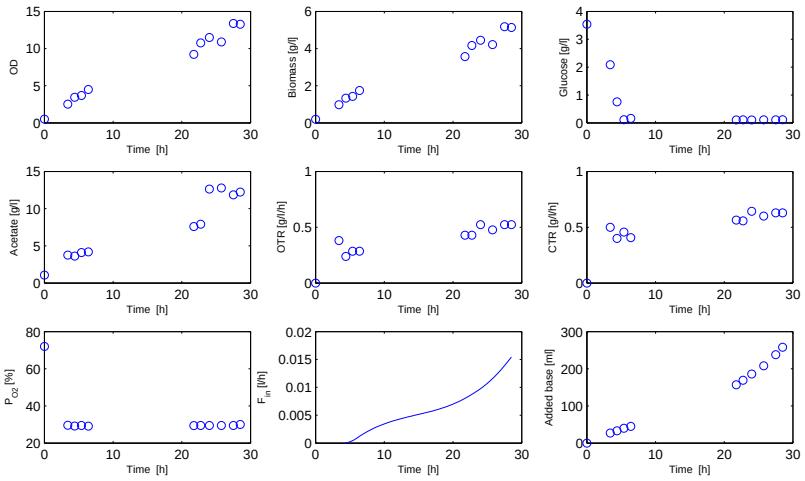

Figure 6.9: Second semi fed-batch experiment. The fed-batch phase is started after 6 *h*. Bubbles: off-line measurements. Solid line: imposed feeding profile.

Table 6.4: Off-line measurements of the third experiment.

Time (h)	Biomass (OD)	Biomass (g/l)	Glucose (g/l)	Acetate (g/l)
0	0,556	0,215	4	0,643
1,75	1,2	0,464	3,647	0,76
3,75	1,842	0,713	2,82	1,218
4,75	2,292	0,887	2,505	1,452
5,75	2,72	1,053	2,166	1,657
6,5	3,264	1,263	1,426	1,757
21,5	7,635	2,955	2,766	3,53
23,25	7,806	3,021	2,783	3,8

$PO_2(\%)$	Added base (ml)
73	0
29,7	6
31,6	22
29,4	27
30,4	31
30,2	35
29,5	117
29,5	131
29,6	140
29,6	157

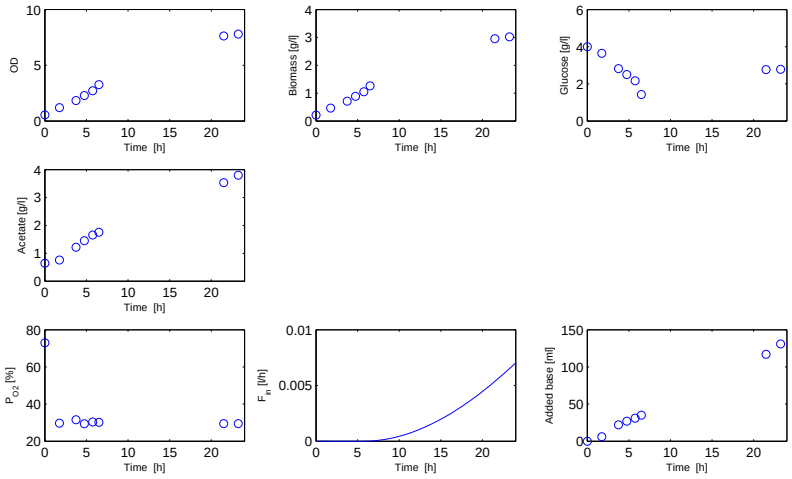

Figure 6.10: Third semi fed-batch experiment. The fed-batch phase is started after 7 *h*. Bubbles: off-line measurements. Solid line: imposed feeding profile.

For the identification procedure using only biomass, substrate and acetate, a simplex method (Nelder-Mead algorithm used in the $MATLAB^{TM}$ function "fminsearch") minimizing, in the Gauss-Markov sense, the following cost function, is used:

$$F_c = \sum_{i=1}^{N} (\xi_{sim}(i) - \xi(i))' Q^{-1} (\xi_{sim}(i) - \xi(i)) \tag{6.12}$$

where

- $\xi = \begin{bmatrix} X & S & A \end{bmatrix}$ is the measured state vector;
- $\xi_{sim} = \begin{bmatrix} X_{sim} & S_{sim} & A_{sim} \end{bmatrix}$ is the state vector generated by the model;
- N is the number of measurements;
- Q is the measurement error covariance (assuming a gaussian measurement noise) of the following form: $Q = \begin{pmatrix} \sigma_X^2 & 0 & 0 \\ 0 & \sigma_S^2 & 0 \\ 0 & 0 & \sigma_A^2 \end{pmatrix}$ where σ_X^2, σ_S^2 and σ_A^2 are respectively the variances of the biomass, substrate and acetate measurement errors. In the following identification procedure, these variances are fixed to 10 % of the relative X, S or A value.

The first identification using 2 batch data sets only, leads to the following parameter vector:

$$\theta_1 = \begin{bmatrix} k_{X1} & k_{X2} & k_{P2} & \mu_S & \frac{\mu_O}{k_{os}} \end{bmatrix} = \begin{bmatrix} 1,451 & 0,3813 & 1,495 & 0,775 & 0,12 \end{bmatrix} \tag{6.13}$$

The second identification is performed using θ_1 as initial conditions and considers K_S and Ki_P (respectively initialized at 0.1 and 5). The following parameter values are obtained:

$$\begin{aligned} \theta_2 &= \begin{bmatrix} k_{X1} & k_{X2} & k_{P2} & \mu_S & \frac{\mu_O}{k_{os}} & K_S & Ki_P \end{bmatrix} \\ &= \begin{bmatrix} 1,742 & 0,305 & 1,196 & 0,72 & 0,096 & 0,05 & 4 \end{bmatrix} \end{aligned} \tag{6.14}$$

Direct validations of the identified set of parameters θ_2 using the complete first two semi fed-batch experiments are presented in Figs. 6.11 and 6.12. The results of the cross-validation using the third data set are presented in Fig. 6.13. As a first visual and qualitative assessment, it can be observed that biomass and acetate are correctly reproduced while the end of the cross-validation misses the last two glucose measurements. However, at this moment, the biomass growth is slowing down, suggesting that the biomass mortality is increased (recall that biomass mortality is not modelled) and the glucose consumption is therefore abnormally limited. These results are also quantitatively assessed by a simple $RMSEP$ cost function comparable to (6.2), amounting to $1,312\ g/l$, $1,505\ g/l$ and $1,38\ g/l$ respectively for the first and

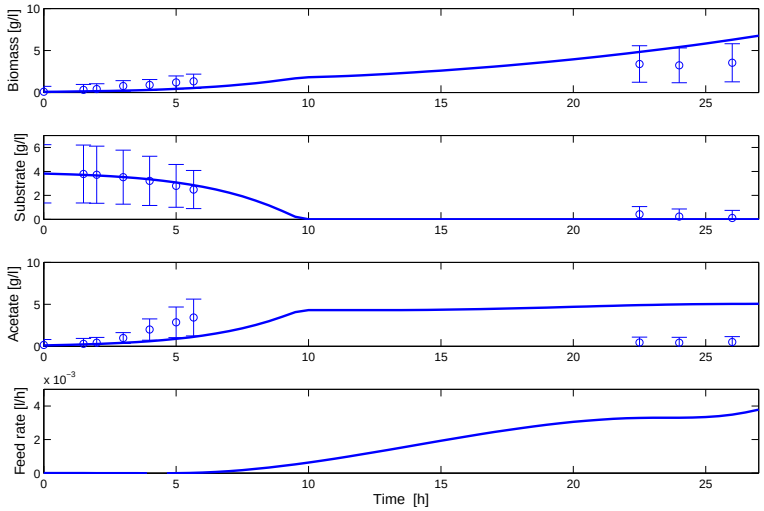

Figure 6.11: First direct validation of model (6.11). Bubbles: off-line measurements. Solid lines: predicted values.

second direct validations and the cross-validation. From these qualitative and quantitative assessments, it can be concluded that this identification is satisfactory.

The last two parameters, k_{O1} and k_{O2}, are identified on the basis of the previously identified parameters (6.14). A quasi-steady state assumption is made on the dissolved oxygen concentration ($\frac{dO}{dt} \approx 0$). This assumption is always verified (except during a very small and negligible transient period after inoculation) during the main part of the culture as the dissolved oxygen is controlled around 30 % by the stirrer speed. After trivial mathematical manipulations and using this assumption, equation (6.11d) can be rewritten as:

$$OTR = (k_{O1}r_1 + k_{O2}r_2)X - DO \tag{6.15}$$

Considering that the dilution term DO is negligible in comparison with the kinetic term $(k_{O1}r_1 + k_{O2}r_2)X$, the following relation holds:

$$OTR = (k_{O1}r_1 + k_{O2}r_2)X \tag{6.16}$$

As a result of the identification, r_1 and r_2 can be considered as perfectly known while OTR and X are measured (note that OTR is only measured in the first two data sets). A linear regression can therefore be performed to recover k_{O1} and k_{O2} values from the following problem:

$$OTR = \varphi\theta_3 \tag{6.17}$$

where $\varphi = \begin{bmatrix} r_1X & r_2X \end{bmatrix}$ and $\theta_3 = \begin{bmatrix} k_{O1} & k_{O2} \end{bmatrix}'$.

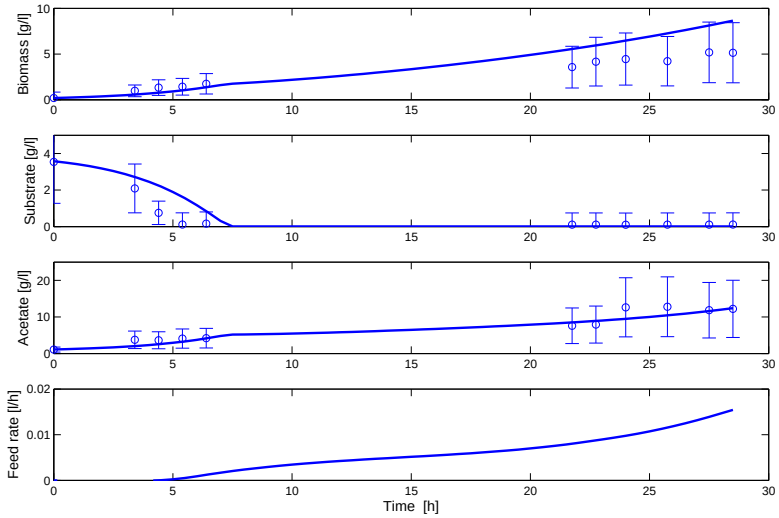

Figure 6.12: Second direct validation of model (6.11). Bubbles: off-line measurements. Solid lines: predicted values.

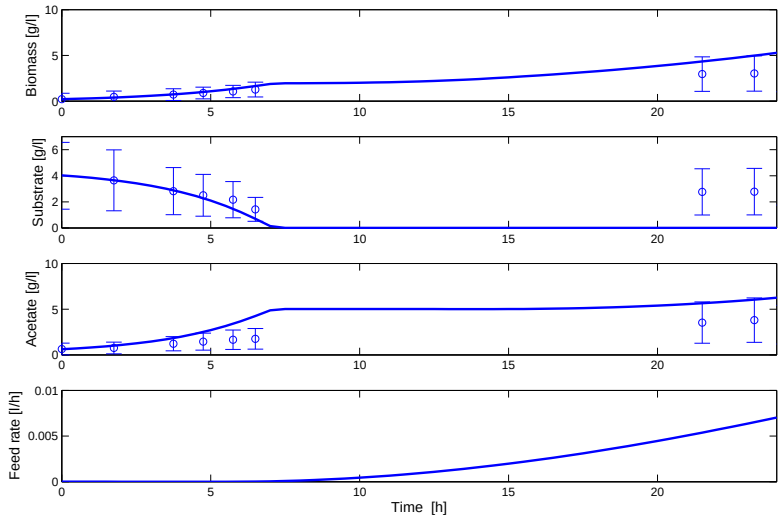

Figure 6.13: Cross-validation of model (6.11). Bubbles: off-line measurements. Solid lines: predicted values.

Table 6.5: Identified parameter values of model 6.11.

k_{X1}	$1,742$
k_{X2}	$0,305$
k_{P2}	$1,196$
k_{O1}	$0,974$
k_{O2}	$0,197$
μ_S	$0,72$
K_S	$0,05$
$\frac{\mu_O}{k_{os}}$	$0,096$
Ki_P	4

The results of this linear regression are obtained using the second data set and are cross-validated using the first one. Fig. 6.14 shows these two validations and, to conclude this section, Table 6.5 summarizes the values of the identified model (6.11).

6.3 Culture optimization

An optimizing regulation comparable to section 5.3 is now considered, where the acetate concentration, measured on-line, following the description of section 6.1.6, is chosen as measured variable. A measurement delay must therefore be considered, taking into account:

- The probe (i.e., the conductimeter) time constant (3 *min*).
- The biological latency preceding the acetate formation.
- The circulation time of the sample in the measurement system (estimated to 12 *min*).

From these last observations, a linearization of the respiro-fermentative model (6.11), comparable to section 5.3, is achieved, considering a measurement delay estimated to 25 *min*. In terms of sampling period T_s, chosen equal to 6 *min*, this delay represents approximately 4 T_s. The discrete time model of the bioreactor is therefore:

$$P(k) = \frac{bq^{-5}}{1-q^{-1}}(F_{in}(k) - d_X(k)) \tag{6.18a}$$

$$d_X(k) = \frac{c}{1-\gamma q^{-1}}\delta(k) \tag{6.18b}$$

where parameters b and c are defined as:

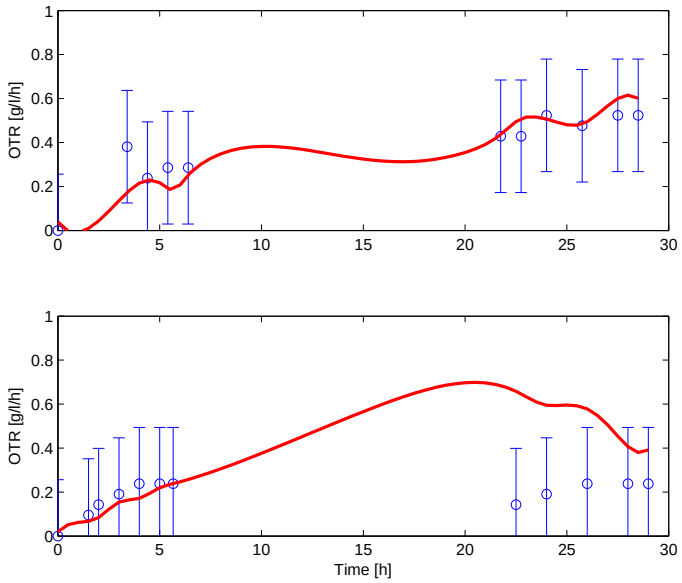

Figure 6.14: Validation of model (6.16). Upper graph: direct validation. Lower graph: cross-validation. Bubbles: off-line OTR measurements. Dashed lines: simulated OTR values.

$$b = T_s \frac{k_{P2} S_{in} - P}{V} \tag{6.19a}$$

$$c = \frac{k_{P2} r_1}{k_{P2} S_{in} - P} V_0 X_0 \tag{6.19b}$$

where V, the medium volume, is estimated by integrating the input F_{in}.

6.3.1 Simulation results

First, a simulation of the *RST* controller applied to the discrete model (6.18) obtained from (6.11) and using parameter values identified in (6.14), is performed. For coherence purpose, operating conditions are chosen so that the simulation is evolving in the respiro-fermentative regime (indeed, as shown by Fig. 6.15, acetate is always produced) and the oxygenation is not limiting. The results of this simulation are shown in Figs. 6.15 and 6.16. In this case, an observer polynomial of the first order ($A_0 = 1 - 0.7q^{-1}$) is sufficient to ensure good robustness conditions as shown by the corrected open-loop function represented in the Black-Nichols diagram in Fig. 6.17. Indeed, the curve is not entering the dashed ellipses representing the direct and complementary sensitivity functions defined in section 5.4.1.

Following these first encouraging results, an experimental investigation on the

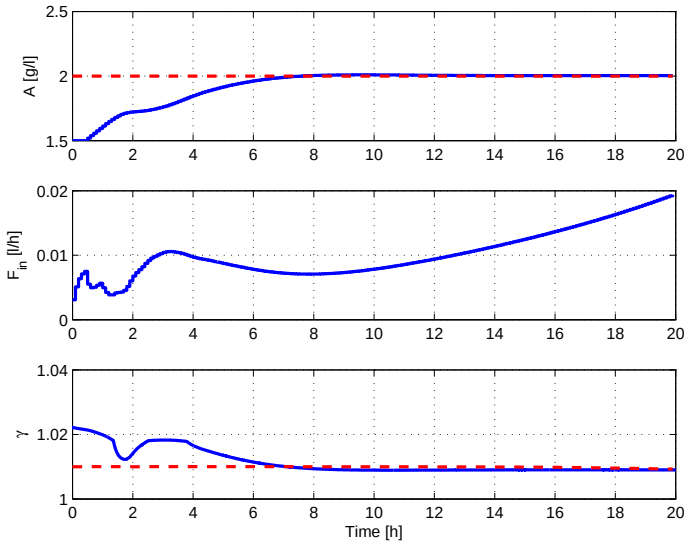

Figure 6.15: Simulation of the RST controller applied to *E.coli* model (6.11) with a large measurement delay (4 T_s). Evolution of the acetate concentration, the feed rate and γ.

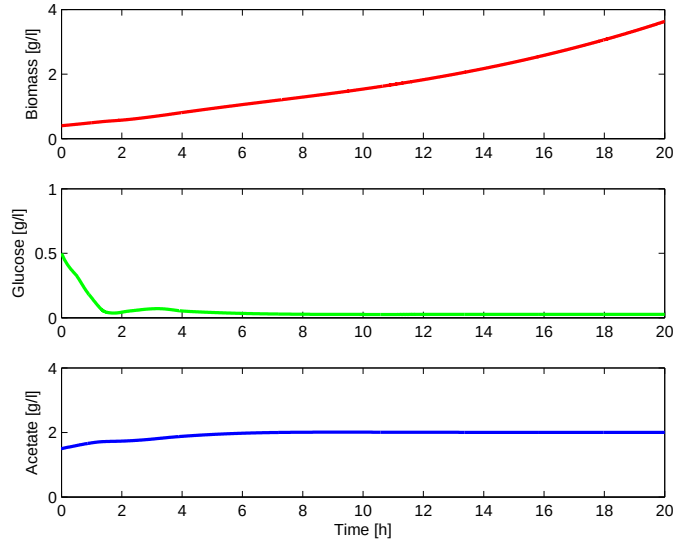

Figure 6.16: Simulation of the RST controller applied to *E.coli* model identified in (6.11) with a large measurement delay (4 T_s). Evolution of the biomass, glucose and acetate concentrations.

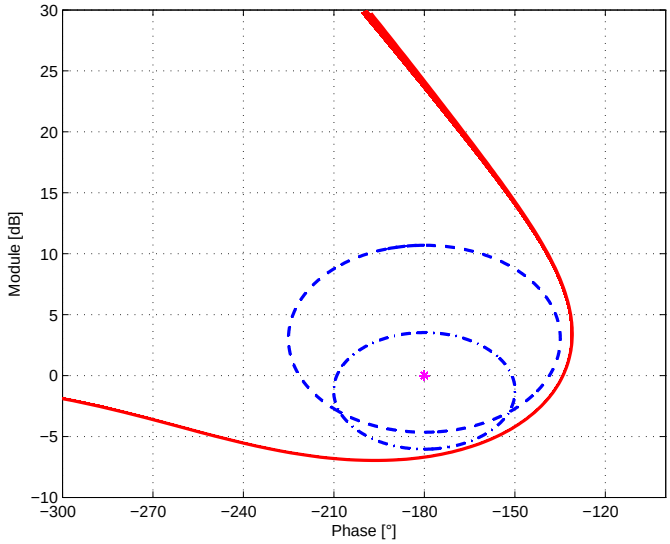

Figure 6.17: Simulation of the RST controller applied to *E.coli* model (6.11) with a large measurement delay (4 T_s). Evolution of the corrected open-loop function in the Black-Nichols diagram.

Table 6.6: Initial and operating conditions of the three experiments.

Experiment	Biomass (g/l)	Glucose (g/l)	Acetate set-point (g/l)
1	0,325	1	2
2	0,478	0,6	3
3	0,277	0,763	2

real pilot plant is presented in the next section.

6.3.2 Experimental results

Three experiments using the previously designed *RST* controller are performed on the *E.coli* pilot plant. Results of these experimental applications are presented in Figs. 6.18, 6.19 and 6.20. Initial and operating conditions of each experiment are represented in Table 6.6.

For the first experiment (Fig. 6.18), the acetate signal is correctly controlled during the first 6 hours. Then, the probe is influenced by a sudden disturbance appearing as a down step. The controller is consequently increasing the feed rate in order to bring the acetate signal back to the neighborhood of its set-point. However, an abnormal accumulation of glucose is observed in an off-line measurement 3 hours later so that the experiment has to be stopped. At this time, the biomass concentration is around 2 g/l. In comparison with the previous simulated results, this value shows that the optimization scheme

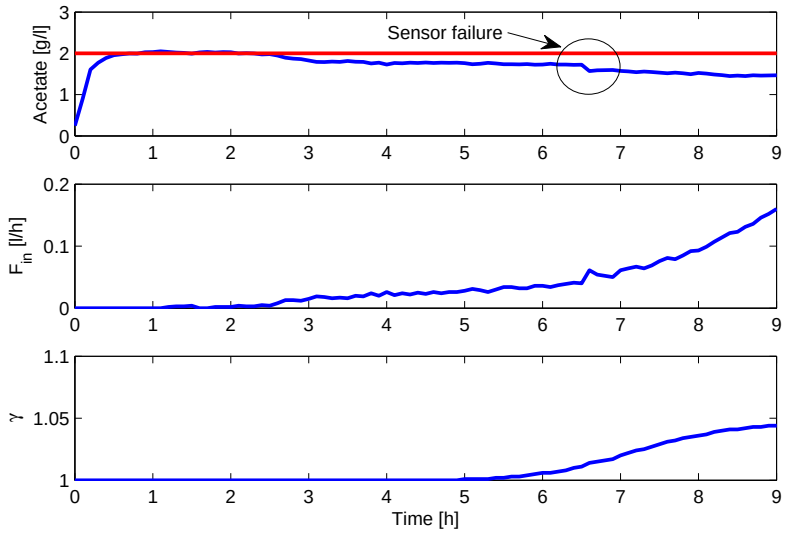

Figure 6.18: Experimental results of the RST controller applied to the *E.coli* pilot plant. First experiment: evolution of the acetate concentration, the feed rate and γ.

has been correctly working until the occurence of this disturbance. Moreover, at the same time, gaz bubbles appeared in the tubes of the assembly measuring on-line acetate, which could possibly influence the conductivity measurement. The apparition of these gaz bubbles could be due to a failure of the microfiltration probe following a too high concentration of biomass accumulating on the membrane and, therefore, partially blocking the broth and only allowing gaz diffusion. Anyway, before drawing too early conclusions, two other experiments are performed for comparison purpose.

In the second experiment, the initial acetate concentration is around 3 g/l and the acetate set-point is increased in order to avoid a switch to the respirative regime and a long reconsumption of acetate (already shown in Fig. 5.23 in section 5.5.2). After a long initial transient period of 10 h (see Fig. 6.19), the feed rate trajectory becomes exponential between 10 and 18 h before the occurence of a new sudden step disturbance (once again, accompanied by gaz bubbles) leading to the same consequences as in the first experiment. At this stage, a biomass concentration equal to $4,257$ g/l is obtained before the probe failure, showing that the controller performs again satisfactorily.

A last experiment is then performed where the probe shows the same behaviour (see Fig. 6.20). The disturbances appear in 6 and 11 h. Note that the second disturbance has less consequences than the first as the step disappears more or less immediately. The final biomass concentration is $1,6$ g/l before the first disturbance.

The next chapter draws the conclusions of these experiments performed on the *E.coli* pilot plant and proposes solutions in view of control improvement.

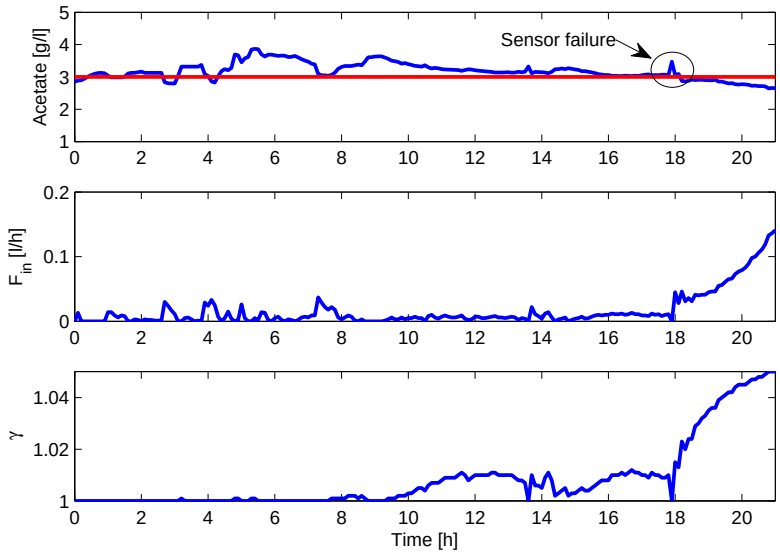

Figure 6.19: Experimental results of the RST controller applied to the *E.coli* pilot plant. Second experiment: evolution of the acetate concentration, the feed rate and γ.

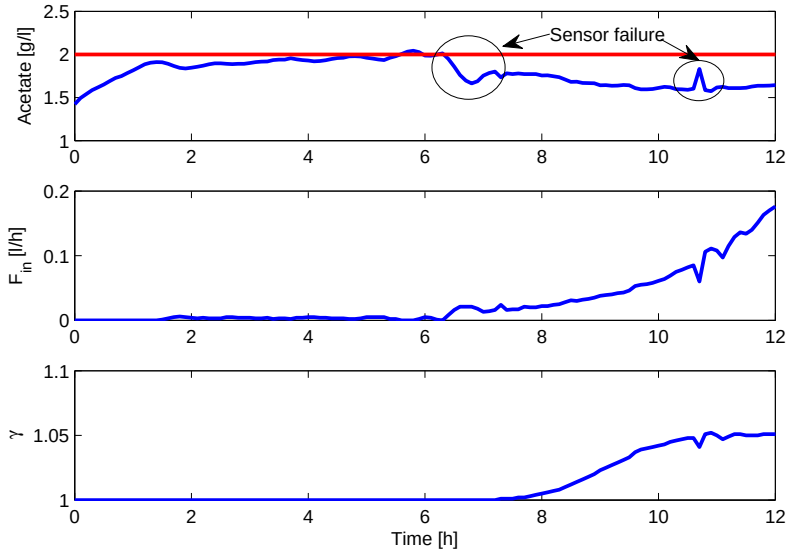

Figure 6.20: Experimental results of the RST controller applied to the *E.coli* pilot plant. Third experiment: evolution of the acetate concentration, the feed rate and γ.

Chapter 7

Perspectives and General Conclusions

7.1 Conclusions

All along this thesis, monitoring and control of bioprocesses is investigated. Starting from primary biological knowledge of the cell catabolism, culture conditions and a brief description of the main physiological feature, called **overflow metabolism**, is provided. A generic mechanistic model that would, in principle, allow the representation of the culture of different strains presenting an overflow metabolism, is then presented. A key feature of mechanistic models allowing the estimation of unmeasured states from measured ones, called **observation**, is also defined and studied for the considered kinetic structure. An illustrative comparison of two different state estimation strategies either based on **mechanistic models** or **data-driven techniques** is presented through simulated and experimental applications.

At this stage of the work, the main concern is to answer the questions:

- What is the plant optimum?

The optimal growth corresponds to the edge between the respirative and respiro-fermentative regimes. A critical substrate level S_{crit} corresponds to this boundary and is influenced by the respiratory capacity of the microorganism. The latter appears to be in turn influenced by several factors including influence of inhibitory byproduct.

- Which state variables should be controlled?

The optimization problem can be stated as a regulation problem either on the substrate concentration at S_{crit} or of the inhibitory byproduct concentration at a as small as possible level. For the substrate regulation, a **model-free**

extremum-seeking strategy is proposed based on 3 measurements. Unfortunately, this method requires also the availability of on-line substrate measurement, which raises the next questions:

- Are the controlled variables measurable?
- If not, is there a way to correctly estimate or observe them?

Substrate concentration measurement around S_{crit} is a difficult task as the concentration level is small and close to the probe sensitivity. However, the substrate estimation using a software sensor could be an alternative.

- Is a suboptimal solution more practical?
- Should the controller have a certain complexity degree? Is the complexity degree a source of limitation?

To alleviate the problem of measuring or estimating the substrate concentration, a suboptimal strategy based on the regulation of the byproduct concentration is proposed. In this context, a comparison of a classical adaptive linearizing control with a novel robust controller using the **LMIs** framework is achieved. At the experimental level, a **RST** control structure including robustification and adaptation mechanisms is applied at the laboratory and industrial scales.

To conclude this work, design, monitoring and control of an *Escherichia coli* **laboratory pilot plant** are achieved. Encouraging simulated and experimental results are finally discussed, highlighting the gradually deteriorating robustness of the current acetate concentration measurement assembly as biomass concentration increases.

7.2 Perspectives

7.2.1 Sensors

Hardware Sensor

Improvements can still be brought to the on-line acetate measurement assembly. As the measurement deterioration occurs immediately after the emergence of gaz bubbles in the assembly tubes, it is legitimate to expect these two phenomenons to be related. From this on, a first degasification cell could be installed upstream of the **A-sep cell**, despite a possible increase of the measurement delay (which, in this case, is still easier to handle than large random step variations).

Software Sensors

As an alternative solution to the acetate hardware sensor, estimators could be build on the basis of available tools presented in chapter 2. Simultaneous sub-

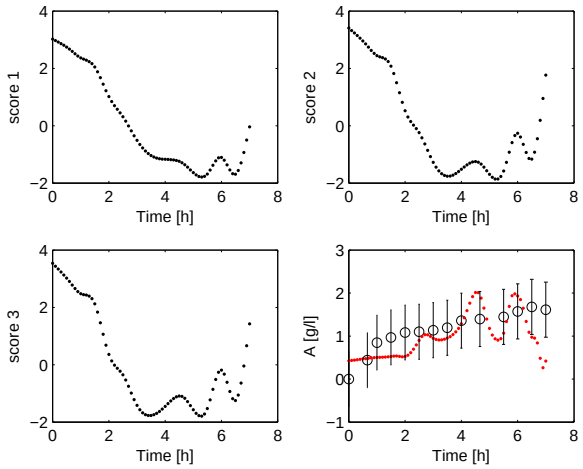

Figure 7.1: Off-line experimental results of the *ANN* applied to the *E.coli* pilot plant data. First direct validation: evolution of the scores and the acetate concentration. Bubbles: off-line measurements. Dotted red line: ANN estimation.

strate and acetate observations from biomass and oxygen measurements using **Continuous-Discrete Extended Kalman Filter** are in the scope of on-going work following this thesis. Moreover, acetate estimation using black-box **RBF-ANN** structures is already being studied. First results are shown from Figs. 7.1 to 7.5. While direct validations of the estimator seem very satisfactory (see Figs. 7.1 to 7.3), cross-validations are still offering poor qualitative results (apparition of abnormal acetate peaks). Nevertheless, qualitative observations indicate more encouraging values as, for instance, an average error of $0,45\ g/l$ for direct validations and $0,65\ g/l$ for cross-validations.

7.2.2 Control

Experimental validations

Extremum-seeking and robust linearizing control are powerful tools that should soon be implemented for their first experimental validations. However, while the first strategy requires substrate concentration measurement which remains below the sensitivity of current available probes, the other one is dependent of the acetate hardware sensor features (particularly the delay and the untimely step variations). Future experimental applications of these two techniques are henceforth linked to the evolution of substrate and acetate software sensor design.

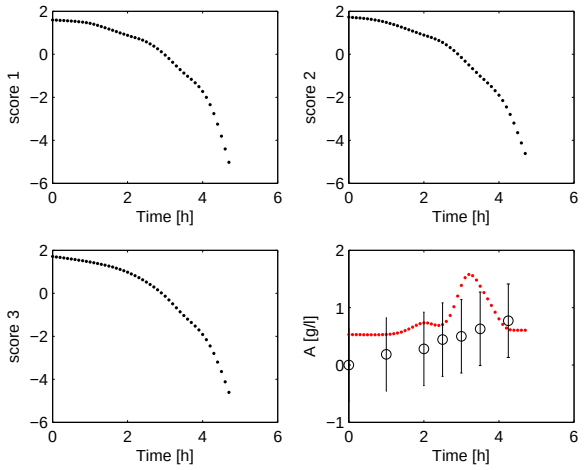

Figure 7.2: Off-line experimental results of the *ANN* applied to the *E.coli* pilot plant data. Second direct validation: evolution of the scores and the acetate concentration. Bubbles: off-line measurements. Dotted red line: ANN estimation.

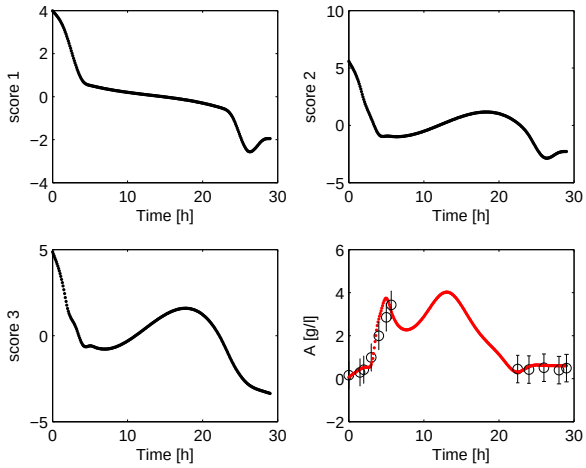

Figure 7.3: Off-line experimental results of the *ANN* applied to the *E.coli* pilot plant data. Third direct validation: evolution of the scores and the acetate concentration. Bubbles: off-line measurements. Dotted red line: ANN estimation.

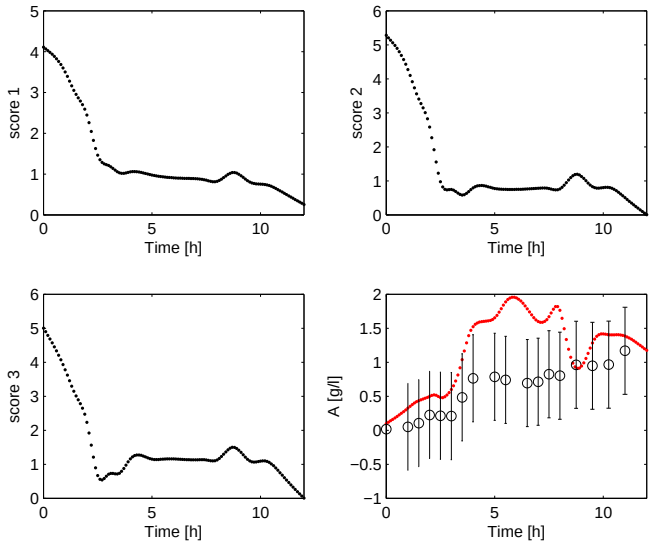

Figure 7.4: Off-line experimental results of the *ANN* applied to the *E.coli* pilot plant data. First cross-validation: evolution of the scores and the acetate concentration. Bubbles: off-line measurements. Dotted red line: ANN estimation.

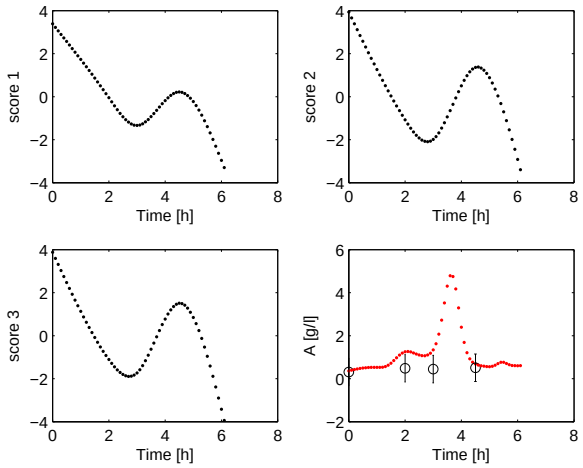

Figure 7.5: Off-line experimental results of the *ANN* applied to the *E.coli* pilot plant data. Second cross-validation: evolution of the scores and the acetate concentration. Bubbles: off-line measurements. Dotted red line: ANN estimation.

New methods

Closed-loop control of fed-batch cultures of microorganisms exhibiting overflow metabolism is of course not limited to the different strategies presented all along this thesis. Model predictive control (**MPC**) is a particularly interesting technique initially applied in its nonlinear form (**NMPC**) to *E. coli* cultures by Hafidi (2008) and recently updated in Santos et al. (2010). Its principle is based on the recurrent optimization of a cost function to be maximized (or minimized) over a certain horizon, taking the control objectives and constraints into account as in:

$$\max_{u} J(\xi) \tag{7.1}$$

$$s.t. \quad \dot{\xi} = f(\xi, u) \tag{7.2}$$

$$h(\xi) \leq 0 \tag{7.3}$$

$$g(\xi) = 0 \tag{7.4}$$

where ξ is the state vector, u is the system input, J is the cost function to be optimized and h and g functions are the constraints.

In the work of Hafidi (2008), an objective cost is considered in order to track the metabolite byproduct (acetate) concentration at a small reference value while constraining the input profile to remain in the neighborhood of the optimal solution. **NMPC** is a very versatile technique which allows the consideration of various cost functions. On-going work Santos et al. (2010) for instance considers the use of the optimality criterion defined in the **RTO** section of this thesis (see section 4.2.1). This strategy uses 3 measurements (OTR, CTR and SIR) to evaluate the optimality criterion. In order to test this conceptual approach maximizing the biomass productivity over a predicted horizon, the following cost function is proposed to be maximized over a finite horizon:

$$J = \sum_{i=1}^{p} (\varphi_{1,k+i} - \varphi_{2,k+i}) - \beta \sum_{i=1}^{m} (F_{in,k+i-1} - F_{in,k+i-1}^{ref})^2 \tag{7.5}$$

where p is the predicted horizon, $m \leq p$ is the input (in this case, the manipulation variable is the feed rate F_{in} and F_{in}^{ref} is its reference) predicted horizon, and β is a strictly positive control penalty constant. First simulation tests have shown very encouraging results. Nevertheless, **NMPC** is based on the full nonlinear model of the process and a study of the robustness is an important issue which is also the subject of on-going workusing a min-max formulation of the optimization problem. In addition, **NMPC** requires the full state measurements for feed-back purpose which implies in turn the design of software sensors.

This last section ends by citing the original **sliding mode control** of fed-batch cultures that has also been investigated in Pico-Marco et al. (2005).

Bibliography

Adetola, V. and Guay, M. (2006). Parameter convergence in adaptive extremum-seeking control. *Automatica*, 43:105–110.

Akesson, M. (1999). *Probing control of glucose feeding in* Escherichia coli *cultivations*. PhD thesis, Lund Institute of Technology, Sweden.

Ariyur, K. B. and Krstic, M. (2003). *Real-time Optimization by Extremum-seeking Control*. John Wiley & Sons, INC, wiley-interscience edition.

Aström, K. J. and Wittenmark, B. (1995). *Adaptive Control, Second Edition*. Addison-Wesley Publishing Company, Inc.

Astrom, K. and Wittenmark, B. (1997). *Computer Controlled Systems Theory and Design*. Information and System Sciences. Prentice Hall.

Axelsson, J. P. (1988). On the role of adaptive controllers in fed-batch yeast production. In *IFAC Adaptive Control of Chemical Processes*, pages 103–108, Copenhagen, Denmark.

Axelsson, J. P. (1989). *Modeling and Control of Fermentation Processes*. PhD thesis, Lund Institute of Technology, Sweden.

Axelsson, J. P., Mandenius, C. F., Holst, O., Hagander, P., and Mattiasson, B. (1988). Experience in using an ethanol sensor to control molasses feed-rates in baker's yeast production. *Bioprocess Engineering*, 3:1–9.

Bastin, G. and Dochain, D. (1990). *On-Line Estimation and Adaptive Control of Bioreactors*, volume 1 of *Process Measurement and Control*. Elsevier, Amsterdam.

Bernaerts, K., Gysemans, K. P. M., Minh, T. N., and Impe, J. F. V. (2005). Optimal experiment design for cardinal values estimation: Guidelines for data collection. *International Journal of Food Microbiology*, 100:153–165.

Betancur, M. J., Titica, M., Moreno, J. A., Dochain, D., and Guay, M. (2004). Event software sensor and adaptive extremum seeking alternatives for optimizing a class of fed-batch bioreactors. In *7th International Symposium on Dynamics and Control of Process Systems*, Boston, USA.

Bogaerts, P. (1999). *Contribution à la Modélisation Mathématique pour la Simulation et l'Observation d'États des Bioprocédés*. PhD thesis, Université Libre de Bruxelles, Brussels.

Bogaerts, P., Castillo, J., and Hanus, R. (1999). A general mathematical modelling technique for bioprocesses in engineering applications. *Syst. Anal. Model. Simul.*, 35:87–113.

Bogaerts, P. and Hanus, R. (2002). *Macroscopic Modelling of Bioprocesses with a View to Engineering Applications*, volume 4 of *Focus on Biotechnology*, pages 77–109. Springer Netherlands.

Bogaerts, P. and Vande Wouwer, A. (2003). Software sensors for bioprocesses. *ISA Transactions*, 42:547–558.

Bogaerts, P. and Vande Wouwer, A. (2004). Parameter identification for state estimation - application to bioprocess software sensors. *Chemical Engineering Science*, 59(12):2465–2476.

Bourlard, H. (1992). Continuous speech recognition: from hidden markov models to neural networks. In *6th European Signal processing Conference, Brussels, Belgium*, pages 63–70.

Boyd, S., El-Ghaoui, L., Feron, E., and Balakrishnan, V. (1994). *Linear Matrix Inequalities in System and Control Theory*. SIAM.

Cappuyns, A. M., Bernaerts, K., Vanderleyden, J., and Impe, J. F. V. (2009). A dynamic model for diauxic growth, overflow metabolism, and al-2-mediated cell-cell communication of salmonella typhimurium based on systems biology concepts. *Biotechnology and Bioengineering*, 102(1):280–293.

Chachuat, B., Srinivasan, B., and Bonvin, D. (2009). Adaptation strategies for real-time optimization. *Computers and Chemical Engineering*, 33:1557–1567.

Chen, L. and Bastin, G. (1996). Structural identifiability of the yield coefficients in bioprocess models when the reaction rates are unknown. *Mathematical Biosciences*, 132:35–67.

Chen, L., Bastin, G., and van V. Breusegem (1995). A case study of adaptive nonlinear regulation of fed-batch biological reactors. *Automatica*, 31(1):55–65.

Chioua, M., Srinivasan, B., Guay, M., and Perrier, M. (2008). Dependence of the error in the optimal solution of perturbation-based extremum seeking methods on the excitation frequency. *The Canadian Journal of Chemical Engineering*, 85(4):447 – 453.

Coutinho, D., Fu, M., Trofino, A., and Danes, P. (2008). L2-gain analysis and control of uncertain nonlinear systems with bounded disturbance inputs. *Int'l J. Robust Nonlinear Contr.*, 18(1):88–110.

Crabtree, H. (1929). Observations on the carbohydrate metabolism of tumors. *Biochemical Journal*, 23:536–545.

Deken, R. H. D. (1966). The crabtree effect: A regulatory system in yeast. *J . gen. Microbiol.*, 44:149–156.

Dewasme, L., Renard, F., and Vande Wouwer, A. (2007a). Experimental investigations of a robust control strategy applied to cultures of s. cerevisiae. In *Preprints of the European Control Conference, Kos, Greece*, pages 4785–4791.

Dewasme, L. and Vande Wouwer, A. (2008). Adaptive extremum-seeking control applied to productivity optimization in yeast fed-batch cultures. In *Preprints of the IFAC World Congress*, Seoul, South Korea.

Dewasme, L., Vande Wouwer, A., Dessoy, S., Dehottay, P., Hulhoven, X., and Bogaerts, P. (2007b). Experimental study of neural network software sensors in yeast and bacteria fed-batch processes. In *10th International IFAC Symposium on Computer Applications in Biotechnology*, volume 1, pages 45–50, Cancun, Mexico.

Francis, B. and Wonham, W. (1975). The internal model principle for linear multivariable regulators. *App. Mathem. Opt.*, 2(2):170–194.

Gauthier, J.-P. and Kupka, I. (1994). Observability and observers for nonlinear systems. *SIAM Journal Control and Optimization*, 32(4):975–994.

Geladi, P. and Kowalski, B. (1986). Partial least squares regression. a tutorial. *Analytica Chimica Acta*, 185:1–17.

Gelb, A. (1974). *The Analytic Sciences Corporation Technical Staff: Applied Optimal Estimation*. MIT Press, Cambridge.

Goffaux, G. and Vande Wouwer, A. (2005). *Bioprocess State Estimation : Some Classical and Less Classical Approaches*, pages 111–128. Control and Observer Design for Nonlinear Finite and Infinite Dimensional Systems. Springer - Verlag Berlin Heidelberg.

Gosselin, B. (1996a). *Application de Réseaux de Neurones Artificiels à la Reconnaissance Automatique de Caractères Manuscrits*. PhD thesis, Faculté Polytechnique de Mons, Belgium.

Gosselin, B. (1996b). Multilayer perceptrons combination applied to handwritten character recognition. *Neural Processing Letters*, 3(1):3–10.

Green, M. and Limebeer, D. (1994). *Linear Robust Control*. Prentice Hall.

Grosfils, A., Vande Wouwer, A., and Bogaerts, P. (2007). On a general model structure for macroscopic biological reaction rates. *Journal of Biotechnology*, 130(3):253–264.

Guay, M. and Zhang, T. (2003). Adaptive extremum seeking control of nonlinear dynamic systems with parametric uncertainties. *Automatica*, 39:1283–1293.

Hafidi, G. (2008). *Commande Prédictive Non-linéaire de Cultures Fed-batch de Bactéries E. coli*. PhD thesis, Université Paris XI.

Henes, B. and Sonnleitner, B. (2007). Controlled fed-batch by tracking the maximal culture capacity. *Journal of Biotechnology*, 132:118–126.

Hulhoven, X., Renard, F., Dessoy, S., Dehottay, P., Bogaerts, P., and Vande Wouwer, A. (2006). Monitoring and control of a bioprocess for malaria vaccine production. In *5th IFAC Symposium on Robust Control Design, Toulouse, France*.

Hulhoven, X., Vande Wouwer, A., and Bogaerts, P. (2005). On a systematic procedure for the predetermination of macroscopic reaction schemes. *Bioprocess and Biosystems Engineering*, 27(5):283–291.

Karim, M. N., Yoshida, T., Rivera, S. L., Saucedo, V. M., Eikens, B., and Oh, G.-S. (1997). Global and local neural network models in biotechnology: Application to different cultivation processes. *Journal of Fermentation and Bioengineering*, 83:1–11.

Krstic, M. and Wang, H. H. (2000). Stability of extremum seeking feedback for general nonlinear dynamic systems. *Automatica*, 36:595–601.

Landau, I. D. (1998). The r-s-t digital controller design and applications. *Control Engineering Practice*, 6:155–165.

Leith, D. and Leithead, W. (2000). Survey of gain-scheduling analysis and design. *International Journal of Control*, 73:1001–1025.

Marchetti, A., Chachuat, B., and Bonvin, D. (2009). Modifier-adaptation methodology for real-time optimization. *Industrial & Engineering Chemistry Research*, 48(13):6022–6033.

Marcos, N. I., Guay, M., and Dochain, D. (2004). Adaptive extremum seeking output feedback control for a continuous stirred tank bioreactor. In *International Symposium on Advanced Control of Chemical Processes*, pages 968–973, Hong Kong, China.

McCulloch, W. S. and Pitts, W. (1943). A logical calculus of the ideas immanent in nervous activity. *Bulletin of Mathematical Biophysics*, 15:115–133.

Methekar, R., Patwardhan, S. C., Gudi, R. D., and Prasad, V. (2010). Adaptive peak seeking control of a proton exchange membrane fuel cell. *Journal of Process Control*, 20:73–82.

Minsky, M. and Papert, S. (1969). Perceptrons: An introduction to computational geometry. *The MIT Press, Cambridge*.

Morgan, N. and Bourlard, H. (1995). Neural networks for statistical recognition of continuous speech. In *Proceedings of the IEEE*, volume 83 of *5*, pages 741–770. Invited Paper.

Peters, N., Guay, M., and DeHaan, D. (2007). Real-time dynamic optimization of batch systems. *Journal of Process Control*, 17:261–271.

Pham, T. B. H. (1999). *Modelling and control of microbii fed-batch and pH-auxostat processes*. PhD thesis, Royal Institute of Technology. Department of Biotechnology. Stockholm, Sweden.

Pico-Marco, E., Pico, J., and Battista, H. D. (2005). Sliding mode scheme for adaptive specific growth rate control in biotechnological fed-batch processes. *Int. Journal of Control*, 78(2):128 – 141.

Pomerleau, Y. (1990). *Modélisation et commande d'un procédé fed-batch de culture des levures à pain*. PhD thesis, Département de génie chimique. Université de Montréal.

Renard, F. (2006). *Commande Robuste de Bioprocédés Opérés en Mode Fed-batch: Application Industrielle à des Cultures de* Saccharomyces cerevisiae. PhD thesis, Faculté Polytechnique de Mons.

Renard, F., Vande Wouwer, A., Valentinotti, S., and Dumur, D. (2006). A practical robust control scheme for yeast fed-batch cultures - an experimental validation. *Journal of Process Control*, 16:855–864.

Renard, F. and Wouwer, A. V. (2008). Robust adaptive control of yeast fed-batch cultures. *Comp. and Chem. Eng.*, 32:1238–1248.

Rocha, I. (2003). *Model-based strategies for computer-aided operation of recombinant E. coli fermentation*. PhD thesis, Universidade do Minho.

Rosenblatt, F. (1958). The perceptron: A probabilistic model for information storage and organization in the brain. *Cornell Aeronautical Laboratory, Psychological Review*, 65(6):386–408.

Santos, L. O., Dewasme, L., and Vande Wouwer, A. (2010). Nonlinear model predictive control of fed-batch cultures of e. coli: Performance and robustness analysis. In *8th IFAC Symposium on Nonlinear Control Systems*, Bologna, Italy. Accepted for oral presentation.

Sastry, S. and Bodson, M. (1989). *Adaptive Control : Stability, Convergence and Robustness*. Prentice Hall Information and System Sciences Series. Prentice Hall, Englewood Cliffs, New Jersey, thomas kailath edition edition.

Skogestad, S. (2000). Self-optimizing control: The missing link between steady-state optimization and control. *Computers and Chemical Engineering*, 24:569–575.

Skogestad, S. (2004). Control structure design for complete chemical plants. *Computers and Chemical Engineering*, 28(1-2):219–234.

Skogestad, S. and Postlethwaite, I. (2001). *Multivariable Feedback Control - Analysis and Design*. John Wiley & Sons, New York, NJ.

Sonnleitner, B. and Käppeli, O. (1986). Growth of *Saccharomyces cerevisiae* is controlled by its limited respiratory capacity : Formulation and verification of a hypothesis. *Biotechnol. Bioeng.*, 28:927–937.

Srinivasan, B. and Bonvin, D. (2002). Interplay between identification and optimization in run-to-run optimization schemes. In *American Control Conference, Anchorage, AK*, pages 2174–2179.

Stephanopoulos, G. (1999). Metabolic fluxes and metabolic engineering. *Metabolic Engineering*, 1:1–11.

Sturm, J. F., Romanko, O., and Pólik, I. (2006). SeDuMi, version 1.1R3. Online – http://sedumi.mcmaster.ca/.

Tan, Y., Nesic, D., and Mareels, I. (2006). On non-local stability properties of extremum seeking control. *Automatica*, 42:889–903.

Tan, Y., Nesic, D., and Mareels, I. (2008). On the choice of dither in extremum seeking systems: A case study. *Automatica*, 44:1446–1450.

Tan, Y., Nesic, D., Mareels, I., and Astolfi, A. (2009). On global extremum seeking in the presence of local extrema. *Automatica*, 45:245–251. Brief Paper.

Titica, M., Dochain, D., and Guay, M. (2003a). Adaptive extremum-seeking control of fed-batch bioreactors. *European Journal of Control*, 9(6):618–631.

Titica, M., Dochain, D., and Guay, M. (2003b). Real-time optimization of fed-batch bioreactors via adaptive extremum-seeking control. *Chemical Engineering Research and Design*, 81(A9):1289–1295.

Valentinotti, S., Cannizzaro, C., Srinivasan, B., and Bonvin, D. (2004). An optimal operating strategy for fed-batch fermentations by feeding the overflow metabolite. In *International Symposium on Advanced Control of Chemical Processes*, Hong Kong.

Valentinotti, S., Srinivasan, B., Holmberg, U., Bonvin, D., Cannizzaro, C., Rhiel, M., and von Stockar, U. (2003). Optimal operation of fed-batch fermentations via adaptive control of overflow metabolite. *Control engineering practice*, 11:665–674.

Vande Wouwer, A., Renotte, C., and Bogaerts, P. (2004). Biological reaction modeling using radial basis function networks. *Computers and Chemical Engineering*, 28:2157–2164.

Vemuri, G., Altman, E., Sangurdekar, D. P., Khodursky, A. B., and Eiteman, M. A. (2006). Overflow metabolism in escherichia coli during steady-state growth: Transcriptional regulation and effect of the redox ratio. *Applied and Environmental Microbiology*, 72(5):3653–3661.

Vemuri, G. N., Eiteman, M. A., McEwen, J. E., Olsson, L., and Nielsen, J. (2007). Increasing nadh oxidation reduces overflow metabolism in saccharomyces cerevisiae. *Proceedings of The National Academy of Sciences of the United States of America*, 104(7):2402–2407.

Versyck, K. J., Bernaerts, K., Geeraerd, A. H., and Impe, J. F. V. (1999). Introducing optimal experimental design in predictive modelling: A motivating example. *International Journal of Food Microbiology*, 51:39–51.

Vidyasagar, M. (1978). *Nonlinear Systems Analysis*. Prentice Hall, Englewood Cliffs.

Wang, H. H., Krstic, M., and Bastin, G. (1999). Optimizing bioreactors by extremum-seeking. *Int. J. Adaptive Control and Signal Processing*, 13:651–669.

Werbos, P. (1974). *Beyond regression: New Tools for Prediction and Analysis in the Behavioural Sciences*. PhD thesis, Harvard University, Cambridge, MA.

Zeitz, M. (1984). Observability canonical (phase-variable) form for nonlinear time-variable systems. *International Journal of System Science*, 15(9):949–958.

Zhang, C. and Ordonez, R. (2009). Robust and adaptive design of numerical optimization-based extremum seeking control. *Automatica*, 45:634–646.

Zhang, Y., Monder, D., and Forbes, J. F. (2002). Real-time optimization under parametric uncertainty: A probability constrained approach. *Journal of Process Control*, 12:373–389.